JANUARY 1986

LIDS-TH-1529

THE BACKPROPAGATED FIELD APPROACH TO MULTIDIMENSIONAL VELOCITY INVERSION

by

Cengiz Esmersoy

This report is based on the unaltered thesis of Cengiz Esmersoy, submitted in partial fulfillment of the requirements for the degree of Doctor of Philosophy at the Massachusetts Institute of Technology in November 1985. The research was conducted at the M.I.T. Earth Resources Laboratory and at the Laboratory for Information and Decision Systems, with support provided in part by the Army Research Office under Grant No. DAAG-29-84-K-0005, and in part by the National Science Foundation under Grant No. ECS-83-12921.

Laboratory for Information and Decision Systems
Massachusetts Institute of Technology
Cambridge, Massachusetts 02139

THE BACKPROPAGATED FIELD APPROACH TO MULTIDIMENSIONAL VELOCITY INVERSION

by

Cengiz Esmersoy

Submitted to the Department of Electrical Engineering

and Computer Science on November 18, 1985

in partial fulfillment of the requirements for the Degree of

Doctor of Philosophy

Abstract

The multidimensional inverse scattering problem for an acoustic medium is considered within the framework of approximate direct inversion. A new approach to direct velocity inversion problem is introduced. The observed scattered field is first backpropagated into the background medium. Then, an image of the velocity variations of the scattering medium is obtained by operating on this backpropagated field. Three types of probing experiments are considered, corresponding to cases when we use a plane-wave source, a point or line source, or an array of coincident source-receiver pairs (zero-offset configuration). The case of incomplete observations of the scattered field is modeled by a receiver array with a finite angle of aperture. The backpropagated field is expressed as a volume integral in terms of the velocity inhomogeneities of the medium. This integral equation, which relates the backpropagated field to the velocities, is derived for all types of probing experiments and for cases of complete and incomplete receiver coverage. It is shown that inversion

of this equation can be achieved by imaging the backpropagated field at time zero or at the source-travel times. In addition to the backpropagated field approach, a slant-stack method of inversion is presented for the case of plane-wave excitation.

Thesis Supervisor: Dr. Bernard C. Levy

Title: Associate Professor of Electrical Engineering

Acknowledgements

I would like to thank my thesis committee members, friends, co-workers, family and parents who became a part of this thesis work by providing valuable suggestions, motivating discussions and support. Let me start with the supervisor of this thesis Prof. Bernard Levy. Throughout this research Bernard has been a constant source of motivation. I have greatly benefited from his guidance and his insights during frequent meetings we had. I would like to thank Bernard for keeping a friendly and productive relationship. It has been a great pleasure to work with him. Prof. Nafi Toksöz, a member of the thesis committee, has supported me prior to and during this study. For over three years I had the privilege of working with him on various projects. Without Nafi this thesis would not have been possible. Another member of the thesis committee, Dr. Michael Oristaglio has made valuable suggestions, that I extensively used in this thesis, while I was a summer student at Schlumberger-Doll Research in 1984. Michael is also responsible for clarifying several issues that came up during the course of this work. Prof. Arthur Baggeroer and Prof. Alan Willsky, members of the thesis committee, contributed by valuable comments and by constructive criticism.

Earth Resources Laboratory has been a big part of my graduate study and my education in the field of seismics. Since I have joined the laboratory in the summer of 1982, I had many opportunities to participate in various consortia and projects. The greatest benefit of being a research assistant at ERL was the interaction that I have had over the years with the graduate students and research scientists. Especially, long

discussions with "Dr. Keho" and Dr. Beydoun has been a part of a typical day. I would like to thank Tim and Wafik for their friendship and for making last years of this thesis work a great experience. Also, thanks go to Dr. Vern Cormier, with whom I had a chance to work in my first year at ERL, and to Dr. Roger Turpening who has always been there whenever I needed to know more about "real" seismic data.

I wish to thank Dr. Ralphe Wiggins and the members of the Schlumberger-Doll Research seismic group for their help during the summers of 1984 and 1985. Special thanks to Dr. Douglas Miller, Dr. Gregory Beylkin and Dr. Anthony Devaney for enlightening discussions. Dr. Thomas Marzetta is responsible for getting me interested in seismic signal processing during my first summer at SDR in 1981.

During the course of this thesis I had the opportunity to meet with distinguished people like Prof. Emil Wolf, Prof. Robert Porter, Dr. Arthur Weglein and Prof. Shimon Coen. Their valuable comments and suggestions are deeply appreciated. In particular, I wish to thank Robert for his guidance that saved me a great deal of time and effort.

Last, and certainly not the least, I would like to thank my wife Ivon and my sons Tan and Cem for their very special support and patience. Also, I wish to thank my parents Mesut and Ayten and my sister Hülya for their unending encouragement.

This work has been supported in part by ONR and by VSP Consortium, ERL, MIT.

Table of Contents

CHAPTER I

Introduction

1.1 Problem Description and Motivation

This thesis treats the inverse scattering problem for an acoustic medium within the framework of approximate direct inversion. Specifically, we consider the following type of scattering experiment. An acoustic medium of variable velocity and constant density is probed by broad-band plane-wave or point sources located outside the region of inhomogeneity of the velocities and the scattered field is recorded at all frequencies with a receiver array also located outside the scattering region. Here, the medium is multidimensional, which means that the velocities vary with two or three space dimensions. The goal of approximate direct inversion is to reconstruct the medium velocities by operating on the observed scattered field. In contrast to iterative inversion methods, no iterations or repeated solutions of the forward problem are used in this approach. In fact, direct inversion is similar to reflector imaging that is commonly called *migration* in the seismics literature, except that in inversion we seek not only the location of velocity inhomogeneities, but also quantitative values for the velocities.

We consider three types of scattering experiments : experiments with plane-wave sources, with point (or line) sources, and with coincident source-receiver pairs ("zero-offset" experiments). Although physical experiments generally involve point

sources, a plane-wave source can be simulated by using a phase shifted array of point sources. Alternatively, if the scatterers are located in the far field of a point source, the effective excitation can be modeled by a plane-wave source with an appropriate angle of incidence. As will be shown later, the zero-offset configuration significantly simplifies the inversion problem. Consequently, most existing multidimensional inversion methods either assume the zero-offset geometry or use monochromatic plane-wave sources with various angles of incidence (as, e.g., in diffraction tomography). In seismic applications, zero-offset data is not collected directly, instead it is obtained from a series of single source experiments by performing a Common Depth Point (CDP) stack. This stacking procedure assumes a layered velocity model in which the velocities are either known a priori or determined from the coherency of the stack over a range of possible velocities. The CDP processing, in general, does not provide the correct common source-receiver data particularly when the lateral velocity changes are significant.

The wideband single source problem (for either a point or a plane-wave source) is significant for many reasons. Unlike in the zero offset case, both the reflected and transmitted waves can be used for inversion. This problem differs also from diffraction tomography by the fact that we perform a single experiment and measure the medium response at all frequencies, whereas in diffraction tomography a large number of experiments are performed by varying the angle of incidence of a probing monochromatic plane wave, but the medium response is measured at a single frequency. The single source problem, therefore, may help to better understand and relate these other inversion methods . Furthermore, this problem is obviously important in appli-

cations such as Vertical Seismic Profiling (VSP) where the coincident source-receiver array configuration or CDP stacking is either impractical or physically impossible. Also, the number and the location of the sources may not be sufficient to produce virtual plane wave sources (by stacking); therefore, each source must be considered separately. Moreover, most seismic reflection data are collected in a single source format. That is, a large receiver array is laid on the surface of the earth and data are collected for a few source locations. The previous inversion schemes perform Fourier transforms with respect to both the receiver and source locations. Therefore, these techniques cannot be directly applied to cases where only a few sources are available. Understanding the single source problem will help to develop direct inversion methods for more realistic problems, such as for multiple bandlimited sources.

1.2 Background

The general inverse scattering problem can be stated as follows. The medium of interest is probed by sources located outside the medium. The field scattered by the medium is recorded at various locations. The problem is to obtain the properties of the medium such as the propagation velocity or the material density from the observed data. Inverse scattering problems of this type arise in areas such as acoustics, electromagnetics and optics, although the corresponding physical phenomena are different. In this thesis, an acoustic medium probed by sound waves is considered. There are three basic approaches to the inversion problem, namely, generalized inversion, exact direct inversion and approximate direct inversion. The method of generalized or iterative inversion is not restricted to scattering problems. It has been widely used for other parametric modelling problems. In the inverse scattering context, this method consists of solving the forward scattering problem for a given set of parameters at each iteration. Depending on the difference between the observed and computed scattered waves, estimates of the medium parameters are updated and the next iteration is performed. Since parameter updating methods are well extablished, current efforts in generalized inversion have concentrated on finding fast and accurate solutions to the forward scattering problem.

The exact direct inversion methods aim at reconstructing the medium properties exactly, by operating on the observed scattered data. There are no iterations or repeated solutions of the forward problem involved. On the other hand these methods require stringent constraints on the observation geometry. Large number of sources and receivers are required to collect the data necessary for direct inversion. One

approach to the exact direct inversion problem is to transform the wave equation into a Schrödinger equation whose potential contains the spatial variations of the medium parameters. Methods developed specifically for this equation are then used to find the potential. In one dimension, a reportedly faster procedure can be obtained by using a two-component wave system instead of the second-order wave equation. The resulting set of linear equations is then solved by the Schur algorithm (Yagle and Levy, 1984). This technique operates directly on the observed data and requires a single recursive solution of the forward problem. Exact direct inversion methods are well developed for one dimensional media (the medium properties change in only one direction). Extension of these techniques to several dimensions has proved to be quite difficult, and is a current area of research.

The differential equation governing wave propagation in a multidimensional inhomogeneous medium can be transformed into an integral equation known as the Lippmann-Schwinger integral equation (Taylor, 1972). It is easily seen from this integral representation that the scattered field is a nonlinear function of the medium parameters. By successively iterating the integral representation of the scattered field, this field can be written as a power series of weighted integrals of the medium parameters. Each term in the series can be physically interpreted as corresponding to waves which have been scattered a fixed number of times. An approximate, linear relationship between the scattered field and the medium velocity function can be obtained by taking the first term of the series. Physically this means that only the first-order scattered waves are taken into account. The approximate direct inversion methods developed in this thesis deals with the direct solution of this linear integral equation.

By direct solution, we mean here that either the velocities are given by an analytical expression containing only the observed scattered field, or that they are obtained by a numerical procedure that does not involve repeated solutions of the forward problem. To better understand the approximations involved and to point out the differences between various inversion schemes, the term "scattered field" needs to be clarified. The scattered field is the difference between the computed background field and the observed total field. The background field is computed by solving the forward problem for a given background velocity model, which is usually based on the a priori knowledge of the medium. The solution of the forward problem can be analytical, if the background model is simple, or it can be obtained by numerical procedures such as the finite difference or geometrical optics (i.e., ray theoretical) methods. The scattered field, therefore, is due to velocity variations of the medium with respect to the background velocity model. With this definition of the scattered field, the linearized or first order scattered field corresponds to the following approximation. The incident field due to sources is propagated within the background model into the medium. At every point, the incident field is scattered (as secondary sources) with an amplitude proportional to the *scattering potential* at that point. The scattering potential is simply related to the difference between the background and true velocities. The scattered waves are propagated to the receivers again within the background model. Note that, depending on the method used to compute the background field, the multiples due to the background model may be included in the scattered field. The multiples due to the residual velocities are neglected. When the background model is a constant velocity medium, this first order approximation of the scattered field is known as the Born approximation. When the background model itself has variations in velocity the first

order approximation is often called the *distorted wave* Born approximation. In this thesis I will use the term Born approximation to cover both cases. Obviously this approximation is a good one when the scattered field is small compared to the incident field inside the medium.

Direct velocity inversion within the Born approximation has been an active research topic in recent years. This problem has been investigated for various dimensions, observation geometries and background velocity models, although most solutions assume an homogeneous background. The simplest problem, namely that of a one dimensional medium probed by a broad band plane wave, was considered by Cohen and Bleistein (1977) who showed that the velocities can be obtained by an inverse Fourier transform with respect to the wavenumber. Although this one dimensional problem may have limited practical importance it nevertheless demonstrates some properties of the Born approximation such as error accumulation with depth. A more interesting problem is the inverse problem for a layered medium probed by a point (or line) source. Exact inversion for this case is also possible, but it requires an array of receivers located on the surface. As was shown by Gray et. al. (1980), the Born inversion can be done with a single receiver in this case. Here again the inversion is obtained via Fourier transforms and a change of variables. For a layered medium, measurements at a minimum of two offsets are required for simultaneous reconstruction of the velocity and the density profiles as was pointed out by Raz (1981a).

Most of the solutions for the multidimensional case assume an observation geometry consisting of coincident sources and receivers (zero-offset). One reason for

the interest in the zero offset problem is that for this geometry the integral representation of the scattered field becomes simpler. As will be seen later, this leads to a one to one mapping between the observed data and the velocity function in the two (or three) dimensional Fourier transform domain. For the inverse seismic problem Cohen and Bleistein (1979) describe a time domain method for zero offset homogeneous background Born inversion, while Norton and Linzer (1981) describe similar methods for ultrasonic reflectivity imaging. Raz (1981b) and Clayton and Stolt (1981) consider the inversion problem with before stack data for the same geometry. In other words, for each source the scattered field is recorded at all receivers rather than only at the coincident receiver, thus resulting in a large amount of data. They showed that with this configuration both the density and the bulk modulus of the acoustic medium can be recovered simultaneously within the homogeneous Born approximation.

A slightly different approach to the study of the direct velocity inversion problem has been developed by extending x-ray tomography techniques to ultrasonic imaging. In this approach, the acoustic medium is probed from various directions by plane waves and the scattered field is recorded for each plane wave separately. At a fixed frequency, plane waves incident on the medium from all directions are required for complete inversion of the velocities. Mueller et al. (1979) discuss the diffraction effects of ultrasound tomography and derive the volume integral representation of the scattered field within the Born and Rytov approximations. Greenleaf (1983) gives some examples of images reconstructed with this approach. In diffraction tomography with plane-wave sources, the incident field becomes a complex exponential, providing a Fourier transform relation between the observed data and the scattering potential. In

fact, the scattered field due to each plane wave gives the velocity function along a circular trajectory in the Fourier transform domain as first pointed out by Wolf (1969). Velocities can be reconstructed by interpolating the available data over a rectangular grid and then taking the inverse Fourier transform in rectangular coordinates. Devaney (1982) introduced the backpropagation method for reconstruction as an alternative to interpolation in the frequency domain. Examples of velocity reconstructions with both incomplete and complete sets of plane waves are given by Devaney (1984), while Devaney and Beylkin (1984) describe the extension of these results to the case of a point source or "fan beam" geometry. As in the wide-band case, most solutions of the diffraction tomography problem assume a homogeneous background velocity model. Devaney and Oristaglio (1983) describe an inversion procedure for the inhomogeneous background case by using the distorted-wave Born approximation. They show that the scattering potential can be approximately recovered by using a complete set of plane-wave sources and receivers surrounding the medium. Their inversion procedure requires finding the inverse of a kernel given by the square of the imaginary part of the background Green's function.

Data processing efforts for single source experiments have mainly concentrated on reflector imaging or migration. The two main approaches to migration - the finite difference method (Claerbout, 1971; Claerbout and Doherty, 1972) and the Kirchhoff integral method for homogeneous background (Schneider, 1978; Jain and Wren, 1980) - are readily applicable to a single source experiment. A review of wavefield extrapolation methods for seismic migration can be found in Berkhout (1981). In general the purpose of migration is to map the locations of sharp velocity changes in

the medium rather than to obtain quantitative estimates of the velocities. For simple structures, such as a horizontal plane reflector, the peak amplitudes along the imaged reflector can be related to the local plane wave reflection coefficients as shown by Temme (1984) using synthetic seismograms. Also, Weglein (1982) observed that for zero-offset reflection data, the normal derivative of the inverted velocities and the migrated image were quite similar. Subsequently, it was shown by Cheng and Coen (1984) that for bandlimited data these quantities are essentially the same and that one can be obtained from the other. Kirchhoff migration can be viewed as a delay and sum array processing. To image a given point in the medium the receiver array is focused on that point by appropriate phase delays, and the image at the point is obtained by integrating over the receivers. The imaged quantity is obviously a function of the amount of scattering from that point but it is also a function of the relative positions of the source, the receiver array and the image point. Therefore, the imaged quantity is not a direct measure of the velocity changes at the image point. Better images of the discontinuities can be obtained by employing a weighted delay and sum operation for focusing, where different receiver weights are used for each point in the medium. Miller et. al. (1984) describe the choice of focusing weights for the case of homogeneous background and illustrate this technique with examples of migrated synthetic data. A formal derivation of the receiver weights for a variable background within the geometrical optics approximation is given by Beylkin (1984). The resulting migration algorithm is interpreted as the first term of the asymptotic expansion (with respect to smoothness) of the velocity inversion solution. This method rests on the use of the geometrical optics approximation for the background Green's function and establishes a connection between the imaging problem and the problem of inverting a

generalized Radon transform.

As was pointed out above, the Born approximation is the linearized (first order) approximation of the scattered field. Therefore, only the first order scattered waves are taken into account. The background model can be inhomogeneous, but is held unchanged during the inversion process. It is reasonable to suspect that one can do better than this for simple structures. For example, consider a one dimensional medium probed by a normally incident plane wave. Obviously, waves reflected from deep layers arrive at later times than those reflected from shallow layers. Therefore, velocities can be inverted sequentially with depth (or travel time) by updating the background model using the previously estimated velocities at each step. This is, in fact, exactly the property exploited by the layer stripping algorithms (Santosa and Schwetlick, 1982, Yagle and Levy, 1984) for exact inversion. This sequential recovery technique has also been used in approximate direct inversion to obtain higher order approximations of the scattered field. Gray (1980) formulates the one dimensional problem in terms of travel times instead of depths. He showed that this results in a second order procedure for the velocity inversion problem. Raz (1981c) considered a one dimensional medium with coincident point source and receiver. He used an approximate WKB formulation in order to correct for the amplitudes as well as the travel times of the incident field. His method, however, corrects only for the travel times because of further approximations that reduced the WKBJ approximation to a Bremmer-like approximation. In Section 3.2.2, a true WKBJ formulation is presented and it is compared with his result. Extension of this higher order procedure to the multidimensional case was investigated by Raz (1982) for the zero offset

configuration. In spite of some questionable assumptions made in inverting the resulting integral, numerical results superior to those given by Born inversion have been reported.

1.3 Contributions

1) In this thesis a different approach to the inversion problem is taken. Instead of operating directly on the observed scattered data, we consider the field extrapolated (backpropagated) with the wave equation from the receivers into the medium. The extrapolated field does not contain more information than the observed scattered field, however, there is more flexibility in the type of operations that can be performed on it. For example, for a two dimensional problem, the observed scattered field $P_s(\xi,\omega)$ is a function of two variables, namely, receiver location ξ and frequency ω (or time). On the other hand the extrapolated field $P_e(x,z,t)$ is a function of two space variables and time or frequency. Therefore, there is one more free parameter in this domain. Furthermore, the extrapolated field and the unknown velocity function $\gamma(x,z)$ share the same spatial parameters. In fact, in this domain migration is an operation where the time variable of the extrapolated field is simply set equal to the travel time corresponding to each point (Claerbout, 1971).

2) The backpropagated field is expressed as a volume integral in terms of the velocity inhomogeneities of the medium. This volume integral representation of the backpropagated field constitutes the starting point of all the results described in this thesis. Integral representations of the backpropagated field for the cases of a single source (plane-wave or point source) and of a zero-offset experiment are derived. The backpropagated field crucially depends on the aperture of the receiver array since only the observed portion of the scattered field can be backpropagated into the medium. We first consider the case where the receiver array surrounds the scatterer, so that the scattered field is observed completely. Then, we examine the more general case of a

receiver array with a finite angle of aperture where the receivers are asymptotic to two lines at the infinity. For example, the straight line array and the right angle array (surface observations combined with vertical observations) are two special cases of this general formulation. In the case of a finite angle aperture only a subset of the plane-wave components of the scattered field is observed. This leads to a partial reconstruction of the medium velocities for the scattering experiment geometries described below.

3) The inversion problem with a single wide-band plane-wave source is considered. Two methods, the slant-stack method and the imaging-filtering method, are obtained for reconstructing the velocities of a multidimensional medium. In the first method it is shown that the projections of the velocity potential at various projection angles can be obtained from the plane-wave scattering amplitudes. Once the projections are obtained, the potential can be reconstructed from its projections via known techniques of tomography. In the second method the backpropagated field formulation is used. The backpropagated field is imaged at the time corresponding to the travel-time from the source to the point - hereafter called the source-travel time. The velocity potential is, then, obtained by filtering this image in the spatial domain with a linear space-invariant filter. The two methods presented here are quite different conceptually and computationally, however, they give mathematically identical results.

4) The inversion problem with a single wide-band point source is considered. Two methods, namely the zero-time imaging and the source-travel time imaging methods are obtained. In both of these methods the backpropagated field formulation is used. The zero-time imaging method is derived for the case where the receiver array surrounds the medium, so that in this case the scattered field is observed

completely. It is shown that a complete set of projections of the velocity potential can be obtained by imaging the backpropagated field at time zero. Again, once the projections are obtained the potential can be reconstructed via the inverse Radon transform. In the second method the backpropagated field is imaged at the source-travel times as in the plane-wave source case. The medium velocities are, then, obtained by a spatial operation on this travel-time image. The source-travel time imaging method is derived for the general case of a receiver array with a finite angle aperture, where the scattered field is observed only partially. The two inversion methods described above are initially derived for the two or three dimensional problems. In this thesis we extend these methods to a third type of problem, namely the 2½ dimensional problem. Compared with the two dimensional problem the 2½ dimensional problem represents a more realistic model for the scattering experiments used in seismic exploration and it is obtained by replacing the line source used in the two dimensional problem by a point source.

5) The inversion problem for the zero-offset experiment is studied with the backpropagated field approach. In particular the 2½ dimensional zero-offset experiment geometry is considered. This experiment geometry represents the theoretical model for one of the most commonly used data reduction methods of reflection seismology, known as the CDP stacking. The backpropagated field approach provides a very simple solution to the zero-offset problem. It is shown that, the scattering potential is directly obtained by imaging the extrapolated field at time zero. Here, the extrapolated field is obtained by backpropagating the filtered observed data into a homogeneous medium, where the medium velocity is equal to the half of the background velocity.

6) Also, in this thesis a unified review of the approximate direct inversion methods is presented. Most of the results in this review have appeared in the literature previously, some of them with different formulations. Some of the results, however, are new and represent more general and improved versions of previous reconstruction techniques.

In Chapter 2, the integral representation and approximations of the scattered field are derived. The equations obtained in this chapter are used in the rest of the thesis, particularly in Chapter 3 where a unified review of previous approximate direct inversion methods is presented. In Chapter 4, the integral representation of the backpropagated field is derived for various experiment geometries. The integral expressions of the backpropagated field and the backpropagated field kernel obtained in this chapter will be used repeatedly in the remainder of this thesis. In Chapter 5, the inversion problem for the plane-wave source experiment is discussed. The slant-stack and imaging-filtering inversion methods are derived. In Chapter 6, the inversion problem for a single wide-band point source excitation is considered. The zero-time imaging and source-travel time imaging methods are obtained. A third experimental configuration, the zero-offset geometry, is discussed in Chapter 7, and conclusions and suggestions for further research are given in Chapter 8.

CHAPTER II

Representation and Approximations of the Scattered Field

In the scattering experiment that we consider, an acoustic medium is probed by sources located outside the medium and the resulting wave field is observed at various locations. In this thesis we are interested in a constant density acoustic medium in which velocities can vary in all directions (the velocity inhomogeneity is multidimensional). In this section the "scattered field" is defined and its volume integral representation in terms of the velocity inhomogeneities of the medium is derived. Also, several approximate forms of this representation, which will be used in the following sections, are obtained.

Let **D** be the wave equation operator of the scattering medium, i.e.

$$\mathbf{D} = \nabla^2 + k^2 n^2(\underline{r}) \ , \tag{2.0.1}$$

where $n(\underline{r}) = \frac{c}{v(\underline{r})}$ is the refraction index, $v(\underline{r})$ is the medium velocity and $c = \frac{\omega}{k}$ is a reference velocity. Define a volume V which contains all the scatterers in the medium and let $P(\underline{r},\omega)$ be the wavefield due to sources located outside V. Then

$$\mathbf{D}P(\underline{r},\omega) = 0 \quad ; \quad \underline{r} \in V \ . \tag{2.0.2}$$

Now, consider the following decomposition of the operator **D** and of the wavefield $P(\underline{r},\omega)$

$$\mathbf{D} = \mathbf{D}_0 + \gamma(\underline{r},\omega) \ , \tag{2.0.3}$$

$$P(\underline{r},\omega) = P_0(\underline{r},\omega) + P_s(\underline{r},\omega) \ . \tag{2.0.4}$$

In this decomposition $\mathbf{D}_0$ is the background wave operator and γ is the scattering potential. For example in the Born approximation discussed in the next section, $\mathbf{D}_0 = \nabla^2 + k^2 n_0^2(\underline{r})$ is the wave operator with background refraction index $n_0(\underline{r}) = c/v_0(\underline{r})$. If no a priori information is available on the medium velocities, a constant velocity background can be specified. In this case the reference velocity c is chosen such that the background refraction index $n_0 = 1$. The background field $P_0(\underline{r},\omega)$ is the portion of the total field that corresponds to the background medium, and it satisfies

$$\mathbf{D}_0 P_0(\underline{r},\omega) = 0 \quad ; \quad \underline{r} \in V \ . \tag{2.0.5}$$

From equation (2.0.4) the remainder of the total field is defined as the scattered field and is denoted by $P_s(\underline{r},\omega)$. The scattered field contains the pertubations of the wavefield due to the variations of the velocity from the background model.

As was mentioned above, in the Born approximation, the background model is chosen such that the background field $P_0(\underline{r},\omega)$ represents the known portion of the total field that corresponds to the a priori velocity information about the medium. Obviously, with this choice $P_0(\underline{r},\omega)$ is independent of the unknown velocity variations

of the medium. However, it is also possible to choose a background field that depends on the unknown scatterers. In this case the decomposition of the wave operator given in equation (2.0.3) becomes more complicated. Nevertheless, it will be shown in Sections 2.3 and 2.4 that this approach leads to higher order approximations of the scattered field.

2.1 Volume Integral Representation

In this section we will derive an exact volume integral representation of the scattered field using the wave operator and wavefield decompositions described in the previous section.

From equations (2.0.2) and (2.0.3) we have

$$\mathbf{D}P(\underline{r},\omega) = \mathbf{D}_0 P(\underline{r},\omega) + \gamma(\underline{r},\omega)\ P(\underline{r},\omega) = 0. \tag{2.1.1}$$

Using the decomposition of the total field in equation (2.0.4)

$$\mathbf{D}_0 P_0(\underline{r},\omega) + \mathbf{D}_0 P_s(\underline{r},\omega) + \gamma(\underline{r},\omega)\ P(\underline{r},\omega) = 0, \tag{2.1.2}$$

and from equation (2.0.5) we obtain

$$\mathbf{D}_0 P_s(\underline{r},\omega) = -\gamma(\underline{r},\omega)\ P(\underline{r},\omega)\ . \tag{2.1.3}$$

This shows that the scattered field is the solution of the background wave equation with the volume source distribution given by the product of the total field and the scattering potential at every point in the medium. Thus, an integral representation of the scattered field is given by

$$P_s(\underline{r},\omega) = \int_V d\underline{r}'\ \gamma(\underline{r}',\omega)\ P(\underline{r}',\omega)\ G_0(\underline{r},\underline{r}',\omega)\ , \tag{2.1.4}$$

where $G_0(\underline{r},\underline{r}',\omega)$ is the Green's function of the background operator $\mathbf{D}_0$, i.e.,

$$\mathbf{D}_0 G_0(\underline{r},\underline{r}',\omega) = -\delta(\underline{r} - \underline{r}') \ . \tag{2.1.5}$$

Equation (2.1.4) is an exact representation of the scattered field as a function of the velocity or scattering potential γ. In general, the inverse problem involves solving this integral equation for γ by using the scattered field observed at the receivers. Substitution of equation (2.1.4) into equation (2.0.4) gives the Lippmann-Schwinger integral equation for the total field $P(\underline{r},\omega)$. By replacing the total field in equation (2.1.4) with its integral representation we obtain

$$P_s(\underline{r},\omega) = \int_V d\underline{r}' \ \gamma(\underline{r}',\omega) \ G_0(\underline{r},\underline{r}',\omega)$$

$$\left\{ P_0(\underline{r}',\omega) + \int_V d\underline{\xi}' \ \gamma(\underline{\xi}',\omega) \ P(\underline{\xi}',\omega) \ G_0(\underline{r}',\underline{\xi}',\omega) \right\} . \tag{2.1.6}$$

This equation shows clearly that the scattered field is a nonlinear function of the scattering potential. By successively replacing the total field with its integral representation, the scattered field can be written as a power series of integrals of the potential. This will be discussed further in the next section.

The integral representation of the scattered field given in equation (2.1.4) can be interpreted as a superposition of secondary sources distributed within the volume V. Each point in the medium can be viewed as a secondary source whose source wavelet is is given by the total field multiplied by the scattering potential at that point. The field created by these sources is propagated by the background Green's function G_0, i.e. the Green's function for the background wave operator $\mathbf{D}_0$. A dual representation of the scattered field can be obtained as follows. From equations (2.0.2) and (2.0.4)

$$\mathbf{D}P(\underline{r},\omega) = \mathbf{D}P_0(\underline{r},\omega) + \mathbf{D}P_s(\underline{r},\omega) = 0, \tag{2.1.7}$$

and, using equations (2.0.3) and (2.0.5), we have

$$\mathbf{D}P_s(\underline{r},\omega) = -\gamma(\underline{r},\omega)P_0(\underline{r},\omega) \ . \tag{2.1.8}$$

Therefore, a second integral representation of the scattered field is given by

$$P_s(\underline{r},\omega) = \int_V d\underline{r}' \ \gamma(\underline{r}',\omega) \ P_0(\underline{r}',\omega) \ G(\underline{r},\underline{r}',\omega) \ , \tag{2.1.9}$$

where $G(\underline{r},\underline{r}',\omega)$ is the Green's function of the full wave operator, i.e.,

$$\mathbf{D}G(\underline{r},\underline{r}',\omega) = -\delta(\underline{r}-\underline{r}') \ . \tag{2.1.10}$$

The dual equation (2.1.9) can also be interpreted as a superposition of secondary sources. In this case, the secondary source wavelets are given by the product of the background field and the scattering potential at each point in the medium. The field created by these sources is propagated with the true wave operator $\mathbf{D}$, instead of the background wave operator $\mathbf{D}_0$.

As was shown previously the scattered field is a nonlinear function of the velocity potential γ that we want to reconstruct. An approximate integral expression for the scattered field is obtained by replacing the total field $P(\underline{r},\omega)$ in equation (2.1.4) with the background field $P_0(\underline{r},\omega)$. With this approximation the integral representation becomes

$$P_s(\underline{r},\omega) = \int_V d\underline{r}'\ \gamma(\underline{r}',\omega)\ G_0(\underline{r},\underline{r}',\omega)\ P_0(\underline{r}',\omega)\ . \tag{2.1.11}$$

Clearly, this approximation is good when the scattered field is small compared to the incident field inside the medium. Note that if the decomposition in equations (2.0.3) and (2.0.4) is such that the background incident field $P_0(\underline{r},\omega)$ is independent of the scatterers, then the above approximation essentially corresponds to the linearization of the exact equation. This linearization corresponds to neglecting the higher order terms in the power series expansion associated with equation (2.1.6). For example, in the Born approximation, the background field is independent of the scatterers, and it will be shown in the next section that the linearized equation is a good approximation at low frequencies.

For a given geometry of experiment - i.e. when the excitation and receiver locations are specified - we can write more explicit expressions for the linearized integral expression of the scattered field. If the medium is excited by plane waves, e.g., then equation (2.1.11) becomes

$$P_s(\underline{r},\underline{k}_s) = \int_V d\underline{r}'\ \gamma(\underline{r}',\omega)\ G_0(\underline{r},\underline{r}',\omega)\ P_0(\underline{r}',\underline{k}_s)\ , \tag{2.1.12}$$

where $P_0(\underline{r}',\underline{k}_s)$ denotes the incident field due to a plane wave propagating in the direction of unit vector $\hat{\underline{k}}_s = \frac{\underline{k}_s}{|\underline{k}_s|}$. For each plane wave source the scattered field observed at $\underline{r}$ is denoted by $P_s(\underline{r},\underline{k}_s)$. For example, in the case of a homogeneous background the incident field is given by $P_0(\underline{r},\omega) = S(\omega)e^{i\underline{k}_s\cdot\underline{r}}$, where $S(\omega)$ is the Fourier component at frequency ω of the source wavelet. In diffraction tomography ,

which will be discussed in Chapter 3, the medium is probed by monochromatic plane waves incident from various directions. Therefore, the scattered field $P_s(\underline{r},\hat{\underline{k}}_s)$ is a function of the plane wave incidence direction and the receiver location. In contrast, for the single wide-band plane wave source problem considered in Chapter 5, the free variable is the frequency ω of excitation, instead of the incidence angle of the probing wave. If the medium is excited by a point source, the background field is given by

$$P_0(\underline{r},\underline{r}_s,\omega) = S(\omega)\ G_0(\underline{r},\underline{r}_s,\omega), \tag{2.1.13}$$

where $\underline{r}_s$ is the source location outside the volume V. From equations (2.1.11) and (2.1.13) the scattered field for a point source excitation can be written as

$$P_s(\underline{r},\underline{r}_s,\omega) = S(\omega) \int_V d\underline{r}'\ \gamma(\underline{r}',\omega)\ G_0(\underline{r}',\underline{r}_s,\omega)\ G_0(\underline{r},\underline{r}',\omega). \tag{2.1.14}$$

A common form of this linearized equation is the zero-offset form, which results when the point source and receiver are coincident. The scattering experiment is repeated for each coincident source-receiver pair. The scattered field in this case is a function of the common source-receiver point $\underline{r}$ and frequency. Replacing $\underline{r}$ with $\underline{r}_s$ in equation (2.1.14) gives the linearized equation for the zero-offset experiment,

$$P_s(\underline{r},\omega) = S(\omega) \int_V d\underline{r}'\ \gamma(\underline{r}',\omega)\ G_0^2(\underline{r},\underline{r}',\omega)\ . \tag{2.1.15}$$

The kernel of the integral in the zero-offset case reduces to a single function which is the square of the Green's function of the background medium. It will be seen in

Chapter 3 that this simplification leads to straightforward inversion procedures. The price for this simplicity is the difficulty of zero-offset experiments, where a scattering experiment must be performed for every point on the observation surface. In some cases it is physically very difficult to perform such experiments, or any other experiment that can simulate the zero-offset data via CDP stacking.

Until now in this section we have considered the integral representation of the scattered field. The inversion problem involves solving this integral equation for the scattering potential γ by operating on the scattered field. We can generalize this approach by considering other functions that are directly obtained from the scattered field and that can also be represented as an integral of the scattering potential. In this thesis we will consider two such functions. One of them is the backpropagated field which is extensively discussed in Chapter 4, and the other one is the Radon transform of the scattered field which is discussed in Chapter 5. As an example of this approach, let $P_h(\underline{r},\underline{k})$ be the solution of the backgorund wave equation $\mathbf{D}_0$ for an incident plane wave with wavenumber $\underline{k}$. Now, define a function $Q_s(\underline{k})$ which is directly obtained from the scattered field by

$$Q_s(\underline{k}) = \int_S d\underline{r}' \, [\, P_s(\underline{r}',\omega) \, \nabla P_h(\underline{r}',\underline{k}) - P_h(\underline{r}',\underline{k}) \, \nabla P_s(\underline{r}',\omega) \,] \cdot \hat{\underline{n}}(\underline{r}') \, , \tag{2.1.16}$$

where the observation surface S surrounds the scatterers contained in the volume V and $\hat{\underline{n}}$ is the normal unit vector. From the second theorem of Green (appendix A) we can replace this surface integral by a volume integral as follows

$$Q_s(\underline{k}) = \int_V d\underline{r}' \, [\, P_s(\underline{r}',\omega)\, \mathbf{D}_0 P_h(\underline{r}',\underline{k}) - P_h(\underline{r}',\underline{k})\, \mathbf{D}_0 P_s(\underline{r}',\omega)\,] \, . \tag{2.1.17}$$

Since $\mathbf{D}_0 P_h(\underline{r}',\underline{k}) = 0 \;\; ; \;\; \underline{r}' \in V$ by definition and using equation (2.1.3) we have

$$Q_s(\underline{k}) = \int_V d\underline{r}' \, \gamma(\underline{r}',\omega)\, P(\underline{r}',\omega)\, P_h(\underline{r}',\underline{k}) \, . \tag{2.1.18}$$

Therefore the new function $Q_s(\underline{k})$ is also represented by a volume integral similar to equation (2.1.4), except that the Green's function is replaced by the known solution $P_h(\underline{r},\underline{k})$ of the background wave equation.

2.2 Born Approximation

One of the most common integral representation of the scattered field is obtained by using the following decomposition of the wave equation operator

$$\mathbf{D} = \mathbf{D}_0 + k^2 \gamma(\underline{r}) \tag{2.2.1}$$

$$\mathbf{D}_0 = \nabla^2 + k^2 n_0^2(\underline{r}) \tag{2.2.2}$$

$$\gamma(\underline{r}) = [\, n^2(\underline{r}) - n_0^2(\underline{r}) \,] \,. \tag{2.2.3}$$

Here $n_0(\underline{r})$ is the refraction index of an assumed background velocity model that incorporates prior knowledge of the medium. With this decomposition, using equation (2.1.4) the scattered field is exactly given by

$$P_s(\underline{r},\omega) = k^2 \int_V d\underline{r}' \, \gamma(\underline{r}') \, P(\underline{r}',\omega) \, G_0(\underline{r},\underline{r}',\omega) \,, \tag{2.2.4}$$

where $P(\underline{r},\omega) = P_0(\underline{r},\omega) + P_s(\underline{r},\omega)$ is the total field and $G_0(\underline{r},\underline{r}',\omega)$ is the Green's function of the operator $\mathbf{D}_0$. Now, for notational simplicity let $\int \gamma G_0 P$ represent the above integral. By successively replacing the total field P with its integral representation $P = P_0 + \int \gamma G_0 P$ we obtain the following power series expansion for the scattered field

$$P_s = k^2 \int \gamma G_0 P_0 + k^4 \int \gamma G_0 \int \gamma G_0 P_0$$

$$+ k^6 \int \gamma G_0 \int \gamma G_0 \int \gamma G_0 P_0 + \cdots \,,$$

(2.2.5)

$$P_s = k^2 \sum_{n=0}^{\infty} k^{2n} \int_{(1)} \gamma G_0 \int_{(2)} \gamma G_0 \cdots \int_{(n+1)} \gamma G_0 P_0 \,. \tag{2.2.6}$$

The physical significance of the successive terms can be interpreted as follows. The first term (n=0) corresponds to waves in which the incident field P_0 is scattered from each point scatterer only once and where the scattered field is propagated to the receivers by using the background Green's function G_0. In the second term (n=1) the primary scattered field given by the first term is scattered at each point scatterer once more. Therefore the second term corresponds to the waves that are scattered twice at any two points in the medium. Similarly, higher order terms in the series corresponds to waves that have been scattered several times at various point scatterers inside the medium. Note that waves are always propagated with the background wave operator $\mathbf{D}_0$ between scattering points. From equation (2.2.6) it is seen that terms involving multiple scattering effects become more important at higher frequencies. The first term in this expansion is called the first Born approximation. Obviously within this approximation the waves which are scattered several times are assumed to be very small compared with the primary scattered field. Also it is interesting to observe that since the higher order terms contain higher powers of frequency, the Born approximation is a better representation of the scattered field at low frequencies.

The Green's function $G_0(\underline{r},\underline{r}',\omega)$ for the background medium is obtained by solving equation (2.1.5) for the given velocity model. In general, closed form solutions for the Green's function and the incident field $P_0(\underline{r},\omega)$ cannot be obtained. One way to handle this problem is to replace the Green's function with its geometrical optics

approximation. For example, for a two dimensional medium

$$G_0(\underline{r},\underline{r}',\omega) \approx e^{i\frac{\pi}{4}}\, k^{-1/2}\, a(\underline{r},\underline{r}')\, e^{iks(\underline{r},\underline{r}')} \quad ; \quad k > 0 \,. \tag{2.2.7}$$

The amplitude and phase functions $a(\underline{r},\underline{r}')$ and $s(\underline{r},\underline{r}')$ can be obtained numerically with the ray approximation.

If an homogeneous background is assumed ($n_0(\underline{r}) = 1$) then the Green's function is given by

$$G_0(\underline{r},\underline{r}',\omega) = \frac{e^{ik|\underline{r}-\underline{r}'|}}{4\pi|\underline{r}-\underline{r}'|} \quad ; \quad \underline{r} = (x,y,z) \,, \tag{2.2.8}$$

for a three dimensional medium and by

$$G_0(\underline{r},\underline{r}',\omega) = \frac{i}{4}\, H_0^{(1)}(k|\underline{r}-\underline{r}'|) \quad ; \quad \underline{r} = (x,z) \,, \tag{2.2.9}$$

for a two dimensional medium (i.e., for line sources and constant velocities along one direction), where $H_0^{(1)}$ is the Hankel function of the first kind which is obtained by integrating equation (2.2.8) over y' and by setting $y = 0$.

An alternative way to derive the Born approximation that will be useful in the following sections is as follows. Instead of choosing the background wave operator $\mathbf{D}_0$ and then computing the background field P_0, first choose P_0. Then compute $\mathbf{D}_0$ and γ such that $\mathbf{D}_0 P_0(\underline{r},\omega) = 0$. For example, let

$$P_0(\underline{r},\omega) = \frac{e^{ik|\underline{r}-\underline{r}_s|}}{4\pi|\underline{r}-\underline{r}_s|} \quad ; \quad \underline{r} = (x,y,z) \ . \tag{2.2.10}$$

Then, it is easy to show that

$$\mathbf{D}_0 = \nabla^2 + k^2 \ , \tag{2.2.11}$$

and the wave operator residual is obtained as

$$\gamma(\underline{r},\omega) = \mathbf{D} - \mathbf{D}_0 = k^2 \left[n^2(\underline{r}) - 1 \right] . \tag{2.2.12}$$

2.3 Phase Corrected Approximation

Instead of assuming that the background field is given by equation (2.2.10), assume that the phase (or slowness) of the background field depends on the unknown velocities. For a point source at the origin we take

$$P_0(\underline{r},\omega) = e^{iks(\underline{r})} , \tag{2.3.1}$$

where $s(\underline{r})$ is a phase function which has the dimension of space. From equations (2.0.3) and (2.0.5) the background field satisfies

$$\mathbf{D}\, P_0(\underline{r},\omega) = \gamma(\underline{r},\omega)\; P_0(\underline{r},\omega) . \tag{2.3.2}$$

Therefore, applying the wave operator **D** given by equation (2.0.1) we obtain

$$ik\nabla^2 s(\underline{r}) - k^2 \mid \nabla s(\underline{r}) \mid^2 + k^2\, n^2(\underline{r}) = \gamma(\underline{r},\omega) . \tag{2.3.3}$$

We can satisfy this equation by requiring

$$\mid \nabla s(\underline{r}) \mid = n(\underline{r}) , \tag{2.3.4}$$

$$\gamma(\underline{r},\omega) = ik\nabla^2 s(\underline{r}) . \tag{2.3.5}$$

Equation (2.3.4) is the eikonal equation of ray theory and it relates the travel times to the medium velocities. Using equations (2.3.4) and (2.3.5), the residual can be represented in terms of the unknown refraction index as

$$\gamma(\underline{r},\omega) = ik\; [\; \nabla n(\underline{r}) \cdot \underline{e}_1(\underline{r}) + n(\underline{r})\; \nabla \cdot \underline{e}_1(\underline{r}) \;] , \tag{2.3.6}$$

where $\underline{e}_1(\underline{r})$ is the unit vector tangent to the ray. In multidimensional problems the integral representation for the phase corrected approximation is more complicated than in the Born case. That is because the phases of the incident field and of the Green's function are also functions of the unknown velocities. However, for some specific cases approximate solutions are possible, as shown in Chapter 3.

2.4 Geometrical Optics Approximation

Extending the ideas in the previous section one can assume a background that corrects for the amplitudes as well as the phases. In a three dimensional medium with a point source located at the origin choose a background field of the form

$$P_0(\underline{r},\omega) = a(\underline{r})\, e^{iks(\underline{r})} . \tag{2.4.1}$$

Substituting this expression inside equation (2.3.2), we have

$$\frac{\nabla^2 a(\underline{r})}{a(\underline{r})} + ik\,[\,2\frac{\nabla a(\underline{r})}{a(\underline{r})} \cdot \nabla s(\underline{r}) + \nabla^2 s(\underline{r})\,] -$$

$$k^2\,|\,\nabla s(\underline{r})\,|^2 + k^2\, n^2(\underline{r}) = \gamma(\underline{r},\omega) . \tag{2.4.2}$$

One way to satisfy this equation is to equate the coefficients of the k and k^2 terms. This gives

$$|\,\nabla s(\underline{r})\,| = n(\underline{r}) , \tag{2.4.3}$$

$$\nabla^2 s(\underline{r}) + 2\frac{\nabla a(\underline{r})}{a(\underline{r})} \cdot \nabla s(\underline{r}) = 0 , \tag{2.4.4}$$

$$\gamma(\underline{r},\omega) = \frac{\nabla^2 a(\underline{r})}{a(\underline{r})} . \tag{2.4.5}$$

Equations (2.4.3) and (2.4.4) are the eikonal and transport equations of ray theory. By substituting expressions (2.4.1) and (2.4.5) into equation (2.1.11) we see that the integral representation of the scattered field in this case is more complicated than for the Born and phase corrected approximations. In some special cases approximate solu-

tions can be obtained by making several assumptions and approximations. Note that for a one dimensional medium the geometrical optics approximation is also known as the WKBJ approximation.

2.5 Higher Order Approximations via Change of Variables

One way to obtain a more accurate representation of the scattered field is to formulate the problem in different spatial coordinates. In the multidimensional case this can only be done approximately. The change of variables should be such that the background incident field for the new variables is a good representation of the true incident field. The following procedure will be considered in this thesis. The wave operator in an inhomogeneous medium is given by

$$\mathbf{D} = \nabla^2 + k^2\, n^2(\underline{r}), \tag{2.5.1}$$

where $n(\underline{r})$ is the refraction index of the scattering medium. Consider the change of variables from the coordinates $\underline{r}$ to the new space coordinates $\underline{s}$ such that

$$\nabla^2 + k^2\, n^2(\underline{r}) \approx \nabla_{\underline{s}}^2 + k^2 + \mathbf{D}_r\ , \tag{2.5.2}$$

where $\nabla_{\underline{s}}^2$ is the Laplacian in the new coordinate system and $\mathbf{D}_r$ is the residual term. Following this transformation, an homogeneous background problem is obtained in the new coordinates by selecting the decomposition of the wave equation

$$\mathbf{D} = \mathbf{D}_0 + \mathbf{D}_r \tag{2.5.3a}$$

$$\mathbf{D}_0 = \nabla_{\underline{s}}^2 + k^2\ . \tag{2.5.3b}$$

Then, from equation (2.1.11) the homogeneous background approximation of the scattered field in the new coordinates is given by

$$P_s(\underline{s},\omega) = \int_V d\underline{s}'\, \mathbf{D}_r P_0(\underline{s}',\omega)\; G_0(\underline{s},\underline{s}',\omega)\ , \tag{2.5.4}$$

where $G_0(\underline{s},\underline{s}',\omega)$ is the free space Green's function. For example in three dimensions

$$G_0(\underline{s},\underline{s}',\omega) = \frac{e^{ik|\underline{s}-\underline{s}'|}}{4\pi|\underline{s}-\underline{s}'|} \quad ; \quad \underline{s} = (s_x, s_y, s_z)\ . \tag{2.5.5}$$

In general, the Laplacian in the original coordinates $\underline{r}$ can be written in terms of the gradients in the new coordinate system $\underline{s}$ as

$$\nabla^2 = \nabla_{\underline{s}} \cdot \mathbf{A} \cdot \nabla_{\underline{s}} + \underline{a} \cdot \nabla_{\underline{s}}\ , \tag{2.5.6}$$

where $\mathbf{A}$ is a dyadic and $\underline{a}$ is a vector, both of which contain derivatives of the coordinates $\underline{s}$ with respect to $\underline{r}$. To obtain a transformation in the form given by equation (2.5.2) we require that the diagonal elements of $\mathbf{A}$ be equal. This will give the $\nabla_{\underline{s}}^2$ term in equation (2.5.2) and the rest of the terms can be included in the residual $\mathbf{D}_r$. The first diagonal term of $\mathbf{A}$ is given by

$$A_{11} = \left(\frac{\partial s_x}{\partial x}\right)^2 + \left(\frac{\partial s_x}{\partial y}\right)^2 + \left(\frac{\partial s_x}{\partial z}\right)^2 . \tag{2.5.7}$$

The other diagonal terms A_{22} and A_{33} have the same form, except that s_x is replaced by s_y and s_z respectively. The elements of the vector $\underline{a}$ in equation (2.5.6) in the general case are given by

$$a_1 = \frac{\partial^2 s_x}{\partial x^2} + \frac{\partial^2 s_x}{\partial y^2} + \frac{\partial^2 s_x}{\partial z^2} , \tag{2.5.8}$$

and a_2 and a_3 have the same form, except that s_x is replaced by s_y and s_z respectively.

The success of the procedure outlined above depends on the choice of the approximate transformation given in equation (2.5.2). In other words, the background field computed in the $\underline{s}$ domain must be a good approximation of the true incident field. In particular, the phase and to some degree the amplitude of the incident field must be corrected properly by this transformation. In the following, a line-ray geometrical optics transformation is defined and the corresponding equations are derived.

2.5.1 An approximate line-ray geometrical optics transformation

Suppose that a scattering medium is probed by a point source located at the origin. Consider the change of variables from the original space variables $\underline{r} = (x,y,z)$ to the new space variables $\underline{s} = (s_x, s_y, s_z)$ such that

$$\underline{s}(\underline{r}) = \hat{\underline{r}} \int_0^r dr' \, n(\hat{\underline{r}} r') , \tag{2.5.9}$$

where $\hat{\underline{r}} = \frac{\underline{r}}{r}$ is a unit vector, $r = |\underline{r}|$ and the integration path is the straight line between the point $\underline{r}$ and the source location. This transformation represents a distortion of space (expansion or compression) along the radial lines starting from the source location. If the velocity at some point is low then $n(\underline{r})$ and the contribution to

the integral of this point are large and vice versa. Therefore, the variables $\underline{s}$ are proportional to the travel times along the straight lines drawn from the source to the scattering points. For a homogeneous medium we have $n(\underline{r}) = 1$ and $\underline{s} = \underline{r}$.

Here we consider the wave equation in the new spatial coordinates described above. It can be shown that, even for this relatively simple transformation the diagonal terms of **A** in equation (2.5.6) are not equal. In the following we will make a series of approximations to obtain the desired property of the dyadic **A**. These approximations cannot easily be justified by the physics of the scattering problem for a multidimensional medium. Nevertheless, the derivation below is useful in understanding the issues involved in higher order approximations obtained by a change of variables. Following Hagin and Gray (1984), the transformation is significantly simplified with the following considerations :

a) The off-diagonal terms of the dyadic **A** are small compared to the other coefficients.

b) If $n(\underline{r})$ does not vary much, then a first order approximation to the transformation in equation (2.5.9) is

$$\underline{s} \approx \underline{r}\, n(\underline{r}) \,, \tag{2.5.10}$$

and the first derivatives can be approximated by

$$\frac{\partial s_x(\underline{r})}{\partial x} \approx n(\underline{r}) \,, \tag{2.5.11a}$$

$$\frac{\partial s_x(\underline{r})}{\partial y} \approx \frac{\partial s_x(\underline{r})}{\partial z} \approx 0 \,. \tag{2.5.11b}$$

Similar expressions for s_y and s_z are obtained by the same argument.

c) The second order derivative terms are more difficult to approximate. From equation (2.5.11a) a first order approximation to the second order derivative is

$$\frac{\partial^2 s_x}{\partial x^2} \approx \frac{\partial n(r)}{\partial x} = n(\underline{s}) \frac{\partial n(\underline{s})}{\partial s_x} , \tag{2.5.12}$$

and similar expressions are obtained for s_y and s_z. With these assumptions the diagonal elements of **A** become equal and are given by

$$A_{11} \approx A_{22} \approx A_{33} \approx n^2(\underline{s}) . \tag{2.5.13}$$

Consequently, the first term in equation (2.5.6) becomes

$$\nabla_{\underline{s}} \cdot \mathbf{A} \cdot \nabla_{\underline{s}} \approx n^2(\underline{s}) \nabla_{\underline{s}}^2 . \tag{2.5.14}$$

Also, from equations (2.5.8) and (2.5.12) we have

$$a_1 = n(\underline{s}) \frac{\partial n(\underline{s})}{\partial s_x} , \quad a_2 = n(\underline{s}) \frac{\partial n(\underline{s})}{\partial s_y} , \quad a_3 = n(\underline{s}) \frac{\partial n(\underline{s})}{\partial s_z} . \tag{2.5.15}$$

Then, the second term in equation (2.5.6) is given by

$$\underline{a} \cdot \nabla_{\underline{s}} = n(\underline{s}) \nabla_{\underline{s}} n(\underline{s}) \cdot \nabla_{\underline{s}} . \tag{2.5.16}$$

Finally, with the line-ray geometrical optics approximation, and with the assumptions stated above, the wave equation in this coordinate system becomes

$$\nabla^2 + k^2 n^2(\underline{r}) \approx n^2(\underline{s}) \left[\nabla_{\underline{s}}^2 + k^2 + \frac{\nabla_{\underline{s}} n(\underline{s})}{n(\underline{s})} \cdot \nabla_{\underline{s}} \right] . \tag{2.5.17}$$

By choosing the reference velocity such that $n(\underline{0}) = 1$ we can divide both sides of the wave equation

$$\mathbf{D} P(\underline{s},\omega) = -\delta(\underline{s}) , \tag{2.5.18}$$

by $n^2(\underline{s})$. Then the residual term in equation (2.5.3a) is identified as

$$\mathbf{D}_r = \frac{\nabla_{\underline{s}} n(\underline{s})}{n(\underline{s})} \cdot \nabla_{\underline{s}} = \nabla_{\underline{s}} \ln n(\underline{s}) \cdot \nabla_{\underline{s}} . \tag{2.5.19}$$

Using this in equation (2.5.4) gives the following approximate integral representation of the scattered field

$$P_s(\underline{s},\omega) = \int_V d\underline{s}' \, \nabla_{\underline{s}'} \ln n(\underline{s}') \cdot \nabla_{\underline{s}'} G_0(\underline{s}',\underline{0},\omega) \; G_0(\underline{s},\underline{s}',\omega) . \tag{2.5.20}$$

The above equation will be considered further in Section 3.4.2.

2.6 2½ Dimensional Problem

Most practical inverse scattering problems three dimensional. Therefore, in all cases the 3-D Laplacian

$$\nabla^2 = \frac{\partial^2}{\partial x^2} + \frac{\partial^2}{\partial y^2} + \frac{\partial^2}{\partial z^2}, \tag{2.6.1}$$

must be used in the wave equation. If the medium properties do not change significantly along one direction, say along the y axis, and if the medium is excited by a line source along this axis, then the wavefield is approximately independent of the variable y. In this case, the wave equation with the 2-D Laplacian can be used. However, in most applications line sources are not used. Instead, if the medium is two dimensional, as described above, point sources and receivers are located in the $y = 0$ plane. This experimental geometry resembles a two dimensional problem, but it is not quite the same. Note in particular that in this case the wavefield depends on y. We will approach this problem by approximating the first order term of the three dimensional scattered field (i.e., the waves which have been scattered only once) by a function defined in the $y = 0$ plane as shown below. In this section, we will denote the three dimensional coordinates by the vector $\underline{R} = (x,y,z)$ and two dimensional coordinates in the source-receiver plane ($y = 0$ plane) by the vector $\underline{r} = (x,0,z)$.

2.6.1 Point source experiment

From equations (2.1.4) and (2.2.8) and for the two dimensional medium described above, the approximate integral representation of the scattered field is given by

$$P_s(\underline{r},\omega) = S(\omega) \int_V d\underline{r}' \, \gamma(\underline{r}',\omega) \, I(\underline{r},\underline{r}',k) \, , \tag{2.6.2}$$

where $\underline{r}$ is the receiver location and

$$I(\underline{r},\underline{r}',k) = \frac{1}{16\pi^2} \int_{-\infty}^{\infty} dy' \, \frac{1}{|\underline{R}'-\underline{r}_s| \, |\underline{r}-\underline{R}'|} \, e^{ik(|\underline{R}'-\underline{r}_s| + |\underline{r}-\underline{R}'|)} \, , \tag{2.6.3}$$

represents the three dimensional first order scattered waves as they are observed in the source-receiver plane ($y = 0$ plane). In the above equations $\underline{r}_s = (x_s,0,z_s)$ is the point source location, and $\underline{R}' = (x',y',z')$ represents the medium coordinates which are chosen such that γ is constant along the y' axis. In the following we will obtain an approximate expression for the first order scattering function I given above. The phase function $|\underline{R}'-\underline{r}_s| + |\underline{r}-\underline{R}'|$ in equation (2.6.3) has a single minimum as a function of y' at $y' = 0$, and one can approximate the integral by the method of stationary phase around this point. In general, the stationary phase approximation of an integral around a single minimum of the phase function is given by (Pilant, 1979)

$$\int_{-\infty}^{\infty} dy' \, f(y') \, e^{ik\phi(y')} \approx e^{\pm i\frac{\pi}{4}} \left\{ \frac{2\pi}{k \, \dfrac{\partial^2\phi(y')}{\partial y'^2}} \right\}^{1/2}_{y'=y'_0} f(y'_0) \, e^{ik\phi(y'_0)} \, , \tag{2.6.4}$$

where

$$\left\{ \frac{\partial\phi(y')}{\partial y'} \right\}_{y'=y'_0} = 0 \quad ; \quad \left\{ \frac{\partial^2\phi(y')}{\partial y'^2} \right\}_{y'=y'_0} \neq 0 \, . \tag{2.6.5}$$

In equation (2.6.3), the phase term $\phi(y') = |\underline{R}'-\underline{r}_s| + |\underline{r}-\underline{R}'|$ satisfies the stationary

point conditions given in equation (2.6.5) at $y' = 0$. Thus, the first order scattering function can be approximated by (for $k > 0$)

$$I(\underline{r},\underline{r}',k) \approx \frac{1}{16\pi^2}\left[\frac{2\pi}{k}\right]^{1/2} e^{i\frac{\pi}{4}} \frac{e^{ik(|\underline{r}'-\underline{r}_s|+|\underline{r}-\underline{r}'|)}}{|\underline{r}'-\underline{r}_s|^{1/2}|\underline{r}-\underline{r}'|^{1/2}(|\underline{r}'-\underline{r}_s|+|\underline{r}-\underline{r}'|)^{1/2}} , \tag{2.6.6}$$

where $\underline{r} = (x,0,z)$ and $\underline{r}' = (x',0,z')$ are the coordinates in the source-receiver plane. Finally, from equation (2.6.2) the scattered field observed in the $y = 0$ plane can be approximately expressed as

$$P_s(\underline{r},\omega) = \frac{(2\pi)^{1/2}}{16\pi^2} e^{i\frac{\pi}{4}} k^{3/2} S(\omega) \int_V d\underline{r}' \frac{\gamma(\underline{r}')}{(|\underline{r}'-\underline{r}_s|+|\underline{r}-\underline{r}'|)^{1/2}} \frac{e^{ik|\underline{r}'-\underline{r}_s|}}{|\underline{r}'-\underline{r}_s|^{1/2}} \frac{e^{ik|\underline{r}-\underline{r}'|}}{|\underline{r}-\underline{r}'|^{1/2}} . \tag{2.6.7}$$

From equation (2.2.9) and the asymptotic approximation of the Hankel function for large arguments, the two dimensional Green's function in the far field is given by

$$G_0(\underline{r},\underline{r}',\omega) \approx \frac{e^{i\frac{\pi}{4}}}{(8\pi)^{1/2}} \frac{e^{ik|\underline{r}-\underline{r}'|}}{k^{1/2}|\underline{r}-\underline{r}'|^{1/2}} \quad ; \quad k > 0 . \tag{2.6.8}$$

Then, the last two terms in equation (2.6.7) are very similar to the two dimensional far field Green's function except for the $k^{-1/2}$ term which represents two dimensional dispersion effects. In some cases the amplitude term $(|\underline{r}'-\underline{r}_s|+|\underline{r}-\underline{r}'|)^{-1/2}$ can be combined with the velocity function as a scaling factor which can be undone after inversion. In that case the last two terms in the integral can be identified as the Green's functions of the problem in the source-receiver plane. If the amplitude term cannot be combined with the velocity function, then we can view it as an extra attenuation

factor of the last term in the integral. We will discuss this issue further in Sections 4.3 and 6.3.

2.6.2 Zero-offset (coincident source-receiver) experiment

Next, we consider the experiment where coincident source-receiver pairs are located along a curve in the $x-z$ plane. Also, the coordinate system is chosen such that the medium velocities are constant along the y axis. Then, the observation geometry consists of a source-receiver pair array in the $y = 0$ plane and the scattering experiment is repeated for each pair. From equations (2.1.15) and (2.2.8) the scattered field is given by

$$P_s(\underline{r},\omega) = S(\omega) \int_V d\underline{r}' \, \gamma(\underline{r}',\omega) \, H(\underline{r},\underline{r}',k) \, , \tag{2.6.9}$$

where $\underline{r} = (x,0,z)$ is the common source-receiver point and

$$H(\underline{r},\underline{r}',k) = \frac{1}{16\pi^2} \int_{-\infty}^{\infty} dy' \, \frac{e^{i2k|\underline{r}-\underline{R}|}}{|\underline{r}-\underline{R}|^2} \, , \tag{2.6.10}$$

represents the three dimensional first order reflections for a coincident source-receiver pair. Here the vector $\underline{R}' = (x',y',z')$ represents the three dimensional cartesian coordinates of an arbitrary point in the scattering medium. Note that the kernel H resembles the field of a line source along the y axis in a homogeneous medium with propagation velocity $v = c/2$, $c = \omega/k$. The only difference is that the denominator in equation (2.6.10) is $|\underline{r}-\underline{R}|^2$, instead of $|\underline{r}-\underline{R}|$, due to the two-way three dimen-

sional spreading attenuation. Now, if we consider the derivative of the kernel H with respect to frequency (this corresponds to multiplication by t in the time domain) we obtain

$$-i\frac{\partial}{\partial k}H(\underline{r},\underline{r}',k) = \frac{1}{2\pi}\int_{-\infty}^{\infty} dy' \, \frac{e^{i2k|\underline{r}-\underline{R}|}}{4\pi|\underline{r}-\underline{R}|} \, . \tag{2.6.11}$$

The right hand side of this equation is the familiar integral representing the field of a line source, therefore

$$-i\frac{\partial}{\partial k}H(\underline{r},\underline{r}',k) = \frac{i}{8\pi} H_0^{(1)}\left(2k|\underline{r}-\underline{r}|^{1/2} \right) , \tag{2.6.12}$$

where $H_0^{(1)}$ is the Hankel function of the first kind. An explicit frequency domain expression for the zero-offset first order scattering kernel H can be obtained by integrating both sides of this equation. This will not be done here, however, since this does not add much to the physical interpretation of the problem. In the time domain the impulse response of the kernel is simply the impulse response of the line source divided by time t, i.e.

$$h(\underline{r},\underline{r}',t) = \frac{c}{4\pi^2} \frac{u\left(t - \frac{2}{c}|\underline{r}-\underline{r}| \right)}{t\left[t^2 - \left(\frac{2}{c}|\underline{r}-\underline{r}| \right)^2 \right]^{1/2}} , \tag{2.6.13}$$

where $u(t)$ denotes the Heaviside step function. Again the additional decrease of the amplitude for increasing times is due to the three dimensional geometrical spreading as opposed to a two dimensional spreading.

CHAPTER III

Review of Previous Approximate Direct Inversion Methods

In this chapter the approximate direct inversion approach is applied to velocity inversion problems with specific observation geometries. Most of the results discussed here have appeared in the literature previously, some of them with different formulations. Some of these results, however, are new and represent more general and improved versions of previous ones. The formulation developed in Section 2 will be employed here. The formulas obtained in that section will be used without repeating their derivations.

In Section 3.1, Born approximation methods are reviewed. Most of the methods discussed assume a homogeneous background. Several observation geometries, such as separated point source and receiver in a one dimensional medium, coincident source-receiver arrays and plane wave sources in a multidimensional medium are considered. A inhomogeneous background Born approximation method is also considered in this section by approximating the Green's functions of the background medium according to ray theory. In Section 3.2, a phase corrected approximation is applied to the problem where a one dimensional medium is excited by plane wave sources or by a point source. The phase corrected approximation is generalized to a WKBJ approximation in Section 3.3. In Section 3.4, two phase corrected background methods are discussed for a multidimensional medium with coincident source-receiver arrays.

3.1 Born Approximation Methods

The most common approach to the direct inversion problem has been the homogeneous backgound Born approximation. In this section, a one dimensional medium with separated point source and receiver and a multidimensional medium with coincident source-receiver arrays are considered by using this approximation. It is shown that, in the Fourier transform domain, there is a one to one mapping between the observed scattered data P_s and the velocity function γ of the medium.

3.1.1 Stratified medium with separated point source and receiver

Consider the experiment where a stratified medium (the velocities vary only with depth z' for $z' > 0$) is probed by a point source located on the surface ($z_s = 0$), and the reflected field is observed by a receiver also located on the surface ($z = 0$). Then, from equations (2.1.14) and (2.2.1-3) the observed data is given by

$$P_s(\underline{r},\omega) = k^2 \int_0^\infty dz'\, \gamma(z') \int_{-\infty}^{\infty}\int_{-\infty}^{\infty} dx'\, dy'\, \frac{e^{ik|\underline{r}-\underline{r}'|}}{4\pi|\underline{r}-\underline{r}'|}\, \frac{e^{ik|\underline{r}'-\underline{r}_s|}}{4\pi|\underline{r}'-\underline{r}_s|} \,. \tag{3.1}$$

The double integral in the above equation can be interpreted as the impulse response of a "plane scatterer" at depth z'. Let us denote it by $H(z',k)$. Now, define the following quantities,

$$\beta(z') = \int_0^{z'} d\xi\, \gamma(\xi) \,,$$

$$F(z',k) = \frac{\partial}{\partial z'} H(z',k)$$

$$= \int_{-\infty}^{\infty}\int_{-\infty}^{\infty} dx'dy' \left\{ \frac{\partial}{\partial z'} \left[\frac{e^{ik|\underline{r}-\underline{r}'|}}{4\pi|\underline{r}-\underline{r}'|} \right] \frac{e^{ik|\underline{r}'-\underline{r}_s|}}{4\pi|\underline{r}'-\underline{r}_s|} + \frac{e^{ik|\underline{r}-\underline{r}'|}}{4\pi|\underline{r}-\underline{r}'|} \frac{\partial}{\partial z'} \left[\frac{e^{ik|\underline{r}'-\underline{r}_s|}}{4\pi|\underline{r}'-\underline{r}_s|} \right] \right\} . \tag{3.2}$$

In terms of these functions equation (3.1) becomes

$$P_s(\omega) = -k^2 \int_0^{\infty} dz' \, \beta(z') \, F(z',k) \, . \tag{3.3}$$

Since there is only one source and one receiver we have dropped the arguments $\underline{r}$ and $\underline{r}_s$. The derivative of the impulse response defined in equation (3.2) can be evaluated easily by noting that each term in the brackets is in the form of a Rayleigh II integral (Berkhout, 1982) consisting of an incident field and a surface Green's function. Then, the first term in equation (3.2) is simply one half of the reflected field due to an interface located at z'. Moreover, due to reciprocity, the contributions from the first and second terms are the same and we have

$$F(z',k) = \frac{-1}{4\pi} \frac{e^{ik|\underline{r}-\tilde{\underline{r}}_s|}}{|\underline{r}-\tilde{\underline{r}}_s|} , \tag{3.4}$$

where $\tilde{\underline{r}}_s$ is the location of the mirror image of the source with respect to the reflector at depth z'. It can be shown that if the origin of the coordinate system is chosen at the midpoint of the source-receiver then

$$| \underline{r} - \underline{\tilde{r}}_s | = 2 \, (x_s^2 + z'^2)^{1/2} \equiv c\tau \, , \tag{3.5}$$

where τ is the travel time associated to a reflection at depth z' and c is the constant background velocity. Then, by changing the variables from depth to travel time in equation (3.3) we have

$$P_s(\omega) = \frac{\omega^2}{8\pi c^2} \int_{-\infty}^{\infty} d\tau \, \frac{\beta(\tau)}{\left[\tau^2 - \frac{4x_s^2}{c^2} \right]^{1/2}} \, e^{i\omega\tau} \, , \tag{3.6}$$

where we have used the fact that $\beta(\tau) = 0$ for $\tau < \frac{2x_s}{c}$. Equation (3.6) represents a Fourier transform relationship between the observed data and the medium velocities. By taking the inverse transform of both sides and by changing the variables from travel time back to depth we obtain

$$\beta(z) = -16\pi c z \int_0^{\frac{2}{c}(x_s^2 + z^2)^{1/2}} dt \left[\frac{2}{c} \, (x_s^2 + z^2)^{1/2} - t \right] \tilde{P}_s(t) \, . \tag{3.7}$$

Finally, according to equation (3.2) by taking the derivative of both sides with respect to z

$$\gamma(z) = -16\pi c \int_0^{\frac{2}{c}(x_s^2 + z^2)^{1/2}} dt \left[\frac{2}{c} \, \frac{x_s^2 + 2z^2}{(x_s^2 + z^2)^{1/2}} - t \right] \tilde{P}_s(t) \, . \tag{3.8}$$

This result was obtained by Gray et. al. (1980a) by using a space-time formulation and by employing prolate spheroidal coordinates. The space-frequency derivation presented

above, however, is more straightforward and more closely related to the physics of the problem.

3.1.2 Multidimensional medium with zero offset experiment

In this section the homogeneous background Born inversion problem is considered for a medium in which velocities vary in all directions. We assume that the medium velocities vary only below the observation surface $z = 0$. For convenience the z axis is chosen such that $z < 0$ in the medium. The reflection experiment is performed by placing a collocated source-receiver pair at some point on the surface and by recording the reflected field. This is repeated at every point on the observation surface. Therefore, the observed data is a function of the common source-receiver point $\underline{r}$ and of time or frequency. This reflection experiment is a mathematical idealization of the beamforming operation (Common Depth Point stacking) commonly used in seismic exploration. In the following we first solve the three dimensional problem where velocities change in all directions below the surface. At the end of the section we will comment on the two dimensional problem.

From equations (2.1.15) and (2.2.1-3), the observed reflected field for impulse sourcesis given by

$$P_s(\underline{r},\omega) = k^2 \int_V d\underline{r}'\, \gamma(\underline{r}')\, \frac{e^{i2k|\underline{r}-\underline{r}'|}}{16\pi^2|\underline{r}-\underline{r}'|^2}\,, \tag{3.9}$$

where $\underline{r} = (x,y,0)$. In order to simplify the above integral the observed time traces can be filtered as follows

$$\phi(x,y,\omega) \equiv -i\frac{\partial}{\partial\omega}\left[\frac{P_s(\underline{r},\omega)}{-\omega^2}\right]$$

$$= \frac{-1}{2\pi c^3}\int_V d\underline{r}'\,\gamma(\underline{r}')\,\frac{e^{i2k|\underline{r}-\underline{r}'|}}{4\pi|\underline{r}-\underline{r}'|}\,. \tag{3.10}$$

We see therefore that for the zero offset case the integral representation becomes very simple containing a single Green's function corresponding to a medium in which the background velocity is $c/2$. The three dimensional Green's function in equation (3.10) can be decomposed into plane waves by the Weyl integral (Aki and Richards, 1980) as

$$\frac{e^{i2k|\underline{r}-\underline{r}'|}}{4\pi|\underline{r}-\underline{r}'|} = \frac{i}{8\pi^2}\int_{-\infty}^{\infty}\int_{-\infty}^{\infty} dk_x\,dk_y\,e^{ik_x(x-x')}\,e^{ik_y(y-y')}\,\frac{e^{ik_z|z-z'|}}{k_z}\,, \tag{3.11}$$

where $k_z = (4k^2 - k_x{}^2 - k_y{}^2)^{1/2}$, $Re(k_z) \geq 0$ and $Im(k_z) \geq 0$. Then, the two dimensional spatial Fourier transform of the filtered data in equation (3.10) gives

$$\tilde{\phi}(k_x,k_y,\omega) = \frac{-i}{4\pi c^3}\int_V d\underline{r}'\,\gamma(\underline{r}')\,e^{-ik_x x'}\,e^{-ik_y y'}\,\frac{e^{-ik_z z'}}{k_z}\,, \tag{3.12}$$

where we have used the facts that $z' \leq 0$ in the volume V and that the observation surface is located at $z = 0$. The critical step in inverting equation (3.12) is to change the free variables (k_x,k_y,ω) to the spatial wavenumbers (k_x,k_y,k_z), $-\infty < k_x,k_y,k_z < \infty$. This is done by viewing ω as a function of the vertical wavenumber k_z such that

$$\omega(k_z) = \frac{c}{2}\, sgn(k_z)\, (k_x^2 + k_y^2 + k_z^2)^{1/2}\,, \tag{3.13}$$

where $sgn(\cdot)$ is the sign function. An important observation at this point is that in the new variables only the real values of k_z are used. The part of the data which corresponds to inhomogeneous waves (i.e., evanescent waves when k_z is purely imaginary) is not used for inversion. From equation (3.11) it is seen that these waves attenuate rapidly for large $|z'|$ and propagate horizontally. Because of the change of variables described above, inhomogeneous waves (most importantly the surface waves) are not included in the reflected field. They must therefore be removed from the observed data before processing. Equation (3.12) is simply a Fourier transform in the wavenumber domain and the medium velocities are obtained by a simple weighted mapping

$$\begin{aligned}\tilde{\gamma}(k_x,k_y,k_z) &= 4\pi c^3 i k_z\, \tilde{\phi}[k_x,k_y,\omega(k_z)] \\ &= -4\pi c^3 k_z \frac{\partial}{\partial\omega}\left[\frac{\hat{P}_s(k_x,k_y,\omega)}{\omega^2}\right].\end{aligned} \tag{3.14}$$

If the velocities in the medium do not vary along, say the y axis (the medium is two dimensional), then the source-receiver pairs need to be placed only along the x axis on the surface. This experiment provides obervations of the scattered field $P_s(x,\omega)$ where x is the common source-receiver location. By performing the same filtering operation on the observed traces as in equation (3.10), the filtered reflected field is given by

$$\phi(x,\omega) = \frac{-i}{8\pi c^3} \int_{-\infty}^{\infty} \int_{-\infty}^{\infty} dx'\, dz'\, \gamma(x',z')\, H_0^{(1)}\left(2k\left[(x-x')^2+z'^2\right]^{1/2}\right), \tag{3.15}$$

where we have used equations (2.2.8) and (2.2.9). The inversion for this case follows exactly the same steps as above, provided that we use the plane wave expansion of the two dimensional Green's function

$$\frac{i}{4} H_0^{(1)}(2k|\underline{r}-\underline{r}'|) = \frac{i}{4\pi} \int_{-\infty}^{\infty} dk_x\, e^{ik_x(x-x')}\, \frac{e^{ik_z|z-z'|}}{k_z}, \tag{3.16}$$

where $k_z = (4k^2 - k_x^2)^{1/2}$, $Re(k_z) \geq 0$ and $Im(k_z) \geq 0$.

The multidimensional inversion for zero offset observations was first studied by Cohen and Bleistein (1979) with a space-time domain formulation for the two dimensional case. The same result was obtained by Raz (1981b) in the space-frequency domain for a three dimensional medium and by Norton and Linzer (1981). Raz also investigated the possibility of simultaneous velocity and density inversion with an experiment where, for each source, data is collected by all receivers instead of only by the coincident receiver (i.e. for unstacked data). He showed that in this case the velocities and vertical density gradients of the medium can be recovered.

3.1.3 Plane-wave sources and receivers surrounding the medium

As was pointed out in Section 2, equations (2.1.11) and (2.1.18) were obtained by making different choices for the arbitrary functions appearing in Green's theorem. With the exception of this section, the rest of this chapter discusses methods derived from equation (2.1.11) or its variants given by equations (2.1.12), (2.1.14) and

(2.1.15). In this section we will consider an inversion procedure for the multidimensional case by using equation (2.1.18). The scattering experiment is as follows. The medium is probed by wide band (containing all frequencies) plane waves incident from all directions. For each plane wave, the scattered field and its normal derivative are observed on a surface surrounding the medium. Apparently, this is not a very practical experiment and the amount of data collected is more than what is neccessary for Born inversion. This will become clear when the diffraction tomography formulation is discussed in the next section.

In equation (2.1.18), let the incident field be a plane wave with wavenumber $\underline{k}$, i.e.

$$P_0(\underline{r}',\omega) = e^{i\underline{k}\cdot\underline{r}'} . \tag{3.17}$$

Choose the arbitrary solution of the wave equation $P_h(\underline{r}',\underline{k})$ equal to the incident field given above. Then, from equations (2.1.18) and (2.2.1-3)

$$k^2 \int_V d\underline{r}' \, \gamma(\underline{r}') \, e^{i2\underline{k}\cdot\underline{r}'} = Q(\underline{k}) , \tag{3.18}$$

where $Q(\underline{k})$ is computed from the scattered field as shown in equation (2.1.18) and $k = |\underline{k}|$. Equation (3.18) is simply a multidimensional spatial Fourier transform of the velocity function γ. Hence, the velocities are given by

$$\gamma(\underline{r}) = \frac{1}{\pi^3} \int_{-\infty}^{\infty} \int_{-\infty}^{\infty} \int_{-\infty}^{\infty} d\underline{k} \, \frac{Q(\underline{k})}{k^2} \, e^{-i2\underline{k}\cdot\underline{r}} . \tag{3.19}$$

This result was obtained by Cohen and Bleistein (1977) by using a derivation similar

to that given above (note that a $1/k^2$ factor is missing in their paper in equation 6.4). They also discussed the the case of single wide band point source with this approach, but an explicit inversion result was not obtained in this case.

3.1.4 Diffraction tomography

A slightly different approach to the velocity inversion problem has been developed, in ultrasonic imaging, by extending x-ray tomography techniques to wave scattering problems. The acoustic medium is excited by monochromatic plane waves incident on the medium from various directions. The scattered field is observed on a surface (or along a line for a two dimensional medium) located on one side of the medium. Note that considerably less of data are collected in this case than in the experiment described in the previous section. In the following we first consider the three dimensional case. The coordinate system is chosen such that the scattering medium lies below ($z < 0$) the observation surface $z = 0$.

Let the incident plane wave be

$$\varphi_0(\underline{r}',\underline{k}_0) = e^{i\underline{k}_0 \cdot \underline{r}'} \quad ; \quad |\underline{k}_0| = k \ . \tag{3.20}$$

From equations (2.1.12) and (2.2.1-3), the scattered field for plane wave sources can be written as

$$P_s(\underline{r},\underline{k}_0) = k^2 \int_V d\underline{r}' \, \gamma(\underline{r}') \, \frac{e^{ik|\underline{r}-\underline{r}'|}}{4\pi|\underline{r}-\underline{r}'|} \, e^{i\underline{k}_0 \cdot \underline{r}'} \ , \tag{3.21}$$

where $\underline{r} = (x,y,0)$ belongs to the observation plane. Now, using the plane wave

expansion of the Green's function given by equation (3.11), the spatial Fourier transform of the observed data is given by

$$\tilde{P}_s(\underline{k},\underline{k}_0) = \frac{ik^2}{2} \int_V d\underline{r}' \, \gamma(\underline{r}') \, \frac{e^{-i\underline{k}\cdot\underline{r}'}}{k_z} \, e^{i\underline{k}_0\cdot\underline{r}'} , \tag{3.22}$$

where we have used the fact that $z' < 0$ in V. For a given k_x and k_y the vertical wavenumber k_z is determined by

$$k_z = (k^2 - k_x{}^2 - k_y{}^2)^{1/2} \quad ; \quad Re(k_z) \geq 0 \quad ; \quad Im(k_z) \geq 0 . \tag{3.23}$$

Equation (3.22) directly gives the multidimensional Fourier transform of the velocity function

$$\tilde{\gamma}(\underline{k}-\underline{k}_0) = \frac{-2ik_z}{k^2} \, \tilde{P}_s(\underline{k},\underline{k}_0) , \tag{3.24}$$

where $\underline{k}_0$ is the wavenumber of the incident plane wave and $\underline{k}$ is the Fourier domain variable for the observed data. Then, for each pair $(\underline{k},\underline{k}_0)$ one point of $\tilde{\gamma}$ is determined. Since $|\underline{k}| = k$, for each plane wave ($\underline{k}_0$ is fixed) $\underline{k}-\underline{k}_0$ is located on a sphere with radius k centered at $\underline{k}_0$. However, because of the constraints on k_z given in equation (3.23), for each plane wave $\tilde{\gamma}$ is determined on the part of the sphere for which $k_z > 0$ (a half sphere). This result was first obtained by Wolf (1969).

If the medium properties are not changing along, for example, the y axis, then observations along a line in the $y = 0$ plane are sufficient for velocity inversion. With plane wave sources (three dimensional plane waves with $k_{0y} = 0$) the Green's

function in equation (3.21) is replaced by the two dimensional Green's function given in equation (2.2.9). Again, using the plane wave expansion in equation (3.16), the inversion procedure described above can be repeated for the two dimensional case. For each plane wave, the velocity function $\tilde{\gamma}(k_x, k_z)$ is obtained along a semicircle ($k_z > 0$) with radius k and centered at $\underline{k}_0$.

The diffraction tomography approach was developed for ultrasonic imaging (Mueller et. al., 1979; Greenleaf, 1983) where, in most cases, the medium can be probed by plane waves from all directions. However, in geophysical problems, even under ideal conditions (infinite aperture source arrays) plane waves with only a limited range of incident angles can be generated (Devaney, 1984). It can be seen from the discussion above that this causes an incomplete determination of the velocity function in the Fourier domain $\tilde{\gamma}(k_x, k_z)$. Finally, from equation (3.24) $\tilde{\gamma}$ is given along semicircles, and there are some computational issues involved in computing the inverse transform γ. One approach is to interpolate the data over a rectangular grid and then to use the Fast Fourier Transform (FFT). Another, and reportedly better, approach is the filtered back propagation method where the scattered data due to each plane wave is first filtered and then backpropagated into the medium. The images obtained for each plane wave are then superimposed to obtain the final reconstruction (Devaney, 1982).

Rytov approximation

In addition to the Born approximation described in Section 2.2, the Rytov approximation has also been used in the diffraction tomography literature. One approximation may be preferred to the other depending on the application. The Lippmann-

Schwinger equation obtained with the Rytov approximation is essentially the same as for the Born approximation except that the definition of the scattered field is different. Therefore, all inversion methods for the Born approximation can be used for the Rytov approximation as well.

In the Born approximation the total field is modeled as the sum of the incident field and the scattered field as in equation (2.0.4). Now, consider the following model for the total field

$$P(\underline{r},\omega) = P_0(\underline{r},\omega)\ e^{ik\Phi(\underline{r},\omega)}\ , \tag{3.25}$$

where $P_0(\underline{r},\omega)$ is the background field for a given background model $n_0(\underline{r})$ and $\Phi(\underline{r},\omega)$ is in general a complex function representing perturbations. If we apply the wave equation on this total field and assume that

$$|\ \nabla\Phi(\underline{r},\omega)\ | \approx 0\ , \tag{3.26}$$

it can be shown that

$$\mathbf{D}_0[\Phi(\underline{r},\omega)P_0(\underline{r},\omega)] \approx ik\gamma(\underline{r})P_0(\underline{r},\omega)\ , \tag{3.27}$$

where $\mathbf{D}_0$ and γ are given in equation (2.2.1-3). Then, the complex phase is given by

$$\Phi(\underline{r},\omega) = \frac{-ik}{P_0(\underline{r},\omega)} \int_V d\underline{r}'\ \gamma(\underline{r}')\ P_0(\underline{r}',\omega)\ G_0(\underline{r},\underline{r}',\omega)\ . \tag{3.28}$$

This equation is similar to equation (2.1.11) for the Born approximation, but Φ and

P_s are defined quite differently. The above equation is used by inversion methods based on the Rytov approximation.

3.1.5 Imaging of discontinuities

In this section the scattering experiment with a single wide band point source and an array of receivers is considered. As in diffraction stack and before stack migration, a set of phase delays are computed for a given point in the medium to focus the receiver array at that point. Moreover, a set of receiver weights are also computed to obtain quantitative estimates of the velocity changes in the medium as well as of their locations. In the following the two dimensional problem is discussed, however, the same discussion can be made for the three dimensional case.

We start by approximating the Green's functions in equation (2.1.14). For a two dimensional medium, the geometrical optics approximation of the Green's function is given by equation (2.2.7). Then, equation (2.1.14) becomes

$$P_s(\underline{r},\omega) = ik \int_V d\underline{r}' \, \gamma(\underline{r}') \, a(\underline{r},\underline{r}') \, e^{iks(\underline{r},\underline{r}')} , \tag{3.29}$$

where $a(\underline{r},\underline{r}')$ and $s(\underline{r},\underline{r}')$ represent the combined amplitudes and phases of the two Green's functions. For example, $s(\underline{r},\underline{r}')/c$ is the total phase shift from the source to the point $\underline{r}'$ and from this point to the receiver located at $\underline{r}$. Since there is only one source the dependence on the source location $\underline{r}_s$ is dropped from the equation. The amplitude and phase functions can be computed numerically and we will assume that they are known. Now, we seek an inverse in the form of a weighted focusing operation

$$\hat{\gamma}(\underline{r}_0) = \frac{i\ sgn(k)}{-4\pi^2} \int_{-\infty}^{\infty} dk \int_S d\underline{r}\ P_s(\underline{r},\omega)\ W(\underline{r},\underline{r}_0)\ e^{-iks(\underline{r},\underline{r}_0)}\ , \tag{3.30}$$

where $\underline{r}$ is the receiver coordinate and S denotes all the receivers. The weighting function W will be computed below. The main idea in this method is to find a weighting function for each point in the medium such that $\hat{\gamma}(\underline{r}_0) \approx \gamma(\underline{r}_0)$. From equations (3.29) and (3.30)

$$\hat{\gamma}(\underline{r}_0) = \frac{1}{4\pi^2} \int_{-\infty}^{\infty} dk \int_S d\underline{r} \int_V d\underline{r}'\ \gamma(\underline{r}')\ a(\underline{r},\underline{r}')\ W(\underline{r},\underline{r}_0)\ |k|\ e^{ik[s(\underline{r},\underline{r}')-s(\underline{r},\underline{r}_0)]}\ . \tag{3.31}$$

The phase function in the integral above is complicated to simplify this expression we approximate the phase term around the focus point $\underline{r}_0$ by the first term of the Taylor series

$$\begin{aligned} k[s(\underline{r},\underline{r}')-s(\underline{r},\underline{r}_0)] &\approx k\nabla_{\underline{r}'}s(\underline{r},\underline{r}')|_{\underline{r}'=\underline{r}_0} \cdot (\underline{r}'-\underline{r}_0) \\ &\equiv \underline{m}(k,\underline{r},\underline{r}_0) \cdot (\underline{r}'-\underline{r}_0)\ . \end{aligned} \tag{3.32}$$

It is seen that, with this approximation the exponent is in the form of an inner product of two vectors. Therefore, the $d\underline{r}'$ integral in equation (3.31) is a Fourier transform from the space variable $\underline{r}'$ to the $\underline{m}$ domain. Note that the medium dimension (dimension of $\underline{m}$) is always one higher than the dimension of S (the receiver space). For example, in the two dimensional problem the receivers are located along a line (or a curve) which is one dimensional. Hence, we can always change the coordinates from $(k,\underline{r})$ to $\underline{m}$. Let the Jacobian of this transformation be $|k|^{-1}J$. From

equation (3.32) the frequency dependence of the Jacobian is simply $|k|^{-1}$. Consequently, J is frequency independent. From equations (3.31) and (3.32) we have

$$\hat{\gamma}(\underline{r}_0) \approx \frac{1}{4\pi^2} \int_{V_m} d\underline{m} \int_V d\underline{r}' \, \gamma(\underline{r}') \, a(\underline{r},\underline{r}') \, J \;\; W(\underline{r},\underline{r}_0) \, e^{i\underline{m} \cdot (\underline{r}'-\underline{r}_0)} \, . \tag{3.33}$$

The integral limits over the variable $\underline{m}$ are determined by the frequency band and the receiver coverage S. Assuming that V_m covers the domain where the medium has Fourier components, the obvious choice for the receiver weights is

$$W(\underline{r},\underline{r}_0) = \frac{1}{a(\underline{r},\underline{r}_0) \, J} \, . \tag{3.34}$$

Now assume that the amplitudes of the Green's functions change slowly, so that $\frac{a(\underline{r},\underline{r}')}{a(\underline{r},\underline{r}_0)} \approx 1$. Then, from equations (3.33) and (3.34) we have

$$\begin{aligned} \hat{\gamma}(\underline{r}_0) &\approx \frac{1}{4\pi^2} \int_{V_m} d\underline{m} \int_V d\underline{r}' \, \gamma(\underline{r}') \, e^{i\underline{m} \cdot (\underline{r}'-\underline{r}_0)} \\ &\approx \gamma(\underline{r}_0) \, . \end{aligned} \tag{3.35}$$

It can be shown that the reconstruction procesdure described above can be implemented by ray tracing from every point in the medium to the receivers and to the source. For every point and receiver, the quantity J in equation (3.34) can be computed from the angle between the source ray and the receiver ray. A simple derivation of the method was given by Miller et. al. (1984). A detailed derivation was given

by Beylkin (1985) where he showed that the migration (or semi-inversion) algorithm described above is, in fact, the first term of an asymptotic expansion of the inverse associated to equation (3.29).

3.2 Phase Corrected Approximation Methods

As was pointed out in the introduction the Born approximation, with either a homogeneous or a varying velocity background, assumes that the incident field is not affected by unknown velocity variations in the medium. Therefore, the Born approximation is valid only for small velocity variations around the background velocity model. However, even if the velocity variations are relatively small an error accumulation is observed at points distant from the source and receivers. This becomes particularly severe if the phase variations of the incident field introduced by the velocity perturbations consistently build up. For example, if the true velocities of the medium are higher than those assumed for the background model, the true incident field arrives at the scatterers before the assumed incident field. The difference in arrival times increases with the distance from the source. One way to overcome this error build up, to some degree, is to employ a background that is dependent on the unknown velocity perturbations. Obviously, the integral representation of the scattered field, in this case, is considerably more complicated since the Green's function and the incident field in equation (2.1.4) are also functions of γ. It will be shown below that, for a one dimensional medium this approach does not complicate the problem. After changing the space variable to travel time, the inversion procedure is similar to the Born case. In the multidimensional case, however, things are more complicated. The only observation geometry that has been considered is the coincident source-receiver array configuration. Even in that case many assumptions, most of which are questionable, must be made to obtain a direct inversion equation. The multidimensional problem will be discussed in Section 3.4. The main feature of phase corrected background

methods is that, at every point in the medium, the incident field is updated with the previously estimated velocities. This can be done only if there is a simple relationship between the location of the scatterers and the arrival times of the corresponding scattered field. In other words, before we compute the velocity at some point in the medium, the portion of the medium in which the incident and scattered fields travel must have already been obtained. Therefore, phase corrected background approximation results have been rectricted to the cases mentioned above. In this section an inversion equation is derived emphasizing the approximations involved. We use a formulation slightly different from what was presented in the literature; however, our results will be compared with the previous ones.

3.2.1 One dimensional problem

First we consider a stratified medium of finite extent excited by a wide band, normally incident plane wave. The reflected field is observed by a receiver located above the medium. The coordinate system is chosen such that the receiver is at the origin ($z = 0$) and the medium is in the region $z > 0$. Using the wave equation decomposition discussed in Section 2.3, we have

$$P_0(z,\omega) = e^{iks(z)} ,$$

$$s(z) = \int_0^z d\xi \; n(\xi) ,$$

$$\gamma(z,\omega) = ik\dot{n}(z) , \tag{3.36}$$

where the derivative with respect to z is indicated as a dot. The Green's function of the one dimensional wave equation $\mathbf{D}_0$ is given by

$$G_0(z,z',\omega) = \frac{1}{-i2kn(z')} e^{ik|\int_{z'}^{z} d\xi\, n(\xi)|} . \tag{3.37}$$

From equations (2.1.11),(3.36) and (3.37) the observed reflected field is

$$P_s(\omega) = -\frac{1}{2}\int_0^\infty dz' \frac{\dot{n}(z')}{n(z')} e^{i2ks(z')} . \tag{3.38}$$

By changing the integration variable from z' to s we have

$$P_s(\omega) = -\frac{1}{2}\int_0^\infty ds \frac{\dot{n}(s)}{n(s)} e^{i2ks} . \tag{3.39}$$

Noting that $\dot{n}(s) = 0$ for $s < 0$ the integral above representes a Fourier transform similar to the one which was obtained for the Born case. Taking the inverse transform of both sides the reflectivity function of the medium is given by

$$q(s) = -\frac{\dot{n}(s)}{2n(s)} = \frac{2}{c}\tilde{P}_s(2\frac{s}{c}) , \tag{3.40}$$

where $\tilde{P}_s(t)$ is the observed scattered field in time domain. Finally by choosing the reference velocity $c = \omega/k = v(0)$, the refraction index of the medium is obtained from

$$\ln n(s) = -\frac{4}{c} \int_0^s ds' \, \tilde{P}_s(2\frac{s'}{c}) \, . \tag{3.41}$$

Since $s(z)$ is known, the refraction index as a function of depth can be obtained by mapping $n(s) \rightarrow n(z)$. This result was obtained by Gray (1980b) with a different approach which can be summarized as follows. If we change the variables from depth z to travel time s/c in the one dimensional wave equation, another differential equation in terms of travel times is obtained. The Born inversion procedure descibed above can, then, be applied to this equation giving the same result.

If the stratified medium is excited by obliquely incident plane waves, the problem can be reduced to the normal incidence case by replacing the refraction index by

$$n'(z) = [\, n^2(z) - \sin^2\theta_0 \,]^{1/2} \, , \tag{3.42}$$

where θ_0 is the incident angle of the plane wave measured with respect to the vertical.

3.2.2 Stratified medium with point source and receiver

In this section the same observation geometry as in Section 3.1.1 is considered, but with the phase corrected background approach. We will assume a coincident source-receiver pair. The results can easily be extended to the small offset case, however, because of the approximations involved this approach cannot be used for large offsets.

The wave equation for a stratified medium with a point source located at the origin is given by $[\, \nabla^2 + k^2 n^2(z) \,] \, P(\underline{r},\omega) = -\delta(\underline{r})$. By taking the Fourier transform with respect to x and y, the wave equation for a plane wave component of the point source

becomes

$$[\ \frac{\partial^2}{\partial z^2} + k^2\ n_e{}^2(k_x,k_y,z)\ ]\ \hat{P}(k_x,k_y,z,\omega) = -\delta(z)\ , \tag{3.43}$$

where

$$n_e{}^2(k_x,k_y,z) = [n^2(z) - \frac{k_x{}^2 + k_y{}^2}{k^2}]\ . \tag{3.44}$$

For each plane wave, equation (3.43) is similar to the plane wave source problem, discussed in the previous section, except for the $\delta(z)$ term on the right hand side. The incident field in this case is not a plane wave but it is given by the Green's function of equation (3.37) after replacing n by n_e. From equation (2.1.14) the reflected field observed at the surface ($z = 0$) is given by

$$\hat{P}_s(k_x,k_y,\omega) = \frac{-i}{4k}\int_0^\infty dz'\ \frac{\dot{n}_e(z')}{n_e(0)\,n_e(z')}\ e^{i2k\hat{s}(z')}\ , \tag{3.45}$$

where $\hat{s}(z)$ is given by equation (3.36) (again, n must be replaced by n_e). Note that n_e and $\hat{s}$ are functions of (k_x,k_y). From properties of the Fourier transform the reflected field observed at the receiver (located at the origin) can be written as

$$P_s(\omega) = \frac{1}{4\pi^2}\int_{-\infty}^{\infty}\int_{-\infty}^{\infty} dk_x\,dk_y\ \hat{P}_s(k_x,k_y,\omega)$$

$$= \frac{-i}{16\pi^2 k} \int_0^\infty dz' \int_{-\infty}^{\infty} \int_{-\infty}^{\infty} dk_x\, dk_y \; \frac{\dot{n}_e(z')}{n_e(0)\, n_e(z')} \; e^{i2k\hat{s}(z')} \; . \tag{3.46}$$

The double integral above represents the scattered waves from a layer at depth z' as a superposition of plane wave reflections. We now approximate this integral by a saddle point integration. It can be seen from the derivatives of the phase term $\hat{s}$ that the main contribution to the integral is from $k_x = k_y = 0$, i.e. from the normal plane wave component. The saddle point approximation is given by (Bleistein and Hanselman, 1975)

$$\int_{R^n} d\underline{x}\; f(\underline{x})\; e^{ik\psi(\underline{x})} \approx \left[\frac{2\pi}{k}\right]^{\frac{n}{2}} \frac{f(\underline{x}_0)}{|\Psi(\underline{x}_0)|^{1/2}}\; e^{ik\psi(\underline{x}_0)}\; e^{i\frac{\pi}{4}m} \; , \tag{3.47}$$

where the stationary point $\underline{x}_0$ and the Hessian matrix $\Psi(\underline{x}_0)$ are given by

$$\nabla\psi(\underline{x}_0)|_{\underline{x}=\underline{x}_0} = 0 \quad ; \quad [\,\Psi(\underline{x}_0)\,]_{ij} = \frac{\partial^2}{\partial x_i x_j}\Big|_{\underline{x}=\underline{x}_0} \; , \tag{3.48}$$

and where it is assumed that $\psi(\cdot)$ has a single stationary point. In equation (3.47) the integer m is the number of positive eigenvalues minus the number of negative eigenvalues of $\Psi(\underline{x}_0)$. Application of the saddle point integration to the $dk_x\, dk_y$ integral in equation (3.46) yields

$$P_s(\omega) \approx -\frac{1}{16\pi} \int_0^\infty dz' \; \frac{\dot{n}(z')}{n(z')} \left[\int_0^{z'} \frac{d\xi}{n(\xi)}\right]^{-1} e^{i2ks(z')} \; , \tag{3.49}$$

where we have defined the background velocity such that $n(0) = 1$ and $s(z')$ is given by equation (3.36). Comparing with equation (3.38), the term in the brackets in equation (3.49) can be interpreted as the amplitude correction for geometrical spreading. As was done in the previous section this equation can be inverted by the change of variables from z' to s followed by an inverse Fourier transform giving

$$q(s) = -\frac{\dot{n}(s)}{2n(s)} = \frac{16\pi}{c}\,\tilde{P}_s(2\frac{s}{c})\int_0^s \frac{ds'}{n^2(s')}\,, \tag{3.50}$$

where $\tilde{P}(t)$ is the observed data in time domain. Finally, the refraction index of the medium is given by the recursive equation

$$\ln n(s) = -\frac{32\pi}{c}\int_0^s ds'\,\tilde{P}_s(2\frac{s'}{c})\int_0^{s'} \frac{ds''}{n^2(s'')}\,. \tag{3.51}$$

This result was obtained by Raz (1981c) with a different approach. He formulated the problem as a WKBJ approximation, i.e. corrections for both the phase and the magnitude of the incident field were sought. However, approximations that were made before inverting the integral representation of the scattered field reduced the problem to a Bremmer-like formulation. Since his result is the same as that of equation (3.51), it only corrects the phase of the incident field. The WKBJ background approximation will be presented in the next section.

Another approach to this problem is to change the spatial variables to travel times in the wave equation. Some of the complicated derivative terms can be simplified by assuming a small offset experiment. The resulting travel time domain wave equation

can then be solved with the Born approximation. This approach was presented in Gray (1981) with some examples demonstrating the improvement over the straightforward Born approximation. His result is not the same as the one obtained above. However, if we take $n(s') \approx 1$ in the second integral in equation (3.51) this integral can be approximated by s' and the two results become the same (modulo a factor of two).

3.3 WKBJ Approximation Methods

In the previous section the phase corrected approximation was discussed. It was seen that when we select a background field whose phase function depends on the unknown velocities, a recursive inversion algorithm can be obtained. In this section we choose a background field whose magnitude and phase functions depend on the medium velocities. It will be shown that new recursive algorithms similar to those in the previous section can be obtained. Since both the magnitude and the phase of the incident field are updated during the inversion process, this approximation is more general and is expected to yield better results than the previous one.

3.3.1 One dimensional problem

The one dimensional problem (with a stratified medium and plane wave source) described in Section 3.2.1 is studied here with a WKBJ incident field. In Section 2.4 the WKBJ approximation was discussed and the corresponding scattering potential and incident field were computed. For a one dimensional medium we have

$$P_0(z,\omega) = a(z)\, e^{iks(z)} ,$$

$$s(z) = \int_0^z d\xi\; n(\xi) ,$$

$$a(z) = n(z)^{-1/2} ,$$

$$\gamma(z,\omega) = \frac{\ddot{a}(z)}{a(z)} = \frac{3}{4}\frac{\dot{n}^2(z)}{n^2(z)} - \frac{1}{2}\frac{\ddot{n}(z)}{n(z)} , \tag{3.52}$$

where the dots indicate derivatives with respect to z. Note that the scattering potential γ is independent of frequency. The WKBJ Green's function can be obtained by the standard procedure (Bender and Orszag, 1978) from the homogeneous solutions of the wave equation $\mathbf{D}_0$,

$$G_0(z,z',\omega) = -\frac{1}{i2k[n(z')n(z)]^{1/2}}\, e^{ik\left|\int_{z}^{z'} d\xi\, n(\xi)\right|} . \tag{3.53}$$

Then, from equations (2.1.11),(3.52) and (3.53) the observed scattered field is given by

$$P_s(\omega) = -\frac{1}{i2k}\int_0^\infty dz' \left[\frac{3}{4}\frac{\dot{n}^2(z')}{n^3(z')} - \frac{1}{2}\frac{\ddot{n}(z')}{n^2(z')} \right] e^{i2ks(z')} , \tag{3.54}$$

where the reference velocity is chosen such that $n(0) = 1$. By the change of variables from z' to s this equation becomes

$$P_s(\omega) = -\frac{1}{i2k}\int_0^\infty ds \left[\frac{1}{4}\frac{\dot{n}^2(s)}{n^2(s)} - \frac{1}{2}\frac{\ddot{n}(s)}{n(s)} \right] e^{i2ks} , \tag{3.55}$$

and the inverse Fourier transform of both sides yields

$$\frac{1}{4}\frac{\dot{n}^2(s)}{n^2(s)} - \frac{1}{2}\frac{\ddot{n}(s)}{n(s)} = \frac{4}{c^2}\,\dot{\tilde{P}}_s(2\frac{s}{c}) , \tag{3.56}$$

where $\dot{\tilde{P}}_s(t)$ is the derivative with respect to time of the observed scattered field. Compared with equation (3.40) for the phase corrected background, the WKBJ

approach gives a similar, but more complicated, inversion procedure for the refraction index of the medium. A more explicit solution can be obtained for the reflectivity function defined by

$$q(s) = \frac{\dot{v}(s)}{2v(s)} = -\frac{\dot{n}(s)}{2n(s)} , \tag{3.57}$$

where $v(s)$ is the velocity. It can be shown that the left hand side of equation (3.56) is simply $\dot{q}(s) - q^2(s)$. Then, the reflectivity function of the medium is given by

$$q(s) = \frac{2}{c}\,\tilde{P}_s(2\frac{s}{c}) + \int_0^s ds'\, q^2(s') . \tag{3.58}$$

If we compare this equation with equation (3.40), the difference between the WKBJ and the phase corrected approximations is the second term in the above equation. Finally, from equation (3.58) the refraction index of the medium is

$$\ln n(s) = -\frac{4}{c}\int_0^s ds'\, \tilde{P}_s(2\frac{s'}{c}) - 2\int_0^s ds'\, (s-s')\, q^2(s') . \tag{3.59}$$

This equation is one of the new results presented in this thesis. The second integral in the above equation corrects for the amplitude variations of the incident field. Note also that, the Riccati equation in (3.56) bears some relation with the equations involved in the Schur algorithm used in the exact inversion for a layered medium (Yagle and Levy, 1984).

3.3.2 Stratified medium with point source and receiver

In the following, the WKBJ approximation is applied to the problem consisting of a stratified medium with a point source which was previously considered in Sections 3.1.1 and 3.2.2 from the point of view of the Born and phase corrected approximations. The method used in Section 3.2.2, where the point source was decomposed into plane waves and the scattered field was approximated will be repeated here for the WKBJ case.

From the discussion at the beginning of Section 3.2.2 and equations (2.1.14) and (3.52), the reflected field for a plane wave component of a wide band point source can be written as

$$\hat{P}_s(k_x,k_y,\omega) = -\frac{1}{4k^2 n_e(0)} \int_0^\infty dz' \left[\frac{3}{4}\frac{\dot{n}_e^2(z')}{n_e^3(z')} - \frac{1}{2}\frac{\ddot{n}_e(z')}{n_e^2(z')} \right] e^{i2k\hat{s}(z')} . \tag{3.60}$$

The reflected field observed at the receiver (located at the origin) can be written as

$$P_s(\omega) = \frac{1}{4\pi^2} \int_{-\infty}^{\infty}\int_{-\infty}^{\infty} dk_x\, dk_y\ \hat{P}_s(k_x,k_y,\omega)$$

$$= -\frac{1}{16\pi^2 k^2} \int_0^\infty dz' \int_{-\infty}^{\infty}\int_{-\infty}^{\infty} dk_x\, dk_y\ \frac{1}{n_e(0)} \left[\frac{3}{4}\frac{\dot{n}_e^2(z')}{n_e^3(z')} - \frac{1}{2}\frac{\ddot{n}_e(z')}{n_e^2(z')} \right] e^{i2k\hat{s}(z')} . \tag{3.61}$$

The $dk_x\, dk_y$ integral above can be approximated by a saddle point integration around the normally incident plane wave component $k_x = k_y = 0$ as shown in equation (3.47). Choosing a background velocity such that $n(0) = 1$, the observed data is

approximately given by

$$P_s(\omega) \approx -\frac{1}{16\pi ik}\int_0^\infty dz' \left[\frac{3}{4}\frac{\dot{n}^2(z')}{n^3(z')} - \frac{1}{2}\frac{\ddot{n}(z')}{n^2(z')}\right]\left[\int_0^{z'}\frac{d\xi}{n(\xi)}\right]^{-1} e^{i2ks(z')} . \tag{3.62}$$

This equation is similar to equation (3.55) of the previous section except for a scaling factor and the second term in the brackets, which corrects for geometrical spreading from the point source. Following the same steps as in the previous section, we now change the spatial variable from z' to s and obtain

$$P_s(\omega) = -\frac{1}{16\pi ik}\int_0^\infty ds \left[\frac{1}{4}\frac{\dot{n}^2(s)}{n^2(s)} - \frac{1}{2}\frac{\ddot{n}(s)}{n(s)}\right]\left[\int_0^{s}\frac{ds'}{n^2(s')}\right]^{-1} e^{i2ks} . \tag{3.63}$$

The inverse Fourier transform of both sides gives

$$\frac{1}{4}\frac{\dot{n}^2(s)}{n^2(s)} - \frac{1}{2}\frac{\ddot{n}(s)}{n(s)} = \frac{32\pi}{c^2}\,\dot{\bar{P}}_s(2\frac{s}{c})\int_0^s \frac{ds'}{n^2(s')} , \tag{3.64}$$

where $\dot{\bar{P}}_s(t)$ is the derivative of the observed reflected field. As was mentioned in the previous section, the left hand side of this equation can be represented by the derivative minus the square of the reflectivity function, defined by equation (3.57). The solution of the resulting differential equation is

$$q(s) = \frac{16\pi}{c}\,\bar{P}_s(2\frac{s}{c})\int_0^s \frac{ds'}{n^2(s')} - \frac{16\pi}{c}\int_0^s ds'\,\frac{\bar{P}_s(2\frac{s'}{c})}{n^2(s')} + \int_0^s ds'\,q^2(s') .$$

(3.65)

Finally, integrating both sides once more, the logarithm of the refraction index is obtained as

$$\ln n(s) = -\frac{32\pi}{c}\int_0^s ds'\,\tilde{P}_s(2\frac{s'}{c})\int_0^{s'}\frac{ds''}{n^2(s'')} +$$

$$\frac{32\pi}{c}\int_0^s ds'\,(s-s')\,\frac{\tilde{P}_s(2\frac{s'}{c})}{n^2(s')} - 2\int_0^s ds'\,(s-s')\,q^2(s')\,. \tag{3.66}$$

This is a new result of approximate direct inversion for a layered medium excited by a point source. A comparison with equation (3.51), shows that the last two terms in equation (3.66) are absent in the phase corrected approach.

3.4 Multidimensional Geometrical Optics Approximation

In this section the multidimensional problem for a coincident source-receiver array is considered within the geometrical optics approximation. Two different methods are discussed. The first method is an extension of the WKBJ approximation to the multidimensional case. It will be seen that several assumptions and approximations must be made to obtain an inversion formula with this approach. Consequently, in the final inversion formula the incident field is not corrected according to the WBKJ approximation as was the case in one dimension. In fact, the nature of the corrections to the incident field is not completely clear, though, better results have been reported with this method than with the Born approximation. The second method consists of applying a line-ray geometrical optics transformation to the wave equation as in Chapter 2. The resulting scattering problem in the new coordinates is then solved within the Born approximation. We will show that these two methods give very similar results. In the following a three dimensional problem is considered, but the same procedure is valid in two dimensions.

3.4.1 Geometrical optics approximation

Since there are many approximations involved in the following discussion we will indicate them with a number in parenthesis. (1) The geometrical optics appproximation to the Green's function of a three dimensional inhomogeneous medium is given by

$$G_0(\underline{r},\underline{r}',\omega) = a(\underline{r},\underline{r}')\ e^{iks(\underline{r},\underline{r}')}\ . \tag{3.67}$$

As shown in Section 2.4 that, with this approximation, the amplitude, phase and scattering potential are given by equations (2.4.3), (2.4.4) and (2.4.5). Note that in this case $n(\underline{r})$ is the total index of refraction instead of the background model index of refraction. Therefore, the Green's function depends on the unknown velocities of the medium. From Section 2.4 it can be shown that

$$s(\underline{r},\underline{r}') = \int_{R:\,\underline{r}'}^{\underline{r}} d\xi \; n(\xi) \quad ; \quad R: \text{along the ray} \tag{3.68a}$$

$$a(\underline{r},\underline{r}') = \frac{1}{4\pi} N^{-1/2}(\underline{r},\underline{r}') \quad ; \quad N(\underline{r},\underline{r}') = n(\underline{r}')\, J(\underline{r},\underline{r}') \tag{3.68b}$$

$$\gamma(\underline{r},\underline{r}') = \frac{\nabla^2 a(\underline{r},\underline{r}')}{a(\underline{r},\underline{r}')} = \frac{3}{4}\frac{|\nabla N(\underline{r},\underline{r}')|^2}{N^2(\underline{r},\underline{r}')} - \frac{1}{2}\frac{\nabla^2 N(\underline{r},\underline{r}')}{N(\underline{r},\underline{r}')}\,, \tag{3.68c}$$

where ∇ is taken with respect to $\underline{r}'$ and $J(\underline{r},\underline{r}')$ is the Jacobian of the coordinate transformation from $\underline{r}$ to ray centered coordinates. The raypaths $R(\underline{r},\underline{r}')$ and the Jacobian can be computed numerically. The scattering potential γ in equation (3.68) is similar to the one dimensional potential given by equation (3.52). However, because of the Jacobian, the scattering potential in the multidimensional case is a function of the coincident source-receiver point $\underline{r}$ as well as of the medium coordinate $\underline{r}'$. (2) We approximate the potential by a function which is independent of $\underline{r}$, i.e., $\gamma(\underline{r},\underline{r}') \approx \gamma(\underline{r}')$. A specific form of this approximation will be given later. (3) Approximate the raypaths $R(\underline{r},\underline{r}')$ by straight lines $L(\underline{r},\underline{r}')$ connecting the points $\underline{r}$ and $\underline{r}'$. It can be shown that with this approximation the Jacobian becomes

$$J(\underline{r},\underline{r}') \approx |\,\underline{r} - \underline{r}'\,|^2 \,, \tag{3.69}$$

and the Green's function is approximated by

$$G_0(\underline{r},\underline{r}',\omega) = \frac{1}{4\pi n^{1/2}(\underline{r}')|\underline{r}-\underline{r}'|}\, e^{iks(\underline{r},\underline{r}')} \,, \tag{3.70}$$

where

$$s(\underline{r},\underline{r}') = \int_{L:\underline{r}}^{\underline{r}'} d\xi\; n(\xi) \,. \tag{3.71}$$

Now, we will make the most crucial assumption of the method. (4) Following Raz (1982), assume that $s(\underline{r},\underline{r}') \approx n_e\,|\underline{r}-\underline{r}'|$, where n_e is a constant average refraction index. This approximation cannot be justified easily because it assumes that the velocity variations are small random perturbations around a constant background. For most problems of interest this is not the case. Also, this approximation looks like the homogeneous Born background assumption. It will be seen shortly that, a Fourier domain mapping similar to the Born approximation is obtained as a result of this assumption. From equations (2.1.15) and (3.70) the scattered field is approximately given by

$$P_s(\underline{r},\omega) = \int_V d\underline{r}'\; \gamma(\underline{r}')\; \frac{e^{i2k_e|\underline{r}-\underline{r}'|}}{16\pi^2|\underline{r}-\underline{r}'|^2} \,. \tag{3.72}$$

This equation is the same as equation (3.9) of the Born approximation except that there is no k^2 term. Following the steps which were used for Born inversion in Section 3.1.2, the potential in the Fourier domain is given by

$$\tilde{\gamma}(k_x, k_y, k_z) = -\frac{4\pi c i k_z}{n_e} \frac{\partial}{\partial \omega} \hat{P}_s(k_x, k_y, \omega) \ . \tag{3.73}$$

Note that the frequency variable ω is replaced by the vertical wave number k_z according to equation (3.13). Next, the inverse Fourier transform of equation (3.73) will be taken and the average refraction index n_e will be replaced by the integral of its previously estimated values. This will lead to a recursive inversion method similar to the one obtained for the one dimensional case. However, before doing this, we must specify the scattering potential γ. Following Raz (1982) we assume that

$$\gamma(\underline{r}') \approx -\frac{1}{2} \nabla^2 \ln n(\underline{r}') \equiv -\frac{1}{2} \nabla^2 u(\underline{r}') \ . \tag{3.74}$$

The above relation not only assumes $J(\underline{r}, \underline{r}') = 1$, but also neglects the terms of order $\frac{|\nabla n(\underline{r}')|^2}{n^2(\underline{r}')}$. Then, from equations (3.73) and (3.74), we have

$$\tilde{u}(k_x, k_y, k_z) = -\frac{2\pi c i k_z}{n_e k_e^2} \frac{\partial}{\partial \omega} \hat{P}_s(k_x, k_y, \omega) \ . \tag{3.75}$$

Taking the inverse transform of both sides gives

$$\ln n(\underline{r}) = -\frac{c}{4\pi^2} \int_{-\infty}^{\infty} \int_{-\infty}^{\infty} \int_{-\infty}^{\infty} dk_x \, dk_y \frac{dk_z \, k_z}{k_e^2} \frac{\partial}{\partial \omega} \hat{P}_s(k_x, k_y, \omega) \ e^{i(k_x x + k_y y + k_z z)} \ . \tag{3.76}$$

According to equation (3.13) by changing variables from k_z to ω we have

$$\ln n(\underline{r}) = -\frac{c}{\pi^2 n_e}\int_{-\infty}^{\infty}\frac{d\omega}{\omega}\int_{-\infty}^{\infty}\int_{-\infty}^{\infty} dk_x\, dk_y\ \frac{\partial}{\partial\omega}\hat{P}_s(k_x,k_y,\omega)\ e^{i(k_x x+k_y y+k_z z)}\ . \tag{3.77}$$

Note that the contribution of the inhomogeneous waves (for which k_z pure imaginary) is neglected here. The $dk_x\, dk_y$ integral above can be computed by Parseval's theorem and the plane wave expansion of the Green's function given by equation (3.11). This gives an integral over the receiver plane (x',y') as follows

$$\ln n(\underline{r}) = \frac{2c}{\pi n_e}\int_{-\infty}^{\infty}\int_{-\infty}^{\infty} dx'dy'\int_{-\infty}^{\infty}\frac{d\omega}{\omega}\ \frac{\partial}{\partial\omega}P_s(x',y',\omega)\ \frac{\partial}{\partial z}\left[\frac{e^{-i2kn_e|\underline{r}-\underline{r}'|}}{|\underline{r}-\underline{r}'|}\right]$$

$$= \frac{2c}{\pi n_e}\ z\int_{-\infty}^{\infty}\int_{-\infty}^{\infty}\frac{dx'dy'}{|\underline{r}-\underline{r}'|^3}\int_{-\infty}^{\infty} d\omega\ \frac{\partial}{\partial\omega}P_s(x',y',\omega)\left[\frac{-1}{\omega}-i\tau_e\right]e^{-i\omega\tau_e}\ , \tag{3.78}$$

where $\tau_e = \frac{2}{c}s(\underline{r},\underline{r}') = \frac{2}{c}n_e|\underline{r}-\underline{r}'|$ is the two way travel time from a point in the medium to the common source-receiver point. Now, evaluate the $d\omega$ integral using Fourier transform relations and move the constant average refraction index inside the integral. Then,

$$\ln n(\underline{r}) = -4cz\int_{-\infty}^{\infty}\int_{-\infty}^{\infty}\frac{dx'dy'}{n_e|\underline{r}-\underline{r}'|^3}\left[\int_0^{\tau} dt\ t\tilde{P}_s(x',y',t) - \tau^2\tilde{P}_s(x',y',\tau)\right]. \tag{3.79}$$

The final step of this method is to undo assumption (4) at this stage. In other words replace the average two way travel time by the line integral of the travel time using the previously estimated velocities. Note that this is possible for the zero offset reflection experiment since reflections from deeper scatterers arrive at later times.

Hence, in equation (3.78) substituting

$$\tau_e \rightarrow \frac{2}{c} \int_{L:\underline{r}'}^{\underline{r}} d\xi \; n(\xi) \equiv \tau(\underline{r},\underline{r}') \; , \tag{3.80}$$

we obtain the recursive inversion equation

$$\ln n(\underline{r}) = -8z \int_{-\infty}^{\infty}\int_{-\infty}^{\infty} \frac{dx'dy'}{n_e|\underline{r}-\underline{r}'|^2}$$

$$\left[\frac{1}{\tau(\underline{r},\underline{r}')} \int_0^{\tau(\underline{r},\underline{r}')} dt \; t\tilde{P}_s(x',y',t) - \tau(\underline{r},\underline{r}')\tilde{P}_s[x',y',\tau(\underline{r},\underline{r}')] \right] . \tag{3.81}$$

3.4.2 Inversion by transforming the wave equation

In Chapter 2, a higher order approximation procedure employing a change of variables was discussed. In particular, an integral representation for the scattered field using an approximate line-ray geometrical optics transformation was obtained in Section 2.5.1. We will now apply the approximate line-ray approach to the zero-offset experiment for a three dimensional medium. The drawbacks of this method are as follows. First, as was pointed out in Chapter 2 the transformation can be done only approximately in the multidimensional case. Second, the inversion in the new coodinate system gives the medium velocities in the new coordinates. Unfortunately, mapping the velocities back to the original variables is not an easy task. Moreover, in the transformation of the wave equation discussed in Section 2.5.1 the new variables were defined by choosing the source location as the origin of both old and new coordinates.

In the zero offset experiment, however, there are many sources, so the transformation defined for a single source cannot be used here. To handle this problem we will follow Hagin and Gray (1984) and assume that the distance $\underline{s}-\underline{s}'$ in the new coordinates is approximately equal to the slowness integral from $\underline{r}$ to $\underline{r}'$. Here $\underline{s}$ and $\underline{r}$ denote the new and the old coordinates and $\underline{r}$ is located on the surface. Obviously, approximations involved in obtaining this method are valid only for a restricted class of multidimensional media where all velocity variations are very weak and lateral velocity variations are even weaker.

From equations (2.5.3b) and (2.5.19), we have the following decomposition of the wave equation operator $\mathbf{D} = \mathbf{D}_0 + \mathbf{D}_r$,

$$\mathbf{D}_0 = \nabla^2 + k^2 , \tag{3.82a}$$

$$D_r = \nabla \ln n(\underline{s}) \cdot \nabla , \tag{3.82b}$$

where ∇^2 and ∇ are defined in the $\underline{s}$ coordinates. Then, from equation (2.1.15) the scattered field for a coincident source-receiver configuration is given by

$$P_s(\underline{s},\omega) = \int_V d\underline{s}' \, \nabla \ln n(\underline{s}') \cdot \nabla G_0(\underline{s}',\underline{s},\omega) \; G_0(\underline{s},\underline{s}',\omega) , \tag{3.83}$$

where G_0 is the free space Green's function. The reciprocity of the Green's function implies that

$$P_s(\underline{s},\omega) = \frac{1}{2} \int_V d\underline{s}' \, \nabla \ln n(\underline{s}') \cdot \nabla G_0^2(\underline{s}',\underline{s},\omega) .$$

(3.84)

Finally, integrating by parts yields the familiar form

$$P_s(\underline{s},\omega) = -\frac{1}{2}\int_V d\underline{s}'\ \nabla^2 \ln\ n(\underline{s}')\ G_0{}^2(\underline{s}',\underline{s},\omega)\ . \tag{3.85}$$

Surprisingly this equation is exactly the same as equation (3.72), with γ is given by equation (3.74). Then, the inverse in the $\underline{s}$ coordinate system is from equation (3.79)

$$\ln\ n(\underline{s}) = -4cs_z \int_{-\infty}^{\infty}\int_{-\infty}^{\infty} \frac{ds_x' ds_y'}{|\underline{s}-\underline{s}'|^3}\left[\int_0^{\tau} dt\ t\tilde{P}_s(s_x',s_y',t) - \tau^2\tilde{P}_s(s_x',s_y',\tau)\right]$$

$$= -\frac{32}{c^2}s_z \int_{-\infty}^{\infty}\int_{-\infty}^{\infty} ds_x' ds_y' \left[\frac{1}{\tau^3}\int_0^{\tau} dt\ t\tilde{P}_s(s_x',s_y',t) - \frac{1}{\tau}\ \tilde{P}_s(s_x',s_y',\tau)\right], \tag{3.86}$$

where the two way travel time is given by $\tau = \frac{2}{c}|\underline{s}-\underline{s}'|$.

CHAPTER IV

Integral Representations of the Backpropagated Field

As pointed out in the introduction, the inverse scattering problem requires the solution of an integral equation (2.1.4) which expresses the scattered field $P_s(\underline{r},\omega)$ as an integral involving the medium velocities. The free variables in this equation are the receiver locations $\underline{r}$ and the frequency ω (or the time t for a time domain formulation). Most of the previous work on multidimensional velocity inversion has focused on finding appropriate processing techniques, which when applied directly to the observed traces give the medium velocities. In this thesis, we break the inversion procedure into two steps, although overall processing is still directly applied to the observed traces. In the first step we operate on the observed scattered field $P_s(\underline{r},\omega)$ and obtain a new function which can also be expressed as an integral of the medium velocities. In the second step, we solve this equation to obtain the velocities. As our first processing step, we will consider two different types of operations, namely backpropagation and Radon transformation, that will lead to two different inversion methods. The Radon transform (or slant-stack) approach will be discussed in Section 5.1. In this chapter the backpropagation approach is considered. More specifically, the extrapolated field $P_e(\underline{r},\omega)$ that is obtained by backpropagating the observed scattered field is investigated. Volume integral representations of the extrapolated field for various receiver array geometries are derived.

Consider the function $P_e(\underline{r},\omega)$ obtained from the scattered field by

$$P_e^*(\underline{r},\omega) = -\int_R d\underline{r}_R \; [\, P_s(\underline{r}_R,\omega)\, \nabla G_0^*(\underline{r},\underline{r}_R,\omega) -$$

$$G_0^*(\underline{r},\underline{r}_R,\omega)\, \nabla P_s(\underline{r}_R,\omega)\,] \cdot \hat{\underline{n}}(\underline{r}_R)\,, \tag{4.0.1}$$

where R denotes the curve (for a two dimensional problem) or the surface (for a three dimensional problem) on which the receivers are located, and $\hat{\underline{n}}(\underline{r}_R)$ is the unit vector normal to R and pointing away from the scattering medium as shown in Figure 4.1. In the above equation G_0 is the Green's function of the background medium, * denotes the complex conjugate and ∇ is the gradient with respect to the variable $\underline{r}_R$. The function P_e will be called as the extrapolated or backpropagated field for the following reasons. First, from integral (4.0.1), we see that the field $P_e^*(\underline{r},\omega)$ can be viewed as obtained by replacing the receiver located at $\underline{r}_R$ by a dipole source and a monopole source which have, respectively, for source wavelets the scattered field $P_s(\underline{r}_R,\omega)$ observed at $\underline{r}_R$ and its normal derivative $\frac{\partial}{\partial n} P_s(\underline{r}_R,\omega)$. Then, $P_e^*(\underline{r},\omega)$ is obtained by summing over all receiver locations $\underline{r}_R$. Second, the field $P_e^*(\underline{r},\omega)$ also satisfies the background wave equation everywhere except on the surface R, i.e.

$$\mathbf{D}_0 P_e(\underline{r},\omega) = 0 \quad ; \quad \underline{r} \text{ not on } R\,, \tag{4.0.2}$$

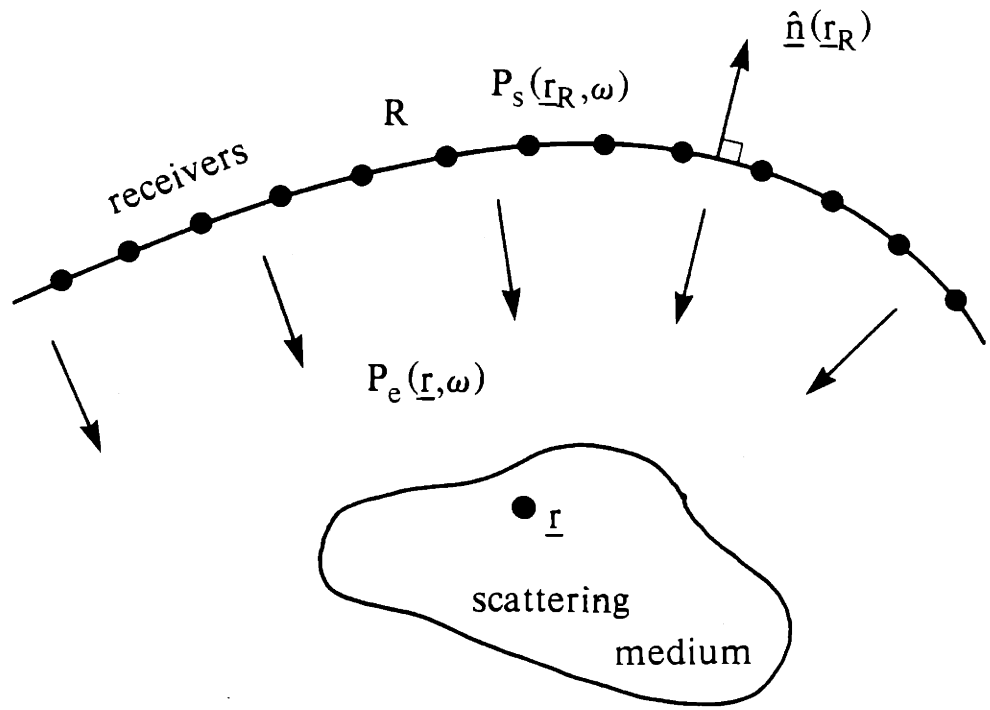

Figure 4.1. The scattered field observed at $\underline{r}_R \in R$ and backpropagated towards the scatterers, producing the extrapolated field $P_e(\underline{r},\omega)$.

and is therefore a wavefield. Finally, since the complex conjugate of the Green's function (or the incoming wave Green's function) G_0^* is used in equation (4.0.1), the observed scattered field P_s is extrapolated from R back into the scattering medium. Therefore, P_e is a backpropagated field. Note that if we replace G_0^* by G_0 in equation (4.0.1) we obtain the well-known Kirchhoff integral (Berkhout, 1982). In this case P_s is extrapolated away from the scatterers and P_e^* gives simply the scattered field in this region.

In the following the extrapolated field is investigated and its volume integral representation as a function of the scattering potential γ is derived for various receiver arrays.

4.1 Field Backpropagated from a Receiver Array Surrounding the Scatterer

First we consider the complete observations case where the receiver array R is located on a closed surface S surrounding the scatterers as shown in Figure 4.2. From equation (4.0.1) the extrapolated field in this case is given by

$$P_e^*(\underline{r},\omega) = -\int_S d\underline{r}_R \; [\; P_s(\underline{r}_R,\omega)\; \nabla G_0^*(\underline{r},\underline{r}_R,\omega) \; - \; G_0^*(\underline{r},\underline{r}_R,\omega)\; \nabla P_s(\underline{r}_R,\omega)\;] \cdot \hat{\underline{n}}(\underline{r}_R) \; . \tag{4.1.1}$$

Using the second theorem of Green, given in Appendix A, we can replace this surface integral with the volume integral

$$P_e^*(\underline{r},\omega) = -\int_V d\underline{r}' \; [\; P_s(\underline{r}',\omega)\; \mathbf{D}_0 G_0^*(\underline{r},\underline{r}',\omega) \; - \; G_0^*(\underline{r},\underline{r}',\omega)\; \mathbf{D}_0 P_s(\underline{r}',\omega)\;] \; , \tag{4.1.2}$$

where V is the volume surrounded by the closed surface S. From equations (2.1.3) and (2.1.5) we have

$$\mathbf{D}_0 P_s(\underline{r}',\omega) = -\gamma(\underline{r}',\omega)\; P(\underline{r}',\omega) \; , \tag{4.1.3a}$$

$$\mathbf{D}_0 G_0^*(\underline{r},\underline{r}',\omega) = -\delta(\underline{r}-\underline{r}') \; . \tag{4.1.3b}$$

Substituting the above equations in equation (4.1.2), we obtain

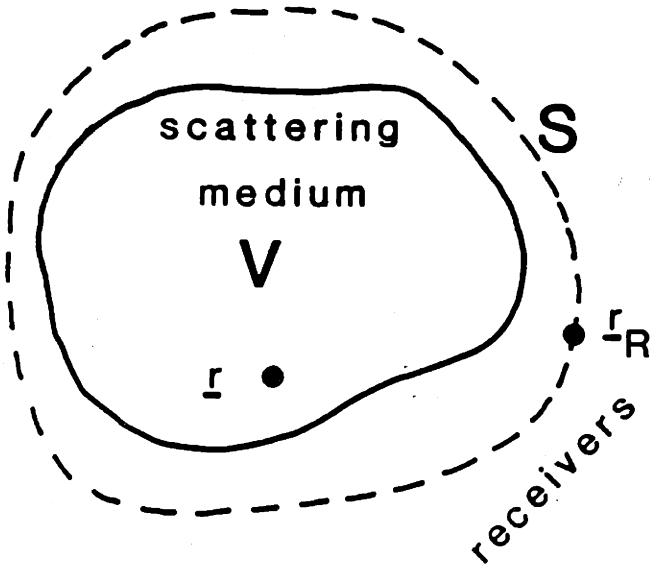

Figure 4.2. Complete observations of the scattered field.

$$P_e^*(\underline{r},\omega) = P_s(\underline{r},\omega) - P_s^-(\underline{r},\omega) \quad ; \quad \underline{r} \in V \,, \tag{4.1.4a}$$

$$= -P_s^-(\underline{r},\omega) \quad ; \quad \text{otherwise} \,, \tag{4.1.4b}$$

where P_s^- is given by

$$P_s^-(\underline{r},\omega) = \int_V d\underline{r}' \, \gamma(\underline{r}',\omega) \; P(\underline{r}',\omega) \; G_0^*(\underline{r},\underline{r}',\omega) \,. \tag{4.1.5}$$

$P_s^-(\underline{r},\omega)$ will be called the *incoming scattered field* for the following reason. From equations (2.1.4) and (4.1.5), we see that $P_s(\underline{r},\omega)$ and $P_s^-(\underline{r},\omega)$ are two solutions of the wave equation given by equation (2.1.3). P_s is the solution given by the outgoing Green's function G_0, whereas P_s^- is the solution given by the incoming Green's function G_0^*. Therefore, P_s^- represents the waves that propagate towards the scatterers as time increases, alternatively, it represents the scattered waves that propagate away from the scatterers in the negative time direction. An example on the relation between the backpropagated field P_e and the scattered field P_s is given in Section 4.5.

Let us now go back to equation (4.1.4). The extrapolated field inside the volume V is the difference between the physical (or outgoing) scattered field P_s and the incoming scattered field P_s^-. Outside the volume V, however the extrapolated field is equal to the incoming scattered field. In this thesis we will be mostly interested in the region inside the volume V. From equations (2.1.4), (4.1.4), (4.1.5) and for $\underline{r} \in V$ the exact volume integral representation of the extrapolated field is given by

$$P_e^*(\underline{r},\omega) = \int_V d\underline{r}' \; \gamma(\underline{r}',\omega) \; P(\underline{r}',\omega) \; E_c(\underline{r},\underline{r}',\omega) \; , \tag{4.1.6}$$

where the extrapolated field kernel E_c is essentially the imaginary part of the background Green's function,

$$E_c(\underline{r},\underline{r}',\omega) = 2i \; \mathrm{Im}[\; G_0(\underline{r},\underline{r}',\omega) \;] \; . \tag{4.1.7}$$

Equations (2.1.4) and (4.1.6) show that the extrapolated field has the same form as the scattered field except that the Green's function is replaced by its imaginary part. Since the impulse response of the imaginary part of the Green's function is odd symmetric in time, the extrapolated field consists of scattered waves propagating in positive and negative time directions. This property will be used in Section 6.1, where equation (4.1.6) is inverted to obtain the scattering potential γ. The extrapolated field due to scattering from each point in the medium can be interpreted as follows. Let the travel time from the source to a point $\underline{r}_0$ be τ_0. When the incident field reaches this point at time τ_0 the waves scattered from the point propagate forward and backward in time. For example, at times $2\tau_0$ and zero, the extrapolated field wavefront due to scattering from $\underline{r}_0$ lies on a curve passing through the source location as shown in Figure 4.3. The shape of the curve is determined by the travel times of the background velocity model. For a homogeneous background the extrapolated field maps onto circles in two dimensions and onto spherical surfaces in three dimensions.

In equation (4.1.1) it appears that both the scattered field P_s and its normal derivative $\hat{\underline{n}} \cdot \nabla P_s$ are needed on the surface S to obtain the extrapolated field. It will be shown in the following that P_s alone is sufficient for backpropagation. Consider the

field P_e which satisfies the background wave equation in V,

$$\mathbf{D}_0 P_e(\underline{r},\omega) = 0 \quad ; \quad \underline{r} \in V \, , \tag{4.1.8}$$

and which has given boundary values $P_e(\underline{r}_R,\omega)$ in the frequency domain or $p_e(\underline{r}_R,t)$ in the time domain, where $\underline{r}_R \in S$ denotes the receiver locations. We can solve this boundary value problem numerically in the time domain by the finite difference method. This is done by running a finite difference algorithm without any sources and by using the boundary values $p_e(\underline{r}_R,t)$ at each time step. From equation (4.1.4a) the extrapolated field on the boundary S is given by (in the time domain)

$$p_e(\underline{r}_R,t) = p_s^+(\underline{r}_R,t) - p_s^-(\underline{r}_R,t) \, , \tag{4.1.9}$$

where p_s^+ and p_s^- denote the outgoing and incoming scattered fields respectively. The scattered field observed in an experiment corresponds to the outgoing waves p_s^+. The incoming scattered field p_s^- is not observed directly, however, it can be obtained numerically from p_s^+ as will be described shortly. In some cases, the time window of interest is such that the extrapolated field within this time window can be obtained by

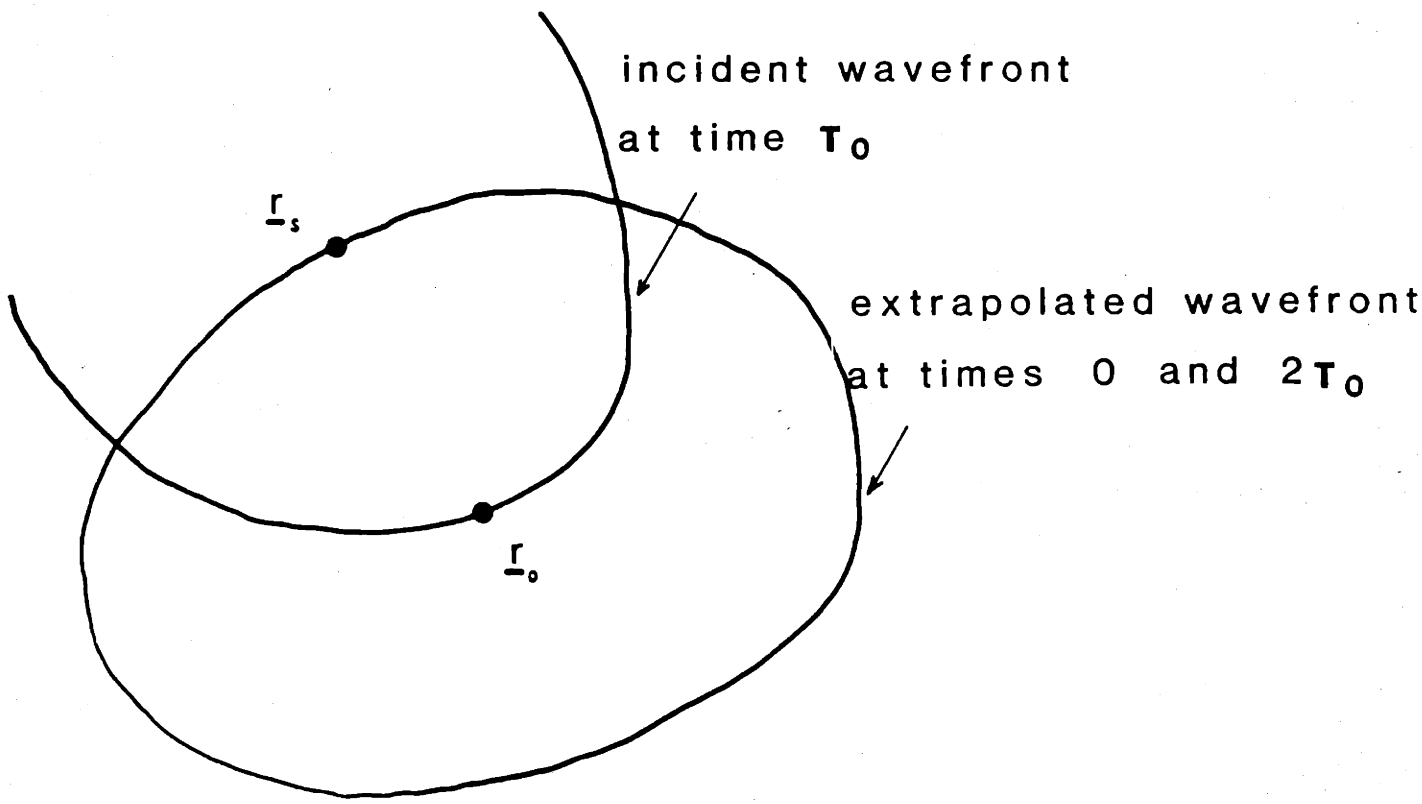

Figure 4.3. Extrapolated field wavefront of a point scatterer, located at $\underline{r}_0$, imaged at times zero and twice the source travel time.

using only p_s^+ as the boundary values. From equations (2.1.4) and (4.1.5), $p_s^+(\underline{r}_R, t)$ and $p_s^-(\underline{r}_R, t)$, associated to a point scatterer, are contained in non-overlapping time windows such that $p_s^-(\underline{r}_R, -t)$ is nonzero for $t > \tau_R - \tau_S$. Here τ_R and τ_S are the travel times from the scattering point to the receiver and to the source respectively. Therefore, within the time segment such that $t < \tau_R - \tau_S$ (for all scatterers and receivers) p_s^- is zero and the boundary values are given by $p_e = p_s^+$.

We now describe what happens at times $t > \tau_R - \tau_S$ if we use the boundary values $p_e = p_s^+$, and how we can obtain p_s^- from p_s^+ numerically. From equation (4.1.4a) at a point $\underline{r}$ very close to the boundary S the extrapolated field is given by the difference of the outgoing and incoming scattered waves. However, on the boundary S we specify only the outgoing waves p_s^+ as boundary values. Therefore the surface S is not transparent to the incoming scattered field p_s^-. Note again that when time is running backwards p_s^- is actually an outgoing wave. For most situations the extrapolated field p_e is not needed for all times and in the time window of interest the field p_s^- does not reach and reflect from the boundary surface S. In general, a boundary transparent to p_s^- can be obtained by specifying the boundary value $p_e = p_s^+ - p_s^-$, instead of $p_e = p_s^+$, on the surface S. First we run the backpropagation algorithm with the boundary values given by $p_e = p_s^+$, on S, and record the *total* field on the boundary. From equation (4.1.4a) the recorded field gives us the transparent boundary conditions $p_e = p_s^+ - p_s^-$, on S. Then, we run the backpropagation algorithm once more with the new boundary values to obtain the extrapolated field.

A simple example of the extrapolated field, computed as described above, is shown in Figure 4.4. Figure 4.4a shows the geometry of a scattering experiment where the

medium consists of two point scatterers. The scattered field due to a point source is computed by a finite difference algorithm, as described in Appendix C, and is recorded at the receivers located on the square frame surrounding the scatterers as shown in Figure 4.4a. This synthetic scattered field is, then, backpropagated into a homogeneous medium given by the background velocity of the scattering medium. The backpropagated field is obtained by running the finite difference algorithm without any sources and with boundary values at the receiver locations given by the time reversed scattered field. Figures 4.4b-4.4h show snapshots of the computed extrapolated field. The snapshot times start at 0.18 sec., in Figure 4b, and decrease (by intervals of 0.03 sec.) to time zero in Figure 4.4h. We note here that the travel times from the source to the point scatterers are given by $\tau_1 = 0.05$ sec. and $\tau_2 = 0.09$ sec. In Figures 4.4b,c,d the corresponding snapshot times, 0.18 sec., 0.15 sec. and 0.12 sec., are larger than both τ_1 and τ_2. Therefore, we observe the outgoing scattered fields (they propagate inwards in reverse time) P_1^+ and P_2^+ corresponding to two scatterers. In Figure 4.4e the snapshot time 0.09 sec. is equal to the travel time τ_2 and we see that the scattered field corresponding to the second scatterer collapses at the location of this scatterer. In Figure 4.4f the snapshot time 0.06 sec. is such that $\tau_1 < 0.06 < \tau_2$ and we observe the incoming field P_2^- (which propagates outwards in reverse time) corresponding to the second scatterer and the outgoind field P_1^+ (the smaller circle) which is just about to collapse at the location of the first scatterer. Finally, in Figures 4.4g,h the snapshot times 0.03 sec. and 0 sec. are smaller than both τ_1 and τ_2 and the imaged field corresponds to P_1^- and P_2^-. Note that in the zero time image shown in Figure 4.4h the scattered fields corresponding to each scatterer are located along circles that pass through the location of the source and that are

centered at the locations of the scatterers. We will discuss this interesting property of the extrapolated field in Chapter 6.

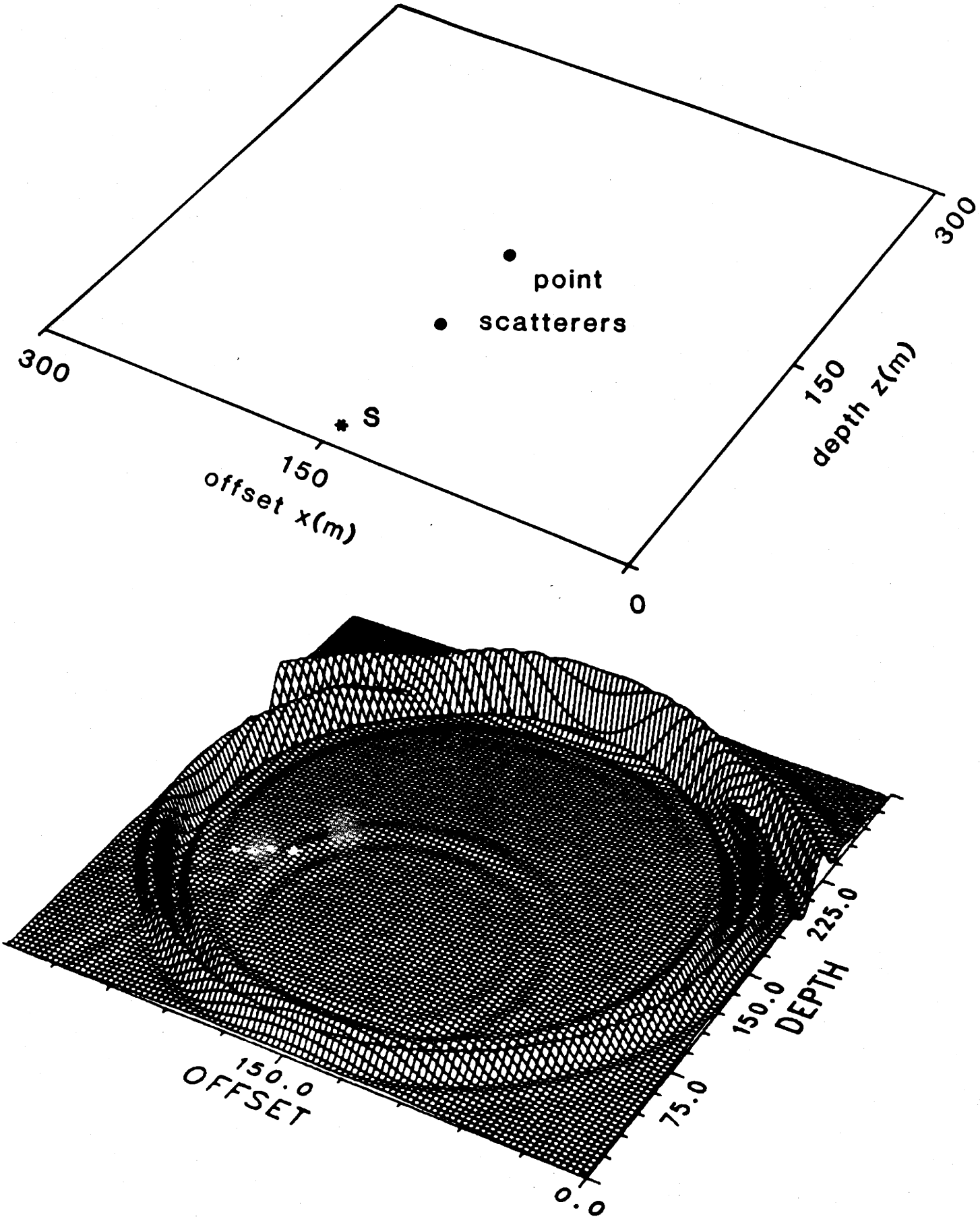

Figure 4.4. Snapshots of the backpropagated field. a) The scattering experiment. b) Snapshot of the extrapolated field at time 0.18 seconds.

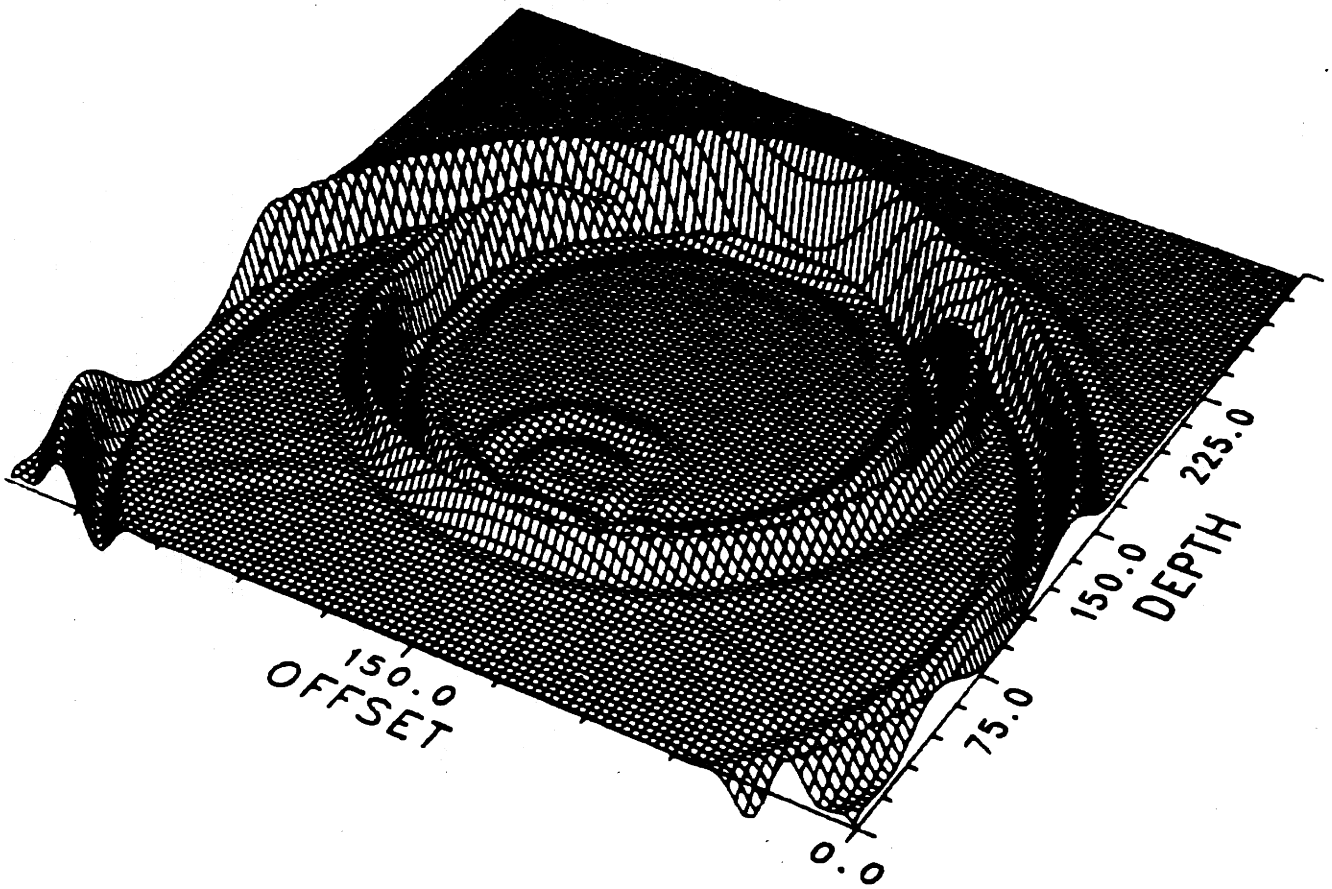

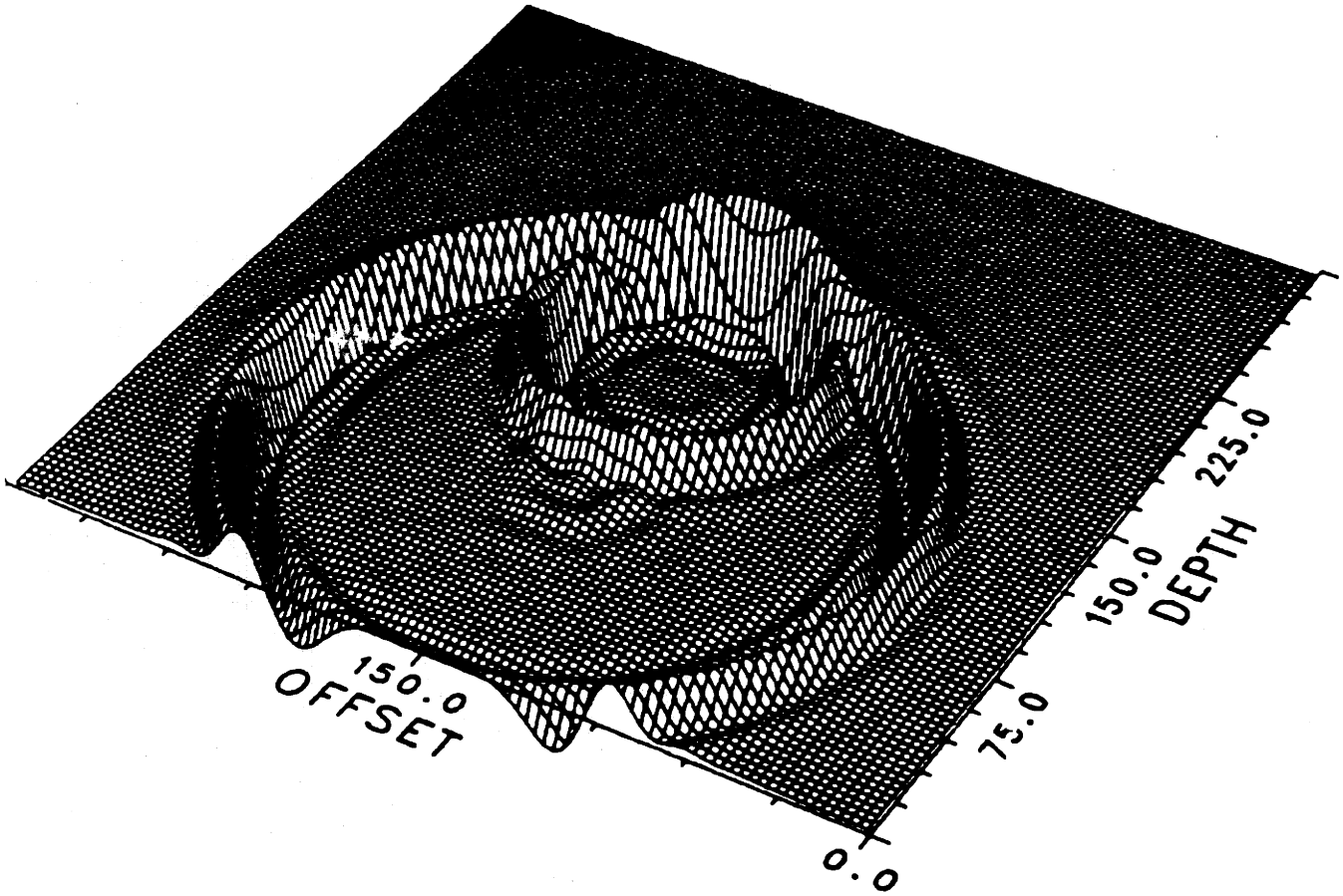

Snapshots of the extrapolated field at times c) 0.15 seconds and d) 0.12 seconds.

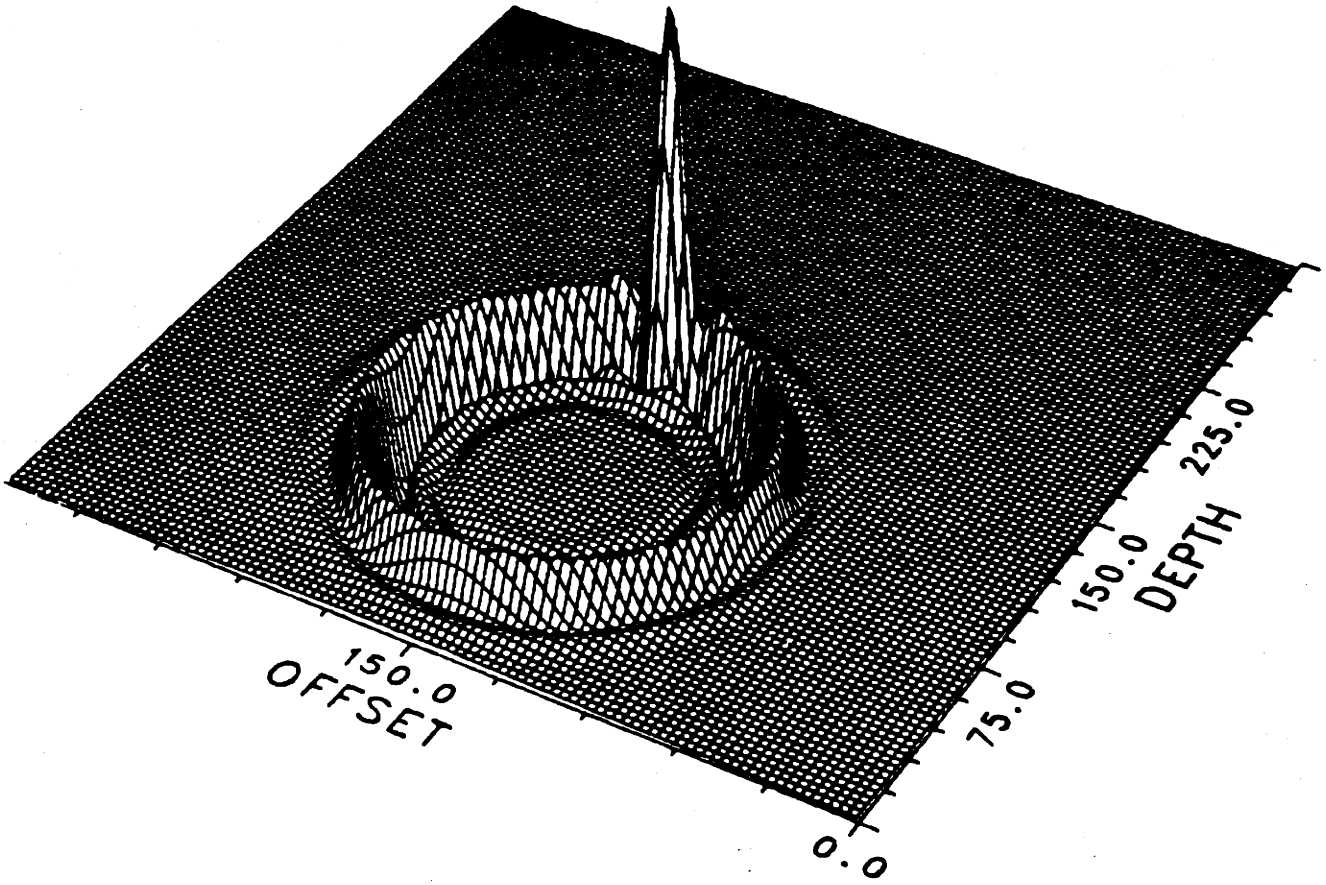

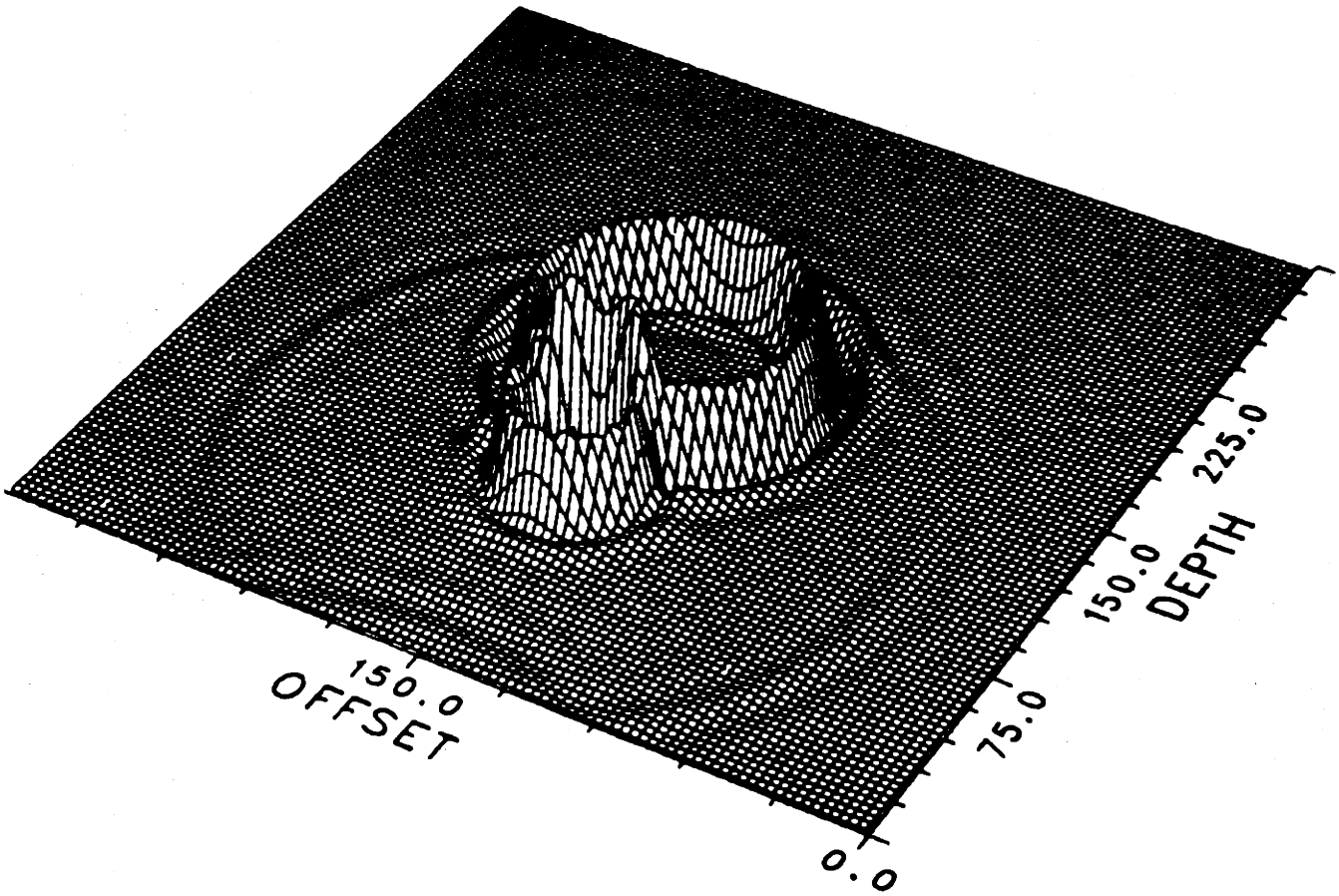

Snapshots of the extrapolated field at times e) 0.09 seconds and f) 0.06 seconds.

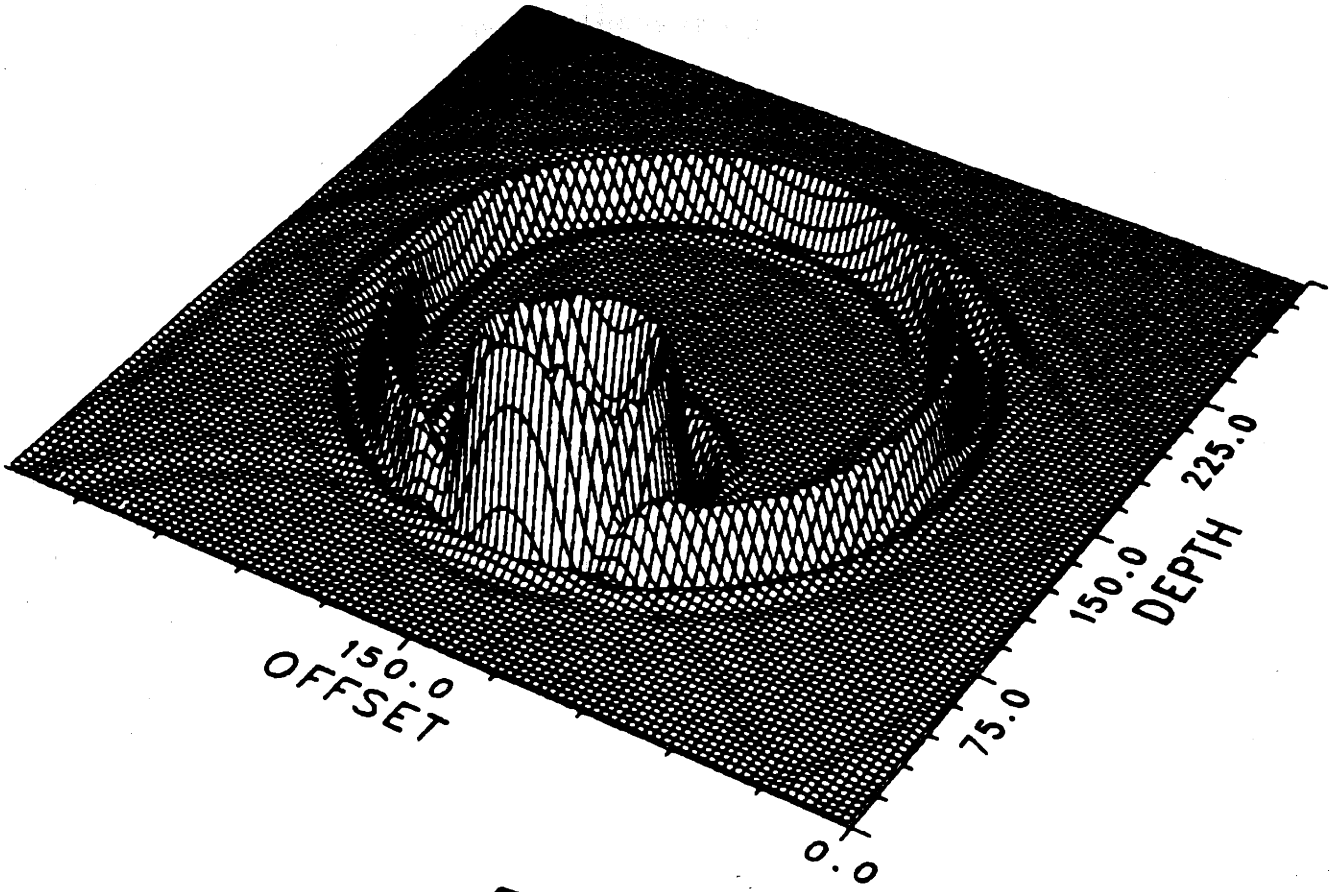

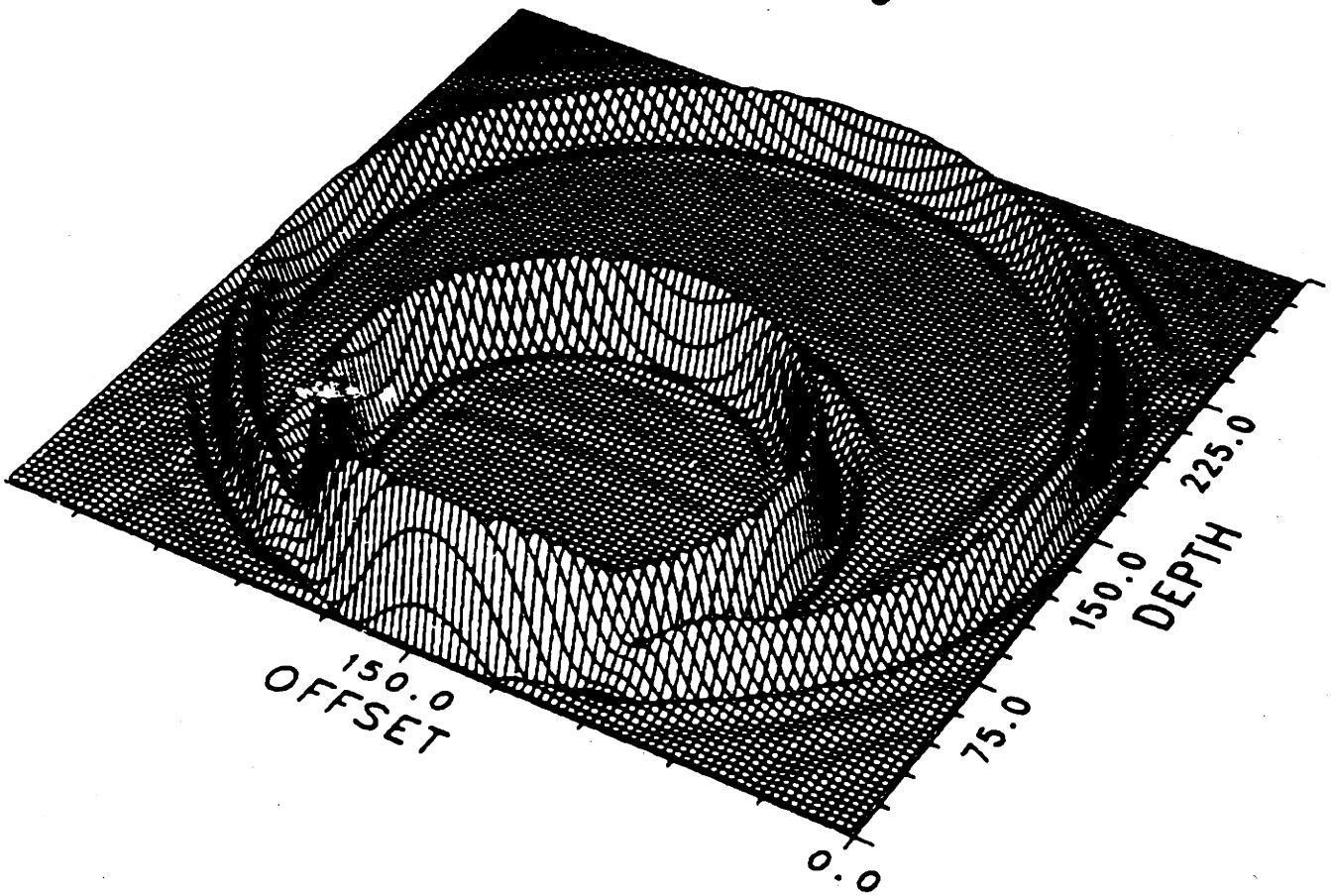

Snapshots of the extrapolated field at times g) 0.03 seconds and h) zero.

4.2 Backpropagated Field for Limited Receiver Coverage

In this section we consider the limited receiver coverage problem where only a portion of the scattered field is observed. In particular, we consider the receiver geometry depicted in Figure 4.5 where the receivers are located on a curve R which is asymptotic to two lines with angles α_1 and α_2 (Porter, 1969). Such a receiver array can represent a variety of receiver configurations such as a line array (with $\alpha_2 = 180°$, $\alpha_1 = 360°$), a horizontal array combined with a vertical array (with $\alpha_2 = 90°$, $\alpha_1 = 360°$) and a horizontal array combined with two vertical arrays on both sides of the scatterer (with $\alpha_2 = 90°$, $\alpha_1 = 450°$). It will be seen that the backpropagated field is independent from the specific shape of the array. The important quantity is the *angular aperture* $[\alpha_2 , \alpha_1]$ of the array. For example let θ_{sc} be the angle corresponding to the propagation direction of a plane-wave component of the scattered field. Then, with a receiver array as in Figure 4.5 the plane-wave components of the scattered field with angles $\alpha_2 < \theta_{sc} < \alpha_1$ are observed. The remaining components are not observed since they propagate away from the receivers.

From the discussion at the beginning of this chapter and from equation (4.0.1) the extrapolated field is given by

$$P_e^*(\underline{r},\omega) = \int_R d\underline{r}_R \; [\, P_s(\underline{r}_R,\omega) \frac{\partial}{\partial n} G_0^*(\underline{r},\underline{r}_R,\omega) - G_0^*(\underline{r},\underline{r}_R,\omega) \frac{\partial}{\partial n} P_s(\underline{r}_R,\omega) \,] \,, \tag{4.2.1}$$

where $\frac{\partial}{\partial n}$ denotes the normal derivative on the curve R, i.e $\frac{\partial}{\partial n} \equiv \hat{\underline{n}}(\underline{r}_R) \cdot \nabla_{\underline{r}_R}$ and

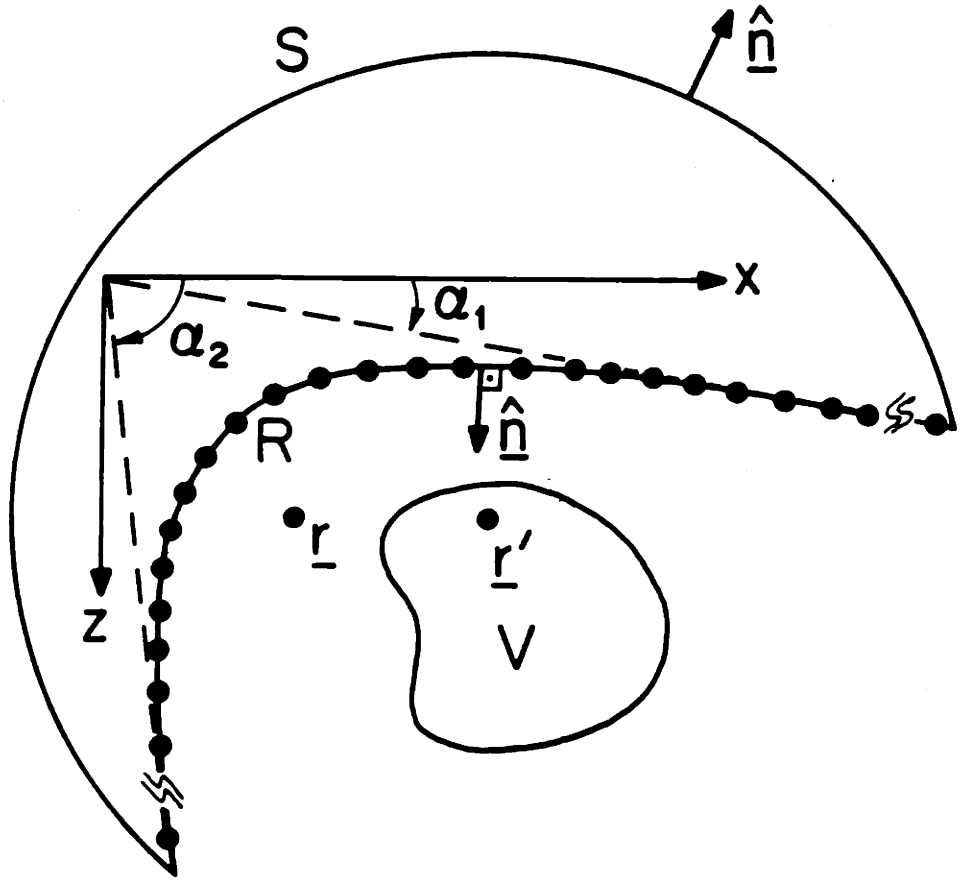

Figure 4.5. A general model for a receiver array with angular aperture [α_1 ; α_2]. R is the curve where the receivers are located and S is the arc of the circle of infinite radius centered at $\underline{r}'$.

$\hat{\underline{n}}(\underline{r}_R)$ is the normal unit vector pointing *towards* the scatterers as shown in Figure 4.5. Substituting the volume integral representation of the scattered field (equation 2.1.4) into the above equation, we obtain the following integral representation of the scattered field

$$P_e^*(\underline{r},\omega) = \int_V d\underline{r}' \, \gamma(\underline{r}',\omega) \, P(\underline{r}',\omega) \, E(\underline{r},\underline{r}',\omega) \, , \tag{4.2.2}$$

where the extrapolated field kernel is given by

$$E(\underline{r},\underline{r}',\omega) = \int_R d\underline{r}_R \, [\, G_0(\underline{r}_R,\underline{r}',\omega) \, \frac{\partial}{\partial n} G_0^*(\underline{r},\underline{r}_R,\omega) - G_0^*(\underline{r},\underline{r}_R,\omega) \, \frac{\partial}{\partial n} G_0(\underline{r}_R,\underline{r}',\omega) \,] \, . \tag{4.2.3}$$

In section 4.1 it was shown that when the receiver array surround the medium the kernel E_c was simply equal to the imaginary part of the Green's function G_0. That result was obtained directly from the second theorem of Green which applied since R was a closed surface surrounding the volume V. Here, we must follow an indirect route to obtain a useful formula for E. Consider the arc S of the circle of infinite radius centered at $\underline{r}'$ as shown in Figure 4.5. Again, from the second theorem of Green now applied to the total surface $R+S$, we have

$$\int_{R+S} d\underline{r}_R \, [\, P_s(\underline{r}_R,\omega) \, \frac{\partial}{\partial n} G_0^*(\underline{r},\underline{r}_R,\omega) - G_0^*(\underline{r},\underline{r}_R,\omega) \, \frac{\partial}{\partial n} P_s(\underline{r}_R,\omega) \,]$$

$$= \int_{V_{RS}} d\underline{r}' \; P_s(\underline{r}',\omega) \; \delta(\underline{r}-\underline{r}') = 0 \quad ; \quad \underline{r} \in V \; , \tag{4.2.4}$$

where V_{RS} is the volume surrounded by the closed surface $R+S$. Here we have used the fact that $\mathbf{D}_0 P_s(\underline{r}',\omega) = 0$ for $\underline{r}' \in V_{RS}$ since there are no scatterers within the volume V_{RS}. Thus, the kernel E can be expressed by an integral over the arc S

$$E(\underline{r},\underline{r}',\omega) = -\int_S d\underline{\xi} \; [\; G_0(\underline{\xi},\underline{r}',\omega) \; \frac{\partial}{\partial n} G_0^*(\underline{r},\underline{\xi},\omega) \; -$$

$$G_0^*(\underline{r},\underline{\xi},\omega) \; \frac{\partial}{\partial n} G_0(\underline{\xi},\underline{r}',\omega) \;] \; . \tag{4.2.5}$$

In two dimensions, the outgoing and incoming Green's functions for a homogeneous background are given by

$$G_0(\underline{\xi},\underline{r}',\omega) = \frac{i}{4} \; H_0^{(1)}(k|\underline{\xi}-\underline{r}|) \; , \tag{4.2.6a}$$

$$G_0^*(\underline{r},\underline{\xi},\omega) = -\frac{i}{4} \; H_0^{(2)}(k|\underline{r}-\underline{\xi}|) \; . \tag{4.2.6b}$$

Now, following Porter (1969), we choose polar coordinates (ρ,ϕ) centered at $\underline{r}'$ (see Figure 4.6) to perform the integration in equation (4.2.5). The asymptotic form of the Green's functions in the new coordinates are

$$G_0(\underline{\xi},\underline{r}',\omega) = \lim_{\rho\to\infty} \frac{e^{i\frac{\pi}{4}sgn(\omega)}}{(8\pi)^{1/2}} \; \frac{e^{ik\rho}}{|k|^{1/2} \; \rho^{1/2}} \; , \tag{4.2.7a}$$

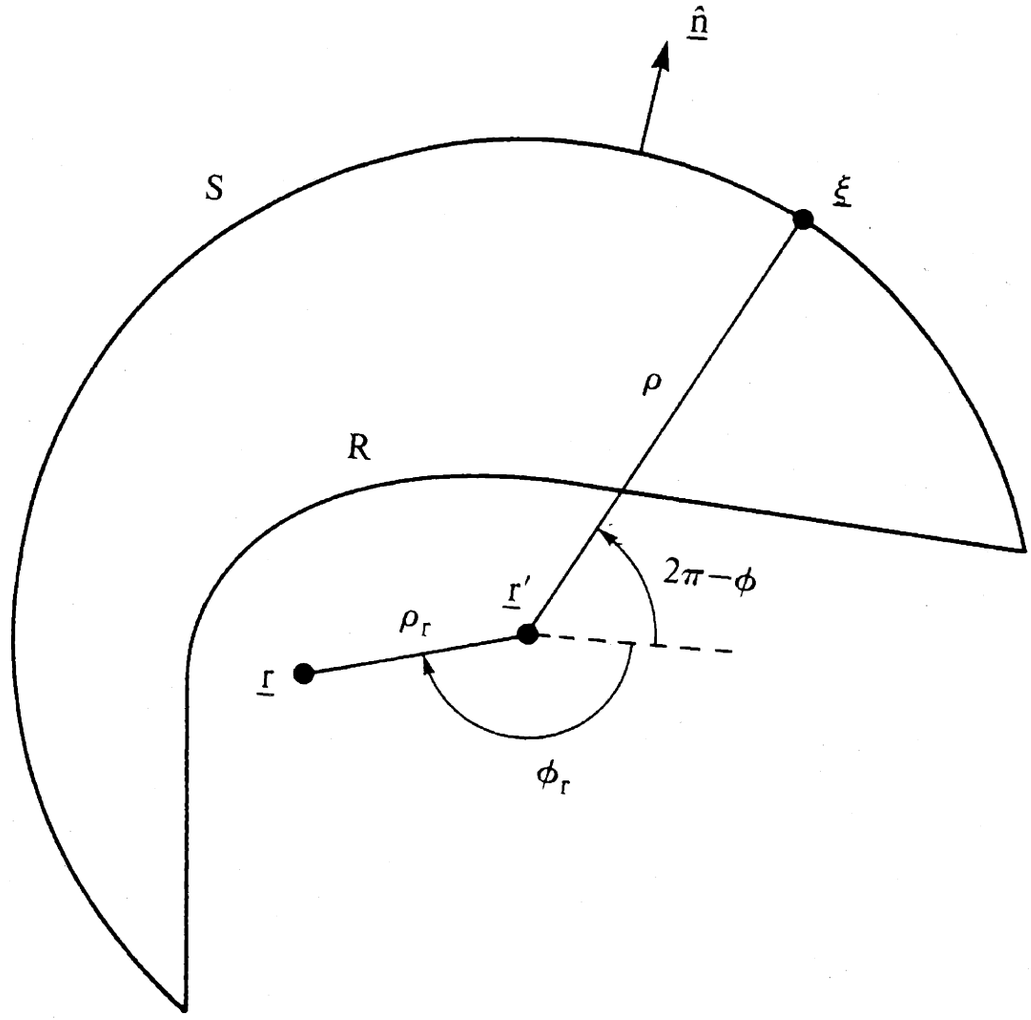

Figure 4.6. Polar coordinate system (ρ , ϕ) centered at $\underline{r}'$.

$$G_0^*(\underline{r},\underline{\xi},\omega) = \lim_{\rho\to\infty} \frac{e^{-i\frac{\pi}{4}sgn(\omega)}}{(8\pi)^{1/2}} \frac{e^{-ik[\rho-\rho_r\cos(\phi-\phi_r)]}}{|k|^{1/2}\,\rho^{1/2}} , \tag{4.2.7b}$$

Also, the normal derivative $\frac{\partial}{\partial n}$ in the new coordinates becomes $\frac{\partial}{\partial \rho}$, the derivative with respect to the radial coordinate. We should note here that since the integral is evaluated for $\rho\to\infty$ the derivatives of the amplitude terms $\rho^{-1/2}$ are neglected. The phase term in equation (4.2.7b) is obtained from the Taylor series expansion

$$|\underline{r}-\underline{\xi}| \approx |\underline{r}'-\underline{\xi}| + (\underline{r}-\underline{r}')\cdot[\nabla|\underline{r}-\underline{\xi}|]_{\underline{r}=\underline{r}'} \tag{4.2.8a}$$

$$= \rho - \rho_r\cos(\phi-\phi_r) . \tag{4.2.8b}$$

From equations (4.2.5) and (4.2.7a,b) the extrapolated field kernel in the new coordinates becomes

$$E(\rho_r,\phi_r;\underline{r}',\omega) = \frac{1}{8\pi}\lim_{\rho\to\infty}\rho\int_{\alpha_2}^{\alpha_1} d\phi\; 2ik\,\frac{e^{ik\rho_r\cos(\phi-\phi_r)}}{|k|\,\rho} , \tag{4.2.9a}$$

$$= \frac{i\,sgn(\omega)}{4\pi}\int_{\alpha_2}^{\alpha_1} d\phi\; e^{ik\rho_r\cos(\phi-\phi_r)} . \tag{4.2.9b}$$

Finally, in the original cartesian coordinates we have

$$E(\underline{r},\underline{r}',\omega) = \frac{i\,sgn(\omega)}{4\pi}\int_{\alpha_2}^{\alpha_1} d\phi\; e^{i\underline{k}\cdot(\underline{r}-\underline{r}')} , \tag{4.2.10}$$

where the wavevector $\underline{k}$ is defined by $\underline{k} = k\hat{\underline{k}}$ and $\hat{\underline{k}}$ is the unit vector corresponding

to the angle ϕ.

Equation (4.2.10) gives the extrapolated field kernel for the general case of incomplete observations. Recall that the kernel $E(\underline{r},\underline{r}',\omega)$ represents the contribution of the scatterer located at $\underline{r}'$ to the extrapolated field observed at $\underline{r}$ (see equation 4.2.2). Therefore, E can be interpreted as the *Green's function* of the backpropagated field. Clearly, E depends only on the asymptotic angles α_2 and α_1, and is independent of the shape of the receiver array between the two asymptotes. From equations (4.1.7) and (4.2.6a) the kernel in the case of complete observations and homogeneous background is given by

$$E_c(\underline{r},\underline{r}',\omega) = \frac{i\ sgn(\omega)}{2} J_0(k|\underline{r}-\underline{r}'|) \ . \tag{4.2.11}$$

Here, the complete case kernel E_c depends only on the distance $|\underline{r}-\underline{r}'|$ between the two points $\underline{r}$ and $\underline{r}'$. By comparison, the incomplete case kernel E depends on the polar angle ϕ_r of $\underline{r}$ as well as its distance ρ_r from $\underline{r}'$. Finally, the complete and incomplete case kernels can be related as follows. If the receivers surround the medium and become asymptotic to two angles such that $\alpha_1 \approx \alpha_2+2\pi$, then from equation (4.2.10)

$$\begin{aligned} E(\underline{r},\underline{r}',\omega) &= \frac{i\ sgn(\omega)}{4\pi} \int_0^{2\pi} d\phi\ e^{ik|\underline{r}-\underline{r}'|\cos(\phi)} \ , \\ &= \frac{i\ sgn(\omega)}{2} J_0(k|\underline{r}-\underline{r}'|) \ , \\ &= E_c(\underline{r},\underline{r}',\omega) \ . \end{aligned} \tag{4.2.12}$$

4.3 Backpropagated Field for the 2½ Dimensional Problem

The 2½ dimensional problem for a point source experiment was described in Section 2.6.1. Recall that in this case we consider a seismic reflection experiment where the medium is probed by a point source and the scattered field is observed on the surface, say the $x-y$ plane. This is a three dimensional problem. The velocity variations in the medium in both the x and y directions can be inverted (partially) with this plane receiver array. Now, suppose we know a priori that the medium velocities do not vary along the y axis, i.e. the medium is two dimensional. If we probe this medium with a point source we still have a three dimensional wavefield since the wavefield changes along the y axis as well. However, variations of the wavefield along the y axis do not contain much information about the variations of the medium velocities along x and z directions. In such cases the practice is to place the source and a one dimensional receiver array in the $y = 0$ plane to reduce the cost of the experiment. Obviously given this one dimensional receiver array data, we cannot backpropagate the field into a three dimensional medium. The aim of 2½ dimensional backpropagation is to obtain approximately the slice of the three dimensional backpropagated field in the source-receiver plane.

The main problem in 2½ dimensional backpropagation is as follows. When the observed data is backpropagated in the $y = 0$ plane, we inherently assume a two dimensional problem. In other words, we are essentially solving a boundary value problem in two dimensions. As a result we obtain a wavefield with incorrect amplitudes and incorrect propagation dispersion due to the two dimensional Green's function involved in backpropagation. A solution to this problem, which is considered

here, is to apply an appropriate filter on the observed traces before backpropagating them into the two dimensional medium. From equations (2.6.2) and (2.6.6), the scattered field within the homogeneous background Born approximation is given by

$$P_s(\underline{r}_R,\omega) = k^2\, S(\omega) \int_V d\underline{r}'\, \gamma(\underline{r}')\, I(\underline{r}_R,\underline{r}',\omega)\ , \tag{4.3.1}$$

where

$$I(\underline{r}_R,\underline{r}',\omega) = \frac{e^{i\frac{\pi}{4}sgn(\omega)}}{(128\pi^3)^{1/2}}\ \frac{e^{ik(|\underline{r}'-\underline{r}_s|+|\underline{r}_R-\underline{r}'|)}}{|k|^{1/2}|\underline{r}'-\underline{r}_s|^{1/2}|\underline{r}_R-\underline{r}'|^{1/2}(|\underline{r}'-\underline{r}_s|+|\underline{r}_R-\underline{r}'|)^{1/2}}\ , \tag{4.3.2}$$

represents the primary scattering for the 2½ dimensional problem. Now, consider the function $\bar{P}_s(\underline{r}_R,\omega)$ obtained by filtering the observed traces as

$$\bar{P}_s(\underline{r}_R,\omega) = -(8\pi)^{1/2}c^3\ W(\omega) * \left[\frac{e^{i\frac{3\pi}{4}sgn(\omega)}}{S(\omega)|\omega|^{3/2}}\ P_s(\underline{r}_R,\omega)\right], \tag{4.3.3}$$

where * denotes the convolution in the frequency domain and the filter W is given by

$$W(\omega) = \frac{i\ sgn(\omega)}{2|\omega|^{3/2}}\ . \tag{4.3.4}$$

The overall filtering operation can be described as follows :

1) Multiplication by $\frac{1}{S(\omega)}$: source signature is deconvolved from the traces (assuming $S(\omega) \neq 0$).

2) Multiplication by $\frac{e^{i\frac{3\pi}{4}sgn(\omega)}}{|\omega|^{3/2}} = \left(\frac{1}{-i\omega}\right)\left(\frac{1}{-i\omega}\right)^{1/2}$: the traces are integrated

in time and convolved with the impulse response of the square-root integrator (see Appendix B).

3) Convolution by $W(\omega)$: the traces are multiplied in time by $(t/2\pi)^{1/2}$ for $t > 0$. This can easily be shown by finding the inverse Fourier transform $w(t)$ of the weighting filter $W(\omega)$,

$$w(t) = \frac{1}{2\pi} \int_{-\infty}^{\infty} d\omega \, \frac{i \, sgn(\omega)}{2|\omega|^{3/2}} \, e^{-i\omega t}$$

$$= \frac{1}{2\pi} \int_{0}^{\infty} d\omega \, \frac{\sin(\omega t)}{\omega^{3/2}} = \left(\frac{|t|}{2\pi} \right)^{1/2} sgn(t) \, . \tag{4.3.5}$$

Let us now obtain the volume integral expression for the filtered field $\bar{P}_s$. From equations (4.3.1), (4.3.2) and (4.3.3) we have

$$\bar{P}_s(\underline{r}_R, \omega) = \frac{1}{4\pi} \int_V d\underline{r}' \, \gamma(\underline{r}') \; W(k) \; * \; \frac{e^{ik(|\underline{r}'-\underline{r}_s|+|\underline{r}_R-\underline{r}'|)}}{|k|^{1/2}|\underline{r}'-\underline{r}_s|^{1/2}|\underline{r}_R-\underline{r}'|^{1/2}(|\underline{r}'-\underline{r}_s|+|\underline{r}_R-\underline{r}'|)^{1/2}} \, . \tag{4.3.6}$$

Here $*$ denotes convolution over the wavenumber k and can be evaluated as follows. Let $d = |\underline{r}'-\underline{r}_s|+|\underline{r}_R-\underline{r}'| > 0$, then

$$W(k) \; * \; e^{ikd} = \int_{-\infty}^{\infty} d\kappa \, \frac{i \, sgn(\kappa)}{2|\kappa|^{3/2}} \, e^{i(k-\kappa)d}$$

$$= (2\pi)^{1/2} \, d^{1/2} \, e^{ikd} \, , \tag{4.3.7}$$

where we have used equation (4.3.5), with ω and t replaced by k and d, respectively. Then the volume integral representation of the scattered field becomes

$$\bar{P}_s(\underline{r}_R,\omega) = \frac{1}{(8\pi)^{1/2}} \int_V d\underline{r}'\, \gamma(\underline{r}')\, \frac{e^{ik|\underline{r}'-\underline{r}_s|}}{|\underline{r}'-\underline{r}_s|^{1/2}}\, \frac{e^{ik|\underline{r}_R-\underline{r}'|}}{|\underline{r}_R-\underline{r}'|^{1/2}} \,. \tag{4.3.8}$$

This equation is similar to the integral representation of the scattered field for a three dimensional problem. The difference is that the above integral is taken over a two dimensional space and that the "Green's functions" in the integrand have an amplitude decay $r^{-1/2}$, whereas in three dimensions the decay is r^{-1}, where r is the distance. A more important property of (4.3.8) is that this equation, when multiplied by ik, gives on the right hand side the scattered field for a two dimensional problem with the two dimensional Green's functions replaced by their asymptotic approximations. Therefore, $\bar{P}_s(\underline{r},\omega)$ satisfies the two dimensional homogeneous wave equation $\mathbf{D}_0\bar{P}_s(\underline{r},\omega) = 0$ outside the volume V. We will use this property shortly.

The extrapolated field P_e is obtained by backpropagating the filtered data $\bar{P}_s$ in a two dimensional medium. Thus

$$P_e^*(\underline{r},\omega) = \int_R d\underline{r}_R \; [\; \bar{P}_s(\underline{r}_R,\omega)\, \frac{\partial}{\partial n} G_0^*(\underline{r},\underline{r}_R,\omega) - G_0^*(\underline{r},\underline{r}_R,\omega)\, \frac{\partial}{\partial n} \bar{P}_s(\underline{r}_R,\omega) \;] \,. \tag{4.3.9}$$

Using equation (4.3.8) in the above expression the volume integral representation of the backpropagated field is given by

$$P_e^*(\underline{r},\omega) = \int_V d\underline{r}'\, \gamma(\underline{r}')\, \frac{e^{ik|\underline{r}'-\underline{r}_s|}}{|\underline{r}'-\underline{r}_s|^{1/2}}\, E_{1/2}(\underline{r},\underline{r}',\omega)\ , \tag{4.3.10}$$

where the extrapolated field kernel $E_{1/2}$ for the 2½ dimensional problem is

$$E_{1/2}(\underline{r},\underline{r}',\omega) = -\frac{1}{(8\pi)^{1/2}} \int_S d\underline{\xi}\ [\ \frac{e^{ik|\underline{\xi}-\underline{r}|}}{|\underline{\xi}-\underline{r}|^{1/2}}\ \frac{\partial}{\partial n} G_0^*(\underline{r},\underline{\xi},\omega)\ -$$

$$G_0^*(\underline{r},\underline{\xi},\omega)\ \frac{\partial}{\partial n}\frac{e^{ik|\underline{\xi}-\underline{r}|}}{|\underline{\xi}-\underline{r}|^{1/2}}\ ]\ . \tag{4.3.11}$$

Here S is the arc of the circle of infinite radius centered at $\underline{r}'$ as shown in Figure 4.5. Note also that we have replaced the surface integral over the receiver locations R by the integral over S as was explained in Section 4.2. From equation (4.2.4) it is seen that this replacement can be done only if $\mathbf{D}_0\bar{P}_s(\underline{r},\omega) = 0$ inside the volume surrounded by the closed surface $R+S$. It was pointed out above that $\bar{P}_s$ indeed satisfies this condition. Now, we will evaluate the integral in (4.3.11) to obtain an explicit expression for the kernel $E_{1/2}$. Since $|\underline{\xi}-\underline{r}|$ is infinitely large on the integration path, if we multiply both sides of equation (4.3.11) by $(-ik)^{-1/2} = \dfrac{e^{i\frac{\pi}{4}sgn(\omega)}}{|k|^{1/2}}$ the exponential terms in the integrand become free space Green's functions evaluated at an infinitely large distance and

$$(-ik)^{-1/2}\ E_{1/2}(\underline{r},\underline{r}',\omega) = -\int_S d\underline{\xi}\ [\ G_0(\underline{\xi},\underline{r}',\omega)\ \frac{\partial}{\partial n} G_0^*(\underline{r},\underline{\xi},\omega)\ -$$

$$G_0^*(\underline{r},\underline{\xi},\omega)\ \frac{\partial}{\partial n} G_0(\underline{\xi},\underline{r}',\omega)\ ] \ , \tag{4.3.12}$$

where G_0 and G_0^* are the two dimensional outgoing and incoming Green's functions. The above equation is identical to equation (4.2.5) for the extrapolated field of the line source problem. Therefore, following the same steps as in Section 4.2 we obtain

$$E_{1/2}(\underline{r},\underline{r}',\omega) = \frac{(ik)^{1/2}}{4\pi} \int_{\alpha_2}^{\alpha_1} d\phi\ e^{i\underline{k}\cdot(\underline{r}-\underline{r}')} \ , \tag{4.3.13}$$

where the wavevector $\underline{k}$ is defined by $\underline{k} = k\hat{\underline{k}}$ and $\hat{\underline{k}}$ is the unit vector corresponding to the angle ϕ. Finally equation (4.3.10) combined with the above equation give the volume integral representation of the extrapolated field in the 2½ dimensional problem. Note that since the whole derivation was done for a fixed frequency, $E_{1/2}$ given above is not the only kernel for this problem. We can obtain various kernels of the form $f(\omega)E_{1/2}$ by simply multiplying $\bar{P}_s$ by $f(\omega)$.

4.4 Backpropagated Field for the 2½ Dimensional Zero-Offset Problem

In Section 2.6, the 2½ dimensional problem was described. In Section 2.6.2 the zero-offset experiment for the 2½ dimensional problem was considered and the scattered field observed in the source-receiver plane was expressed in terms of a kernel $H(\underline{r},\underline{r}',\omega)$. The function H represents the three dimensional scattering observed by the coincident source-receiver pair. Also in Section 2.6.2 an explicit expression of H interms of the two dimensional Green's function was derived. In the following we discuss the backpropagated field for the 2½ dimensional zero-offset problem and derive its volume integral representation within the homogeneous background Born approximation. In this section we consider the general receiver array model R described in Section 4.2 and shown in Figure 4.5, with the exception that the receivers are replaced by source-receiver pairs in this case.

There are two interesting issues in this experiment geometry. First, unlike the single source problems considered before, the zero-offset experiment involves a large number of separate experiments with many coincident source/receiver pairs. At each receiver the observed field is due to a different point source which is collocated with that receiver. Thus, the scattered field along the receivers does not correspond to a single physical wavefield. In particular, from equation (2.6.9) the scattered field within the Born approximation for this experiment is given by

$$P_s(\underline{r},\omega) = k^2\, S(\omega) \int_V d\underline{r}'\, \gamma(\underline{r}')\, H(\underline{r},\underline{r}',\omega) \,, \tag{4.4.1}$$

where the kernel H is described in Section 2.6.2. If we apply the two dimensional

background wave operator $\mathbf{D}_0$ on both sides, we see that P_s does not satisfy the wave equation $\mathbf{D}_0 P_s = 0$ anywhere in space. Thus, the field that is obtained by backpropagating P_s does not have much physical meaning. Second, as was pointed out in the previous section, the actual field in the 2½ dimensional configuration varies in all three dimensions but we observe it only in the $y = 0$ plane. If we backpropagate the observed data in a two dimensional medium without any prefiltering we cannot obtain the $y = 0$ slice of the true field. Fortunately, in the zero-offset configuration both of these problems can be eliminated by a simple prefiltering operation applied on the observed scattered data before backpropagating it into a two dimensional medium. Define the filtered scattered field $\bar{P}_s$ obtained from the observed data by

$$\bar{P}_s(\underline{r},\omega) = -i2\pi c^3 \frac{\partial}{\partial\omega}\left[\frac{P_s(\underline{r},\omega)}{\omega^2\, S(\omega)}\right], \tag{4.4.2}$$

where $c = \omega/k$ is the background velocity. In the time domain, $\bar{P}_s(\underline{r},t)$ is obtained by the following steps :

1) Multiplication by $\dfrac{1}{S(\omega)}$: source signature is deconvolved from the traces (assuming $S(\omega) \neq 0$).

2) Multiplication by $-\dfrac{1}{\omega^2}$: the traces are integrated twice in time.

3) Derivative $-i\dfrac{\partial}{\partial\omega}$: the traces are multiplied by the time t, for $t > 0$.

From equations (4.4.1) and (4.4.2), the volume integral representation of the filtered scattered field is given by

$$\bar{P}_s(\underline{r},\omega) = -2\pi \int_V d\underline{r}' \, \gamma(\underline{r}') \, i\frac{\partial}{\partial k} H(\underline{r},\underline{r}',\omega) \, , \tag{4.4.3}$$

and using equation (2.6.12) we obtain

$$\bar{P}_s(\underline{r},\omega) = \int_V d\underline{r}' \, \gamma(\underline{r}') \, \frac{i}{4} \, H_0^{(1)}(2k|\underline{r}-\underline{r}'|) \, . \tag{4.4.4}$$

The above expression provides the following interesting interpretation for the function $\bar{P}_s$. All the scatterers in the medium can be viewed as *sources* with an identical source time function $\delta(t)$. The field created by these distributed sources propagates in the background medium with velocity $v = c/2$, which is half the reference velocity. The difference between the scattered field for a single source given by equation (2.1.11) and that for the zero-offset case is that in the first case the scatterers are secondary sources, each with a different source function given by the incident field P_0. In the latter case, all secondary sources are turned on simultaneously at time zero with an impulsive time function. Note also that, the filtered scattered field given by equation (4.4.4) has the same interpretation as the *exploding reflector model* used in migration of stacked data.

Let $P_e(\underline{r},\omega)$ be the extrapolated field obtained by backpropagating $\bar{P}_s$ in a medium with constant velocity $v = c/2$. Then the volume integral representation of the extrapolated field for this experiment is obtained as

$$P_e^*(\underline{r},\omega) = \int_V d\underline{r}' \, \gamma(\underline{r}') \, E_0(\underline{r},\underline{r}',\omega) \, , \tag{4.4.5}$$

where the 2½ dimensional zero-offset extrapolated field kernel is given by

$$E_0(\underline{r},\underline{r}',\omega) = -\int_S d\underline{\xi}\ [\ \bar{G}_0(\underline{\xi},\underline{r}',\omega)\ \frac{\partial}{\partial n}\bar{G}_0^*(\underline{r},\underline{\xi},\omega) -$$

$$\bar{G}_0^*(\underline{r},\underline{\xi},\omega)\ \frac{\partial}{\partial n}\bar{G}_0(\underline{\xi},\underline{r}',\omega)\ ]\ , \tag{4.4.6}$$

where $\bar{G}_0$ denotes the two dimensional free space Green's function of a homogeneous medium with a velocity equal to the half of the background velocity, i.e.

$$\bar{G}_0(\underline{\xi},\underline{r}',\omega) = \frac{i}{4}\ H_0^{(1)}\ (2k|\underline{\xi}-\underline{r}|)\ , \tag{4.4.7a}$$

$$\bar{G}_0^*(\underline{r},\underline{\xi},\omega) = -\frac{i}{4}\ H_0^{(2)}\ (2k|\underline{r}-\underline{\xi}|)\ . \tag{4.4.7b}$$

In equation (4.4.6), S is the arc of the infinite radius circle centered at $\underline{r}'$ as shown in Figure 4.5. Again we have replaced the integral over the receiver curve R with the integral over S by the same argument in Section 4.2 and by using the fact that the filtered scattered field satisfies $\mathbf{D}_0\bar{P}_s(\underline{r},\omega) = 0$ outside the volume V. It is seen that the surface integral in equation (4.4.6) is the same as equation (4.2.5) except that the wavenumber k is replaced by $2k$. Therefore, equations (4.2.7-4.2.10) can be repeated here by substituting $2k$ for k. Finally, from equation (4.2.10) the end result is given by

$$E_0(\underline{r},\underline{r}',\omega) = \frac{i\ sgn\,(\omega)}{4\pi}\int_{\alpha_2}^{\alpha_1} d\phi\ e^{i2\underline{k}\cdot(\underline{r}-\underline{r}')}\ ,$$

(4.4.8)

where the wavevector $\underline{k}$ is defined by $\underline{k} = k\hat{\underline{k}}$ and $\hat{\underline{k}}$ is the unit vector corresponding to the angle ϕ. The angles α_2 and α_1 represent the angle aperture of the zero-offset array as was described previously. Equations (4.4.5) and (4.4.8) give the desired volume integral representation of the extrapolated field for the 2½ dimensional zero-offset experiment.

4.5 An Example on the Relation Between the Backpropagated and Scattered Fields

It was shown in Section 4.1 that, the field obtained by backpropagating the scattered field recorded at receivers surrounding the medium is given by (in the time domain)

$$p_e(\underline{r},-t) = p_s^+(\underline{r},t) - p_s^-(\underline{r},t) \ , \tag{4.5.1}$$

where p_s^+ and p_s^- are the outgoing and incoming scattered fields respectively. In this section we will demonstrate this relation between the backpropagated and scattered fields with a numerical example. More specifically, we will compare the scattered field and backpropagated field traces recorded at several locations inside the medium. Figure 4.7 shows the geometry of the scattering experiment used in this example. First, we probed the medium with a point source, denoted by S, and recorded the synthetic scattered field (obtained by using a finite difference algorithm) at the receivers located on the rectangular frame and at three locations inside the medium denoted by R_1, R_2 and R_3 (Figure 4.8(a)). Note that in an actual experiment the scattered field is obtained by subtracting the known background field from the observed total field. Then, we backpropagated the scattered field from the receivers into a homogeneous medium (with the background velocity) and recorded the field at the same locations R_1, R_2 and R_3 (Figure 4.8(b)). It is seen in Figure 4.8 that the outgoing part $p_s^+(\underline{r},t)$ of the backpropagated field $p_e(\underline{r},-t)$ is identical to the scattered field $p_s(\underline{r},t)$. The rest of the backpropagated field is the incoming scattered field $p_s^-(\underline{r},t)$.

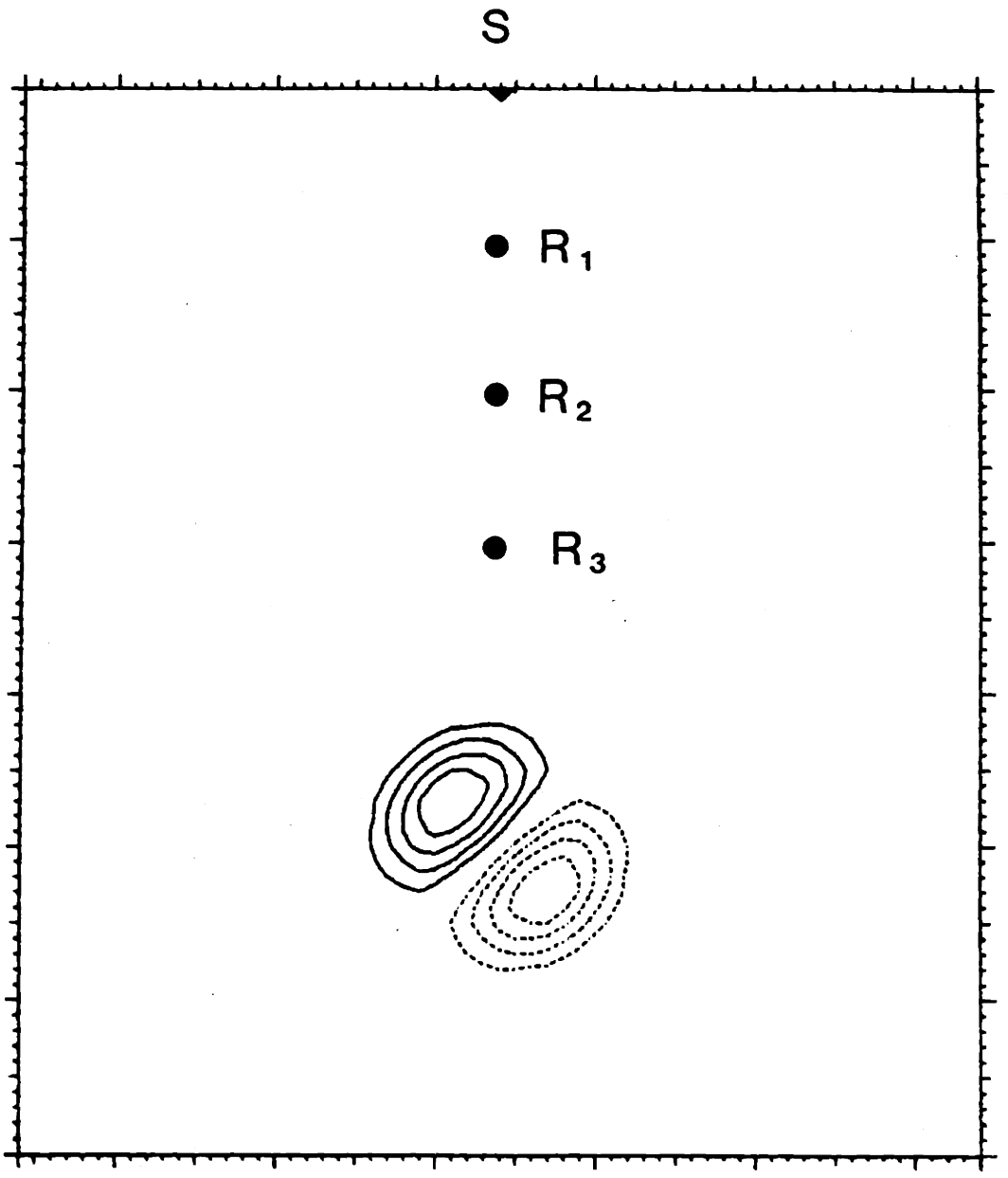

Figure 4.7. Scattering experiment. Solid and dotted contours represent velocities higher and lower than the background velocity respectively. The medium is probed by a point source denoted by S and the scattered field is recorded at receivers located on the rectangular frame. The scattered and backpropagated fields are observed at three locations R_1, R_2 and R_3.

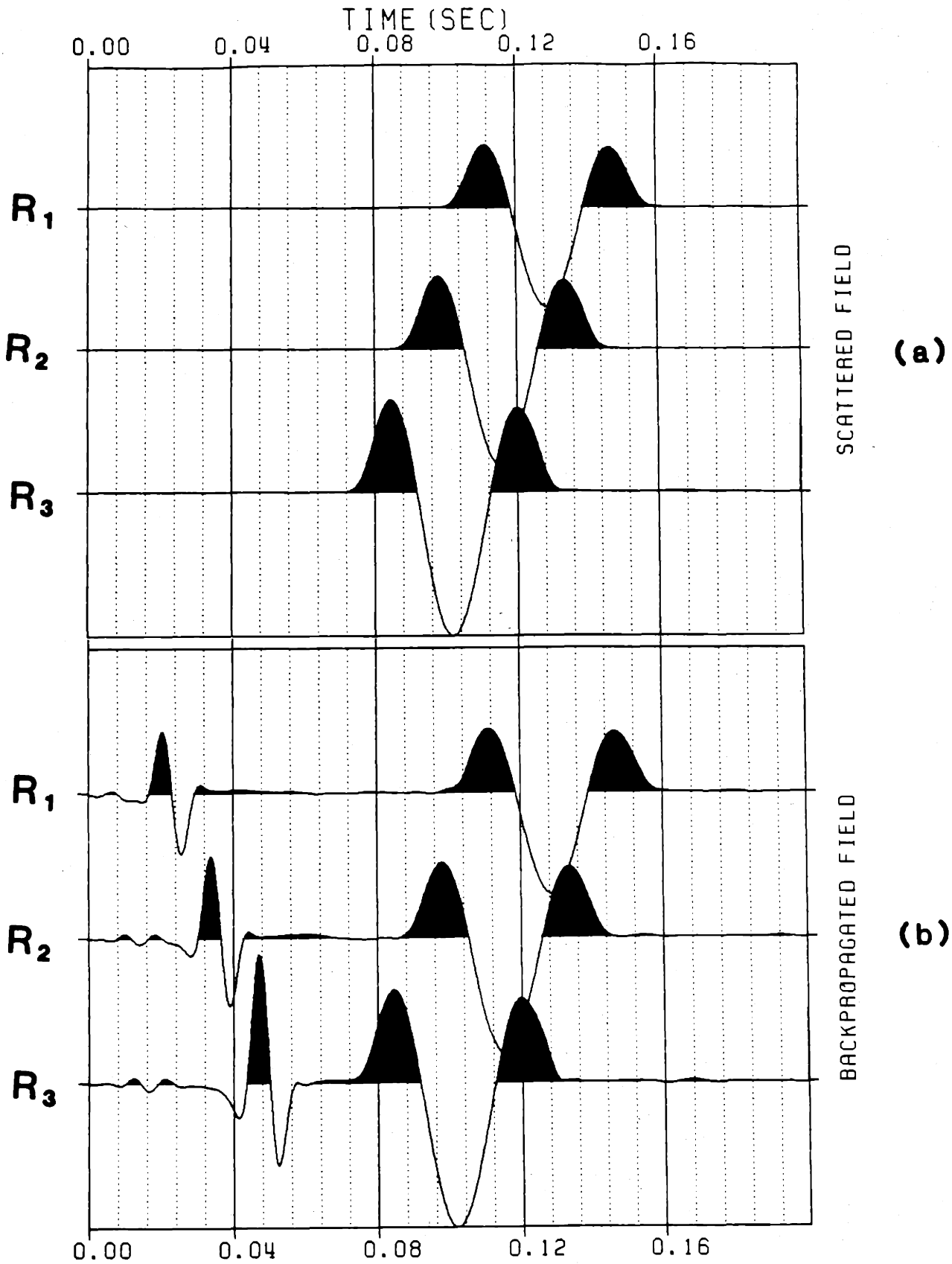

Figure 4.8. Scattered and backpropagated fields observed at R_1, R_2 and R_3; a) $p_s(\underline{r},t)$ b) $p_e(\underline{r},-t)$.

CHAPTER V

Inversion for a Wide-Band Plane-Wave Source

In this chapter we consider the scattering experiment described in Figure 5.1. A constant density acoustic medium is probed by a wide-band plane wave and the scattered field is observed along a receiver array. From equation (2.1.4) the scattered field observed at a receiver located at $\underline{r}_R$ is, within the homogeneous background Born approximation,

$$P_s(\underline{r}_R,\omega) = k^2\, S(\omega) \int_V d\underline{r}'\, \gamma(\underline{r}')\, e^{i\underline{k}_s \cdot \underline{r}'}\, G_0(\underline{r}_R,\underline{r}',\omega)\ , \tag{5.0.1}$$

where $G_0(\underline{r},\underline{r}',\omega)$ is the free space Green's function and $\underline{k}_s$ is the wave-vector of the incident plane wave. As before $S(\omega)$ denotes the Fourier transform of the source excitation, $k = \omega/c$ is the wavenumber, c is a reference velocity and $\gamma(\underline{r}) = \dfrac{c^2}{v(\underline{r})^2} - 1$ is the scattering potential associated to the medium velocity function $v(\underline{r})$. In a scattering experiment the scattered field $P_s(\underline{r},\omega)$ in equation (5.0.1) is not directly observed at the receivers, but can be obtained by subtracting the probing source field (which can be expressed analytically) from the observed total field. Equation (5.0.1) represents the homogeneous background Born approximation of the scattered field. In this approximation it is assumed that the field created by the source propagates through the medium undistorted by the velocity variations. Thus, each point in the

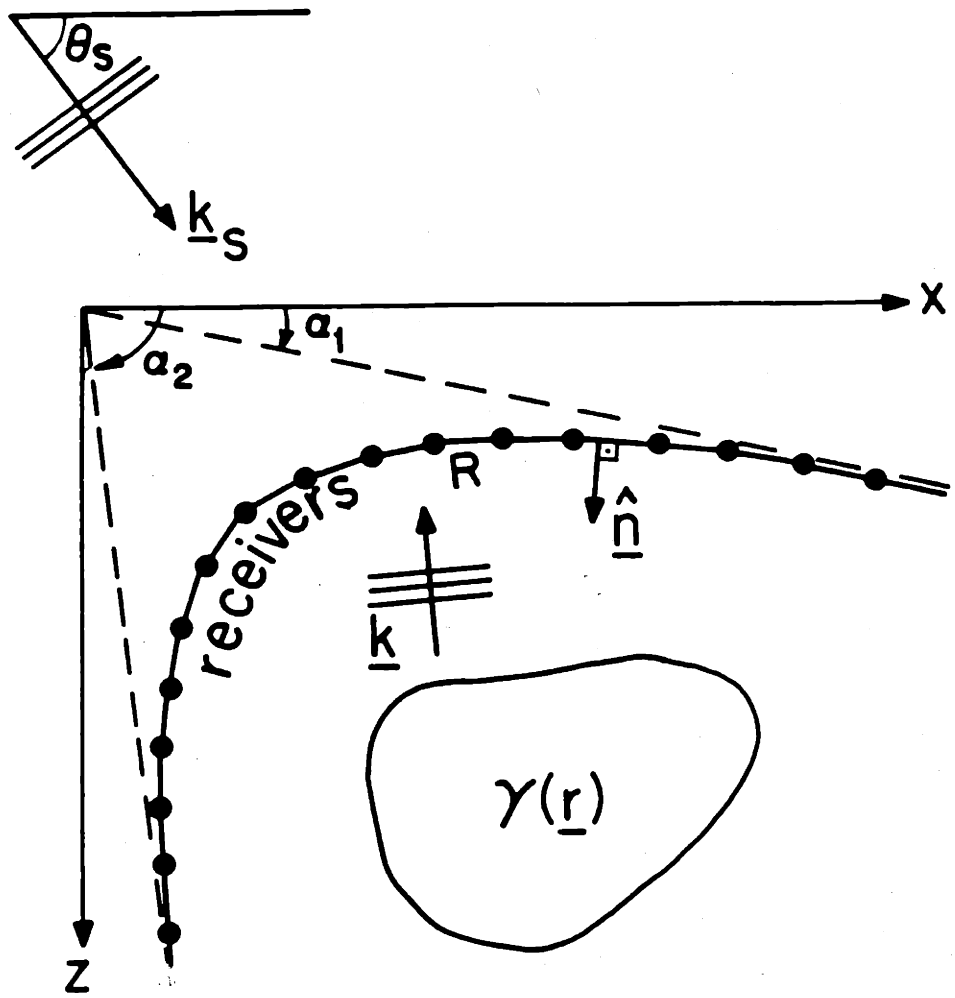

Figure 5.1. Scattering experiment. The medium is probed by a wide-band plane wave and the scattered field is observed along a receiver array asymptotic to angles α_1 and α_2.

medium becomes a secondary point source with source excitation given by $k^2 S(\omega)\gamma(\underline{r})e^{i\underline{k}_s \cdot \underline{r}}$ in the Fourier domain. The scattered field is the field radiated by these secondary sources. Since the field incident on the scatterers is assumed to be independent of the velocity variations, multiple scattering effects are neglected in this model. The inversion problem considered here consists of reconstructing the scattering potential $\gamma(\underline{r})$ from observations of the scattered field at various locations outside the medium. In some cases this can be accomplished only approximately due to insufficient receiver coverage, and/or because the source has only a finite bandwidth.

In this chapter we consider the inversion problem with a single wide-band plane-wave source. This is the dual of the diffraction tomography problem, i.e., instead of using one frequency and all angles of incidence, we use one angle of incidence and all frequencies. We present two methods, which we call the slant-stack and imaging-filtering methods, for partially reconstructing the velocity potential from the observed scattered field. First, it is shown that there is a simple map between the plane-wave component of the scattered field at a fixed angle θ and the projection of the potential at an angle ϕ which is algebraically related to θ and θ_s, where θ_s is the angle of incidence of the probing plane wave. Therefore, projections of the potential at various projection angles can be obtained from the plane-wave scattering amplitudes. The plane-wave scattering amplitudes are obtained from the scattered field by performing a slant-stack or Radon transform. If the receiver array does not surround the medium (incomplete coverage), only an incomplete set of projections can be obtained. For example, if the receivers are located on the surface, the available projection angles are contained in a cone of $\pi/2$. Once the projections are obtained, the velocity potential is

reconstructed either by using the filtered backprojection method for the available angles, or by a multidimensional inverse Fourier transform (after invoking the projection slice theorem). In both cases, we set the missing projections to zero.

The imaging-filtering method consists of two steps. The first step is similar to migration. The observed traces are filtered in time, extrapolated back into the medium and imaged at the source-travel times. The velocity potential is, then, obtained by filtering this image in the spatial domain with a linear space-invariant filter. The filter is independent of the specific geometry of the receiver array and is completely determined by the angle of incidence of the probing plane wave. Again, if the receiver coverage is incomplete, the potential can only be recovered partially. The two methods presented here are quite different conceptually and computationally, however, it can be shown that they give mathematically identical inversion results.

In the following section we obtain the relation between the slant-stack of the scattered wavefield and the projections of the scattering potential γ for the general case when the receiver coverage is incomplete. The slant-stack method of inversion is discussed in Section 5.2. In Sections 5.2.1 and 5.2.2 we consider the special cases of straight-line and weak-curvature receiver arrays, respectively. In Section 5.3 the imaging-filtering method is presented. Several experiments involving plane waves with different angles of incidence and/or different receiver arrays may be performed for a given medium. In such cases inversion results obtained from each experiment must be combined properly in the final result. This issue is discussed in Section 5.4. Synthetic examples illustrating both reconstruction methods for various receiver geometries are given in Section 5.5.

5.1 Relation Between Plane-Wave Components of the Scattered Field and Projections of the Scattering Potential

In this section the relation between the plane-wave scattering amplitude and the velocity scattering potential is derived for an arbitrary receiver array with angular-aperture $[\alpha_2 ; \alpha_1]$ as shown in Figure 4.5. The plane-wave scattering amplitude is obtained from the scattered field by

$$A(\hat{\underline{k}},\omega) = -\int_R d\underline{r}_R \; [\, P_s(\underline{r}_R,\omega)\, \nabla e^{-i\underline{k}\cdot\underline{r}_R} - \nabla\, P_s(\underline{r}_R,\omega)\, e^{-i\underline{k}\cdot\underline{r}_R} \,] \cdot \hat{\underline{n}}(\underline{r}_R) \;, \tag{5.1.1}$$

where R is the surface where the receivers are located, $\hat{\underline{n}}$ is the unit normal vector pointing *towards* the scatterers as in Figure 4.5 and $\underline{k} = k\hat{\underline{k}}$. Let us briefly compare the above equation with the backpropagated field given by equation (4.0.1). It is seen that the Green's function $G_0^*(\underline{r},\underline{r}_R,\omega)$ in equation (4.0.1) is replaced by the exponential $e^{-i\underline{k}\cdot\underline{r}_R}$ in equation (5.1.1). The extrapolated field P_e^* is obtained by collapsing or concentrating the scattered field back inside the medium. In contrast we will see that the scattering potential A is obtained by decomposing the scattered field into its plane-wave components. From equations (5.0.1) and (5.1.1) we have

$$A(\hat{\underline{k}},\omega) = k^2\, S(\omega) \int_V d\underline{r}'\, \gamma(\underline{r}')\, e^{i\underline{k}\cdot\underline{r}'}\, F(\underline{k},\underline{r}') \;, \tag{5.1.2}$$

where the slant-stack kernel F is given by

$$F(\underline{k},\underline{r}') = -\int_R d\underline{r}_R \; [\, G_0(\underline{r}_R,\underline{r}',\omega)\, \nabla e^{-i\underline{k}\cdot\underline{r}_R} - \nabla\, G_0(\underline{r}_R,\underline{r}',\omega)\, e^{-i\underline{k}\cdot\underline{r}_R} \,] \cdot \hat{\underline{n}}(\underline{r}_R) \;.$$

(5.1.3)

Here, $G_0(\underline{r}_R, \underline{r}', \omega)$ is the free space Green's function, and in two-dimensions it is given by

$$G_0(\underline{r}_R, \underline{r}', \omega) = \frac{i}{4} H_0^{(1)}(k|\underline{r}_R - \underline{r}'|) . \tag{5.1.4}$$

Now, consider the arc S of the circle of infinite radius centered at $\underline{r}'$ which is shown in Figure 4.5. Since there are no scatterers within the volume surrounded by the closed surface $R+S$, from the second theorem of Green

$$F(\underline{k}, \underline{r}') = \int_S d\underline{\xi} \left[\frac{i}{4} H_0^{(1)}(k|\underline{\xi} - \underline{r}'|) \frac{\partial}{\partial n} e^{-i\underline{k} \cdot \underline{\xi}} - \frac{\partial}{\partial n} \frac{i}{4} H_0^{(1)}(k|\underline{\xi} - \underline{r}'|) e^{-i\underline{k} \cdot \underline{\xi}} \right] , \tag{5.1.5}$$

where $\frac{\partial}{\partial n}$ denotes the normal derivative on the arc S, i.e. $\frac{\partial}{\partial n} \equiv \hat{\underline{n}}(\underline{\xi}) \cdot \nabla_{\underline{\xi}}$ and $\hat{\underline{n}}$ is the unit normal vector as shown in Figure 4.5. Let (ρ, ϕ) be the polar coordinates centered at $\underline{r}'$, as shown in Figure 4.6, and let θ be the angle corresponding to the unit vector $\hat{\underline{k}}$. Then, in this coordinate system the boundary integral in equation (5.1.5) takes the form

$$F(\underline{k}, \underline{r}') = e^{-i\underline{k} \cdot \underline{r}'} \lim_{\rho \to \infty} \rho \int_{\alpha_2}^{\alpha_1} d\phi \left[\frac{i}{4} H_0^{(1)}(k\rho) \frac{\partial}{\partial \rho} e^{-ik\rho\cos(\phi - \theta)} - \right.$$

$$\left. \frac{\partial}{\partial \rho} \frac{i}{4} H_0^{(1)}(k\rho) e^{-ik\rho\cos(\phi - \theta)} \right] . \tag{5.1.6}$$

For $\rho \to \infty$ and $k \neq 0$, we have the following asymptotic expansion of the Green's

function and its normal derivative

$$\lim_{\rho \to \infty} \frac{i}{4} H_0^{(1)}(k\rho) = \lim_{\rho \to \infty} \frac{e^{i\frac{\pi}{4} sgn(\omega)}}{(8\pi)^{1/2}} \frac{e^{ik\rho}}{|k|^{1/2}\rho^{1/2}} , \tag{5.1.7}$$

$$\lim_{\rho \to \infty} \frac{\partial}{\partial \rho} \frac{i}{4} H_0^{(1)}(k\rho) = \lim_{\rho \to \infty} ik \frac{i}{4} H_0^{(1)}(k\rho) . \tag{5.1.8}$$

Here, the derivative of the amplitude term $\rho^{-1/2}$ is neglected as ρ goes to infinity. Consequently, as $\rho \to \infty$, the boundary integral becomes

$$F(\underline{k},\underline{r}') = -e^{-i\underline{k}\cdot\underline{r}'} \lim_{\rho \to \infty} \frac{i}{4} H_0^{(1)}(k\rho)\, ik\rho$$

$$\int_{\alpha_2}^{\alpha_1} d\phi \, [\cos(\phi - \theta) + 1] \, e^{-ik\rho\cos(\phi - \theta)} . \tag{5.1.9}$$

The above integral can be evaluated by the method of stationary phase. The stationary points ϕ_0 of the phase function are given by

$$\frac{\partial}{\partial \phi} k\cos(\phi - \theta) \,|_{\phi = \phi_0} = 0 , \tag{5.1.10}$$

so that $\phi_0 = \theta$, $\theta+\pi$. For $\phi_0 = \theta + \pi$ the integrand of equation (5.1.9) vanishes, therefore the only stationary point to be considered is $\phi_0 = \theta$. Now, if θ is not within the integration range $[\alpha_2 ; \alpha_1]$, there is no contribution from this point and the integral is zero. However, if $\theta \in [\alpha_2 ; \alpha_1]$ equation (5.1.9) becomes

$$F(\underline{k},\underline{r}') = -e^{-i\underline{k}\cdot\underline{r}'} \lim_{\rho\to\infty} \frac{i}{4} H_0^{(1)}(k\rho)\, ik\rho\, e^{i\frac{\pi}{4}sgn(\omega)} \left(\frac{2\pi}{k\rho}\right)^{1/2} 2e^{-ik\rho} . \tag{5.1.11}$$

Finally, using the asymptotic form of the Green's function given in equation (5.1.7), and noting that

$$ik\rho\, e^{i\frac{\pi}{2}sgn(\omega)} = -|k\rho| , \tag{5.1.12}$$

we obtain

$$\begin{aligned} F(\underline{k},\underline{r}') &= e^{i\underline{k}\cdot\underline{r}'} \quad ; \quad \theta \in [\alpha_2 ; \alpha_1] \\ &= 0 \quad ; \quad \text{otherwise} . \end{aligned} \tag{5.1.13}$$

Using this expression in equation (5.1.2), we find that the plane-wave scattering amplitude is given by

$$\begin{aligned} A(\hat{\underline{k}},\omega) &= k^2 S(\omega) \int_V d\underline{r}'\, \gamma(\underline{r}')\, e^{-i(\underline{k}-\underline{k}_s)\cdot\underline{r}'} \quad ; \quad \theta \in [\alpha_2 ; \alpha_1] \\ &= 0 \quad ; \quad \text{otherwise} , \end{aligned} \tag{5.1.14}$$

where θ is the angle corresponding to the unit vector $\hat{\underline{k}}$. The above relation between the plane-wave components of the scattered field and the potential is valid even if the receivers provide incomplete coverage of the scattering medium. This means that the receiver array does not completely surround the domain V where the scattering potential $\gamma(\underline{r})$ is nonzero. When R is an open surface asymptotic to radial lines with angles

α_1 and α_2 (as indicated in Figure 5.1) we have shown that $A(\hat{\underline{k}},\omega)$ is given by equation (5.1.14). It is seen from this identity that, for fixed $\hat{\underline{k}}$ and ω, the plane-wave amplitude is related to one point in the Fourier transform of the potential. If the receiver array surrounds the medium, we have $[\alpha_2;\alpha_1] = [0;2\pi]$ and equation (5.1.14) corresponds to the complete coverage case considered by Devaney and Beylkin (1984).

We will now derive a relationship between the plane-wave scattering amplitude for fixed $\hat{\underline{k}}$ and the projection of the potential onto a line defined by a unit vector $\hat{\underline{u}}$. We consider a two-dimensional problem (the receivers are located on a curve and the velocity is a function of x and z), however, the three-dimensional formulation can be obtained following similar steps. Let

$$\hat{\underline{u}} = \begin{bmatrix} \cos\phi \\ \sin\phi \end{bmatrix} \equiv \frac{\hat{\underline{k}} - \hat{\underline{k}}_s}{|\hat{\underline{k}} - \hat{\underline{k}}_s|} , \tag{5.1.15a}$$

$$u \equiv k\,|\hat{\underline{k}} - \hat{\underline{k}}_s| = k\,2\,|\hat{\underline{u}} \cdot \hat{\underline{k}}_s| , \tag{5.1.15b}$$

i.e., $\hat{\underline{u}}$ is the unit vector along the direction $\underline{k}-\underline{k}_s$, and u is obtained by multiplying the wavenumber k by the length of $\hat{\underline{k}}-\hat{\underline{k}}_s$ as shown in Figure 5.2. The angle ϕ and the magnitude u can be simply related to the angles θ and θ_s as follows

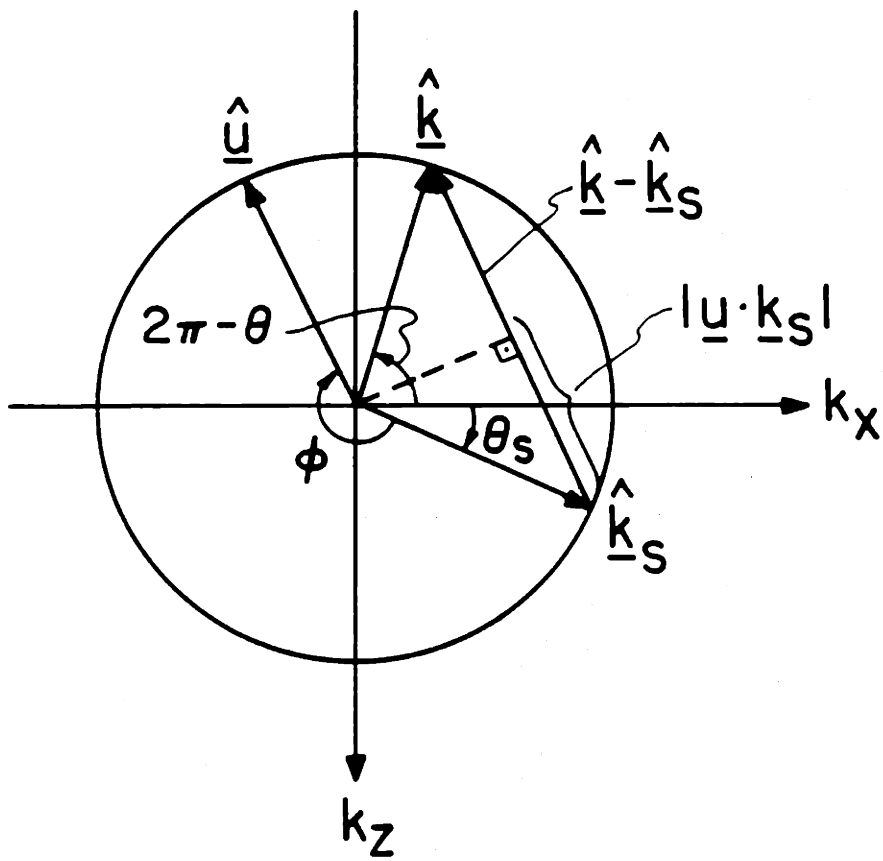

Figure 5.2. The relation between the angle of incidence θ_s of the plane-wave source, the angle θ of the scattered plane wave and the projection angle ϕ.

$$\phi = \frac{\theta + \theta_s \pm \pi}{2} , \tag{5.1.16a}$$

$$u = k\ 2|\cos(\phi - \theta_s)| = k\ 2|\sin(\frac{\theta - \theta_s}{2})| , \tag{5.1.16b}$$

where the sign of ϕ in equation (5.1.16a) is chosen such that $\theta_s + \pi/2 < \phi < \theta_s + 3\pi/2$. Replacing the exponent $\underline{k} - \underline{k}_s$ in equation (5.1.14) by $u\hat{\underline{u}}$, we find that for an angle θ which belongs to the angular aperture of the receiver array (i.e., $\theta \in [\ \alpha_2\ ;\ \alpha_1\ ]$) we have

$$A(\hat{\underline{k}},\omega) = k^2\ S(\omega) \int_V d\underline{r}'\ \gamma(\underline{r}')\ e^{-iu\hat{\underline{u}}\cdot\underline{r}'} . \tag{5.1.17}$$

Thus, for fixed $\hat{\underline{k}}$ and varying ω, the plane-wave scattering amplitude gives the Fourier transform of γ along a line with angle ϕ, where ϕ is algebraically related to the angle θ of $\hat{\underline{k}}$ via equation (5.1.16a). If we consider all available plane-wave components we obtain a cone in the Fourier transform domain of γ, where the angles ϕ contained in this cone are given by

$$\phi \in \Phi = \left[\frac{\alpha_2 + \theta_s \pm \pi}{2} ;\ \frac{\alpha_1 + \theta_s \pm \pi}{2} \right] , \tag{5.1.18}$$

as shown in Figure 5.3. By taking the Fourier transform of both sides of equation (5.1.17) the projection of the potential onto the line defined by $\hat{\underline{u}}$ is given by

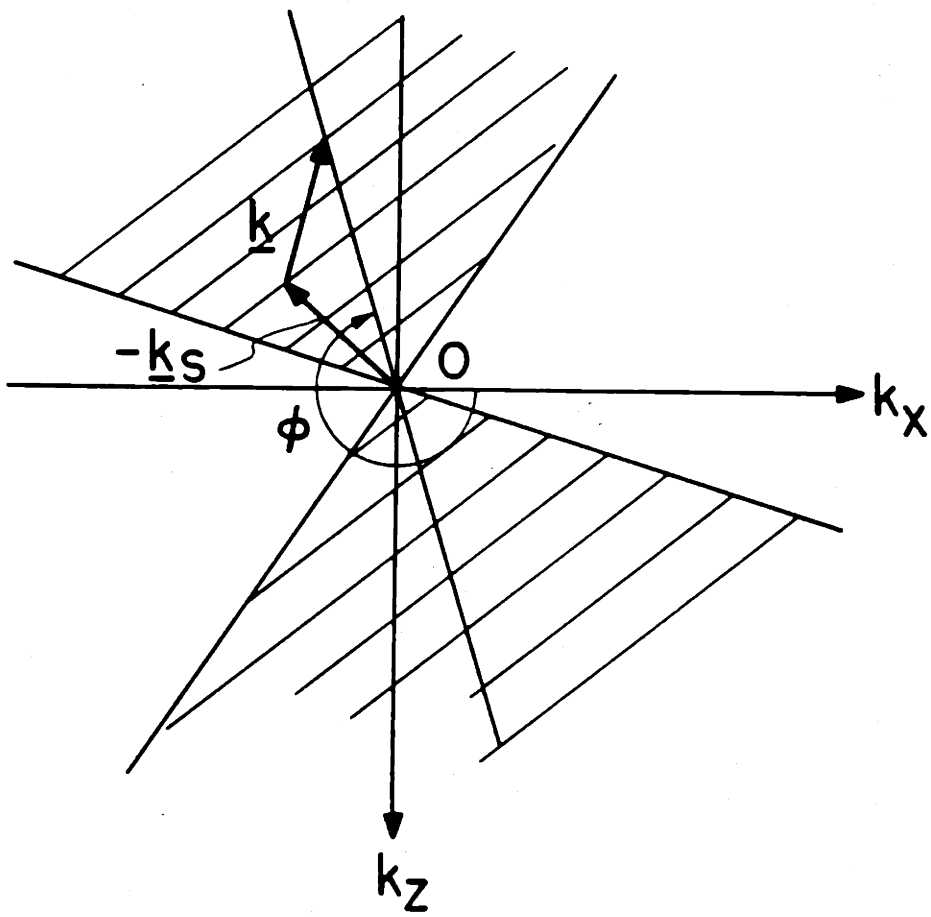

Figure 5.3. Coverage in the Fourier transform domain of the potential γ.

$$\hat{\gamma}(\hat{\underline{u}},s) = \int_V d\underline{r}'\, \gamma(\underline{r}')\, \delta(\hat{\underline{u}} \cdot \underline{r}' - s)$$

$$= \frac{1}{2\pi} \int_{-\infty}^{\infty} du\, \frac{A(\hat{\underline{k}},\omega)}{k^2 S(\omega)}\, e^{ius} . \tag{5.1.19}$$

Finally, changing the integral variable from u to k according to equation (5.1.15b), we obtain

$$\hat{\gamma}(\hat{\underline{u}},s) = \frac{1}{\pi} |\hat{\underline{u}} \cdot \hat{\underline{k}}_s| \int_{-\infty}^{\infty} dk\, \frac{A(\hat{\underline{k}},\omega)}{k^2 S(\omega)}\, e^{ik2|\hat{\underline{u}} \cdot \hat{\underline{k}}_s|s} . \tag{5.1.20}$$

5.2 Inversion by Slant-Stack

The projections of the velocity potential are given by equation (5.1.20) when $\hat{\underline{k}}$ is within the angular-aperture of the receiver array. The projections for the remaining angles cannot be obtained from the data. Therefore, if the receivers do not surround the medium, only a subset of the projections can be recovered. In this case, the reconstruction problem is similar to the limited angle tomography problem. The range of available projection angles is determined by the angles α_1, α_2 specifying the receiver array and by the angle θ_s of the incident plane wave (equation (5.1.15a)). In the discussion above we have seen that for fixed $\hat{\underline{k}}$ and varying ω the plane-wave scattering amplitude gives the Fourier transform of γ along a line with angle ϕ. From the projection-slice theorem the inverse Fourier transform along this line gives the projection of the potential γ onto the line defined by the angle ϕ. This is the dual of the problem considered in diffraction tomography, where for fixed ω and varying $\hat{\underline{k}}$ the plane-wave scattering amplitude gives the Fourier transform of the potential along semi-circular trajectories.

The velocity potential is reconstructed from its projections by Radon's inversion formula (Dudgeon and Mersereau, 1984)

$$\gamma(\underline{r}) = \frac{1}{2\pi} \int_{\Phi} d\hat{\underline{u}}\ \hat{\gamma}_f(\hat{\underline{u}}, \hat{\underline{u}} \cdot \underline{r}) , \tag{5.2.1}$$

where Φ is the range of available projections specified by equation (5.1.18), and where the filtered projections are defined as

$$\hat{\gamma}_f(\hat{\underline{u}},\rho) \equiv \frac{1}{2\pi} \int_{-\infty}^{\infty} du\ e^{iu\rho}\,|u| \int_{-\infty}^{\infty} ds\ e^{-ius}\ \hat{\gamma}(\hat{\underline{u}},s)\ . \tag{5.2.2}$$

From equations (5.1.15b) and (5.1.19), the filtered projections can be written in terms of the scattering amplitude as

$$\hat{\gamma}_f(\hat{\underline{u}},\rho) = \frac{2}{\pi}\,|\hat{\underline{u}}\cdot\hat{\underline{k}}_s|^2 \int_{-\infty}^{\infty} dk\ \frac{A(\hat{\underline{k}},\omega)}{|k|S(\omega)}\ e^{ik|\hat{\underline{u}}\cdot\hat{\underline{k}}|\rho}\ . \tag{5.2.3}$$

For a given array geometry, the scattering amplitude obtained in equation (5.1.1) can be substituted in the above equation, thus providing a direct relation between the observed data and the projections of the potential.

From equation (5.1.1), we see that both the scattered field and its normal derivative are needed to obtain the plane-wave scattering amplitude. It is easy to show that for a straight-line receiver array the two terms inside the brackets in equation (5.1.1) become identical, so that only the scattered field itself is needed to obtain the scattering amplitude. In general the normal derivative of the scattered field along a curve (or surface) can be obtained from the field itself, but there is no simple analytical expression between these two quantities. In the next section we consider the case of a straight-line receiver array.

5.2.1 Straight-line receiver array

Consider the observation geometry shown in Figure 5.4, where receivers are located on a straight line defined by the unit vector $\hat{\underline{s}}$. In this case, the plane-wave scattering amplitude becomes

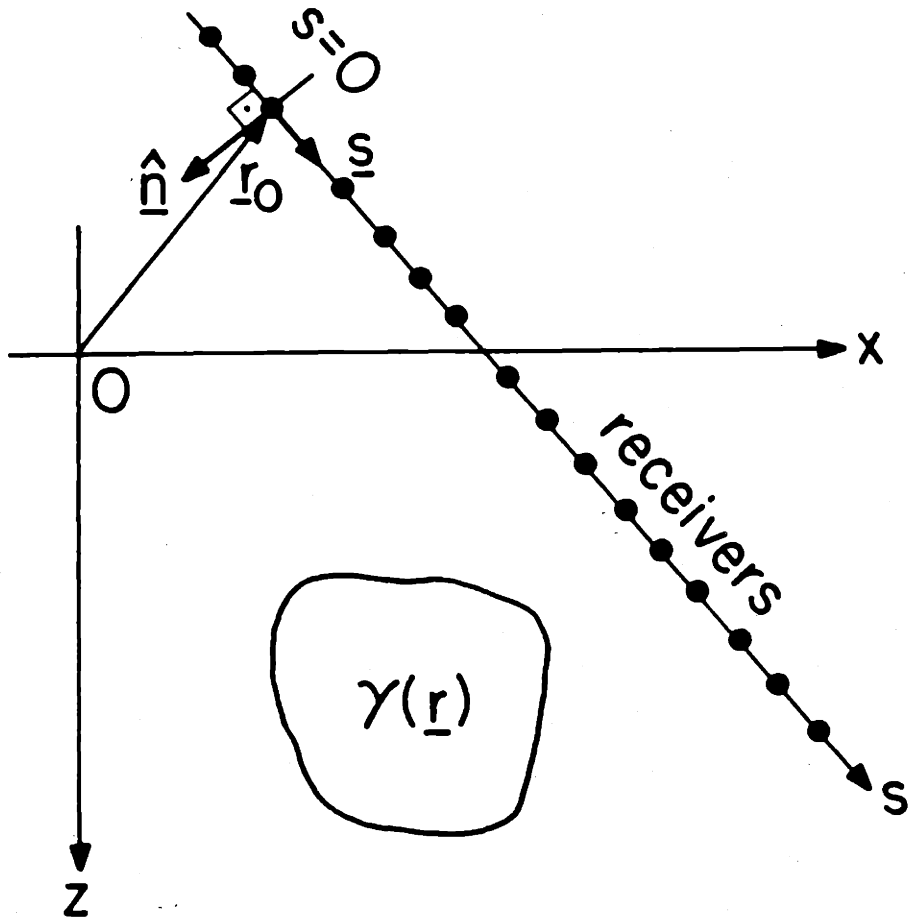

Figure 5.4. Straight-line receiver array; $\hat{\underline{s}}$ is the unit vector along the array, $\hat{\underline{n}}$ the normal unit vector pointing towards the scatterers, $\underline{r}_0$ an arbitrary origin along the array.

$$A(\hat{\underline{k}},\omega) = 2\,\hat{\underline{n}} \cdot \hat{\underline{k}} \int_{-\infty}^{\infty} ds\; ik\; P_s(s,\omega)\; e^{-i\underline{k} \cdot (\underline{r}_0 + s\hat{\underline{s}})}\,, \tag{5.2.4}$$

where $\hat{\underline{n}}$ is the unit vector pointing towards the scatterers and $\underline{r}_0$ is the origin of the receiver array indicated in Figure 5.4. From equations (5.2.3) and (5.2.4), the filtered projections of the potential can be expressed directly in terms of the observed scattered field as follows

$$\hat{\gamma}_f(\hat{\underline{u}},\rho) = \frac{4}{\pi} |\hat{\underline{u}} \cdot \hat{\underline{k}}_s|^2\, \hat{\underline{n}} \cdot \hat{\underline{k}}$$

$$\int_{-\infty}^{\infty} ds \int_{-\infty}^{\infty} dk\; i\; sgn(\omega)\; \frac{P_s(s,\omega)}{S(\omega)}\; e^{-ik[\hat{\underline{k}} \cdot (\underline{r}_0 + s\hat{\underline{s}}) - 2|\hat{\underline{u}} \cdot \hat{\underline{k}}_s|\rho]}\,, \tag{5.2.5}$$

where $sgn(\omega)$ denotes the sign of ω. The expression inside the integral in equation (5.2.5) can be interpreted as follows :

1) First, the source signature is deconvolved, so that $P_s(s,\omega)$ is divided by $S(\omega)$.

2) The deconvolved data is then Hilbert transformed, which corresponds to a multiplication by $i\; sgn(\omega)$.

3) The dk integral corresponds to an inverse Fourier transform.

The filtered projections can therefore be expressed in the time domain as

$$\hat{\gamma}_f(\hat{\underline{u}},\rho) = \frac{8}{c} |\hat{\underline{u}} \cdot \hat{\underline{k}}_s|^2\, \hat{\underline{n}} \cdot \hat{\underline{k}}\,,$$

$$\int_{-\infty}^{\infty} ds\ P_d^H(s,\ t = \frac{1}{c}\ \hat{\underline{k}} \cdot \underline{r}_0 - \frac{2}{c}\ |\hat{\underline{u}} \cdot \hat{\underline{k}}_s|\ \rho + \frac{1}{c}\ \hat{\underline{k}} \cdot \hat{\underline{s}}\ s)\ , \tag{5.2.6}$$

where $P_d^H(s,t)$ is the deconvolved and Hilbert transformed data and where the ds integral corresponds to a slant-stack operation.

5.2.2 Weak-curvature receiver array

If the receiver array is not a straight-line both the scattered field and its normal derivative are needed to obtain the projections. It can be seen from equations (5.1.1) and (5.2.3) that in this case the projections are obtained by slant-stacking both the field and its normal derivative. This increases the processing time by a factor of two. Moreover, if the normal derivative field is not observed, it must be obtained from the field observations numerically. However, if the local radius of curvature of the receiver array is much larger than the dominant wavelength, the normal derivative field can be approximately written in terms of the field along the array. The simplest way is to assume that the receiver array is locally a straight line (Devaney and Beylkin, 1984). With this assumption the plane-wave scattering amplitude becomes

$$A(\hat{\underline{k}},\omega) = 2 \int_{-\infty}^{\infty} ds\ \hat{\underline{n}}(s) \cdot \hat{\underline{k}}\ ik\ P_s(\underline{r},\omega)\ e^{-i\underline{k} \cdot [\underline{r}_0 + s\hat{\underline{s}}(s)]}\ . \tag{5.2.7}$$

This is essentially the same expression as in equation (5.2.4) except that the tangent ($\hat{\underline{s}}$) and normal ($\hat{\underline{n}}$) unit vectors are functions of the receiver location. Therefore, the filtered projections in this case are given by

$$\hat{\gamma}_f(\hat{\underline{u}},\rho) = \frac{8}{c}\,|\hat{\underline{u}}\cdot\hat{\underline{k}}_s|^2$$

$$\int_{-\infty}^{\infty} ds\ \hat{\underline{n}}(s)\cdot\hat{\underline{k}}\ P_d^H[s,\ t = \frac{1}{c}\,\hat{\underline{k}}\cdot\underline{r}_0 - \frac{2}{c}\,|\hat{\underline{u}}\cdot\hat{\underline{k}}_s|\,\rho + \frac{1}{c}\,\hat{\underline{k}}\cdot\hat{\underline{s}}(s)\ s]\ . \tag{5.2.8}$$

For straight-line and weak-curvature receiver arrays, the slant-stacking reconstruction method consists therefore in obtaining first the filtered projections $\hat{\gamma}_f(\hat{\underline{u}},\rho)$ via equations (5.2.6) or (5.2.8), and then in using (5.2.1) to reconstruct the potential $\gamma(\underline{r})$.

5.3 Inversion by Imaging-Filtering

The second inversion method considered here consists of a sequence of steps where the scattered field is first backpropagated inside the medium, imaged at the travel times from source to image point and then filtered in space. We consider the extrapolated wavefield $P_e(\underline{r},\omega)$ defined by

$$P_e^*(\underline{r},\omega) \equiv \int_R d\underline{r}_R \; [\; P_s(\underline{r}_R,\omega)\; \nabla G_0^*(\underline{r},\underline{r}_R,\omega) \; - \; \nabla P_s(\underline{r}_R,\omega)\; G_0^*(\underline{r},\underline{r}_R,\omega)\;] \cdot \hat{\underline{n}}(\underline{r}_R)\;, \tag{5.3.1}$$

where R denotes the curve where the receivers are located, $\hat{\underline{n}}$ is the normal unit vector pointing towards the scatterers, and G_0^* is the complex conjugate of the Green's function. The backpropagated field obtained by this equation was discussed in Chapter 4. From equation (4.2.2) and by using the homogeneous Born approximation, i.e. by substituting $P(\underline{r}',\omega) \approx k^2\, S(\omega)\, e^{i\underline{k}\cdot\underline{r}'}$, the extrapolated field for a plane-wave source is represented by

$$P_e^*(\underline{r},\omega) = k^2\, S(\omega) \int_V d\underline{r}'\; \gamma(\underline{r}')\; e^{i\underline{k}\cdot\underline{r}'}\; E(\underline{r},\underline{r}',\omega)\;. \tag{5.3.2}$$

From equation (4.2.10) the extrapolated field kernel for the experiment geometry shown in Figure 5.1 is given by

$$E(\underline{r},\underline{r}',\omega) = \frac{i\; sgn(\omega)}{4\pi} \int_{\alpha_2}^{\alpha_1} d\theta\; e^{i\underline{k}\cdot(\underline{r}-\underline{r}')}\;, \tag{5.3.3}$$

where θ is the angle corresponding to the unit vector $\hat{\underline{k}}$ and $\underline{k} = k\hat{\underline{k}}$. Let now

$$\beta(\underline{r}) \equiv -\frac{1}{2\pi} \int_{-\infty}^{\infty} d\omega \, \frac{P_e^*(\underline{r},\omega)}{i\omega \, S(\omega)} \, e^{-i\underline{k}_s \cdot \underline{r}} \, , \tag{5.3.4}$$

be the function obtained by filtering the extrapolated field and then imaging it at the source travel times $\tau(\underline{r}) = \frac{1}{c} \, \hat{\underline{k}}_s \cdot \underline{r}$ (which corresponds to a plane-wave source and a homogeneous background). Here the filter $[i\omega S(\omega)]^{-1}$ corresponds to a deconvolution followed by integration in time. Equation (5.3.1) implies that the filtered extrapolated field can be obtained by first filtering the scattered field and then backpropagating the resulting traces into the medium. The travel time image $\beta(\underline{r})$ is similar to the migrated image except for the time integration performed before extrapolation. It turns out that $\beta(\underline{r})$ is simply a spatially filtered version of the velocity potential $\gamma(\underline{r})$ where the filter impulse response depends on the incidence angle of the plane wave and the angle-aperture of the receiver array. To see this, combine equations (5.3.2), (5.3.3) and (5.3.4). Then, the travel time image can be expressed as

$$\beta(\underline{r}) = \int_V d\underline{r}' \, \gamma(\underline{r}') \, g(\underline{r}-\underline{r}') \, , \tag{5.3.5}$$

where $g(\cdot)$ is a space-invariant filter with point spread function

$$g(\underline{r}) = -\frac{1}{8\pi^2} \int_{\alpha_2}^{\alpha_1} d\theta \int_{-\infty}^{\infty} dk \, |k| \, e^{ik(\hat{\underline{k}}-\hat{\underline{k}}_s) \cdot \underline{r}} \, . \tag{5.3.6}$$

Thus, the image $\beta(\underline{r})$ represents the velocity potential filtered by the space-invariant filter given above. This filter has a simple interpretation in the Fourier domain.

Consider the change of variables given by equations (5.1.15a,b) and let ϕ be the angle corresponding to the unit vector $\hat{\underline{u}}$. In the new coordinates (ϕ , u) the filter can be written as

$$g(\underline{r}) = -\frac{1}{16\pi^2} \int_{\Phi} \frac{d\phi}{|\hat{\underline{u}} \cdot \hat{\underline{k}}_s|^2} \int_{-\infty}^{\infty} du\, |u|\, e^{iu\hat{\underline{u}} \cdot \underline{r}} , \tag{5.3.7}$$

where Φ is the integration range for the angles ϕ corresponding to $\theta \in [\alpha_2 ; \alpha_1]$. Define an extended range of angles Θ such that if $\phi \in \Phi$ then both ϕ and $\phi + \pi \in \Theta$. Then, equation (5.3.7) becomes

$$g(\underline{r}) = -\frac{1}{4\pi^2} \int_{\Theta} d\phi \int_{0}^{\infty} du\; u\; e^{iu\hat{\underline{u}} \cdot \underline{r}} \frac{1}{4|\hat{\underline{u}} \cdot \hat{\underline{k}}_s|^2} ,$$

$$= \mathbf{FT}^{-1} \left\{ -\frac{N_{\Theta}}{4|\hat{\underline{u}} \cdot \hat{\underline{k}}_s|^2} \right\} , \tag{5.3.8}$$

where $\mathbf{FT}^{-1}$ denotes the multidimensional inverse Fourier transform and

$$N_{\Theta} = 1 \qquad \phi \in \Theta$$

$$= 0 \quad ; \quad \text{otherwise} . \tag{5.3.9}$$

The Fourier magnitude of the filter $g(\underline{r})$ for a line array with the plane wave at normal incidence is shown in Figure 5.5. From equation (5.3.5), we see that the potential $\gamma(\underline{r})$ can be obtained by deconvolving the image $\beta(\underline{r})$ with the filter $g(\underline{r})$. However, in general the inverse filter does not exist because of the zero region of N_{Θ}

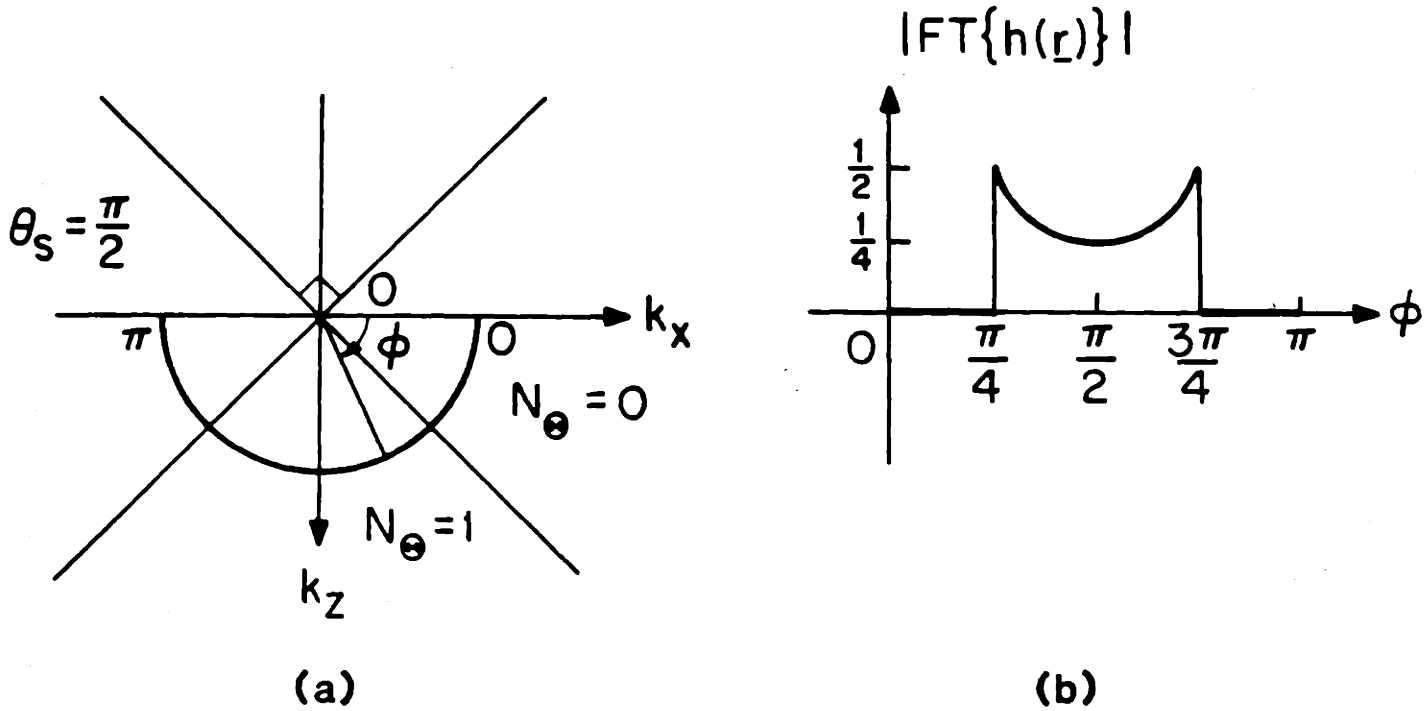

Figure 5.5. Fourier domain representation of the filter relating the migrated image to the velocity potential. The filter which is shown corresponds to the experiment where the receiver array is on the surface (x axis) and the probing plane-wave is normally incident ($\theta_s = \pi/2$). (a) Zero and nonzero regions in the Fourier domain. (b) Fourier magnitude of the filter along the semi-circle shown in (a).

in the Fourier transform of $h(\underline{r})$. This zero region is determined by the array geometry and the incidence angle of the plane wave. It can be shown that, in fact, the zero region N_Θ corresponds to the missing projections of the potential discussed in Section 5.2. Since we cannot deconvolve in this region, the Fourier transform of γ cannot be recovered in the domain where N_Θ is zero. Although other choices could be made, we simply set the Fourier transform of γ to zero in this region. This corresponds to setting the missing projections to zero in the slant-stack method. A partial reconstruction $\gamma_{REC}(\underline{r})$ of the potential is then given by

$$\gamma_{REC}(\underline{r}) = \mathbf{FT}^{-1}\left\{ -4|\hat{\underline{u}} \cdot \hat{\underline{k}}_s|^2 \, \tilde{\beta}(u\hat{\underline{u}}) \right\}, \tag{5.3.10}$$

where $\tilde{\beta}(\underline{u})$ is the spatial Fourier transform of $\beta(\underline{r})$.

The imaging-filtering method can be summarized as follows. In the first step, the observed scattered field is deconvolved by the source wavelet, integrated in time and backpropagated into the medium. The backpropagation can be done by using the Kirchhoff integral in equation (5.3.1). Note that, except for the straight-line array case, both the field and its normal derivative are required in the Kirchhoff integral. An alternative way to obtain the extrapolated field is to solve the boundary value problem numerically by the finite-difference method. As we showed before the observations of the field alone are sufficient to obtain the extrapolated field. This is done by running the finite-difference algorithm without any sources, but with the time-reversed scattered field as the boundary values at the receiver locations. In the second step of the imaging-filtering method the extrapolated field is imaged at every point in the medium

at the time corresponding to the travel time of the incident source field to that point. For the homogeneous background problem, the travel times can be computed analytically. In the third and final step, the resulting travel time image is filtered by the approximate inverse filter of the point spread function (equation 5.3.10).

5.4 Multiple Source Experiment

In the previous sections it was shown that if the receiver array does not surround the scatterers, the velocities of the medium can only be reconstructed partially. In the case of a plane-wave excitation the partial coverage can be best understood in the Fourier transform domain of the scattering potential. For a receiver array with angular aperture [α_1 ; α_2] the observable region of the Fourier space is contained in a cone given by equation (5.1.18), where θ_s is the angle of incidence of the probing plane wave. The region of coverage of a straight line array located along the x axis is shown in Figure 5.3 as a function of the source wave-vector $\underline{k}_s$. In practice, since the receivers arrays are not infinitely long the actual coverage is somewhat less than what is predicted for infinite arrays. One way to obtain more coverage is to perform several experiments with sources arranged in such a way that each source covers a different region in the Fourier space. The images reconstructed for each source separately can then be added together in the space domain to obtain a combined image. For example, suppose that for a straight line array located along the x axis we perform two scattering experiments with plane wave sources such that $\underline{k}_{s_2} = -\underline{k}_{s_1}$, where $\underline{k}_{s_1}$ and $\underline{k}_{s_2}$ are the wave-vectors of the probing waves. Then, as shown in Figure 5.6, these two experiments provide complementary coverage in the Fourier domain so that the scattering potential can be reconstructed completely by simply adding the corresponding images in the space domain. However, in general the regions of coverage provided by several experiments overlap. In such cases the images reconstructed from each experiment should not be averaged in the space domain. This is because

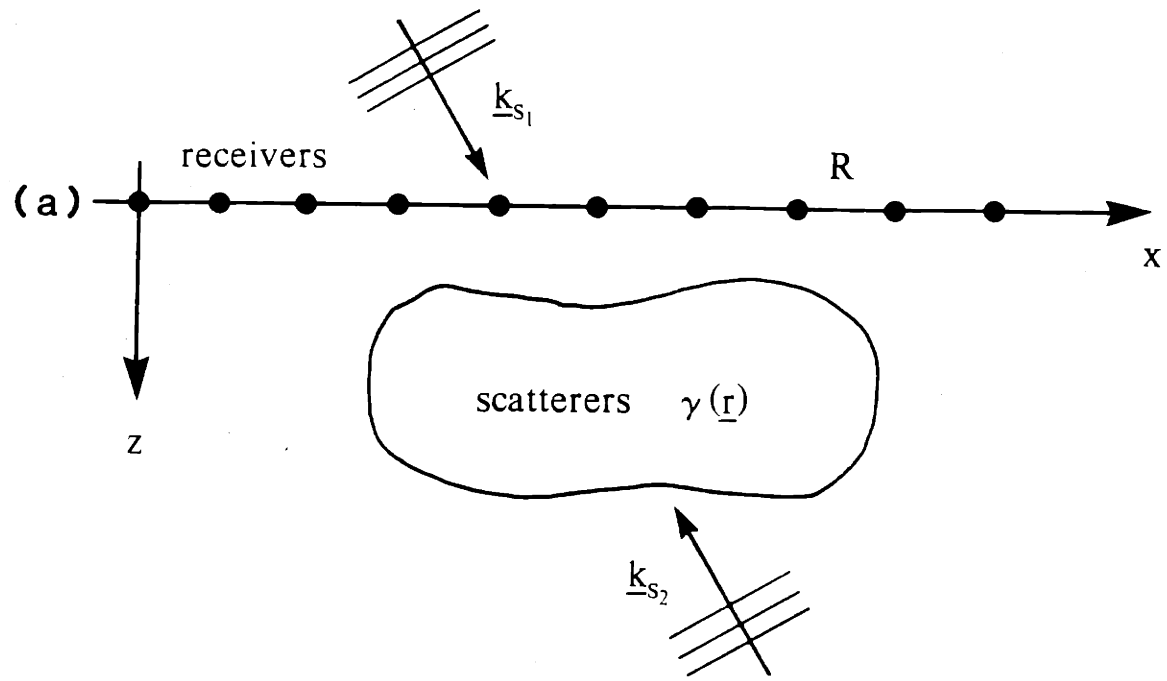

Figure 5.6. Complete coverage in the Fourier domain from two experiments. (a) Two scattering experiments are performed with probing wave-vectors $\underline{k}_{s_1}$ and $\underline{k}_{s_2}$ such that $\underline{k}_{s_2} = -\underline{k}_{s_1}$. The scattered field is observed along the x axis. (b) Region of coverage in the Fourier domain of the potential $\tilde{\gamma}(k_x, k_z)$.

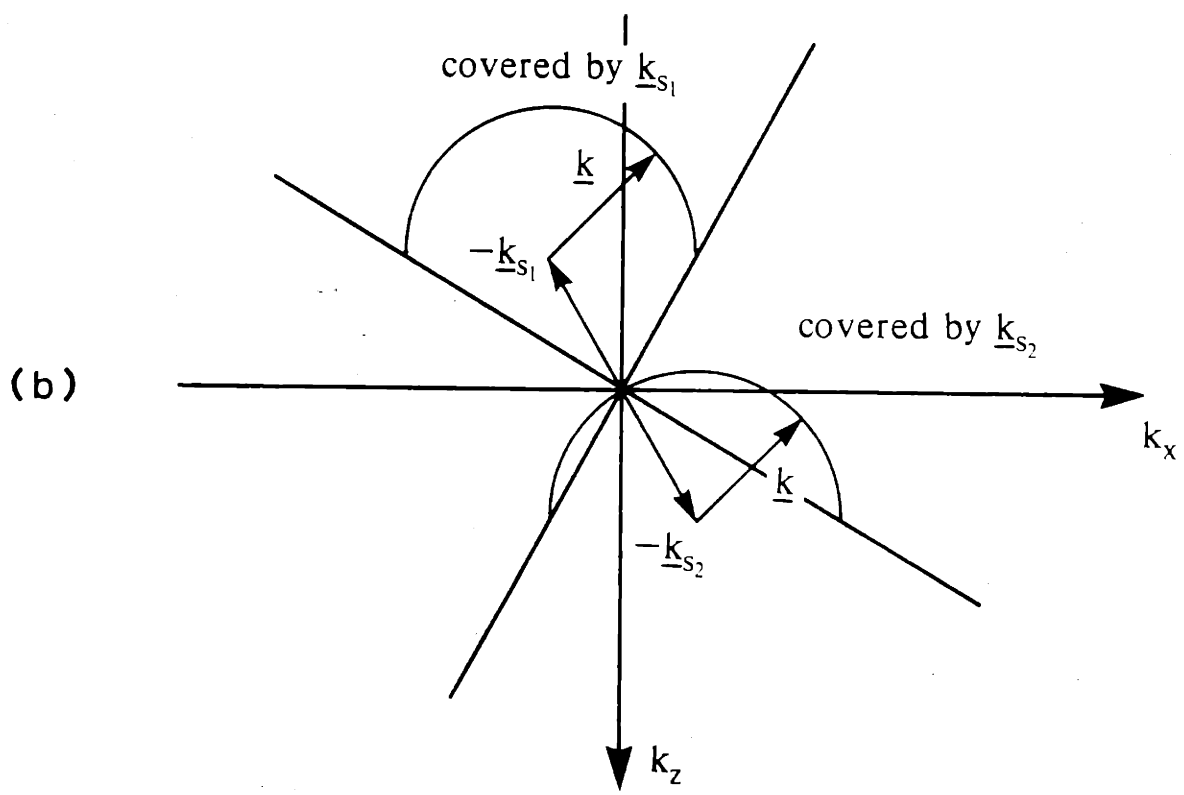

averaging in space is the same as averaging at every point in the Fourier domain. Consequently, this procedure amplifies the overlapping regions with respect to the other Fourier components, resulting in a distorted image. Instead, averaging should be performed directly in the Fourier domain by taking the redundancy into account at each point separately. In other words, the images obtained from several experiments are added together and Fourier transformed. The region of coverage for each experiment depends only on the location of the receiver array and the angle of incidence of the source. Then, at every point in the Fourier domain, the values should be divided by the redundancy. After this weighting the final image is obtained by an inverse Fourier transform. A simple example for a two source experiment is shown in Figure 5.7

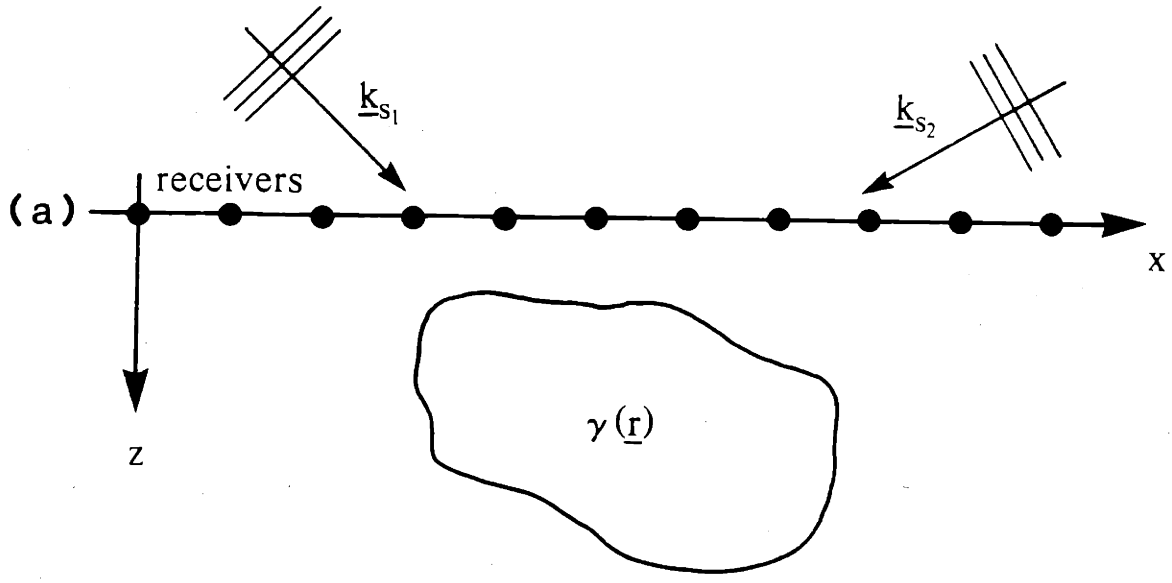

Figure 5.7. Averaging in the Fourier domain for a multiple source experiment. (a) Experiment geometry. (b) Regions of coverage in the Fourier domain of the potential $\tilde{\gamma}(k_x, k_z)$. Averaging is done only in the region of overlap.

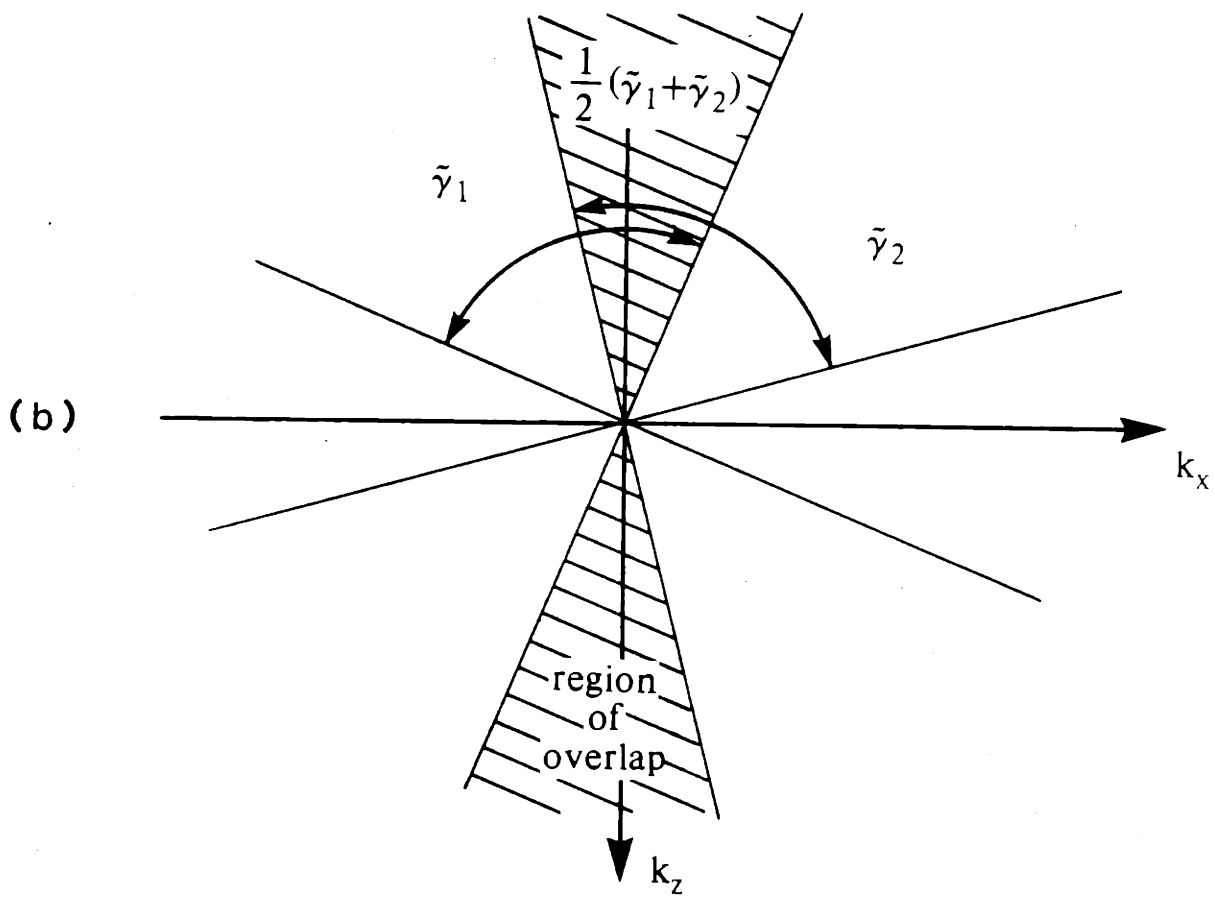

5.5 Synthetic Examples

In this section we give some examples of the slant-stack and imaging-filtering methods discussed in the previous sections. We consider a two dimensional medium in which velocities do not vary along the y axis. The data used in the examples are obtained by a finite difference algorithm. In all cases a four point Blackman window with approximately 50 Hz bandwidth (corresponding to pulse duration of 0.02 seconds) is used as the source wavelet. The synthetic traces are deconvolved, with a Wiener inverse filter, before further processing.

The velocity structure and the observation geometry of the first example is shown in Figure 5.8(a). In this example the scatterer is a high velocity cylindrical object (the figure shows the cross-section in the plane $y = 0$) with a diameter of 14 meters, which is approximately equal to the smallest wavelength contained in the incident wavelet. The medium is probed by a normally incident plane wave and the scattered field is recorded on the surface ($z = 0$) along a 128 meter horizontal array, and along a 64 meter vertical array. The scattered field is shown in Figure 5.8(b) where h and v indicate the horizontal and vertical arrays respectively. The projections of the velocity potential are shown in Figure 5.9. Note that by simply using appropriate phase shifts on the data we can choose any point in the medium as the origin for the projections. Here we choose the center of the scatterer ($x = 64$, $z = 18$) as the origin to display the projections. The projections obtained from the actual velocity model used to create the synthetics are shown in Figure 5.9(a). Since the object is circularly symmetric, the projections at all angles are the same. Figure 5.9(b) shows the projections obtained from the scattered field observed along the horizontal receiver array only.

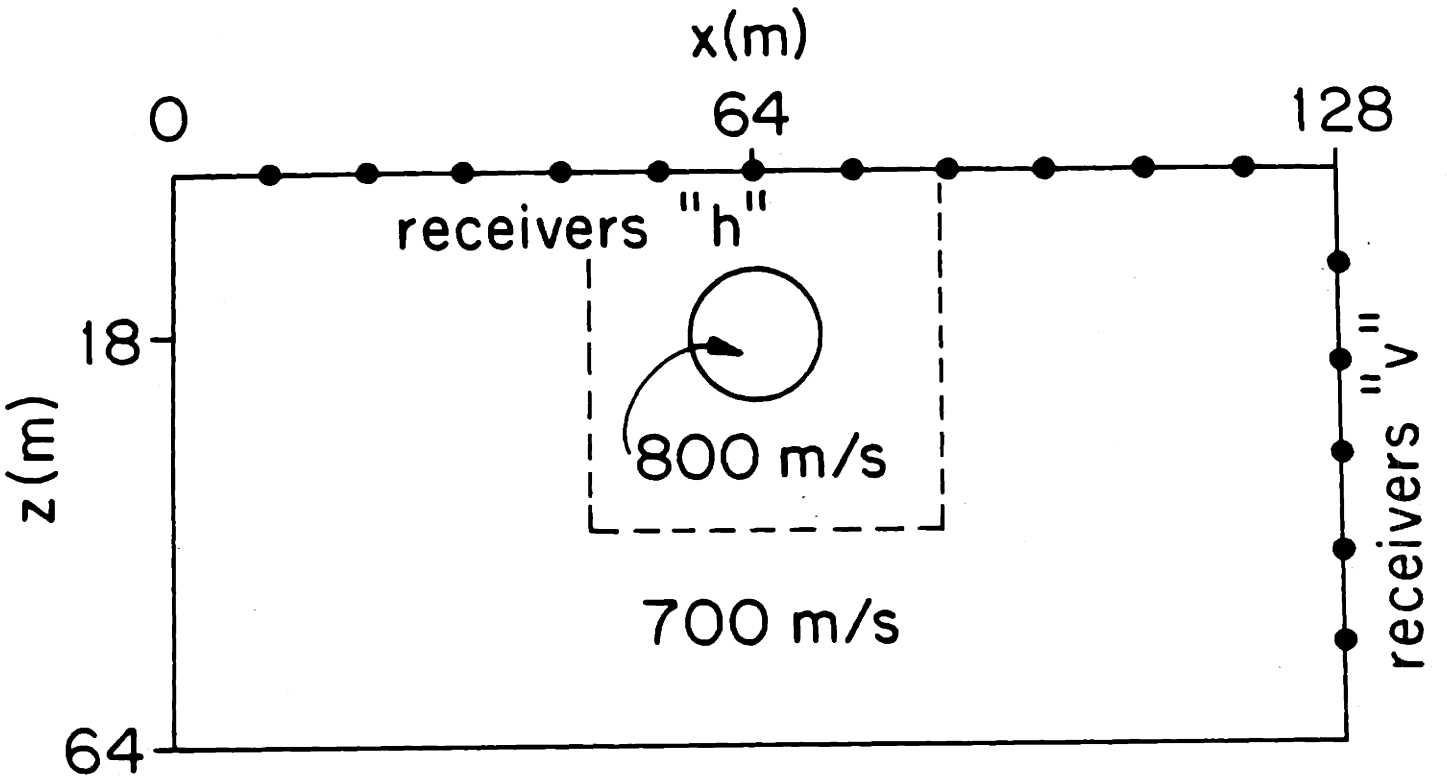

(a)

Figure 5.8. Scattering experiment. (a) High velocity cylindrical object probed by a normally incident plane wave.

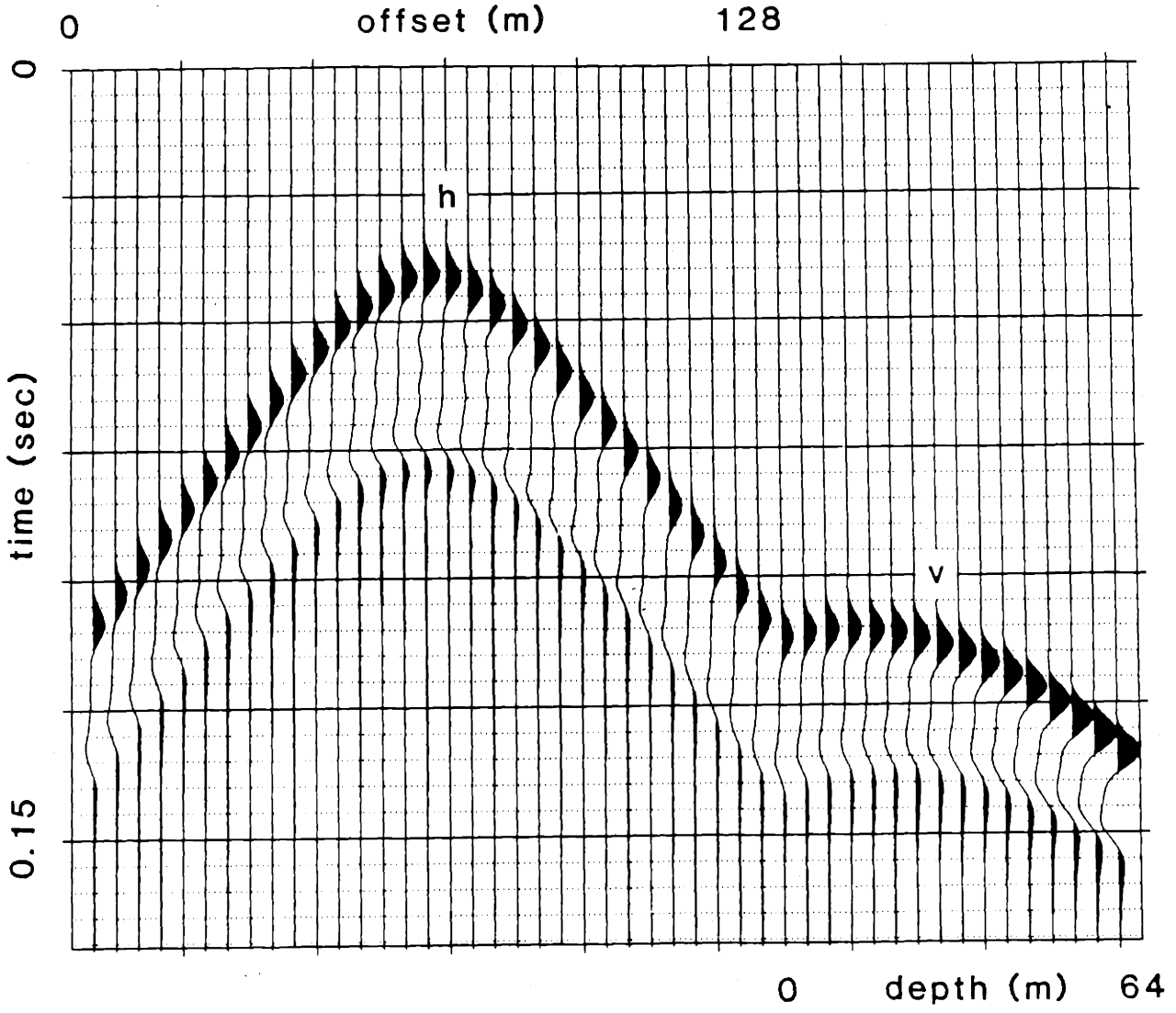

(b) Observed scattered field. The horizontal array on the surface is indicated by "*h*" and the vertical array is indicated by "*v*".

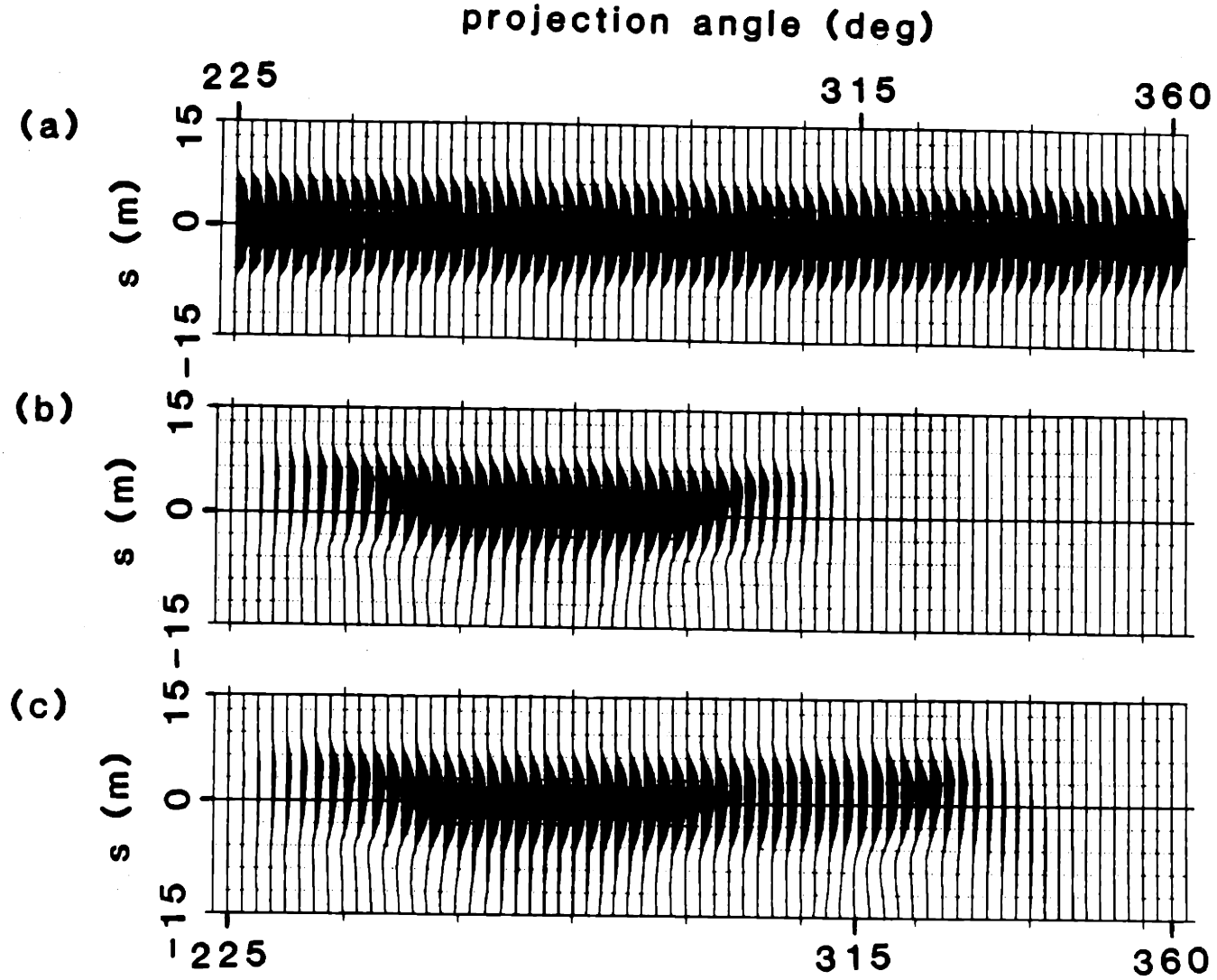

Figure 5.9. Projections $\hat{\gamma}(\hat{\underline{u}},s)$ of the velocity potential. The origin for the projections is chosen at the center of the object. The horizontal axis is the projection angle ϕ corresponding to the unit vector $\hat{\underline{u}}$, where the angle is measured clockwise from the x axis. The vertical axis is the variable s. (a) True projections. (b) Projections obtained from the surface array only. (c) Projections recovered from the combined horizontal and vertical arrays.

Figure 5.9(c) describes the projections recovered from the horizontal array combined with the vertical array. From equation (5.1.18), for an infinite horizontal array ($\alpha_2 = 180°$, $\alpha_1 = 360°$) the range of available projections is $225° < \phi < 315°$ and for an infinite horizontal-vertical array ($\alpha_2 = 180°$, $\alpha_1 = 450°$) the range is given by $225° < \phi < 360°$. For arrays of finite length, however, only some of these projections can be recovered as seen in Figures 5.9(b,c). The slant-stack inversion result is shown in Figure 5.10 for the region indicated in Figure 5.8(a) by dashed lines. Figures 5.10(a) and 5.10(b) are the results obtained by using only the horizontal array, and the combined horizontal and vertical arrays, respectively. Figures 5.11(a) and 5.11(b) show the velocity structure obtained by the imaging-filtering method for the same data sets. It is seen that the two methods give very similar results.

In the second example, shown in Figure 5.12, the scattering medium consists of two halves of a cylinder. The velocities in the top and bottom halves are lower and higher than the background velocity, respectively. The velocity contrast between the two regions is about 14% and the radius of the cylinder is 15 meters, approximately one minimum wavelength. The medium is probed by a plane wave with angle of incidence $\theta_s = 45°$, and the scattered field is observed on the surface and along two vertical arrays on two sides of the object. The length of each line array is about ten minimum wavelengths or five times the size of the scatterer. The scattered fields observed along the vertical array located at offset $x = 0$, on the surface, and along the vertical array located at offset $x = 150$ meters are shown in Figures 5.13(a), (b) and (c), respectively.

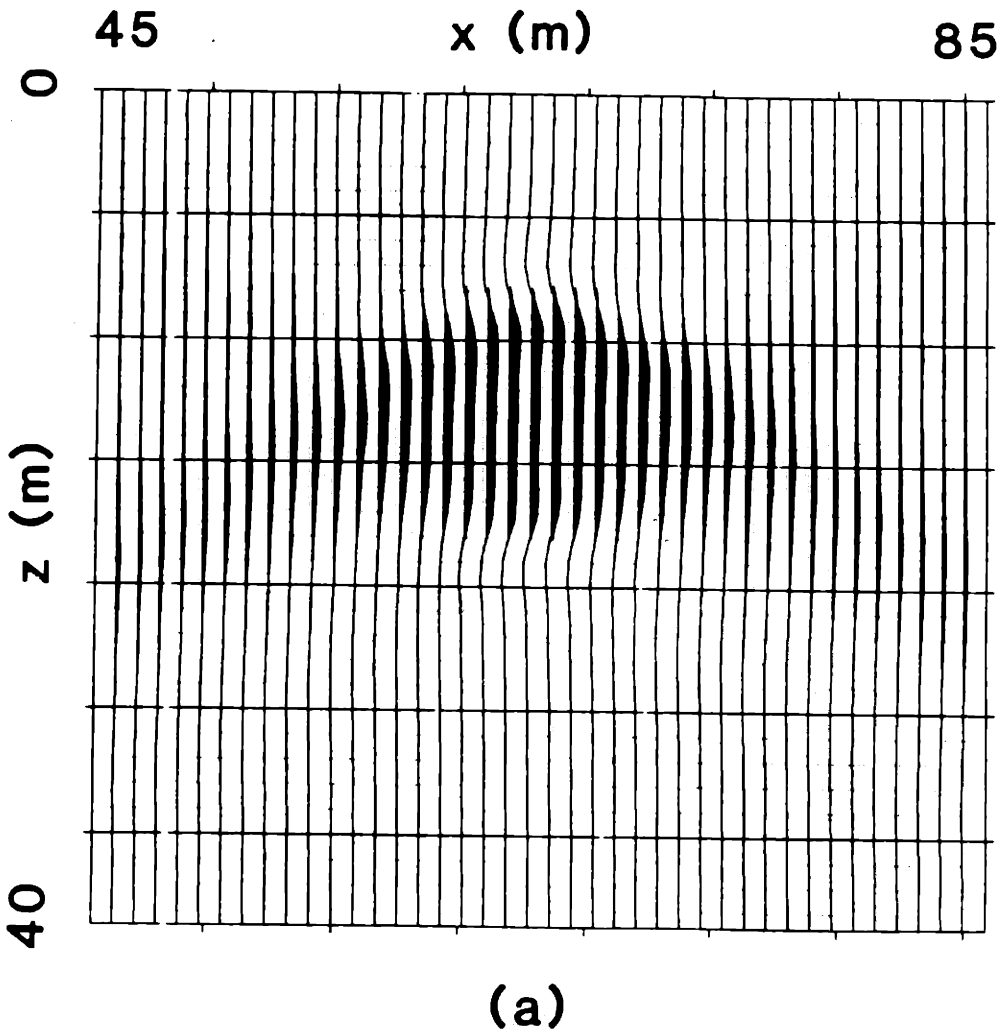

Figure 5.10. The slant-stack inversion result for the region shown inside the dashed lines in Figure 6(a). One trace spacing corresponds to a 100 m/s velocity difference from the background. Reconstruction (a) using only surface data,

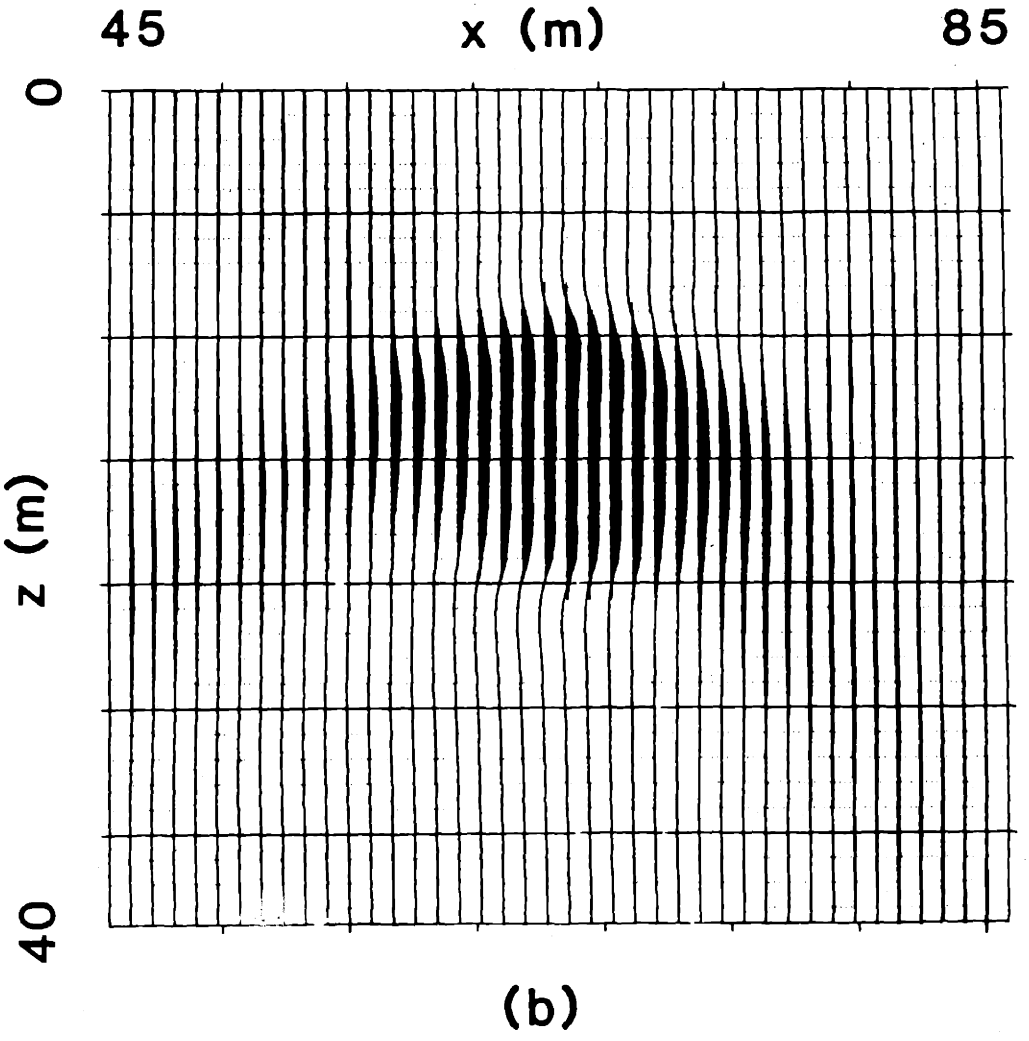

(b) using the combined surface and vertical data.

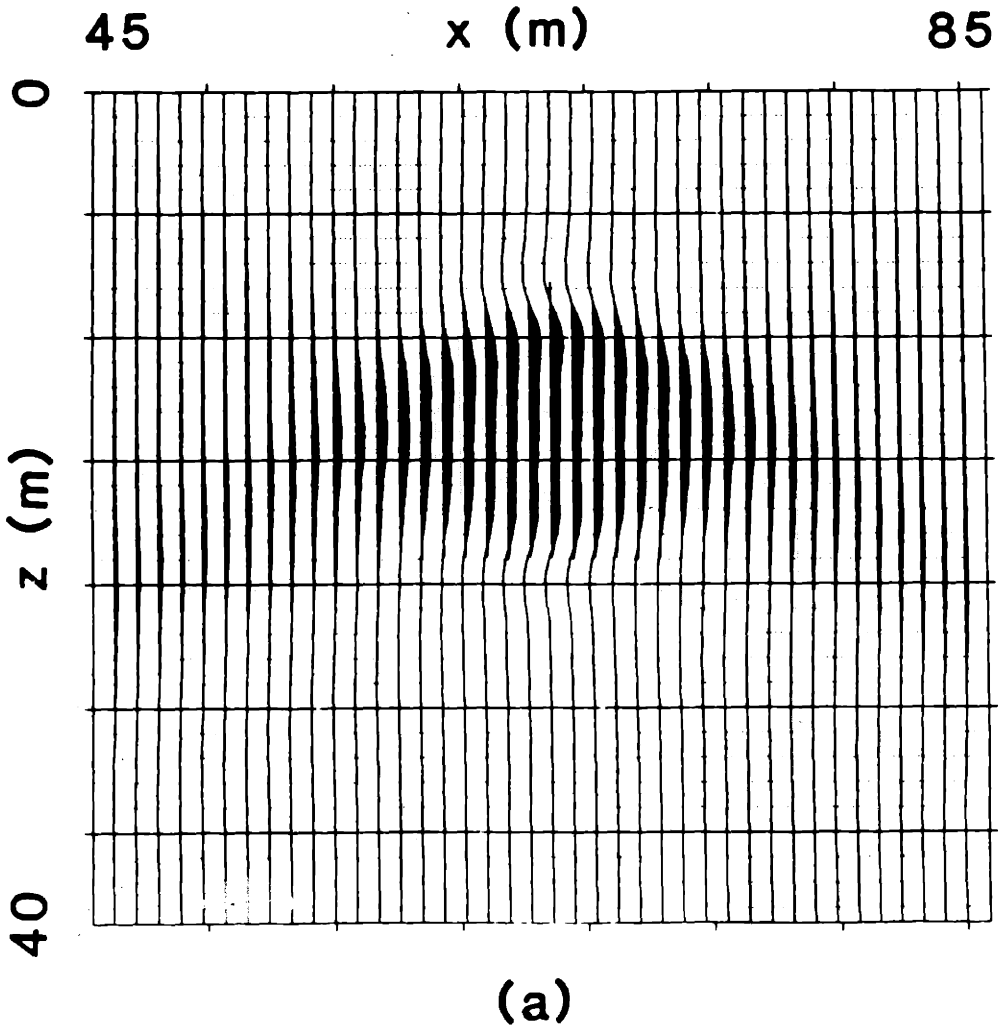

Figure 5.11. The imaging-filtering inversion result for the same region as in Figure 8. One trace spacing corresponds to $100m/s$ velocity difference from the background. Reconstruction (a) using surface data only,

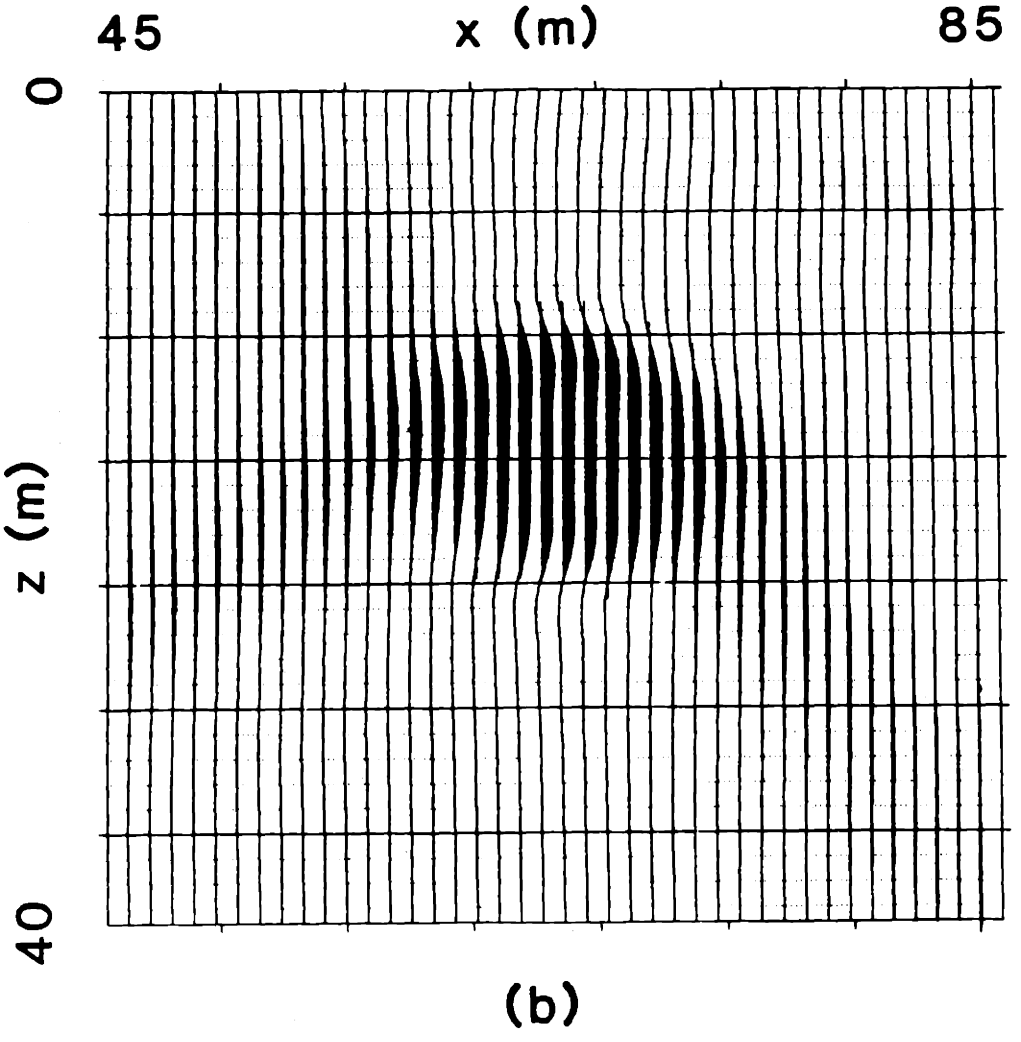

(b) using both surface and vertical data.

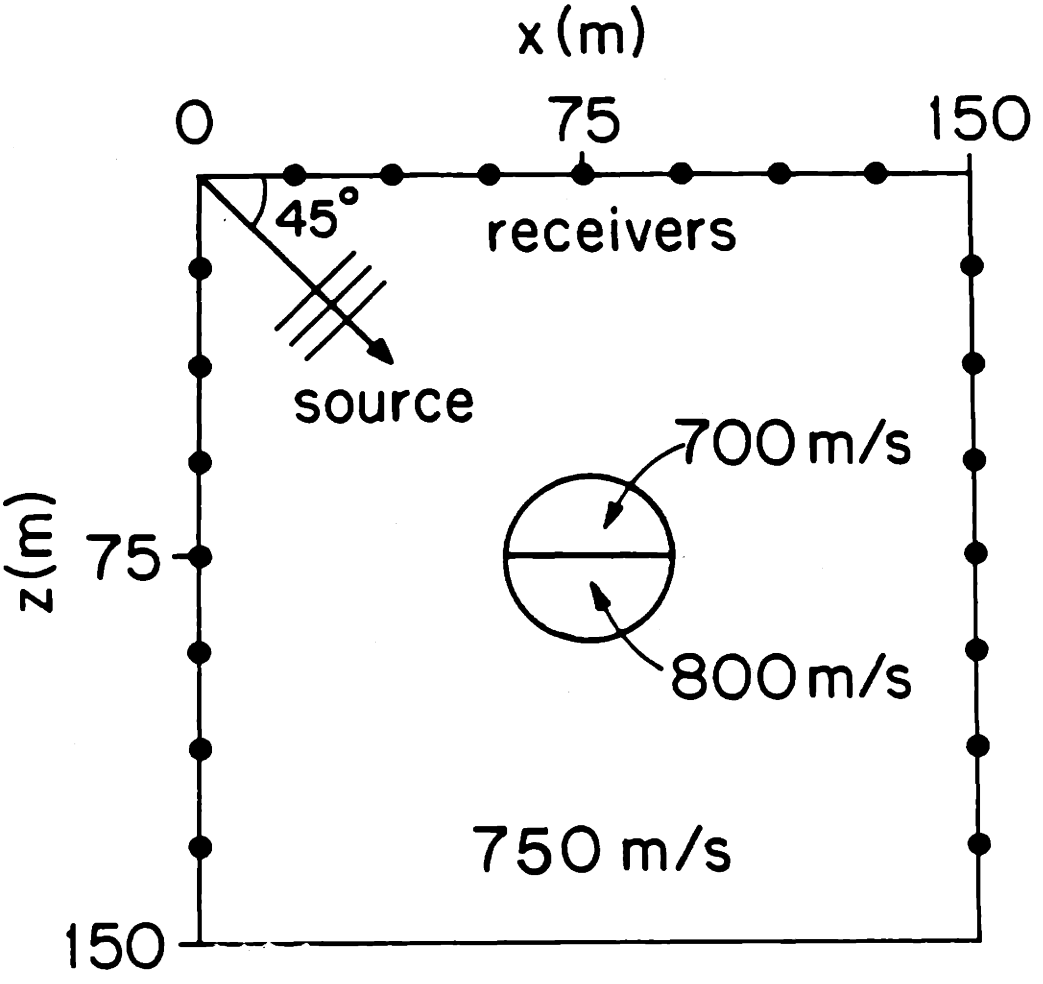

Figure 5.12. Scattering experiment. The medium is probed by a plane wave with 45° angle of incidence. The scattered field is observed on the surface and along two vertical arrays on both sides of the scatterer.

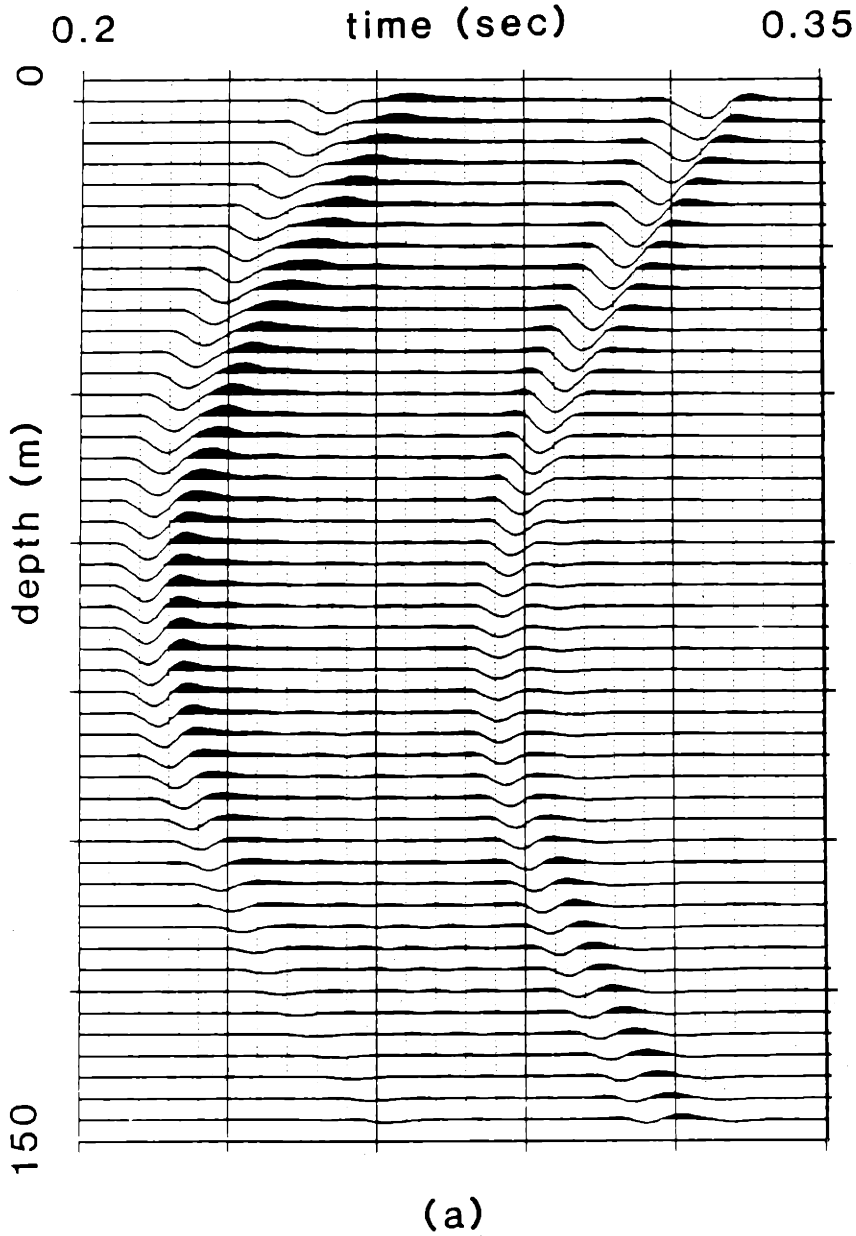

Figure 5.13. Observed scattered field in the time window 0.2–0.35 seconds. (a) The vertical array at zero offset (amplitude scale 0.1).

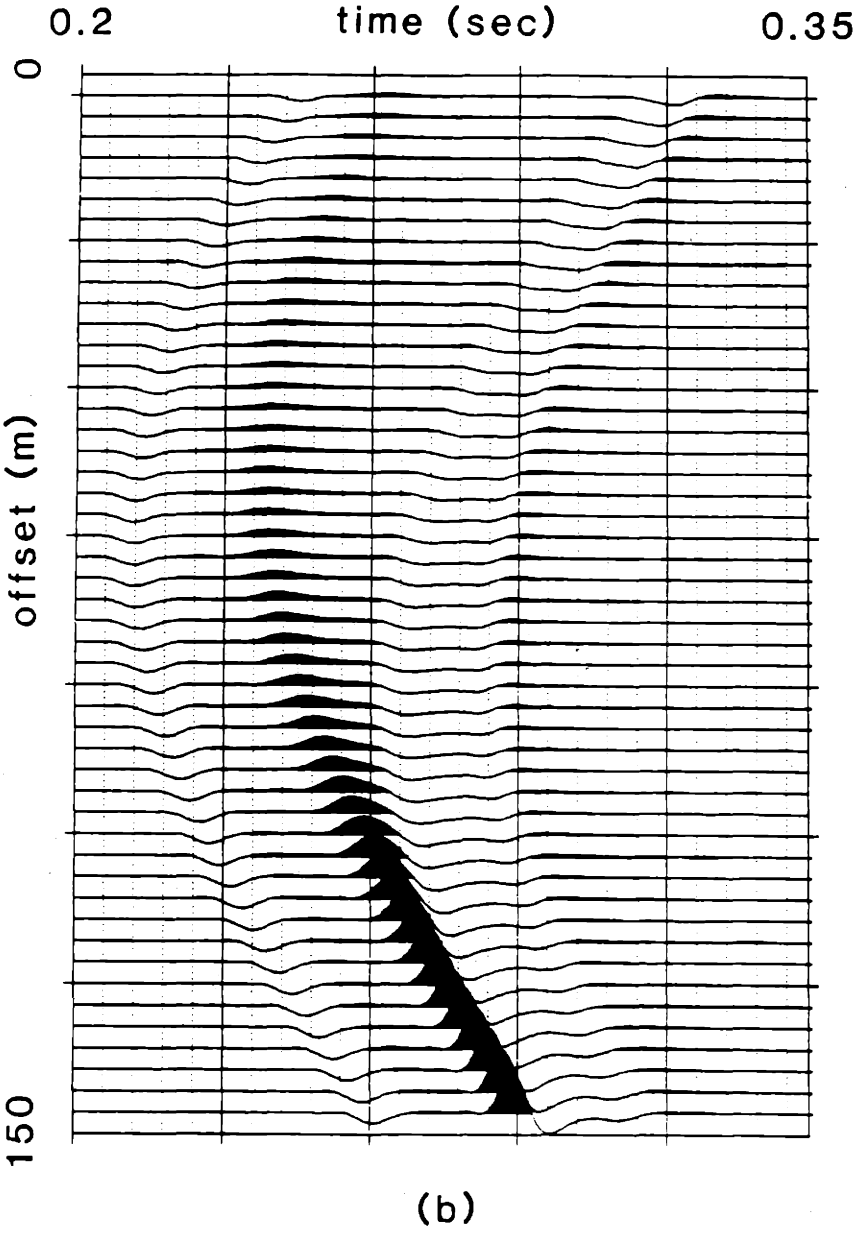

(b) The surface array (scale 0.24).

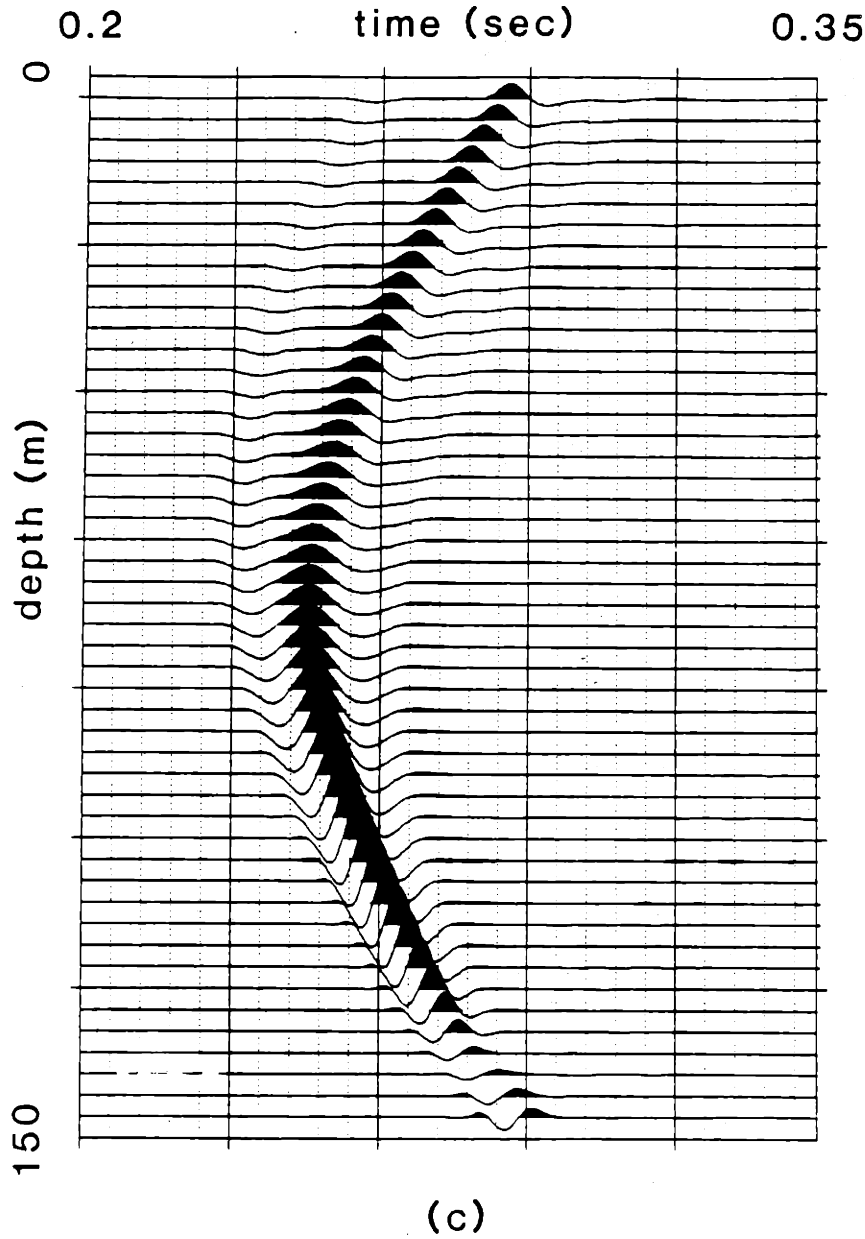

(c) The vertical array at offset 150 meters (scale 0.71).

The projections of the velocity potential are shown in Figure 5.14, where the projection origin is chosen at $x = z = 75$ meters. The projections obtained from the actual velocity model are shown in Figure 5.14(a), where the shaded region corresponds to the positive values of γ, i.e. velocities lower than the background velocity. Figures 5.14(b), (c) and (d) are the projections obtained from the observed data. Figure 5.14(b) shows the image obtained by using the surface array only, (c) the image from the surface array combined with the vertical array at zero offset and (d) the image obtained by using all three arrays. Note that the projections in the range of angles 135° to 315° represent a complete set from which the potential can be totally reconstructed. However, due to the finite extent of the arrays and the fact that the data is bandlimited , we can recover only a portion of the projections with this experiment. In general, the missing projections can be obtained by performing several experiments with appropriately chosen probing waves. For example, for the receiver geometry used in this example, a second probing wave with an angle of incidence equal to 135° could provide the proper complementary coverage. Figure 5.15 shows the inversion results using all three receiver arrays. Figure 5.15(a) is the result of the slant-stack method. Figure 5.15(b) shows the travel time image $\beta(\underline{r})$ (defined by equation (5.3.4)), and Figure 5.15(c) is the result obtained by filtering $\beta(\underline{r})$ via equation (5.3.10). Figure 5.15(d) shows the inversion result for the case where a second probing wave with an angle of incidence equal to 135° is used to obtain a complementary coverage.

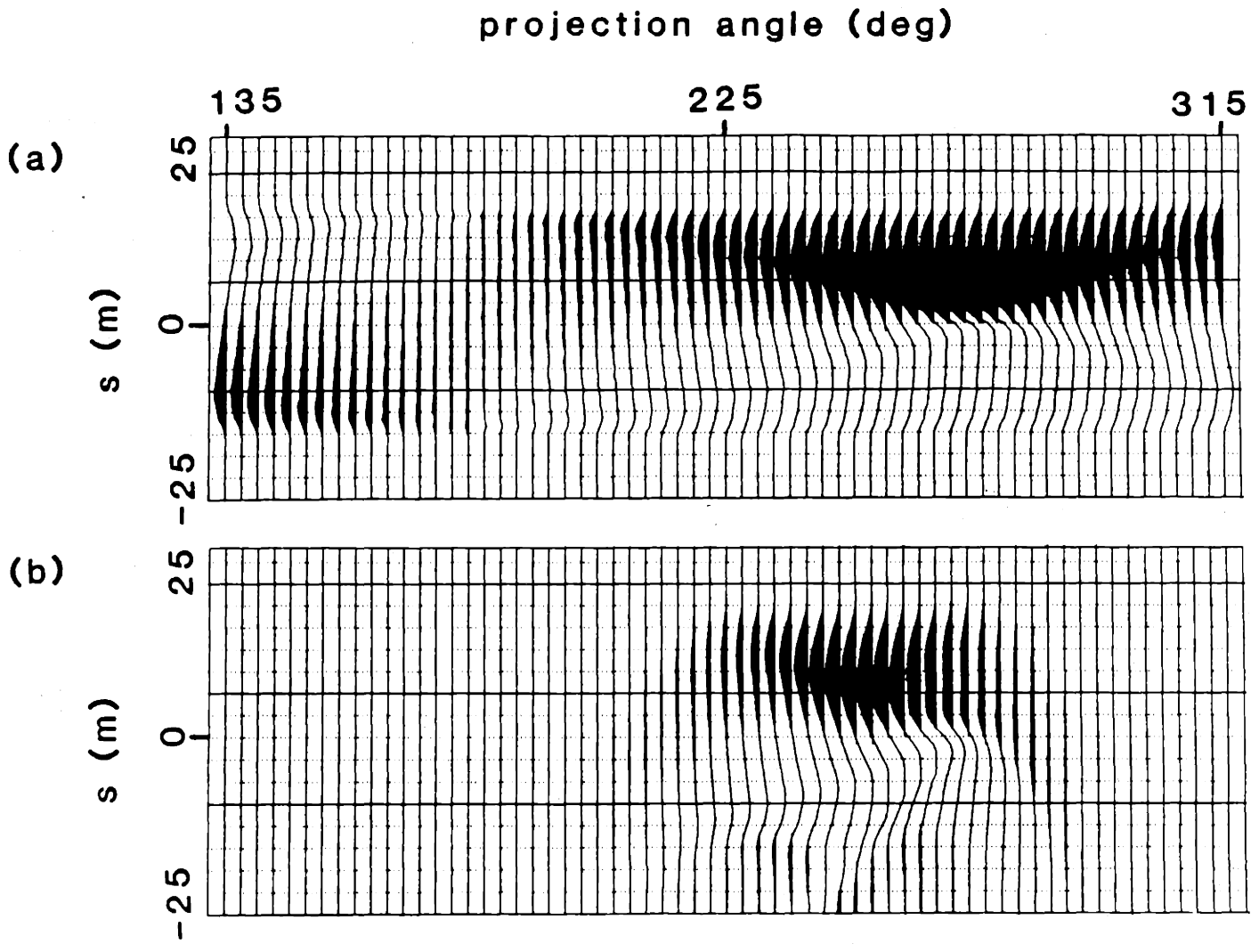

Figure 5.14. Projections $\hat{\gamma}(\hat{\underline{u}},s)$ of the velocity potential. The origin for the projections is at $x = z = 75$ meters. The horizontal axis is the projection angle ϕ measured clockwise from the x axis. The vertical axis is the variable s. (a) True projections. (b) Projections obtained from the surface array only.

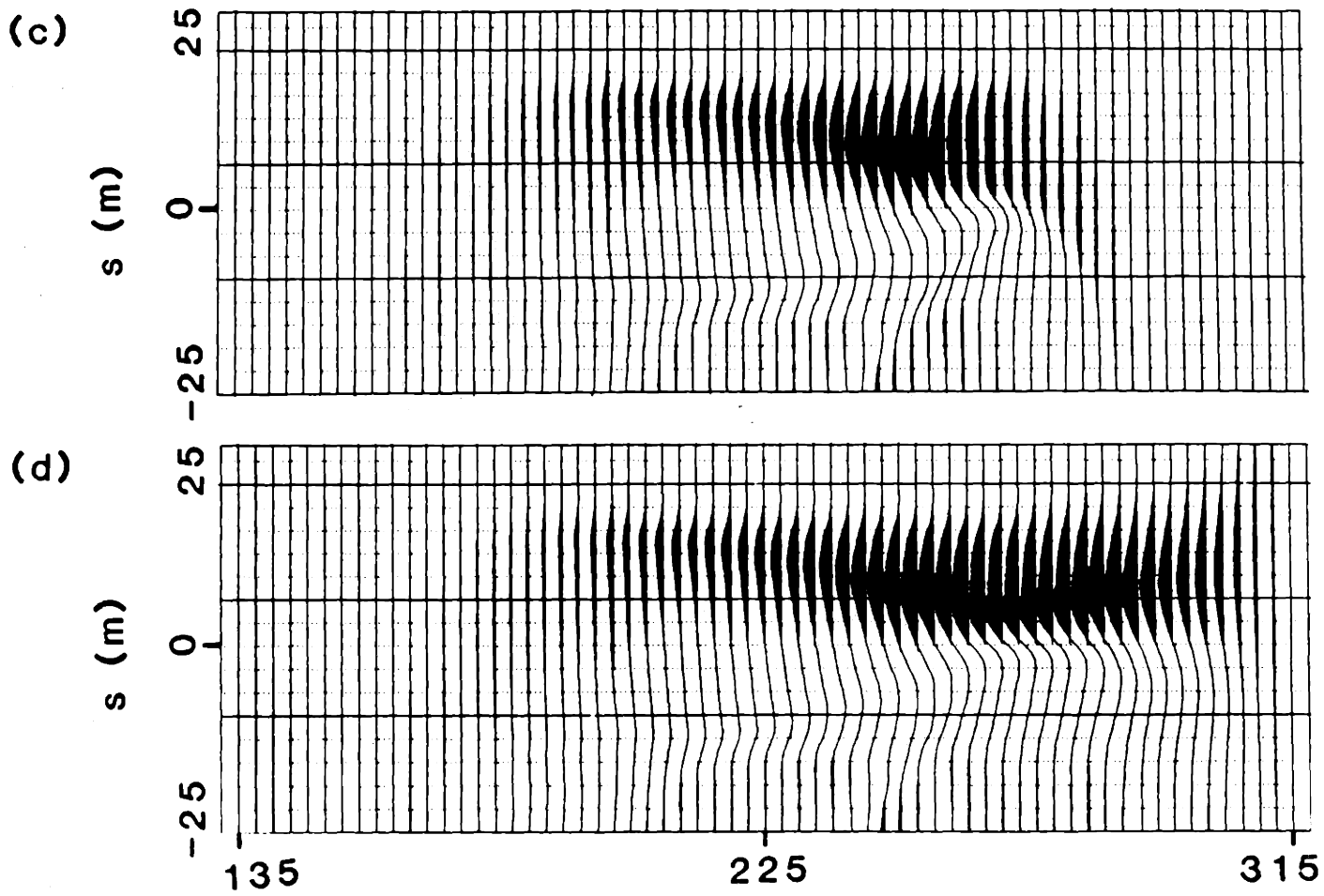

(c) Projections obtained from the surface array combined with the vertical array at zero offset. (d) Projections recovered from all three arrays.

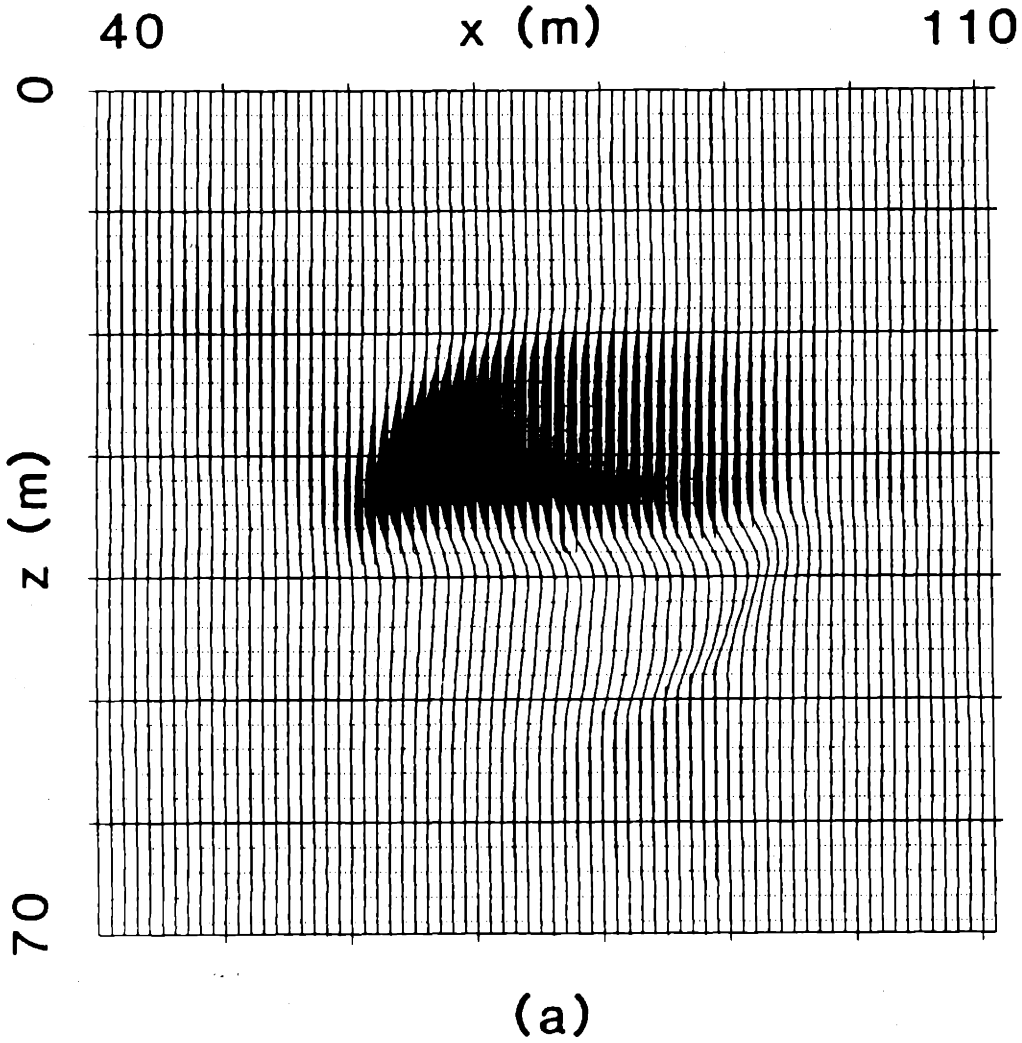

Figure 5.15. Reconstruction. One trace spacing corresponds to a 50 m/s velocity difference from the background. (a) Slant-stack inversion result.

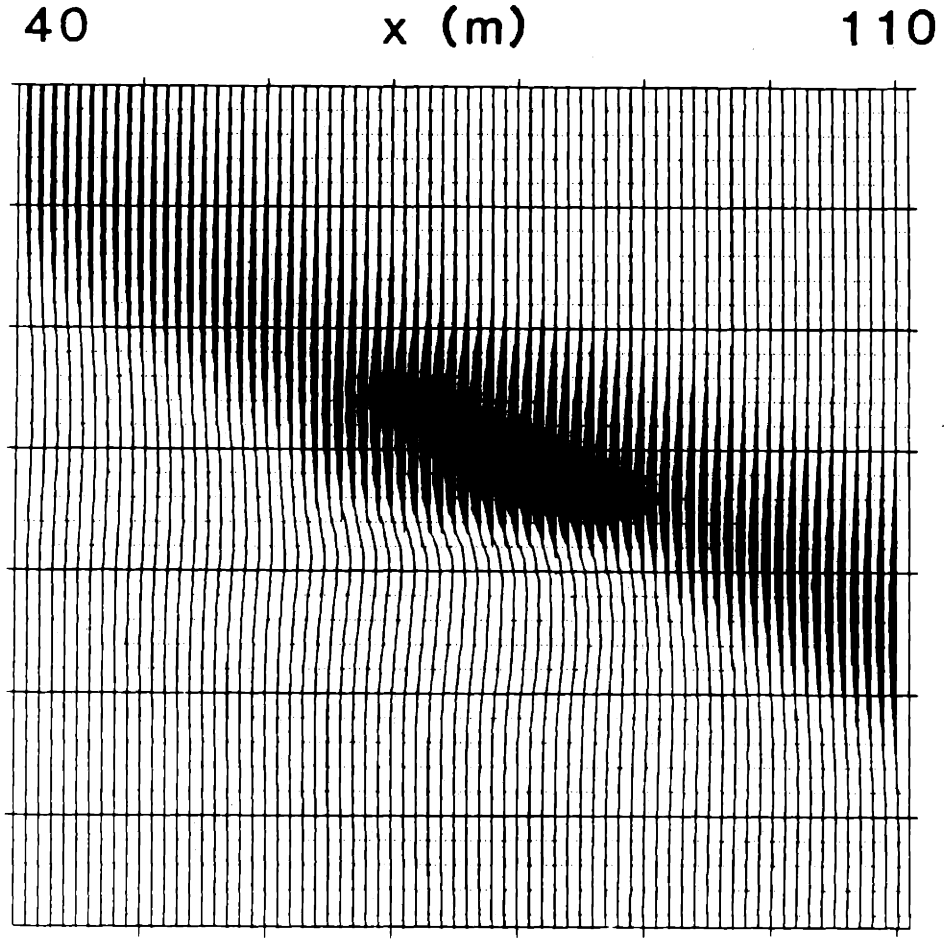

(b)

(b) Travel time image $\beta(\underline{r})$.

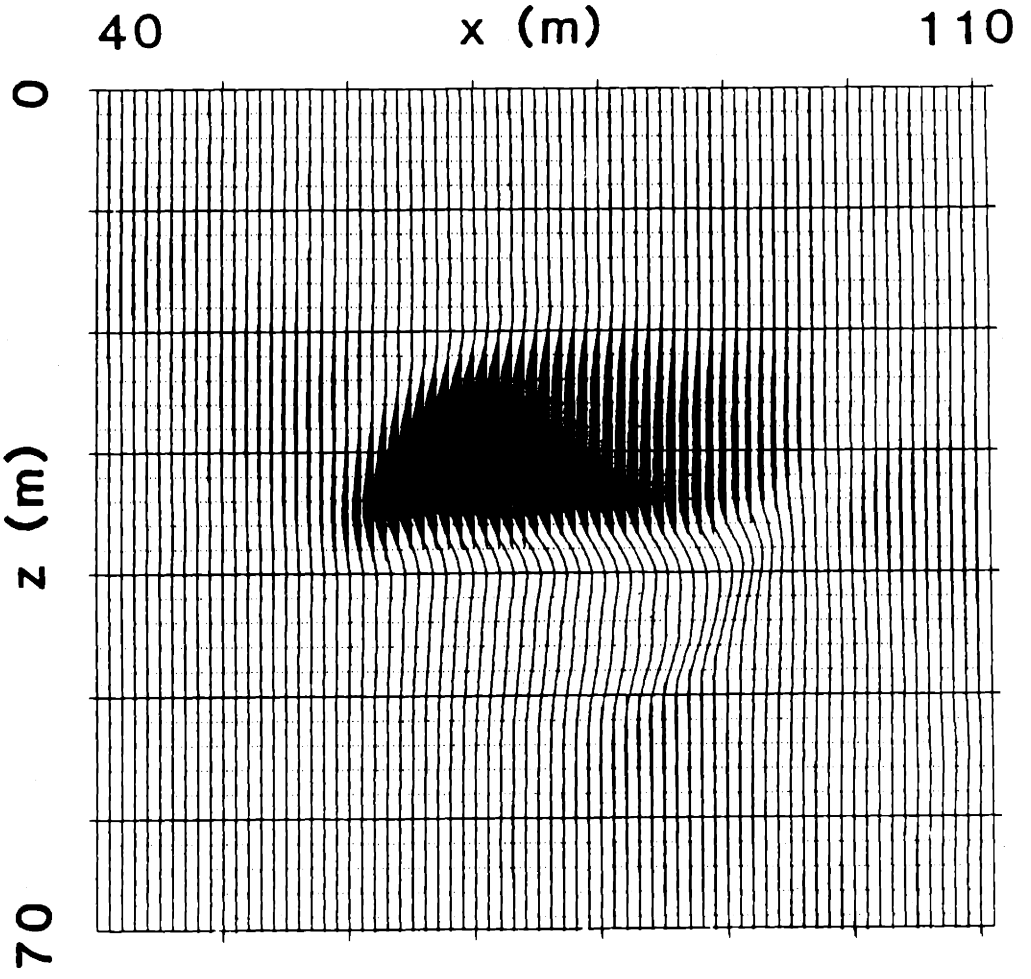

(c)

(c) The result obtained by filtering $\beta(\underline{r})$ with the space-invariant filter $h(\underline{r})$.

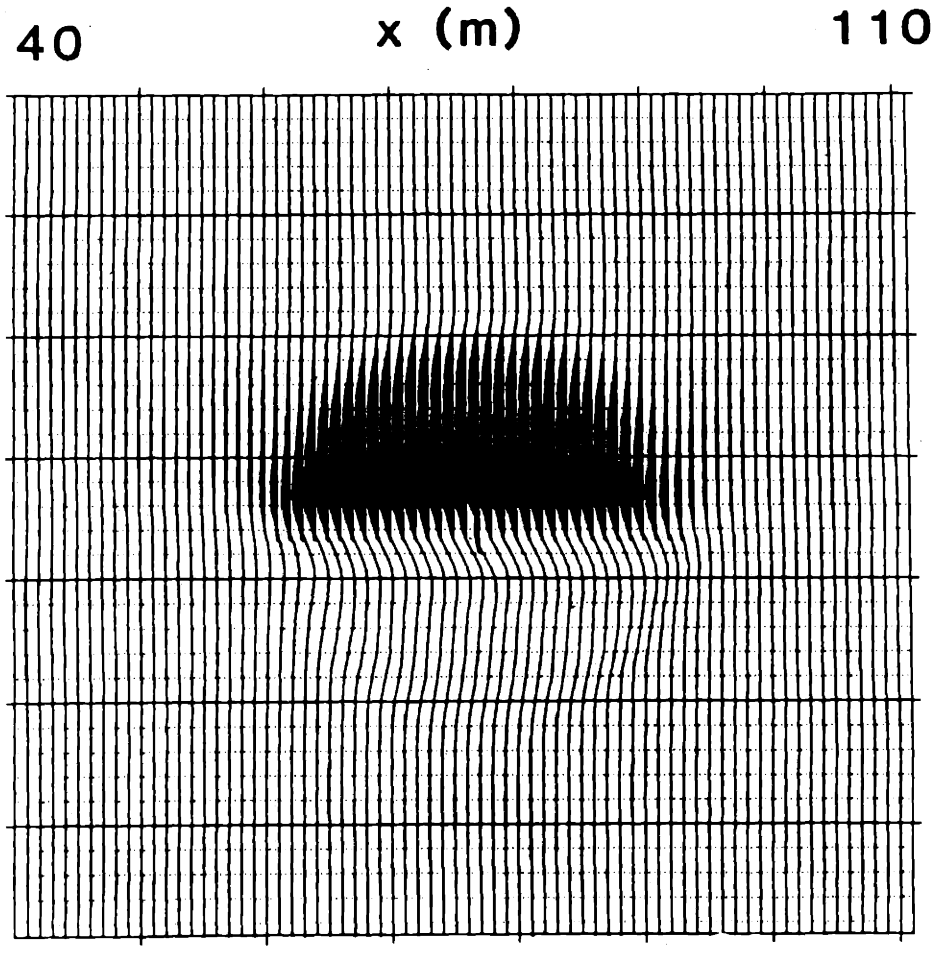

(d)

(d) Slant-stack inversion result for two probing plane waves with angles of incidence 45° and 135°.

Uncorrelated noise

The purpose of the following example is to demonstrate that uncorrelated noise added to the receivers is handled properly by the backpropagated field method of inversion. In general, one must consider various factors, such as signal to noise ratio, receiver aperture, noise characteristics and the size and location of the scatterers, to investigate the effects of the noise on the reconstructed images. Here, we examine a simple case where a scatterer, which has a diameter of one dominant wavelength, is probed by a normally incident plane wave. The scattered field is observed at the surface along a straight-line receiver array with an aperture of thirty dominant wavelengths, as shown in Figure 5.16(a). Synthetic data, generated by using a finite difference algorithm, is shown in Figure 5.16(b). Figure 5.16(c) shows the inversion result obtained with the imaging-filtering method by using the noise-free traces shown in Figure 5.16(b). Noisy traces, shown in Figure 5.17(a), were obtained by adding white noise to the synthetic traces in Figure 5.16(b). The noise was generated by a random number generator with a uniform probability distribution. The maximum amplitude of the noise samples was set to two times the maximum amplitude of the original synthetics. Figure 5.17(b) shows the noisy data after a Wiener deconvolution filter was applied to the traces. Although deconvolution filter suppresses the high frequency noise, the scattered field is still buried in the components of the noise that are inside the signal frequency band. Finally, Figure 5.17(c) shows the reconstructed image obtained from the noisy data with the imaging-filtering method.

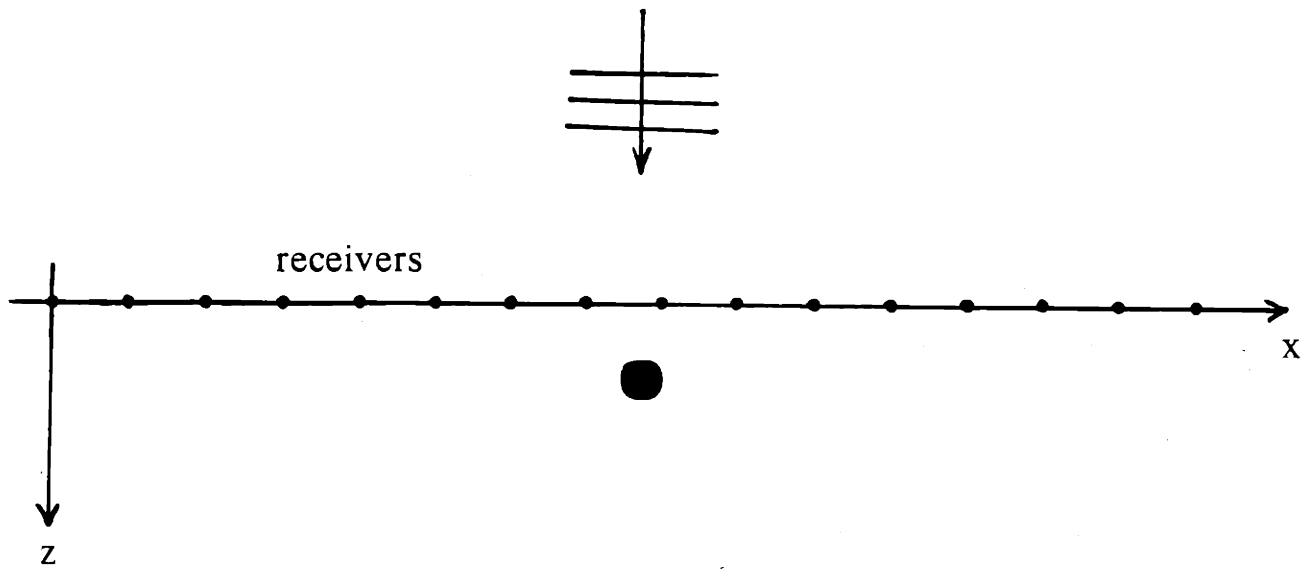

Figure 5.16. (a) Scattering experiment.

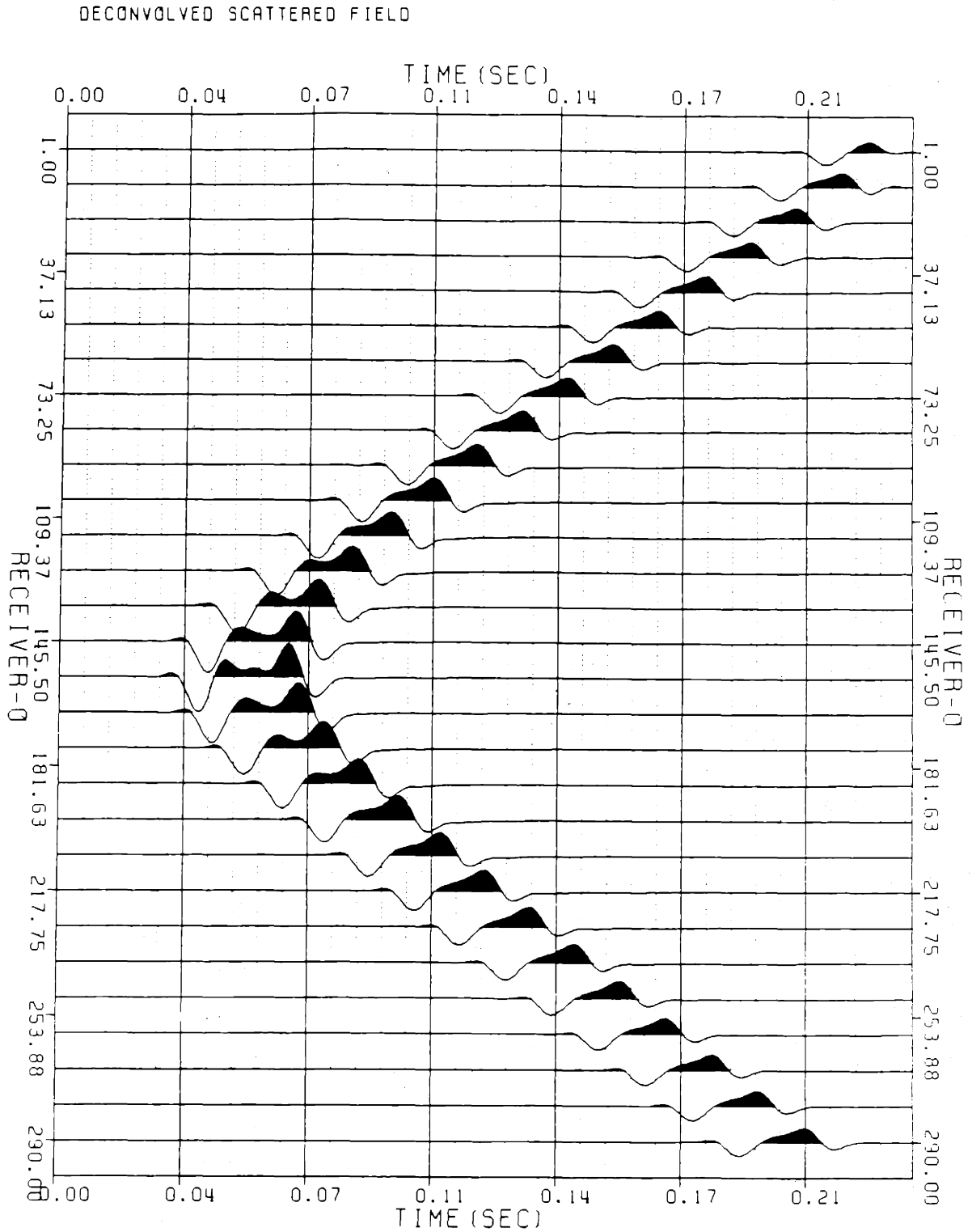

(b) Synthetic scattered field traces.

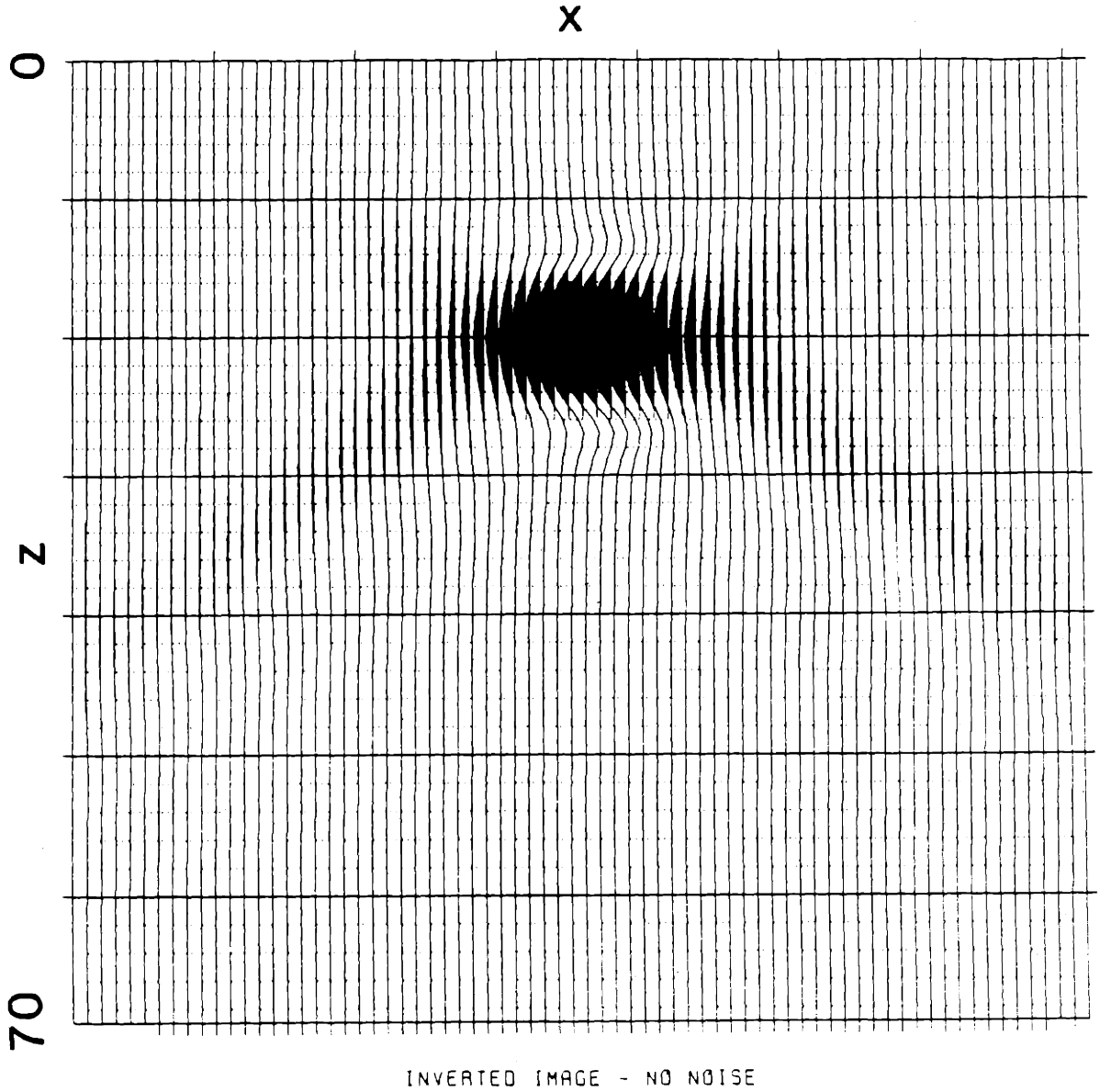

(c) Image obtained from noise-free data.

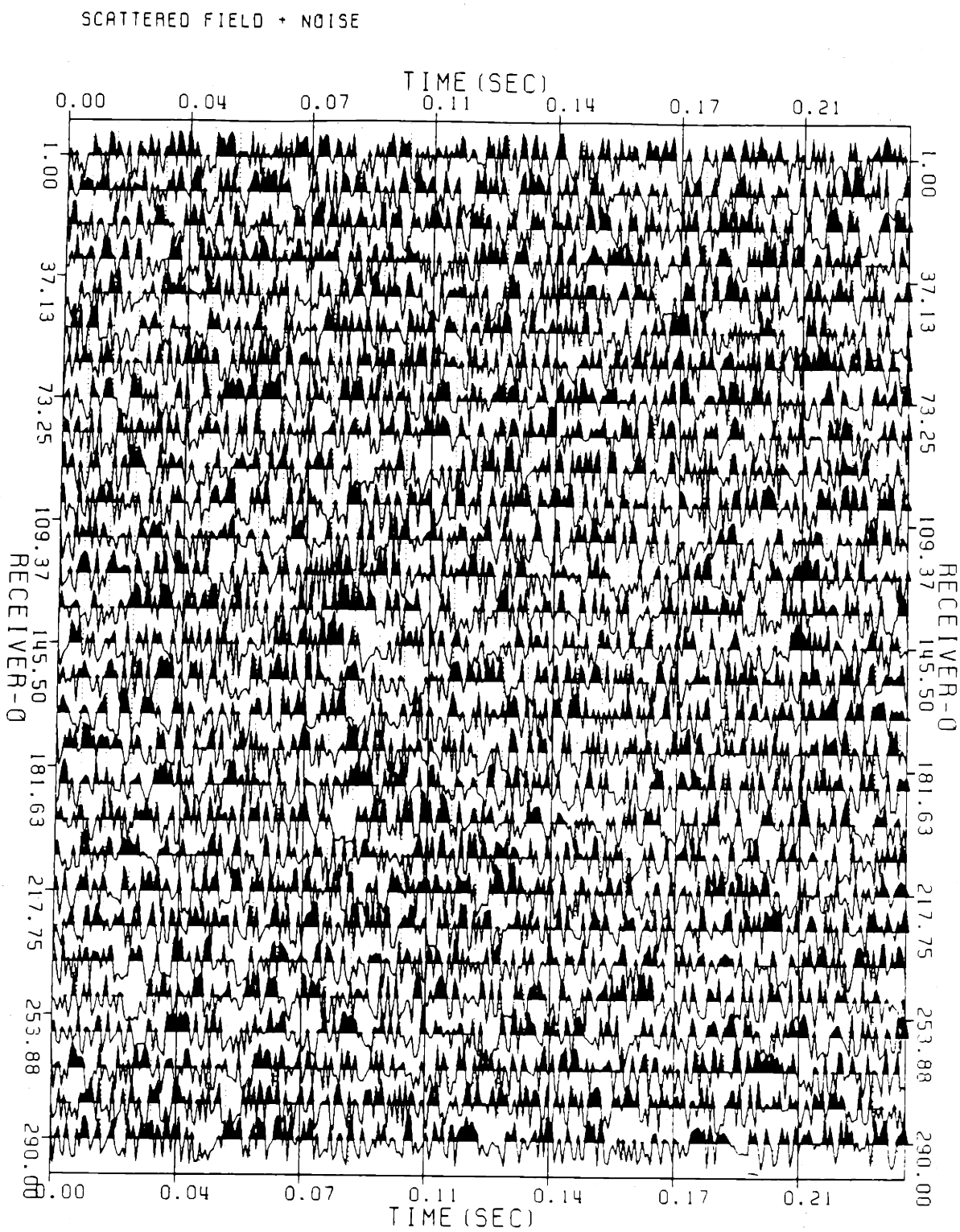

Figure 5.17. (a) Noisy scattered field traces.

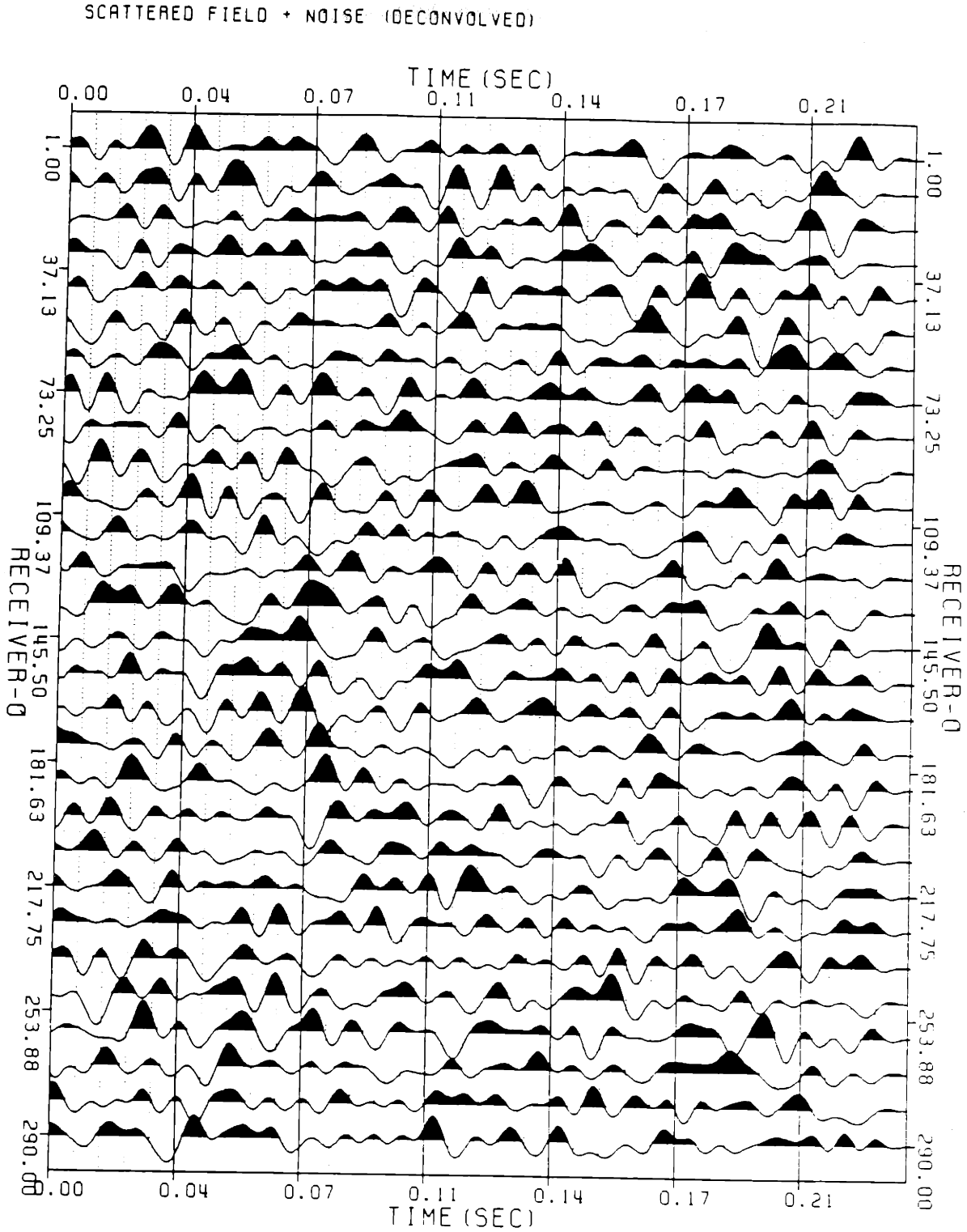

(b) Noisy traces after deconvolution.

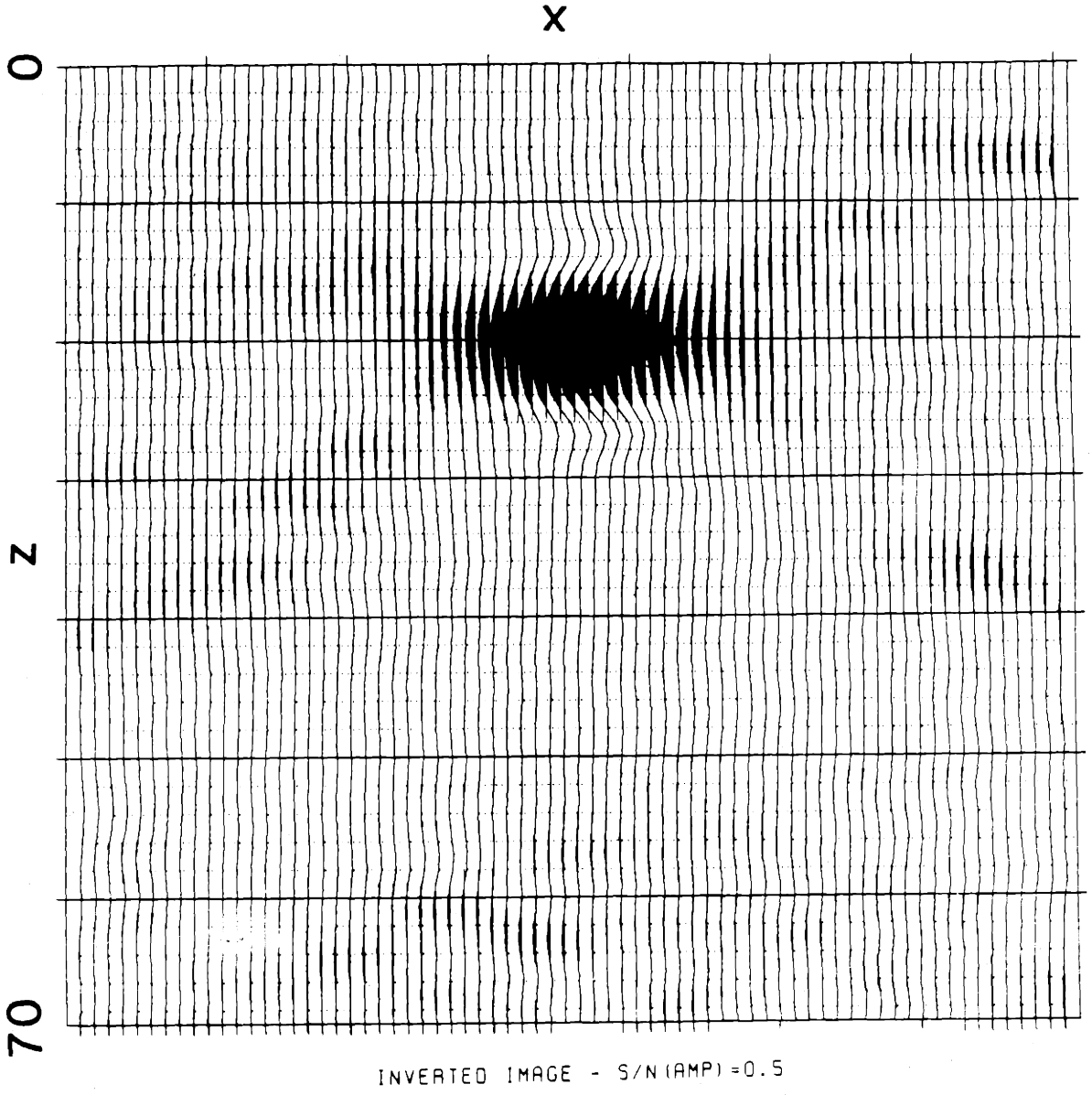

(c) Image obtained from noisy data.

CHAPTER VI

Inversion for a Wide-Band Point Source

In this chapter we consider the inverse scattering problem where the medium is probed by a wide-band point source. Inversion for a wide-band plane-wave excitation was discussed in the previous chapter. It was seen that within the homogeneous background Born approximation, the probing plane wave stays as a plane wave across the medium. In terms of the mathematics of the problem, the incident field term in the integral representation of the scattered field was a simple exponential. As a result of this, straightforward inversion methods were obtained for a plane-wave excitation. For example, in the method of inversion by imaging the backpropagated field, it was shown in Section 5.3 that the inversion process consists in applying a space invariant filter to the source-travel time image of the extrapolated field. The velocity inversion problem for a point source excitation is relatively more complicated as will be seen in this chapter. Nevertheless, the point source problem is important because, within the wavelengths of interest, sources used in most experiments can be modeled as point sources. As was pointed out previously, a virtual plane-wave source can be obtained from an array of point sources. Also, if the scatterer is in the far field of a point source, the effective excitation can be modeled by a plane wave. However, in many experiments an array of point sources is not available due to either financial or physical reasons. If the size of the scatterers is of the order of its distance from the point

source we cannot assume approximately planar wavefronts either. In such cases we must use the point source formulation.

The major difference between the point source and plane-wave source problems is that the incident field created by the point source contains a wavefront curvature and an amplitude decay. The point source excitation, in a sense, is richer than the plane-wave field in that it contains many plane-wave components. The difficulty in inverting the point source data arises from the fact that the observed scattered field is the sum of many scattered fields which are each due to a different plane-wave component of the point source. It is well-known that in a one dimensional (layered) medium the lateral wavenumber of the field due to a plane wave excitation remains constant (Snell's law). In this case, if the scattered field of a point source is observed along a lateral receiver array, components of the scattered field corresponding to the plane-wave components of the source can be extracted from the observed data. Therefore, the point source problem in a layered medium can be regarded as a plane-wave excitation problem involving many experiments each with a different angle of incidence. Unfortunately, in a multidimensional medium this approach cannot be used since the horizontal wavenumber of the field excited by a plane wave is no longer constant throughout the medium.

There are three types of multidimensional point source problems that will be considered in this thesis. The three dimensional problem consists of a point source, a three dimensional medium and receivers located on a two dimensional surface. The two dimensional problem consists of a *line* source along the y axis, a two dimensional medium and receivers located on a curve in the $y = 0$ plane. By convention we

choose the y axis along the direction in which the medium velocities are constant. This experiment geometry corresponds to a two dimensional problem because the wavefield is independent of the variable y. Therefore, we can formulate an equivalent problem in the $y = 0$ plane in terms of the variables x and z. In this two variable problem the line source becomes a point source located at the point where the source line intersects the $y = 0$ plane. Also, the wave equation in the $x-z$ plane is obtained by using the two dimensional Laplacian. It is generally true that most inversion methods obtained for the two dimensional problem can easily be extended to the three dimensional problem. Another reason for our interest in the two dimensional problem is that it is easier to test inversion methods on some numerical examples in two dimensions. This is because generating synthetic data can be quite difficult and costly in three dimensions compared to the two dimensional case. The third type of problem considered here is the 2½ dimensional problem. This problem is specific to the point source case, there is no counterpart of this problem for a plane-wave excitation for obvious reasons. A description and a study of the main features of the 2½ dimensional problem were presented in Sections 2.6 and 4.3 and these will not be repeated here. Briefly, the 2½ dimensional problem is obtained from the two dimensional problem by replacing the line source by a point source.

In this chapter we present two methods for velocity inversion using a single wideband point source. Both of these methods are obtained by using the backpropagated field approach which was discussed in Chapter 4. In Section 6.1 the method of inversion by zero-time imaging is presented for the case of complete observations of the scattered field. In this method the observed scattered field is backpropagated into the

medium and imaged at time zero at all points simultaneously. It is shown that a complete set of projections of the scattering potential can be obtained from this zero-time image. For each projection angle, the projection function of the potential is obtained by reading the zero-time image along a line passing through the source location. Then, the potential is reconstructed from its projections using the inverse Radon transform. In Section 6.2 the method of inversion by source-travel time imaging is presented for the general receiver array model depicted in Figure 4.5. In this method the backpropagated field is imaged at every point at the corresponding source-travel times, as in migration. The scattering potential is then partially reconstructed by a spatial operation acting on the travel-time image. In Section 6.3 the inversion problem for the 2½ dimensional case is discussed by using the backpropagated field formulation described in Section 4.3. It is shown that the inversion procedure for this case is very similar to the two dimensional problem except for a prefiltering operation applied to the observed traces before backpropagation. Numerical examples of both inversion methods for various receiver array configurations are given in Section 6.4.

6.1 Inversion by Zero-Time Imaging

In this section we present a new method of velocity inversion for the wide-band point source excitation problem. Consider an experiment where a two dimensional medium is probed by a line source (a point source in the $x-z$ plane) and the scattered field is observed on the surface S as shown in Figure 6.1. The volume integral representation of the field backpropagated into the medium from a receiver array surrounding the medium was derived in Section 4.1. From equations (4.1.6) and (4.1.7) the volume integral for the extrapolated field within the homogeneous Born approximation is given by

$$P_e^*(\underline{r},\omega) = k^2 \int_V d\underline{r}' \, \gamma(\underline{r}') \, G_0(\underline{r}',\underline{r}_s,\omega) \, 2i \, Im[\, G_0(\underline{r},\underline{r}',\omega) \,] \, , \tag{6.1.1}$$

where $\underline{r}_s$ is the location of the source and G_0 is the free space Green's function. Here we assume that the scattered field is deconvolved by the source wavelet before back-propagation. A geometric interpretation of the extrapolated field can be made as follows. Let the travel time from the source to a point $\underline{r}_0$ be $\tau_0 = |\underline{r}_0|/c$, where $c = \omega/k$ is the background velocity. When the incident field reaches this point at time τ_0 the waves scattered from the point propagate forward and backward in time. This is due to the fact that the extrapolated field kernel (in this case the imaginary part of the Green's function) has an odd symmetric impulse response in the time domain. At times $2\tau_0$ and zero, the extrapolated field due to scattering from $\underline{r}_0$ lies on a circle centered at $\underline{r}_0$ and passing through the location of the source as shown in Figure 6.2. Note that this geometrical picture is the same for every scattering point in the

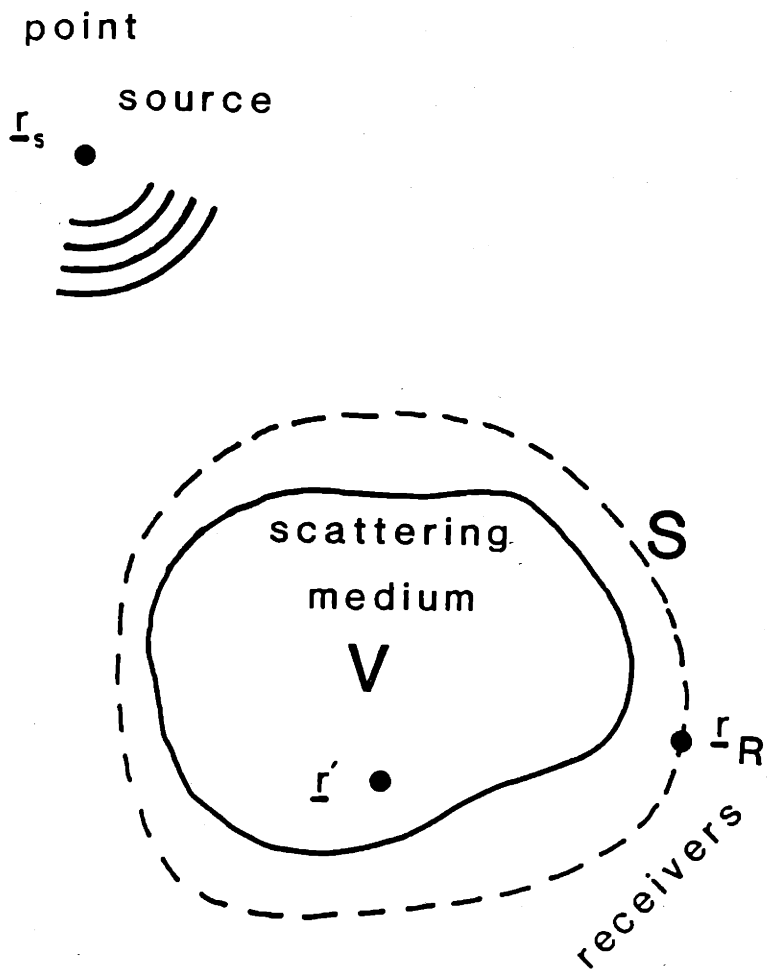

Figure 6.1. Single source scattering experiment.

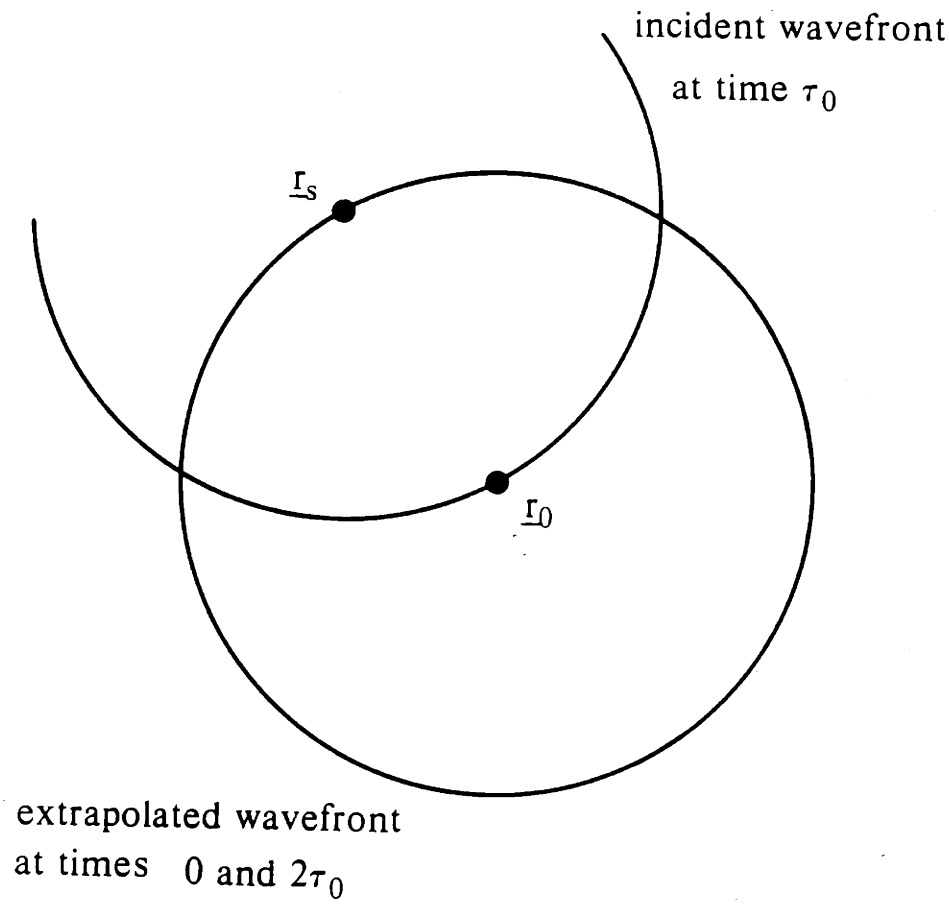

Figure 6.2. Extrapolated field of a point scatterer imaged at times zero and twice the source travel time.

medium. In the following, this property of the extrapolated field will be exploited to obtain an analytical solution for the potential in equation (6.1.1).

The derivation of the inversion procedure is the same for the two dimensional medium with a line source and for the three dimensional medium with a point source. We will consider the 2-D case. The Green's function of a two dimensional homogeneous medium is given by

$$G_0(\underline{r},\underline{r}',\omega) = \frac{i}{4} H_0^{(1)}(k|\underline{r}-\underline{r}'|), \tag{6.1.2}$$

and its imaginary part is

$$Im[G_0(\underline{r},\underline{r}',\omega)] = \frac{1}{4} sgn(k) J_0(k|\underline{r}-\underline{r}'|), \tag{6.1.3}$$

where $H_0^{(1)}(\cdot)$ and $J_0(\cdot)$ are the Hankel and Bessel functions of the first kind and $sgn(k) = \pm 1$ denotes the sign of k. Also, recall that for a homogeneous background the scattering potential is defined as

$$\gamma(\underline{r}) = n^2(\underline{r}) - 1, \tag{6.1.4}$$

where $n(\underline{r})$ is the refraction index of the medium. From equations (6.1.1), (6.1.2) and (6.1.3) the extrapolated field can be written as

$$P_e^*(\underline{r},\omega) = -\frac{k^2}{8} sgn(k) \int_V d\underline{r}' \, \gamma(\underline{r}') \, H_0^{(1)}(k|\underline{r}'-\underline{r}_s|) \, J_0(k|\underline{r}-\underline{r}'|). \tag{6.1.5}$$

Since the scattering potential is real (we assume that the medium is lossless) the only

complex quantity on the right hand side of this equation is the Hankel function $H_0^{(1)}$. By taking the real parts of both sides, we obtain

$$P_e^R(\underline{r},\omega) = -\frac{k^2}{8} \int_V d\underline{r}' \, \gamma(\underline{r}') \, J_0(k|\underline{r}'-\underline{r}_s|) \, J_0(k|\underline{r}-\underline{r}'|). \tag{6.1.6}$$

Note that we prefer to work with the above equation instead of equation (6.1.5) mainly because the Bessel functions J_0 appearing in the integrand are finite everywhere and are orthogonal with respect to integration over the wavenumber k. Now consider the following function obtained from the extrapolated field imaged at time zero (imaging at time zero corresponds to simply integrating $P_e(\underline{r},\omega)$ with respect to ω),

$$\hat{\gamma}(\underline{r}) = -4\,|\underline{r}-\underline{r}_s| \int_{-\infty}^{\infty} d\omega \, \frac{P_e(\underline{r},\omega)}{|\omega|} \, . \tag{6.1.7}$$

Here the filter $|\omega|^{-1}$ can be implemented in the time domain by an integration in time followed by a Hilbert transform. The function $\hat{\gamma}(\underline{r})$ can be expressed as

$$\hat{\gamma}(\underline{r}) = -8\,|\underline{r}-\underline{r}_s| \int_0^{\infty} dk \, \frac{P_e^R(\underline{r},\omega)}{k}$$

$$= |\underline{r}-\underline{r}_s| \int_V d\underline{r}' \, \gamma(\underline{r}') \int_0^{\infty} dk \; k \; J_0(k|\underline{r}'-\underline{r}_s|) \; J_0(k|\underline{r}-\underline{r}'|) \, . \tag{6.1.8}$$

Using the orthogonality property of Bessel functions, we obtain

$$\hat{\gamma}(\underline{r}) = |\underline{r}-\underline{r}_s| \int_V d\underline{r}' \, \frac{\gamma(\underline{r}')}{|\underline{r}'-\underline{r}_s|} \, \delta(\,|\underline{r}'-\underline{r}_s| - |\underline{r}-\underline{r}'|\,). \tag{6.1.9}$$

The roots of the argument of the delta function in the above equation clearly lie along the line perpendicular to the $\underline{r}-\underline{r}_s$ vector at its midpoint. To obtain the appropriate weights for integrating along this line the variables in the integral (6.1.9) can be changed from (x',z') to (ρ,ξ) by shifting the origin to the source location $\underline{r}_s$ and by rotating the coordinate axes as shown in Figure 6.3. It follows that

$$\hat{\gamma}(\hat{\underline{r}},r) = r \int_{\xi_1(\underline{r})}^{\xi_2(\underline{r})} d\xi \int_{\rho_1(\underline{r})}^{\rho_2(\underline{r})} d\rho \, \frac{\gamma(\rho,\xi;\,\hat{\underline{r}})}{(\rho^2+\xi^2)^{1/2}} \, \delta\left\{ (\rho^2+\xi^2)^{1/2} - [(\rho-r)^2+\xi^2]^{1/2} \right\}, \tag{6.1.10}$$

where $r = |\underline{r}|$ and $(\rho,\xi;\,\hat{\underline{r}})$ denotes the coordinates (ρ,ξ) of point $\underline{r}'$ with respect to the axes specified by the direction $\hat{\underline{r}}$ as shown in Figure 6.3. Note that $\hat{\gamma}(\hat{\underline{r}},0) = 0$ for all directions $\hat{\underline{r}}$. For $r \neq 0$, this integral is evaluated as follows. Viewing ξ as a parameter, the second integral is of the form

$$\int_{\rho_1(\underline{r})}^{\rho_2(\underline{r})} d\rho \; b(\rho,\xi) \; \delta[a(\rho,\xi)] = \left\{ b(\rho,\xi) \left| \frac{\partial a(\rho,\xi)}{\partial \rho} \right|^{-1} \right\}_{\rho=\rho_0} \quad ; \quad \rho_1 < \rho_0 < \rho_2$$

$$= 0 \quad ; \quad \text{otherwise}, \tag{6.1.11}$$

where ρ_0 is the only root of $a(\rho,\xi)$ for all ξ. In equation (6.1.10) the only root of the argument is $\rho_0 = r/2$ and

$$\left\{ \frac{\partial a(\rho,\xi)}{\partial \rho} \right\}_{\rho=\rho_0} = \frac{\rho}{(\rho^2+\xi^2)^{1/2}} - \frac{\rho-r}{[(\rho-r)^2+\xi^2]^{1/2}} = \frac{r}{[(\frac{r}{2})^2+\xi^2]^{1/2}}. \quad (6.1.12)$$

Therefore, for $r \neq 0$ we obtain

$$\hat{\gamma}(\hat{\underline{r}},r) = \int_{\xi_1(\underline{r})}^{\xi_2(\underline{r})} d\xi \; \gamma(\frac{r}{2},\xi;\hat{\underline{r}})$$

$$= \int_{(\underline{r}'-\underline{r}_s)\cdot\hat{\underline{r}}=\frac{r}{2}} dl \; \gamma(\underline{r}') \; . \quad (6.1.13)$$

This simply means that $\hat{\gamma}(\hat{\underline{r}},2r)$ for $\hat{\underline{r}}$ fixed is the projection of $\gamma(\underline{r}')$ onto the line defined by the unit vector $\hat{\underline{r}}$ as shown in Figure 6.4. Since the function $\hat{\gamma}(\underline{r})$ is known everywhere in the medium, projections at all angles $\hat{\underline{r}} = \frac{\underline{r}}{r}$ are obtained by equation (6.1.13). Recovering $\gamma(\underline{r})$ from its projections $\hat{\gamma}(\hat{\underline{r}},2r)$ is exactly the problem solved by Radon (1917) and can be done by an inverse Radon transform (Ludwig, 1966). This reconstruction method has been extensively used in x-ray tomography. From the projection-slice theorem

$$\tilde{\gamma}(k\hat{\underline{k}}) = \int_{-\infty}^{\infty} d\rho \; \hat{\gamma}(\hat{\underline{k}},2\rho) \; e^{-ik\rho}, \quad (6.1.14)$$

where $\tilde{\gamma}(\underline{k})$; $\underline{k} = k\hat{\underline{k}}$, is the Fourier transform of $\gamma(\underline{r})$.

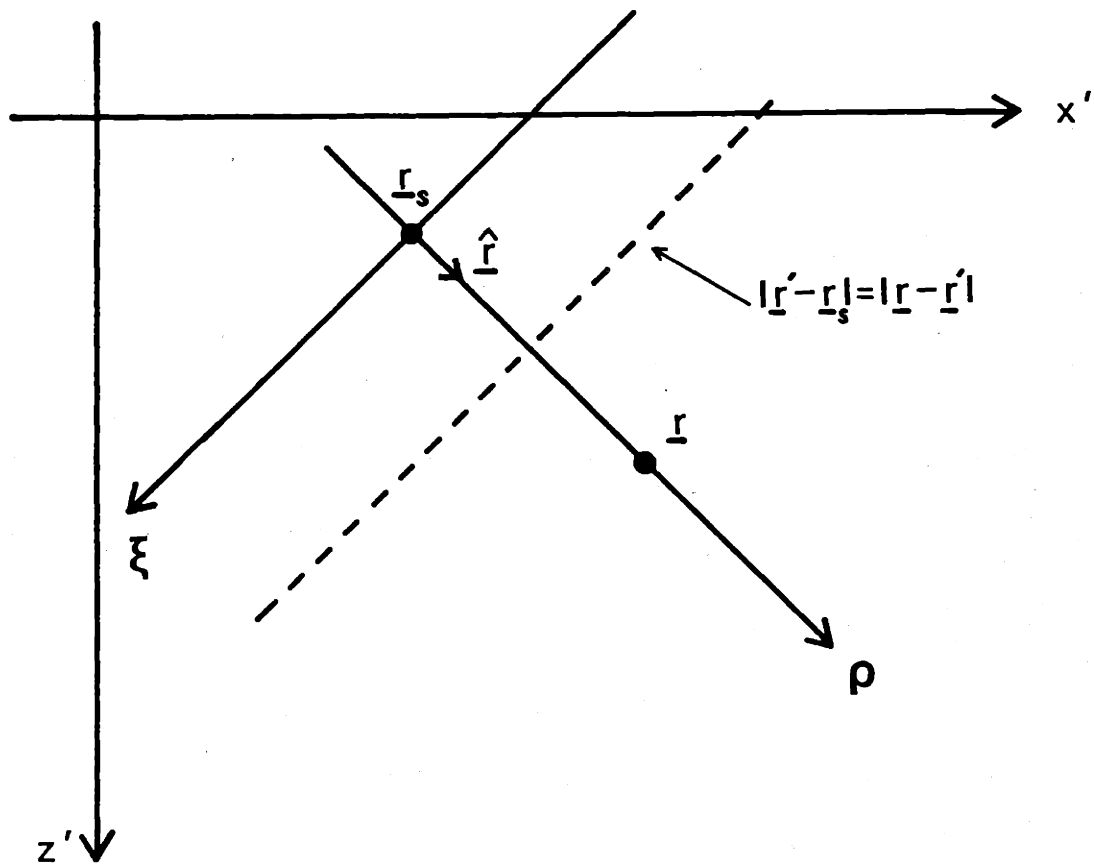

Figure 6.3. Change of coordinates for a given source location and an image point in the medium. The zero-time image at a point $\underline{r}$ is the integral of the potential along the dashed line.

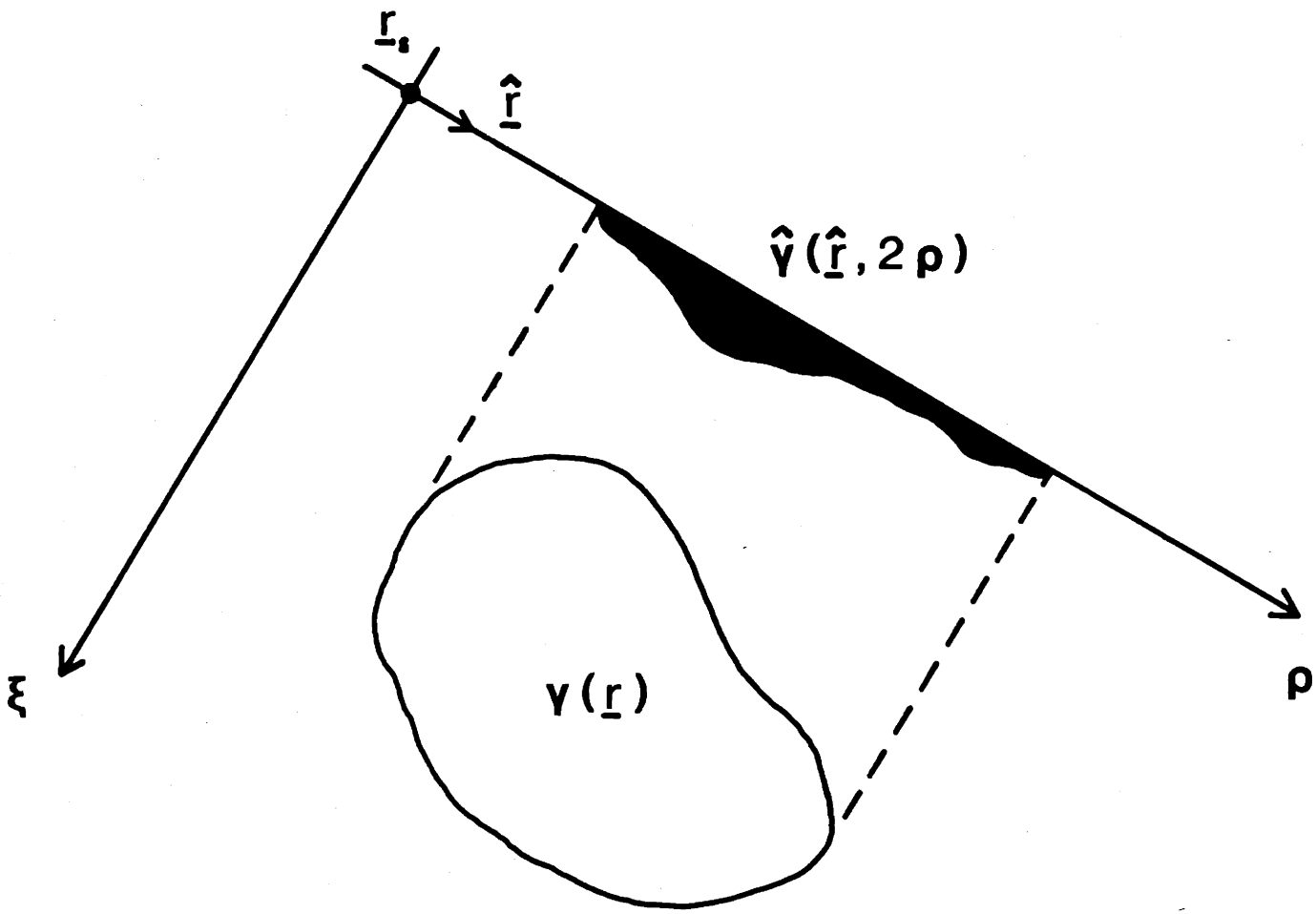

Figure 6.4. One projection of the velocity function obtained by the method of zero-time imaging.

From the Fourier representation of $\gamma(\underline{r})$ and using equation (6.1.14), it can be shown that

$$\gamma(\underline{r}) = \frac{1}{4\pi^2} \int_0^{2\pi} d\hat{\underline{k}} \int_0^{\infty} dk\ k\ e^{ik\hat{\underline{k}}\cdot\underline{r}} \int_{-\infty}^{\infty} d\rho\ \hat{\gamma}(\hat{\underline{k}},2\rho)\ e^{-ik\rho}. \tag{6.1.15}$$

This equation gives the reconstruction of $\gamma(\underline{r})$ from its projections and it can be implemented by mapping the polar coordinates into cartesian coordinates in the Fourier domain.

An alternative implementation can be obtained by noting that $\hat{\gamma}(-\hat{\underline{k}},-2\rho) = \hat{\gamma}(\hat{\underline{k}},2\rho)$. Using this property, equation (6.1.15) can be written as

$$\gamma(\underline{r}) = \frac{1}{8\pi^2} \int_0^{2\pi} d\hat{\underline{k}} \int_{-\infty}^{\infty} dk\ e^{ik\hat{\underline{k}}\cdot\underline{r}}\ |k| \int_{-\infty}^{\infty} d\rho\ \hat{\gamma}(\hat{\underline{k}},2\rho)\ e^{-ik\rho}. \tag{6.1.16}$$

This shows that for reconstruction the projections are first filtered with the filter $|k|$, then they are backprojected into the medium. Equation (6.1.16) can also be written in compact form

$$\gamma(\underline{r}) = \frac{1}{4\pi} \int_0^{2\pi} d\hat{\underline{k}}\ \mathbf{H} \left\{ \frac{\partial}{\partial s}\ \hat{\gamma}(\hat{\underline{k}},s) \right\}_{s=2\hat{\underline{k}}\cdot\underline{r}}, \tag{6.1.17}$$

where **H** denotes the Hilbert transform.

As was pointed out previously, the projections of $\gamma(\underline{r})$ along the lines that go through the origin are not obtained, instead we have the constraint that $\hat{\gamma}(\hat{\underline{r}},0) = 0$. Nevertheless, this has no effect on the reconstructed velocities within the volume V.

From equation (6.1.13)

$$\hat{\gamma}(\hat{\underline{r}},2r) = \int_{-\infty}^{\infty} d\xi\ \gamma(r,\xi;\hat{\underline{r}}) \quad ; \quad r \neq 0$$

$$= 0 \quad ; \quad r = 0 \,. \tag{6.1.18}$$

The integration limits are extended to infinity since $\gamma(r,\xi;\hat{\underline{r}})$ is zero outside $[\ \xi_1(\underline{r})\ ;\ \xi_2(\underline{r})\ ]$. Let the reconstructed velocity function $\gamma_r(\underline{r})$ be the sum of the true velocity function and an error term

$$\gamma_r(\underline{r}) = \gamma(\underline{r}) + \gamma_e(\underline{r}) \tag{6.1.19a}$$

$$\hat{\gamma}(\hat{\underline{r}},2r) = \int_{-\infty}^{\infty} d\xi\ \gamma_r(r,\xi;\hat{\underline{r}}) \,. \tag{6.1.19b}$$

It follows from equations (6.1.18) and (6.1.19a,b) that the projections of the error term are given by

$$\int_{-\infty}^{\infty} d\xi\ \gamma_e(r,\xi;\hat{\underline{r}}) = -\int_{-\infty}^{\infty} d\xi\ \gamma(r,\xi;\hat{\underline{r}}) \quad ; \quad r = 0$$

$$= 0 \quad ; \quad \text{otherwise.} \tag{6.1.20}$$

Therefore, the only region where the error term is nonzero is an infinitely close neighbourhood of the source location. Since the source is located outside the medium this does not effect the reconstruction and

$$\gamma_r(\underline{r}) = \gamma(\underline{r}) \quad ; \quad \underline{r} \in V . \tag{6.1.21}$$

In summary, the velocity function $\gamma(\underline{r})$ is obtained from the observed scattered field in three steps :

1) Extrapolate the observed data to obtain $P_e(\underline{r},\omega)$. The extrapolation can be done directly by solving the boundary value problem numerically with a finite difference method. Alternatively, the Kirchhoff integral form in equation (4.1.1) can be used.

2) Obtain the zero time image field $\hat{\gamma}(\underline{r})$ by equation (6.1.7). In the time domain, equation (6.1.7) can be implemented by integrating and Hilbert transforming the observed traces before extrapolation. Then, the extrapolated field is imaged at time zero and scaled at all image points by $8\pi|\underline{r}-\underline{r}_s|$.

3) Reconstruct $\gamma(\underline{r})$ from its projections $\hat{\gamma}(\hat{\underline{r}},r)$. From equation (6.1.16) this reconstruction can be done in two steps:

a) Filter the projections

$$F(k,\hat{\underline{k}}) = |k| \int_{-\infty}^{\infty} d\rho \; \hat{\gamma}(\hat{\underline{k}},2\rho) \; e^{-ik\rho}, \tag{6.1.22a}$$

$$f(\underline{r},\hat{\underline{k}}) = \frac{1}{2\pi} \int_{-\infty}^{\infty} dk \; F(k,\hat{\underline{k}}) \; {}^{ik\hat{\underline{k}}\cdot\underline{r}}. \tag{6.1.22b}$$

b) Backproject the filtered projections

$$\gamma(\underline{r}) = \frac{1}{4\pi} \int_{0}^{2\pi} d\hat{\underline{k}} \; f(\underline{r},\hat{\underline{k}}). \tag{6.1.23}$$

6.2 Inversion by Source-Travel Time Imaging

In the previous section the zero-time imaging inversion method for the point source case was discussed. It was shown that if the receiver array surround the scattering medium then a complete set of projections of the velocity potential can be obtained from the zero-time image. In this section we consider another inversion method for the wide-band point source excitation problem for the general receiver array model shown in Figure 4.5. The method consists of three steps. First the observed scattered traces are filtered in time. Then, the filtered traces are backpropagated and imaged at the source-travel times. Finally, the travel-time image is filtered in space. The method is similar to the imaging-filtering method for the plane-wave case, discussed in Section 5.3. The temporal and spatial filters are quite different, however, as will be shown below.

It was shown in Section 4.2 that, for a receiver array asymptotic to a wedge with angular range $[\alpha_1 ; \alpha_2]$ the backpropagated (extrapolated) field can be represented by the volume integral

$$P_e^*(\underline{r},\omega) = k^2 \int_V d\underline{r}' \, \gamma(\underline{r}') \, P(\underline{r}',\omega) \, E(\underline{r},\underline{r}',\omega) \, , \tag{6.2.1}$$

where the extrapolated field kernel is given by

$$E(\underline{r},\underline{r}',\omega) = \frac{i \, sgn(\omega)}{4\pi} \int_{\alpha_2}^{\alpha_1} d\theta \, e^{i\underline{k} \cdot (\underline{r}-\underline{r}')} \, . \tag{6.2.2}$$

Here, θ is the angle corresponding to the unit vector $\hat{\underline{k}}$ and $\underline{k} = k\hat{\underline{k}}$. Using the Born

approximation we replace the total incident field $P(\underline{r}',\omega)$ in equation (6.2.1) by the background incident field $P_0(\underline{r}',\omega)$. The incident field in 2-D involves the Hankel function $H_0^{(1)}$, but when the source is a few wavelengths from the scatterers, we can approximate the Hankel function by its asymptotic expansion, thus,

$$P_0(\underline{r}',\omega) = S(\omega)\ \frac{i}{4}\ H_0^{(1)}\,(k|\underline{r}'-\underline{r}_s|) \approx S(\omega)\ \frac{e^{i\frac{\pi}{4}sgn(\omega)}}{(8\pi)^{1/2}}\ \frac{e^{ik|\underline{r}'-\underline{r}_s|}}{|k|^{1/2}\,|\underline{r}'-\underline{r}_s|^{1/2}}\ , \tag{6.2.3}$$

where $S(\omega)$ is the Fourier transform of the source wavelet. Substituting the integral representation of the kernel E and the asymptotic form of the incident field into equation (6.2.1), gives the following explicit expression for the extrapolated field

$$P_e^*(\underline{r},\omega) = \frac{i\ sgn(\omega)\,e^{i\frac{\pi}{4}sgn(\omega)}}{4\pi\,(8\pi)^{1/2}}\ |k|^{3/2}\ S(\omega)$$

$$\int_V d\underline{r}'\ \gamma(\underline{r}')\ \frac{e^{ik|\underline{r}'-\underline{r}_s|}}{|\underline{r}'-\underline{r}_s|^{1/2}} \int_{\alpha_2}^{\alpha_1} d\theta\ e^{i\underline{k}\cdot(\underline{r}-\underline{r}')}\ . \tag{6.2.4}$$

As in the plane-wave source case, we define the travel-time image $\beta(\underline{r})$ as follows

$$\beta(\underline{r}) = \left(\frac{8}{\pi}\right)^{1/2} \int_{-\infty}^{\infty} dk\ \frac{e^{-i\frac{\pi}{4}sgn(\omega)}}{|k|^{3/2}\ S(\omega)}\ P_e^*(\underline{r},\omega)\ e^{-ik|\underline{r}-\underline{r}_s|}\ . \tag{6.2.5}$$

The travel-time image $\beta(\underline{r})$ is obtained by first filtering the observed scattered field with the temporal filter

$$-4(2\pi c)^{1/2}\ \frac{e^{i\frac{3\pi}{4}sgn(\omega)}}{S(\omega)\ |\omega|^{3/2}} = \frac{4(2\pi c)^{1/2}}{S(\omega)} \left[\frac{1}{-i\omega}\right] \left[\frac{1}{-i\omega}\right]^{1/2} \tag{6.2.6}$$

and then by backpropagating and imaging at the travel times. The above filter can be implemented in three steps; 1) Deconvolve the time traces with the source wavelet. 2) Integrate the traces in time. 3) Apply a square-root integration filter. An impulse invariant design of the digital square-root integration filter is described in Appendix B. From equations (6.2.4) and (6.2.5) the travel-time image can be written as

$$\beta(\underline{r}) = \int_V d\underline{r}'\ \frac{\gamma(\underline{r}')}{|\underline{r}'-\underline{r}_s|^{1/2}}\ g(\underline{r},\underline{r}')\ , \tag{6.2.7}$$

where

$$g(\underline{r},\underline{r}') = \frac{1}{4\pi^2} \int_{\alpha_1}^{\alpha_2} d\theta \int_{-\infty}^{\infty} dk\ i\ sgn(k)\ e^{ik[|\underline{r}'-\underline{r}_s|-|\underline{r}-\underline{r}_s|+\hat{\underline{k}}\cdot(\underline{r}-\underline{r}')]}\ . \tag{6.2.8}$$

The relation (6.2.7) is similar to equation (5.3.5) of the plane-wave source case, and the travel-time image $\beta(\underline{r})$ represents the velocity potential filtered by $g(\underline{r},\underline{r}')$. The major difference, however, is that in this case the filter is not spatially invariant as can be seen from the above equation. In the following we will show that the inverse spatial filtering operation for the point source case consists in taking the radial gradient (with respect to the source location) of the image field. Define an estimate $\hat{\gamma}(\underline{r})$ of the potential as

$$\hat{\gamma}(\underline{r}) = |\underline{r}-\underline{r}_s|^{1/2}\ \hat{\underline{k}}_s(\underline{r}) \cdot \nabla\beta(\underline{r}) \tag{6.2.9a}$$

$$= |\underline{r}-\underline{r}_s|^{1/2} \int_V d\underline{r}'\ \frac{\gamma(\underline{r}')}{|\underline{r}'-\underline{r}_s|^{1/2}}\ \hat{\underline{k}}_s(\underline{r}) \cdot \nabla g(\underline{r},\underline{r}') \tag{6.2.9b}$$

$$\equiv |\underline{r}-\underline{r}_s|^{1/2} \int_V d\underline{r}'\ \frac{\gamma(\underline{r}')}{|\underline{r}'-\underline{r}_s|^{1/2}}\ h(\underline{r},\underline{r}')\ , \tag{6.2.9c}$$

where $\hat{\underline{k}}_s \equiv \dfrac{\underline{r}-\underline{r}_s}{|\underline{r}-\underline{r}_s|}$ and ∇ denotes the gradient operating on the variable $\underline{r}$. The new image $\hat{\gamma}(\underline{r})$, therefore, represents the velocity potential filtered by $h(\underline{r},\underline{r}') = \hat{\underline{k}}_s(\underline{r}) \cdot \nabla g(\underline{r},\underline{r}')$. For complete recovery of the potential the filter $h(\underline{r},\underline{r}')$ must be a delta function. However, if the receivers do not surround the medium we cannot expect to recover the potential completely. With an array of angular aperture $[\alpha_1\ ;\ \alpha_2]$ only the plane wave components of the scattered field within this range are observed. Since there is no obvious relation between the missing plane wave components and the observed components in the multidimensional case, we can only expect to obtain a partial reconstruction. In the following it will be shown that, in fact, in the incomplete observations case the filter $h(\underline{r},\underline{r}')$ is a partial delta function (i.e., a function reconstructed from a subset of the projections of a delta function by setting the missing projections to zero).

From equation (6.2.8), and using the fact that

$$\nabla[\,|\underline{r}'-\underline{r}_s| - |\underline{r}-\underline{r}_s| + \hat{\underline{k}} \cdot (\underline{r}-\underline{r}')\,] = \hat{\underline{k}} - \hat{\underline{k}}_s(\underline{r}) \tag{6.2.10}$$

the filter $h(\underline{r},\underline{r}')$ is given by

$$h(\underline{r},\underline{r}') = -\frac{1}{4\pi^2}\int_{\alpha_1}^{\alpha_2} d\theta \int_{-\infty}^{\infty} dk\,|k|\,\hat{\underline{k}}_s(\underline{r})\cdot(\hat{\underline{k}}-\hat{\underline{k}}_s)\,e^{ik[|\underline{r}'-\underline{r}_s|-|\underline{r}-\underline{r}_s|+\hat{\underline{k}}\cdot(\underline{r}-\underline{r}')]}\,. \tag{6.2.11}$$

For $\underline{r}'$ close to $\underline{r}$ the phase term in the integrand can be approximated by the first term of its Taylor series expansion, i.e.

$$|\underline{r}'-\underline{r}_s| - |\underline{r}-\underline{r}_s| \approx \frac{\underline{r}-\underline{r}_s}{|\underline{r}-\underline{r}_s|}\cdot(\underline{r}'-\underline{r}) = \hat{\underline{k}}_s(\underline{r})\cdot(\underline{r}'-\underline{r})\,. \tag{6.2.12}$$

Therefore the point spread function of the filter in the point source case can be approximately written as

$$h(\underline{r},\underline{r}') = -\frac{1}{4\pi^2}\int_{\alpha_1}^{\alpha_2} d\theta \int_{-\infty}^{\infty} dk\,|k|\,\hat{\underline{k}}_s(\underline{r})\cdot[\hat{\underline{k}}-\hat{\underline{k}}_s(\underline{r})]\,e^{ik[\hat{\underline{k}}-\hat{\underline{k}}_s(\underline{r})]\cdot(\underline{r}-\underline{r}')}\,. \tag{6.2.13}$$

Note that this point spread function is similar to the point spread function for the plane wave case, except that the incidence angle $\hat{\underline{k}}_s$ in the plane-wave source case is replaced here by the *local incidence angle* $\hat{\underline{k}}_s(\underline{r}) = \frac{\underline{r}-\underline{r}_s}{|\underline{r}-\underline{r}_s|}$. As in the plane wave case, we consider the change of intgeration variables from (θ,k) to (ϕ,u) such that

$$\hat{\underline{u}}(\underline{r}) = \begin{bmatrix}\cos\phi(\underline{r})\\ \sin\phi(\underline{r})\end{bmatrix} \equiv \frac{\hat{\underline{k}}-\hat{\underline{k}}_s(\underline{r})}{|\hat{\underline{k}}-\hat{\underline{k}}_s(\underline{r})|}\,, \tag{6.2.14a}$$

$$u(\underline{r}) \equiv k\,|\hat{\underline{k}}-\hat{\underline{k}}_s(\underline{r})| = k\;2\,|\hat{\underline{u}}\cdot\hat{\underline{k}}_s(\underline{r})|\,, \tag{6.2.14b}$$

i.e., $\hat{\underline{u}}(\underline{r})$ is the unit vector along the direction $\underline{k}-\underline{k}_s(\underline{r})$, and $u(\underline{r})$ is obtained by

multiplying the wavenumber k by the length of $\hat{\underline{k}}-\hat{\underline{k}}_s(\underline{r})$. The angle $\phi(\underline{r})$ can be simply related to the angles θ and $\theta_s(\underline{r})$ as follows

$$\phi(\underline{r}) = \frac{\theta + \theta_s(\underline{r}) \pm \pi}{2} , \tag{6.2.15}$$

where $\theta_s(\underline{r})$ is the polar angle of the image point $\underline{r}$ with respect to the point source location $\underline{r}_s$. By noting that $\hat{\underline{u}}(\underline{r}) \cdot \hat{\underline{k}}_s(\underline{r}) = -|\hat{\underline{u}}(\underline{r}) \cdot \hat{\underline{k}}_s(\underline{r})|$, with respect to the new variables the point spread function becomes

$$h(\underline{r},\underline{r}') = \frac{1}{4\pi^2} \int_{\phi_1(\underline{r})}^{\phi_2(\underline{r})} d\phi \int_{-\infty}^{\infty} du\, |u|\, e^{iu\hat{\underline{u}} \cdot (\underline{r}-\underline{r}')} , \tag{6.2.16}$$

where the integration limits, which specify the range of available projection angles at the reconstruction point $\underline{r}$, are given by

$$\phi \in \Phi(\underline{r}) = \left[\frac{\alpha_2 + \theta_s(\underline{r}) \pm \pi}{2} ; \frac{\alpha_1 + \theta_s(\underline{r}) \pm \pi}{2} \right] . \tag{6.2.17}$$

Finally, the point spread function can be expressed in cartesian coordinates as

$$h(\underline{r},\underline{r}') = \frac{1}{4\pi^2} \int_{U_\Phi(\underline{r})} d\underline{u}\, e^{i\underline{u} \cdot (\underline{r}-\underline{r}')} , \tag{6.2.18}$$

where $\underline{u} = u\hat{\underline{u}}$ and $U_\Phi(\underline{r})$ denotes the region in cartesian coordinates contained in the cone given by equation 6.2.17, as shown in Figure 6.5. Therefore the filter $h(\underline{r},\underline{r}')$, in general, is a function obtained from a subset of projections of the delta function.

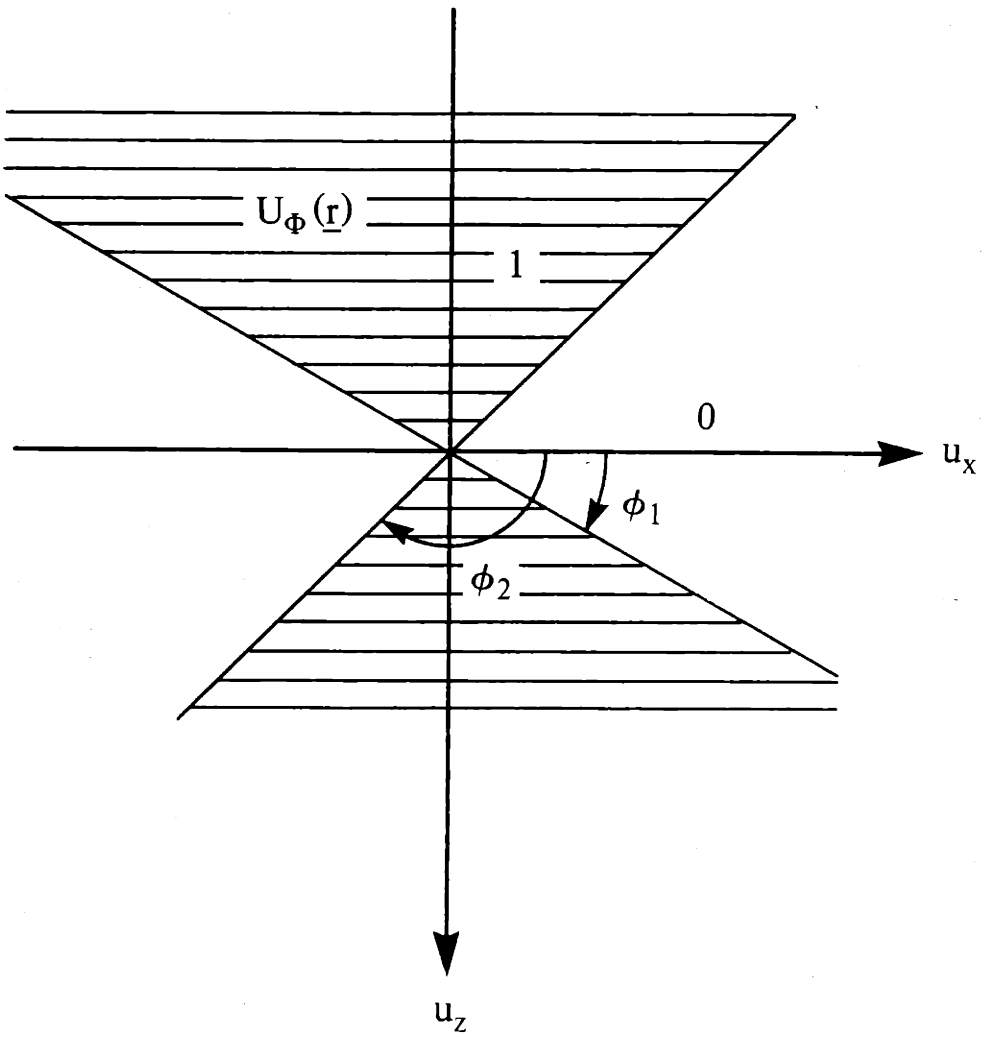

Figure 6.5. Fourier transform of the point spread function at point $\underline{r}$. The value of the transform is 1 in the shaded area and 0 elsewhere.

Since the range of available projection angles $[\phi_1(\underline{r})\ ;\ \phi_2(\underline{r})]$ depends on the angular position of the imaged point with respect to the source, the resolution at a given point depends on its location as well as on the angular aperture of the receiver array. Also note that, if the receivers surround the medium, i.e. $\Phi = [0\ ;2\pi]$, then $U_\Phi(\underline{r})$ covers the whole plane and from equation 6.2.18 we have $h(\underline{r},\underline{r}') = \delta(\underline{r}-\underline{r}')$. The potential can be completely recovered by imaging at the source-travel times as well as by imaging at zero time (as discussed in the previous section).

From equation (6.2.9a) an estimate $\hat{\gamma}(\underline{r})$ of the potential can be obtained by taking the radial derivative of the source-travel times image $\beta(\underline{r})$, where the radial direction is defined with respect to the location of the source. Alternatively, $\hat{\gamma}(\underline{r})$ can be obtained directly from the extrapolated field $P_e^*(\underline{r},\omega)$ as follows. From equations (6.2.5) and (6.2.9a) it can be shown that

$$\hat{\gamma}(\underline{r}) = -4(2\pi c)^{1/2}\,|\underline{r}-\underline{r}_s|^{1/2}\,\frac{1}{2\pi}\int_{-\infty}^{\infty} d\omega\,\frac{1}{(-i\omega)^{1/2}\,S(\omega)}$$

$$\left[\frac{1}{c}\,P_e^*(\underline{r},\omega) - \hat{\underline{k}}_s(\underline{r})\cdot\nabla\frac{P_e^*(\underline{r},\omega)}{i\omega}\right] e^{-ik|\underline{r}-\underline{r}_s|}\,, \tag{6.2.19}$$

where $c = \omega/k$ is the background velocity. Then $\hat{\gamma}(\underline{r})$ can be obtained from the observed scattered field with the following steps :

1) First, we deconvolve the observed traces with the source wavelet and we apply a square-root integration filter. This corresponds to multiplication by $\dfrac{1}{(-i\omega)^{1/2}\,S(\omega)}$ in the above equation.

2) Then, we backpropagate the filtered traces with a finite difference algorithm.

At each time step of the algorithm we obtain the extrapolated field $P_e^*(\underline{r},\omega)$ in the time domain at every point $\underline{r}$ in the medium. Also, at every point $\underline{r}$ we integrate the backpropagated field by adding the field obtained in the current time step to the previous integrated field. This integrated field corresponds to the term $\frac{P_e^*(\underline{r},\omega)}{i\omega}$ in equation (6.2.19).

3) Next, at each point $\underline{r}$ in the medium we image the quantity in the brackets in equation (6.2.19) at the time equal to the travel time from the source to $\underline{r}$. The first term in the brackets is simply the image of the field divided by the velocity c. The second term in the brackets can be written as

$$\frac{1}{|\underline{r}-\underline{r}_s|}\left[(x-x_s)\frac{\partial}{\partial x}\frac{P_e^*(\underline{r},\omega)}{i\omega} + (z-z_s)\frac{\partial}{\partial z}\frac{P_e^*(\underline{r},\omega)}{i\omega} \right], \tag{6.2.20}$$

where $\underline{r} = (x,z)$, and $\underline{r}_s = (x_s,z_s)$ is the location of the source. The derivative terms in the above expression can be obtained by taking the difference of the integrated field between adjacent grid points of the finite difference algorithm. In summary, at every point $\underline{r}$ when the time is equal to the travel time $\tau_r = |\underline{r}-\underline{r}_s|/c$, we evaluate expression (6.2.20) and we subtract it from the image of the extrapolated field divided by c.

4) In the final step, after all points in the medium are imaged as described above, we multiply the resulting image by $-4(2\pi c)^{1/2}\,|\underline{r}-\underline{r}_s|^{1/2}$.

6.3 Inversion for the 2½ Dimensional Problem

The inversion methods presented in the previous sections of this chapter were derived for the two and three dimensional problems. As was pointed out previously, the two dimensional problem consists of a two dimensional medium and a line source located along the direction in which the medium velocities are constant. The receivers are contained inside a plane which is perpendicular to the line source. In this section we will consider the same observation geometry as in the two dimensional problem except that we replace the line source by a point source located in the receiver plane. We choose the y axis to be the direction in which the medium velocities are constant and we assume that the source and receivers are contained in the $y = 0$ plane. The main differences between the 2½ dimensional problem and the two and three dimensional problems are;

1) Unlike in the two dimensional problem the wavefield varies along the y axis.

2) Unlike in the three dimensional problem the scattered field is not observed over a two-dimensional array, instead it is observed only along a one-dimensional array located in the $y = 0$ plane.

The volume integral representation of the backpropagated field for the 2½ dimensional problem was derived in Section 4.3. From equation (4.3.10) we have

$$P_e^*(\underline{r},\omega) = \int_V d\underline{r}'\, \gamma(\underline{r}')\, \frac{e^{ik|\underline{r}'-\underline{r}_s|}}{|\underline{r}'-\underline{r}_s|^{1/2}}\, E_{1/2}(\underline{r},\underline{r}',\omega)\ , \tag{6.3.1}$$

where from equation (4.3.13) the extrapolated field kernel $E_{1/2}$ for the 2½ dimensional problem is given by

$$E_{1/2}(\underline{r},\underline{r}',\omega) = \frac{(ik)^{1/2}}{4\pi} \int_{\alpha_2}^{\alpha_1} d\theta \; e^{i\underline{k}\cdot(\underline{r}-\underline{r}')} \; . \tag{6.3.2}$$

Here, θ is the angle corresponding to the unit vector $\hat{\underline{k}}$, and $k = k\hat{\underline{k}}$. Equation (6.3.2) gives the kernel $E_{1/2}$ for a receiver array with an angular aperture [α_1 ; α_2], as shown in Figure 4.5. If the receivers surround the scatterer, the angular aperture of the array becomes [0 ; 2π] and the kernel is

$$E_{1/2}(\underline{r},\underline{r}',\omega) = \frac{(ik)^{1/2}}{2} J_0(k|\underline{r}-\underline{r}'|) \; , \tag{6.3.3}$$

where J_0 is the Bessel function of the first kind. In the following two sections we present the zero-time imaging and source-travel time imaging methods for reconstructing the potential γ in equation (6.3.1).

6.3.1 2½ dimensional inversion by zero-time imaging

First we consider the zero-time imaging method for the case of complete receiver coverage. From equations (6.3.1) and (6.3.3) the extrapolated field can be written as

$$P_e^*(\underline{r},\omega) = \frac{(ik)^{1/2}}{2} \int_V d\underline{r}' \; \gamma(\underline{r}') \; \frac{e^{ik|\underline{r}'-\underline{r}_s|}}{|\underline{r}'-\underline{r}_s|^{1/2}} \; J_0(k|\underline{r}-\underline{r}'|) \; . \tag{6.3.4}$$

In the 2½ dimensional case the exponential term in the above integral replaces the Hankel function that appears in the two dimensional case (equation 6.1.5). Now, if the scatterers are at least a few dominant wavelengths away from the point source, using the asmptotic expansion of the Hankel function for large arguments, we can

approximate the exponential term in equation (6.3.4) by

$$\frac{(ik)^{1/2}}{2} \frac{e^{ik|\underline{r}'-\underline{r}_s|}}{|\underline{r}'-\underline{r}_s|^{1/2}} \approx (2\pi)^{1/2} |k| \frac{i}{4} H_0^{(1)}(k|\underline{r}'-\underline{r}_s|) . \tag{6.3.5}$$

Then, the integral expression for the extrapolated field in the 2½ dimensional case becomes similar to the the integral expression for the two dimensional case given in equation (6.1.5). However, this does not mean that the 2½ and two dimensional problems can be treated in the same way. Recall that the extrapolated field in the 2½ dimensional case is obtained by backpropagating the filtered scattered field $\bar{P}_s$ given by equation (4.3.3), whereas in the two dimensional problem the extrapolated field is obtained directly from P_s. Using the property (6.1.3), if we first take the imaginary parts of both sides in equatin (6.3.4) and then multiply the result by $-k/(8\pi)^{1/2}$ we obtain the following relation

$$-\frac{k}{(8\pi)^{1/2}} \operatorname{Im}\{ P_e^*(\underline{r},\omega) \} = -\frac{k^2}{8} \int_V d\underline{r}' \, \gamma(\underline{r}') \, J_0(k|\underline{r}'-\underline{r}_s|) \, J_0(k|\underline{r}-\underline{r}'|) . \tag{6.3.6}$$

The right hand side of this equation is the same as the right hand side of equation (6.1.6). Consequently, equation (6.3.6) can be inverted by following the same steps as in Section 6.1.

In particular, consider the function $\hat{\gamma}(\underline{r})$ obtained from the 2½-D extrapolated field by imaging at time zero as

$$\hat{\gamma}(\underline{r}) = -\frac{(2/\pi)^{1/2}}{c} |\underline{r}-\underline{r}_s| \int_{-\infty}^{\infty} d\omega \; isgn(\omega) \; P_e^*(\underline{r},\omega) \tag{6.3.7}$$

The filter $isgn(\omega)$ appearing in the above equation corresponds to the Hilbert transform and can be combined with the other filters appearing in equation (4.3.3), which are applied to the scattered field before backpropagation. Using the fact that the real part of $P_e(\underline{r},\omega)$ is even symmetric with respect to ω, the function $\hat{\gamma}(\underline{r})$ can be expressed as

$$\hat{\gamma}(\underline{r}) = (8/\pi)^{1/2} |\underline{r}-\underline{r}_s| \int_0^{\infty} dk \; \mathrm{Im}\{ P_e^*(\underline{r},\omega) \}$$

$$= |\underline{r}-\underline{r}_s| \int_V d\underline{r}' \; \gamma(\underline{r}') \int_0^{\infty} dk \; k \; J_0(k|\underline{r}'-\underline{r}_s|) \; J_0(k|\underline{r}-\underline{r}'|) \; . \tag{6.3.8}$$

The zero-time image $\hat{\gamma}$ given above is exactly the same as the image obtained for the two dimensional problem in equation (6.1.8). It was shown in Section 6.1 that, for a fixed direction $\hat{\underline{r}} = (\underline{r}-\underline{r}_s)/|\underline{r}-\underline{r}_s|$, $\hat{\gamma}(\hat{\underline{r}},r)$ is the projection of $\gamma(\underline{r})$ onto the line defined by $\hat{\underline{r}}$, as shown in Figure 6.4. Here, $r = |\underline{r}-\underline{r}_s|$ denotes the distance from the source location. In the complete coverage case, projections at all angles corresponding to the unit vector $\hat{\underline{r}}$ are obtained from the zero-time image $\hat{\gamma}(x,z)$ by mapping the cartesian coordinates (x,z) into the polar coordinate system centered at the source location $\underline{r}_s$. Then, the image $\hat{\gamma}$ can be written as

$$\hat{\gamma}(\hat{\underline{r}},r) = \int_{(\underline{r}'-\underline{r}_s)\cdot\hat{\underline{r}} = \frac{r}{2}} dl \; \gamma(\underline{r}') \; , \tag{6.3.9}$$

where $(\hat{\underline{r}}, r)$ is the polar coordinate system centered at $\underline{r}_s$. Finally, the potential $\gamma(\underline{r})$ can be recovered from its projections by the inverse Radon transform as described in Section 6.1.

6.3.2 2½ dimensional inversion by source-travel time imaging

Next we consider the source-travel time imaging method for the 2½ dimensional problem. From equations (6.3.1) and (6.3.2) the extrapolated field associated with a receiver array with angular aperture $[\,\alpha_1\,;\,\alpha_2\,]$ is given by

$$P_e^*(\underline{r},\omega) = \frac{(ik)^{1/2}}{4\pi} \int_V d\underline{r}'\, \gamma(\underline{r}')\, \frac{e^{ik|\underline{r}'-\underline{r}_s|}}{|\underline{s}-\underline{s}'|^{1/2}} \int_{\alpha_2}^{\alpha_1} d\theta\, e^{i\underline{k}\cdot(\underline{r}-\underline{r}')}\,, \tag{6.3.10}$$

where θ is the angle corresponding to the unit vector $\hat{\underline{k}} = \underline{k}/|\underline{k}|$. Let the travel-time image $\beta(\underline{r})$ be defined as follows

$$\beta(\underline{r}) = \frac{c^{1/2}}{\pi} \int_{-\infty}^{\infty} d\omega\, \frac{e^{i\frac{\pi}{4}sgn(\omega)}}{|\omega|^{1/2}}\, P_e^*(\underline{r},\omega)\, e^{-ik|\underline{r}-\underline{r}_s|}\,, \tag{6.3.11}$$

where $c = \omega/k$ is the background velocity. An impulse invariant design of the above square-root integrator $(-i\omega)^{-1/2} = e^{i\pi/4 sgn(\omega)}\,|\omega|^{-1/2}$ above is presented in Appendix B. From equations (6.3.10) and (6.3.11) we obtain

$$\beta(\underline{r}) = \int_V d\underline{r}'\, \frac{\gamma(\underline{r}')}{|\underline{r}'-\underline{r}_s|^{1/2}}\, g(\underline{r},\underline{r}')\,, \tag{6.3.12}$$

where the function $g(\underline{r},\underline{r}')$ is given by

$$g(\underline{r},\underline{r}') = \frac{1}{4\pi^2} \int_{\alpha_1}^{\alpha_2} d\theta \int_{-\infty}^{\infty} dk \; i \; sgn(k) \; e^{ik[|\underline{r}'-\underline{r}_s|-|\underline{r}-\underline{r}_s|+\hat{\underline{k}}\cdot(\underline{r}-\underline{r}')]} \; . \tag{6.3.13}$$

Equations (6.3.12) and (6.3.13) which express the source-travel time image in terms of the scattering potential in the 2½ dimensional problem are exactly the same as equations (6.2.7) and (6.2.8) obtained for the two dimensional problem. Therefore, inversion in this case can be carried out by following the same steps as described in Section 6.2. In summary, an estimate $\hat{\gamma}(\underline{r})$ of the potential is obtained from the travel-time image $\beta(\underline{r})$ by

$$\hat{\gamma}(\underline{r}) = |\underline{r}-\underline{r}_s|^{1/2} \; \hat{\underline{k}}_s(\underline{r}) \cdot \nabla\beta(\underline{r}) \; , \tag{6.3.14}$$

where $\hat{\underline{k}}_s(\underline{r}) = (\underline{r}-\underline{r}_s)/|\underline{r}-\underline{r}_s|$ is the local direction of incidence of the incident field and ∇ denotes the gradient with respect to the variable $\underline{r}$. The estimate $\hat{\gamma}$ of the potential is related to the true potential via

$$\hat{\gamma}(\underline{r}) = |\underline{r}-\underline{r}_s|^{1/2} \int_V d\underline{r}' \; \frac{\gamma(\underline{r}')}{|\underline{r}'-\underline{r}_s|^{1/2}} \; h(\underline{r},\underline{r}') \; , \tag{6.3.15}$$

where the point spread function h is given by

$$h(\underline{r},\underline{r}') = \hat{\underline{k}}_s(\underline{r}) \cdot \nabla g(\underline{r},\underline{r}') \; . \tag{6.3.16}$$

Finally, it was shown in Section 6.2 that the point spread function h corresponds, in general, to a partial reconstruction of a delta function from a subset of its projections. The point spread function is approximately given by the following inverse Fourier

transform

$$h(\underline{r},\underline{r}') = \frac{1}{4\pi^2} \int_{U_\Phi(\underline{r})} d\underline{u}\ e^{i\underline{u}\cdot(\underline{r}-\underline{r}')} . \tag{6.3.17}$$

Here, $U_\Phi(\underline{r})$ is the spatially variant region of coverage in the Fourier domain in which the Fourier transform of h is nonzero. This region of coverage consists of a cone containing the range of angles given in equation (6.2.17). To conclude we have shown that the inversion procedure for the 2½ dimensional problem is similar to that obtained for the two dimensional inversion problem with the exception that the extrapolated field is obtained from the filtered scattered field $\overline{P}_s$, given in equation (4.3.3), instead of from the scattered data itself.

6.4 Synthetic Examples

In this section we present various numerical examples for the zero-time imaging and source-travel time imaging inversion methods described in Sections 6.1 and 6.2. We consider a two dimensional medium in which the velocities are constant along the y axis. The synthetic scattered field data used in these examples was obtained by a finite difference algorithm as described in Appendix C.

Inversion by zero-time imaging with complete observations

Figure 6.6 shows the contour plot of the velocity structure used in the first example. Solid and dotted contours represent velocities that are higher and lower than the background velocity (750 m/s) respectively, with contour increments of 10 m/s. The difference between the peak velocities is about 14% of the background velocity and the distance between the peaks corresponds to approximately one dominant wavelength. As shown in Figure 6.6 the distance between the point source and the scatterers is on the order of the size of the scattering region. The source wavelet consists of a 4 point Blackman window (Blackman-Harris window) with a pulse duration of 0.02 seconds. Receivers are located on the square frame surrounding the scatterers as shown in Figure 6.6. Inversion is done as follows :

1) According to equation (6.1.7), the observed traces are Hilbert transformed and then integrated in time.

2) The resulting traces are backpropagated with a finite difference scheme by using the time reversed scattered field as to specify the boundary values at the receiver locations. The finite difference algorithm is run for all observed time samples and the backpropagated field is imaged at the last sample (time zero) simultaneously

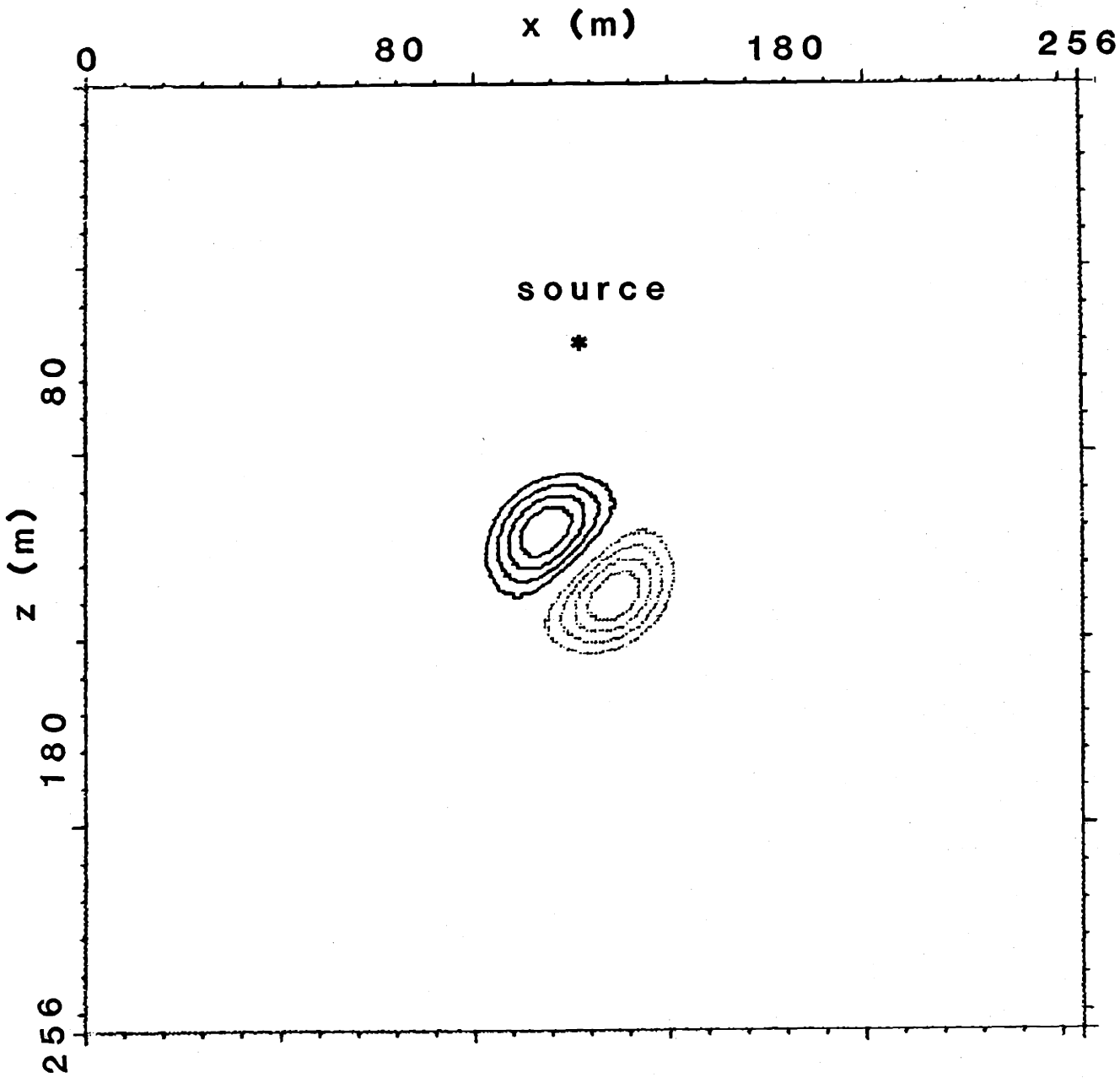

Figure 6.6. Velocity structure and the experiment geometry of the first example. Receivers are located on the square frame surrounding the medium.

at all grid points. The obtained zero-time image is shown in Figure 6.7a where the positive values of the image are shaded. It is seen in this figure that the scattered field is mapped onto circles which are centered at the scatterers and which also pass through the source location. This zero-time image is then weighted at each point by the radial distance from the source according to equation (6.1.7). The projections of the potential, $\hat{\gamma}(\hat{\underline{r}},r)$ in equation (6.1.13), are obtained from the image by picking up points along the radial lines passing through the source location. This is shown in Figure 6.7b where the vertical axis denotes the polar angle, measured clockwise from the x axis, and the horizontal axis denotes the distance from the source. Some characteristic features of the scattering medium can be readily seen from these projections. For example, projections in the vicinity of 135° are very small because of the cancellation of the potentials in the high and low velocity regions. On the other hand for an angle of projection in the vicinity of 45° the high and low velocity regions do not block each other and projections of the negative and positive potentials corresponding to these regions can clearly be seen.

3) The last step of inversion is to reconstruct the potential from the projections shown in Figure 6.7b by using either equation (6.1.16) or equations (6.1.22) and (6.1.23). The obtained potential is then converted to velocities. Figures 6.8a,b show the true and reconstructed velocities respectively with identical contour levels of 15, 25 and 35 m/s. It is seen that the locations, shapes and the values of the velocity changes are obtained by this method with reasonable accuracy. The main differences between the true and reconstructed velocities are as follows. First, the magnitudes of the reconstructed velocities are smaller than the true velocities. One reason for this is the spatial smoothing due to the bandlimited source wavelet used to probe the

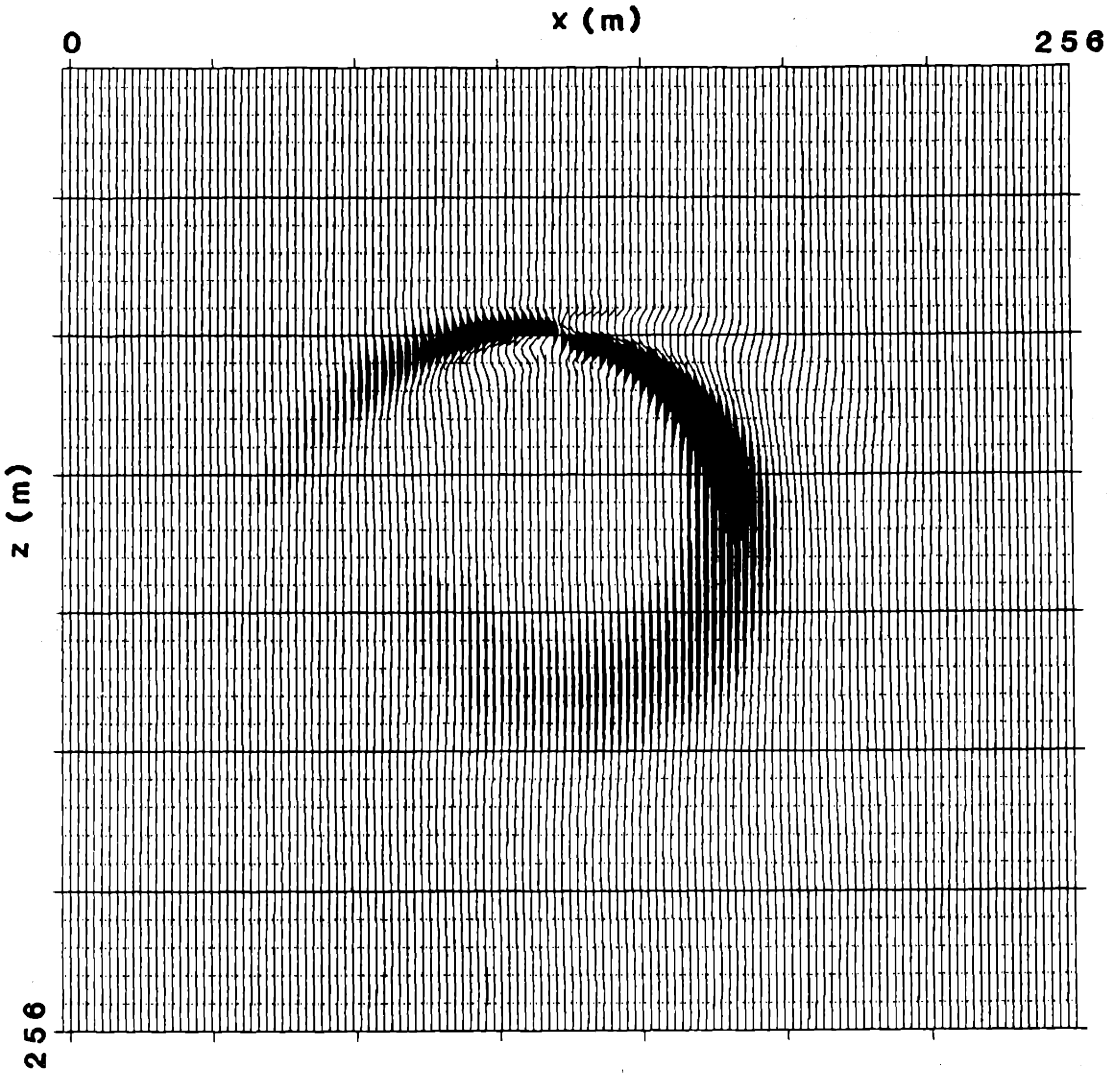

Figure 6.7. (a) The zero-time image obtained from the scattered field.

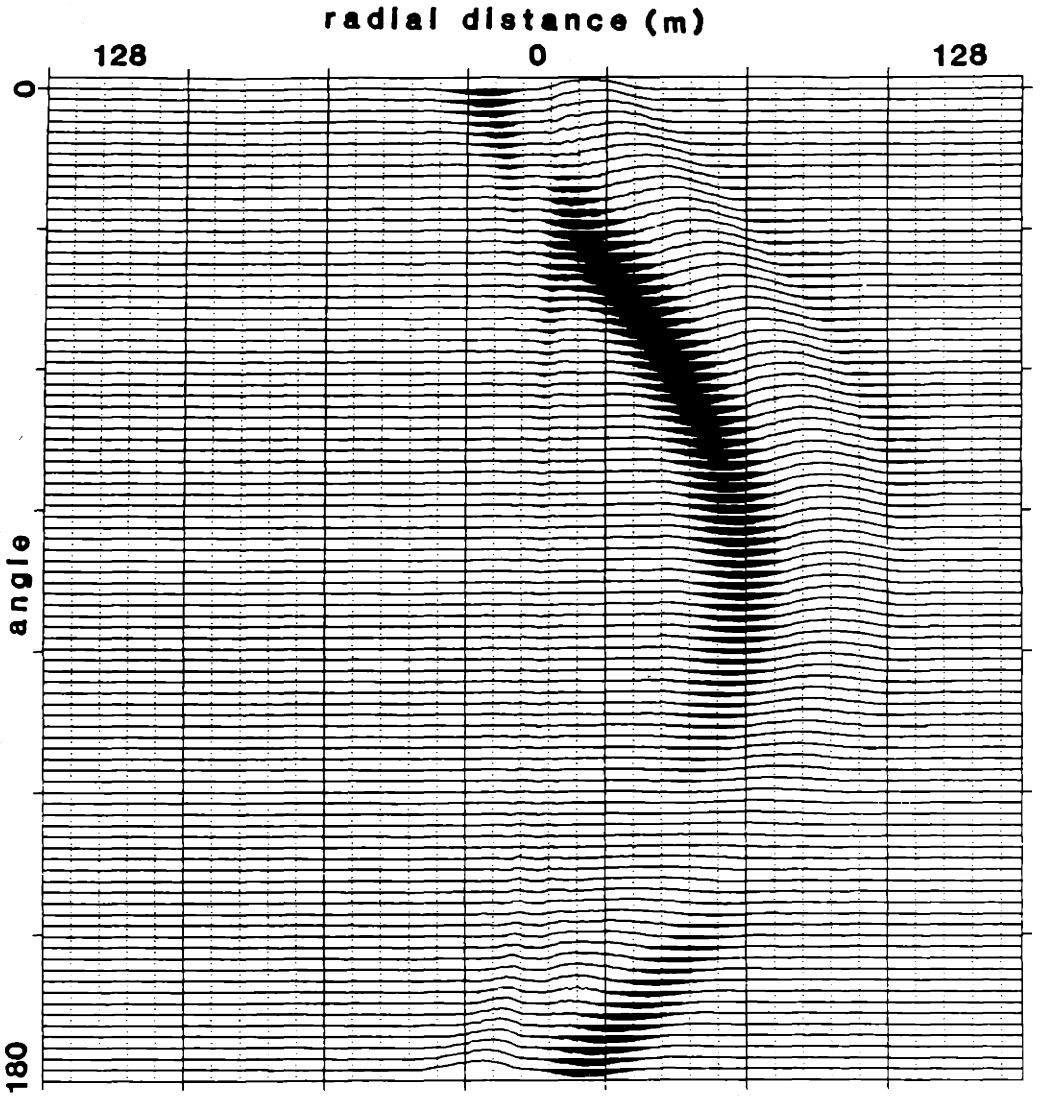

(b) Projections obtained from the zero-time image. Part (b) is obtained from the image shown in part (a) by plotting it in the polar coordinates centered at the source location. Vertical and horizontal axes correspond to polar angle and range respectively.

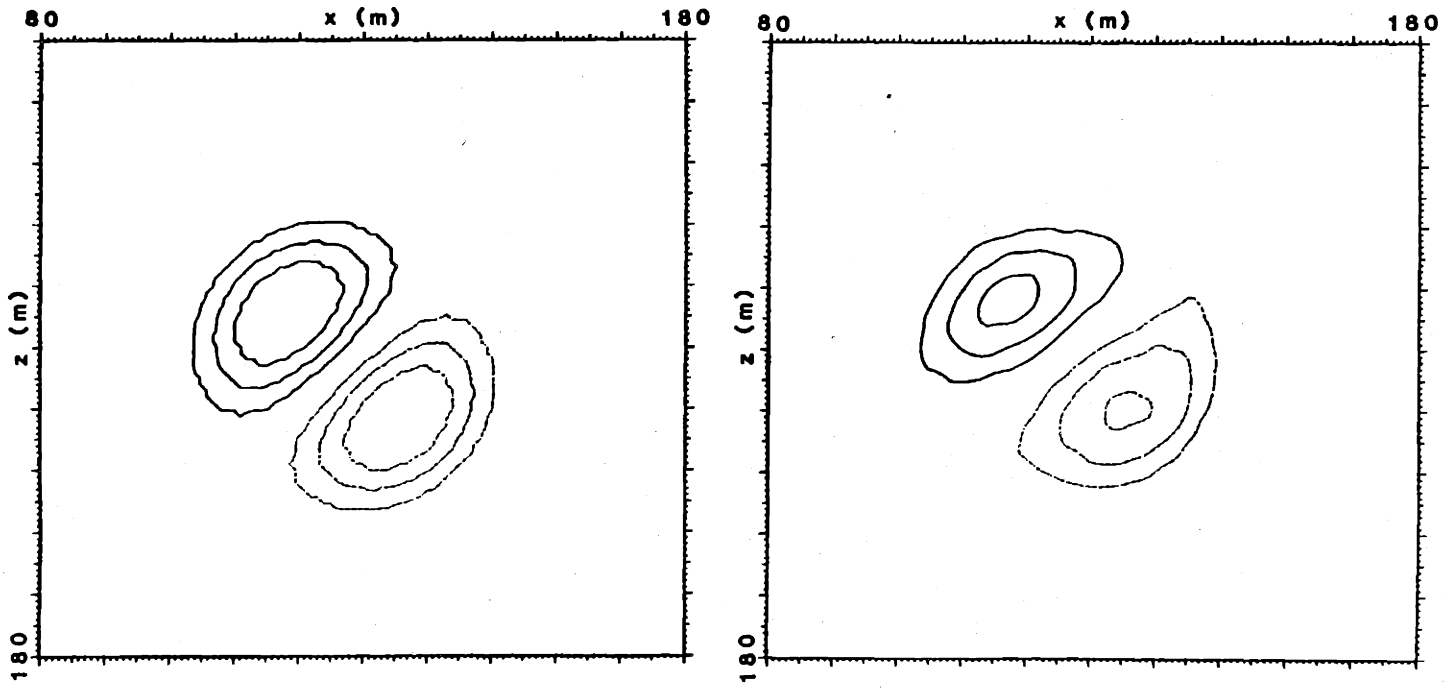

Figure 6.8. Inversion result. (a) True velocity structure. (b) Velocities reconstructed from the projections shown in Figure 6.7b.

medium. This smoothing reduces the absolute values of the reconstructed velocities since the size of the region of inhomogeneity is on the order of the dominant wavelength in the background medium. Second, the location of the low velocity region is slightly shifted upwards compared to its true position. This is essentially due to the Born approximation which was assumed in deriving the inversion method. From Figure 6.6 it is seen that the high velocity region of the scatterer lies between the source and the low velocity region. Therefore, there is a difference between the true travel times of the field incident on the low velocity region and the travel times that are obtained by the homogeneous background approximation. Since the true travel times in this region are smaller than the background travel times the reconstructed image is slightly shifted towards the source.

Inversion by travel-time imaging with incomplete observations

Figure 6.9 shows the contour plot of the velocity structure used in the next example. Solid and dotted contours represent velocities higher and lower than the background velocity respectively, with contour increments of 50 m/s. The source wavelet consists of a 4 point Blackman window with a pulse duration of 0.02 seconds. Receivers are located on the square frame surrounding the scatterers shown in Figure 6.9. Figures 6.10a,b,c,d show the scattered field observed at the receivers located on the left, top, right and bottom sides of the frame respectively. Inversion was done by using equation (6.2.19) by following the steps described in the section following this equation. Figures 6.11a,b,c show the velocities reconstructed by using several subsets of the receiver array. In these figures, the vertical axis shows the difference velocity obtained by subtracting background velocity from the reconstructed velocities. The

horizontal axes (depth and offset) correspond to a region (from 50 meters to 350 meters in both directions) around the scatterers. Velocities obtained by using only the receivers located on the left and top sides of the receiver frame are shown in Figure 6.11a. Figure 6.11b shows the reconstructed velocities when we use the receivers on the left, top and right sides of the frame. Figure 6.11c, is the inversion result when we use all the receivers. The true velocity model is shown in Figure 6.11d for comparison.

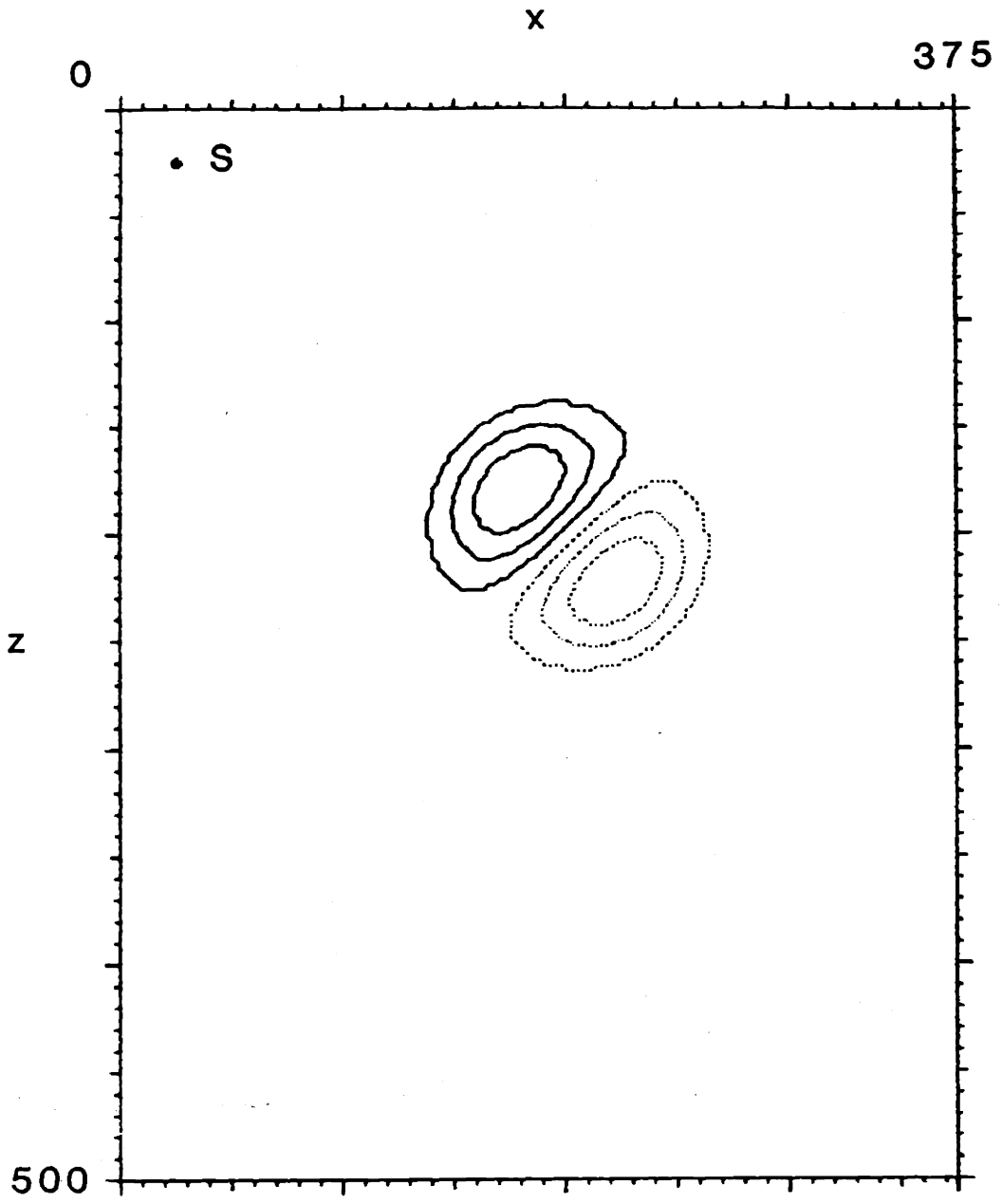

Figure 6.9. Velocity structure and the experiment geometry of the second example. Receivers are located on the square frame surrounding the medium.

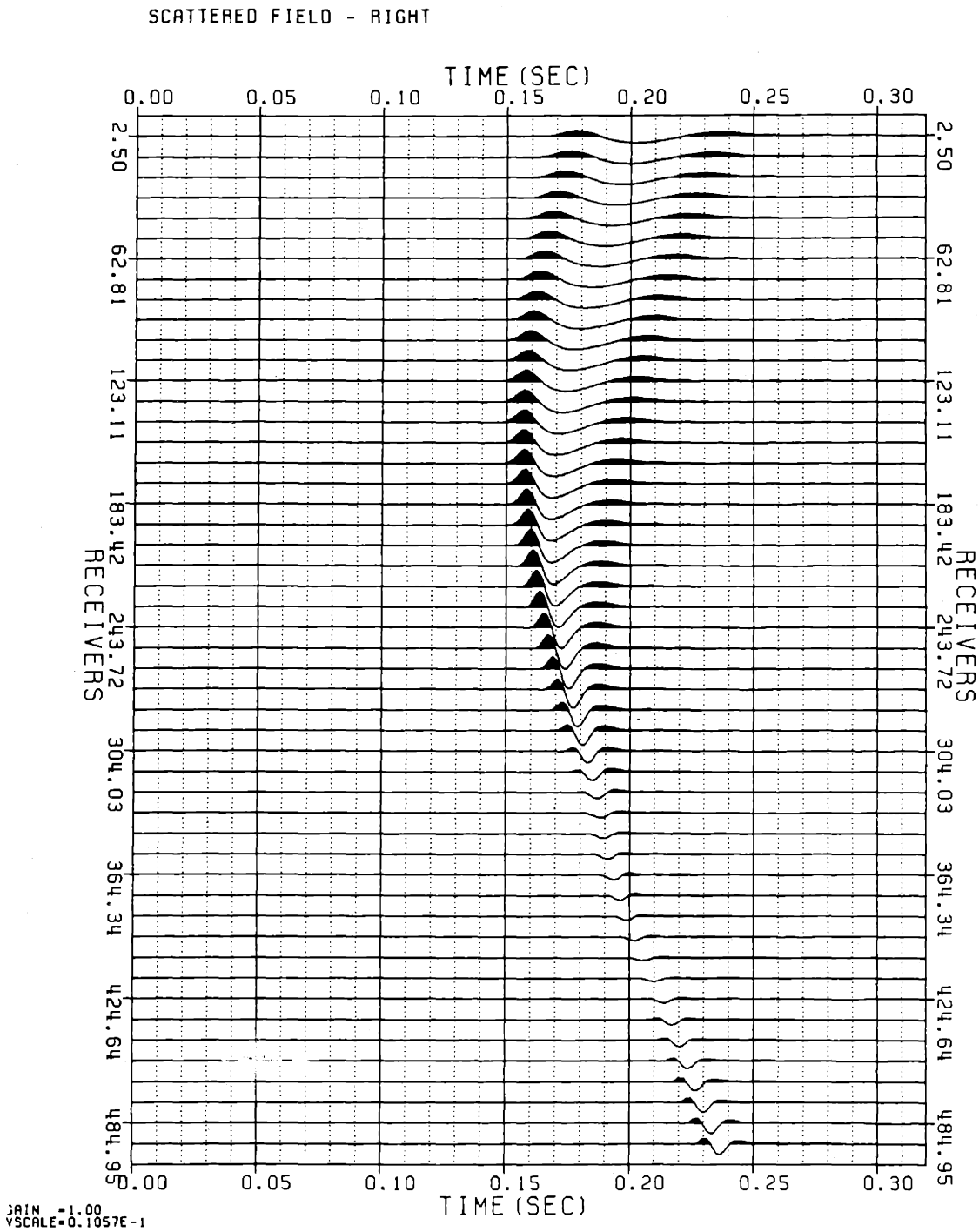

Figure 6.10 a) Scattered field recorded at the receivers located on the left side of the medium.

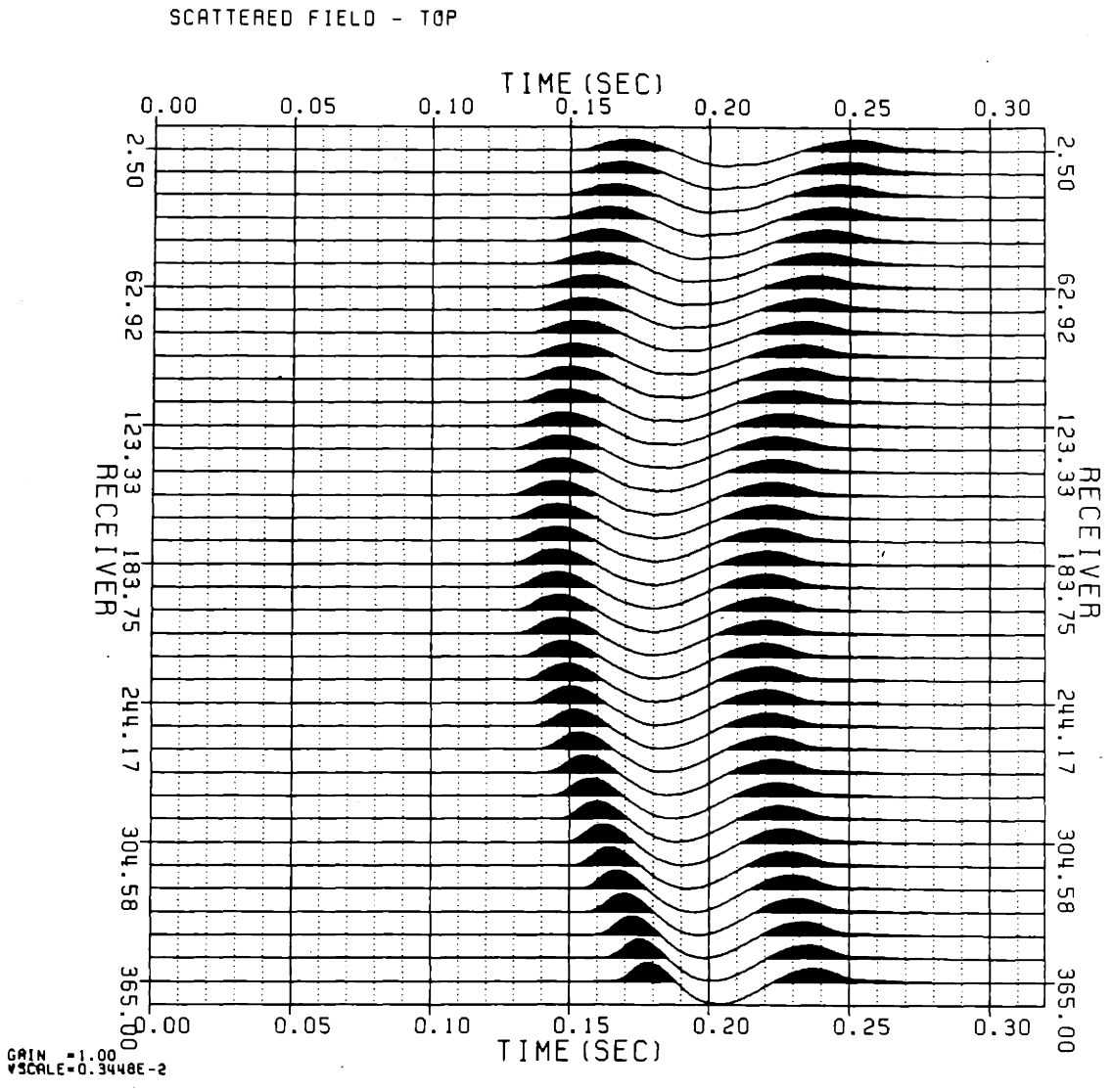

Figure 6.10 b) Scattered field recorded at the receivers located above the medium.

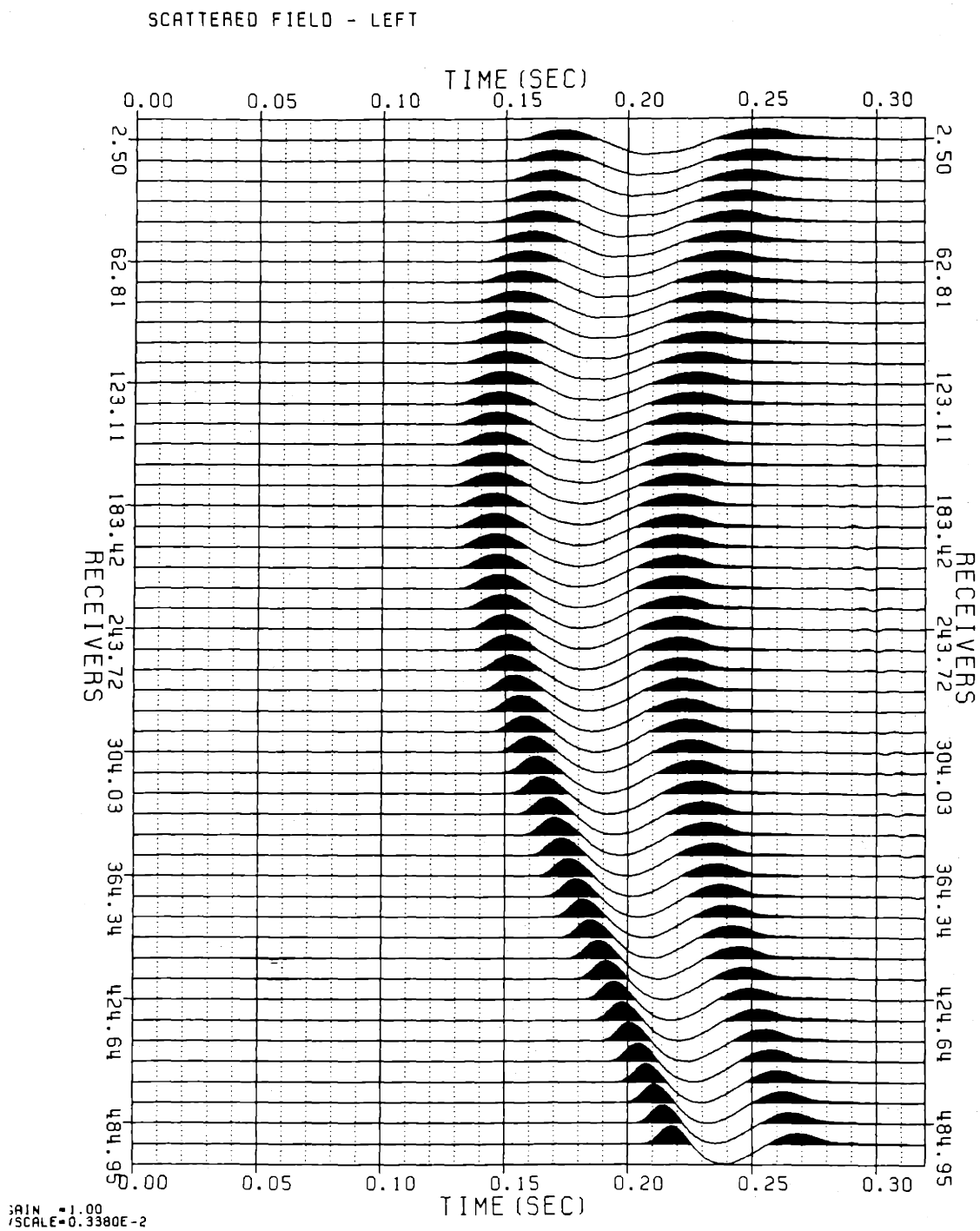

Figure 6.10 c) Scattered field recorded at the receivers located on the right side of the medium.

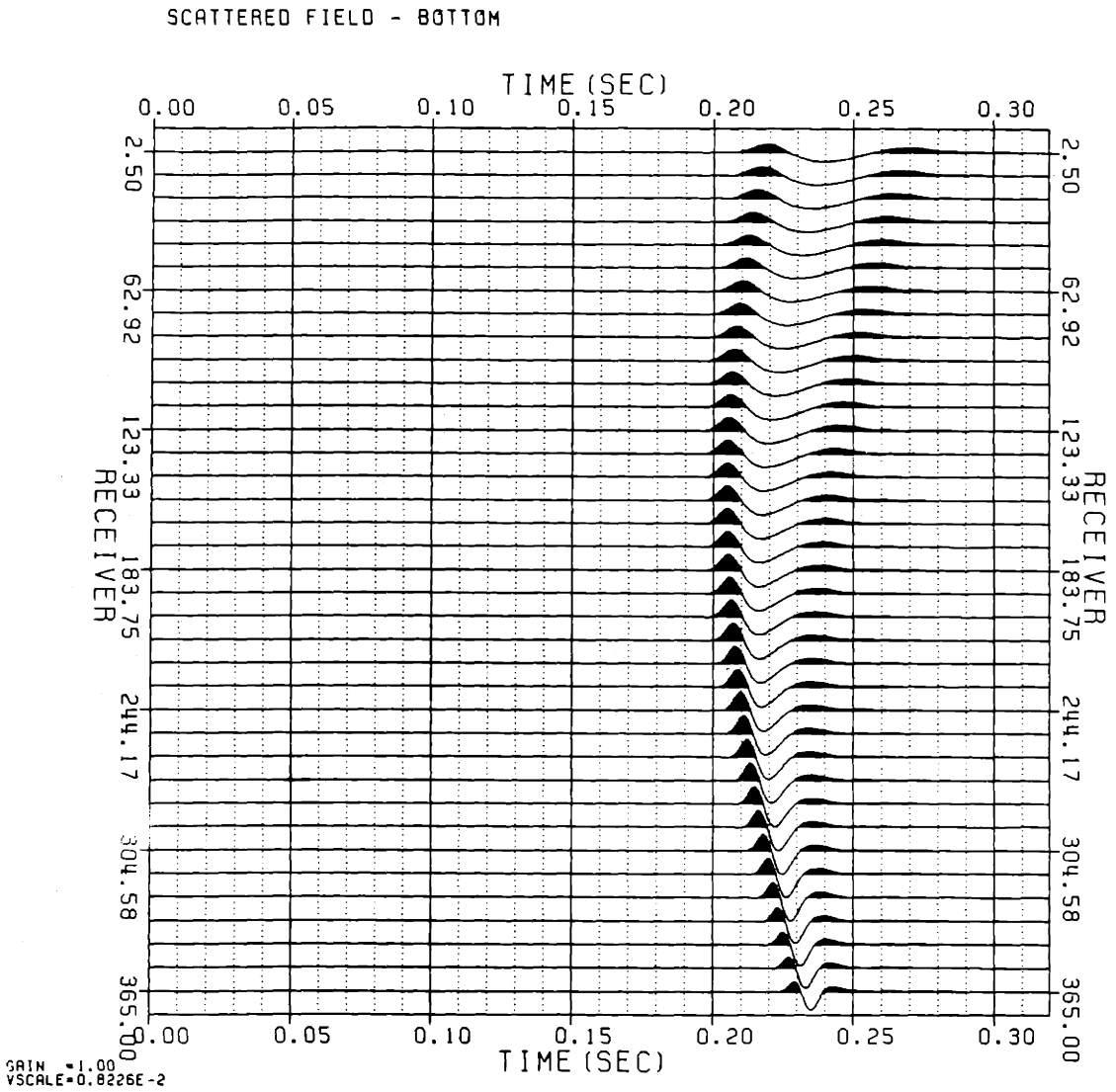

Figure 6.10 d) Scattered field recorded at the receivers located below the medium.

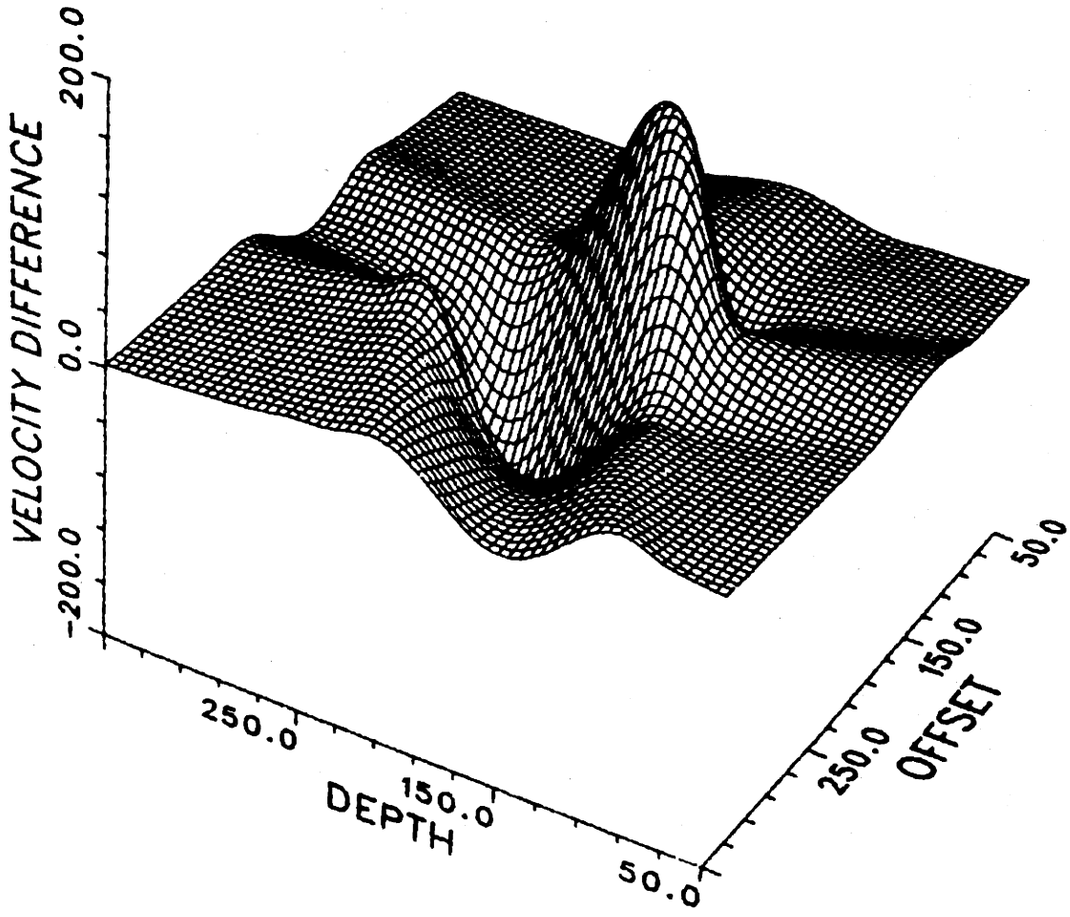

Figure 6.11 a) Velocities reconstructed by using only the receivers located on the left side and above the medium.

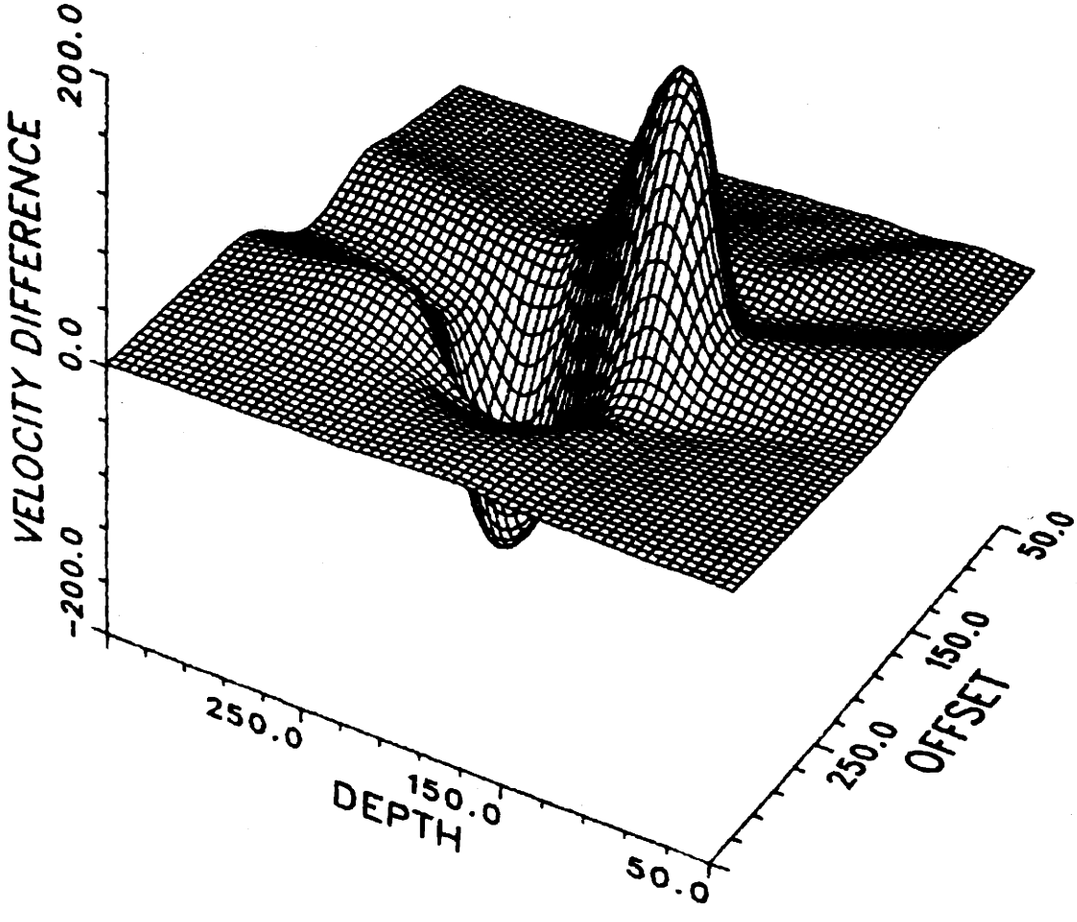

Figure 6.11 b) Velocities reconstructed by using the receivers located on the left side, above and on the right side of the medium.

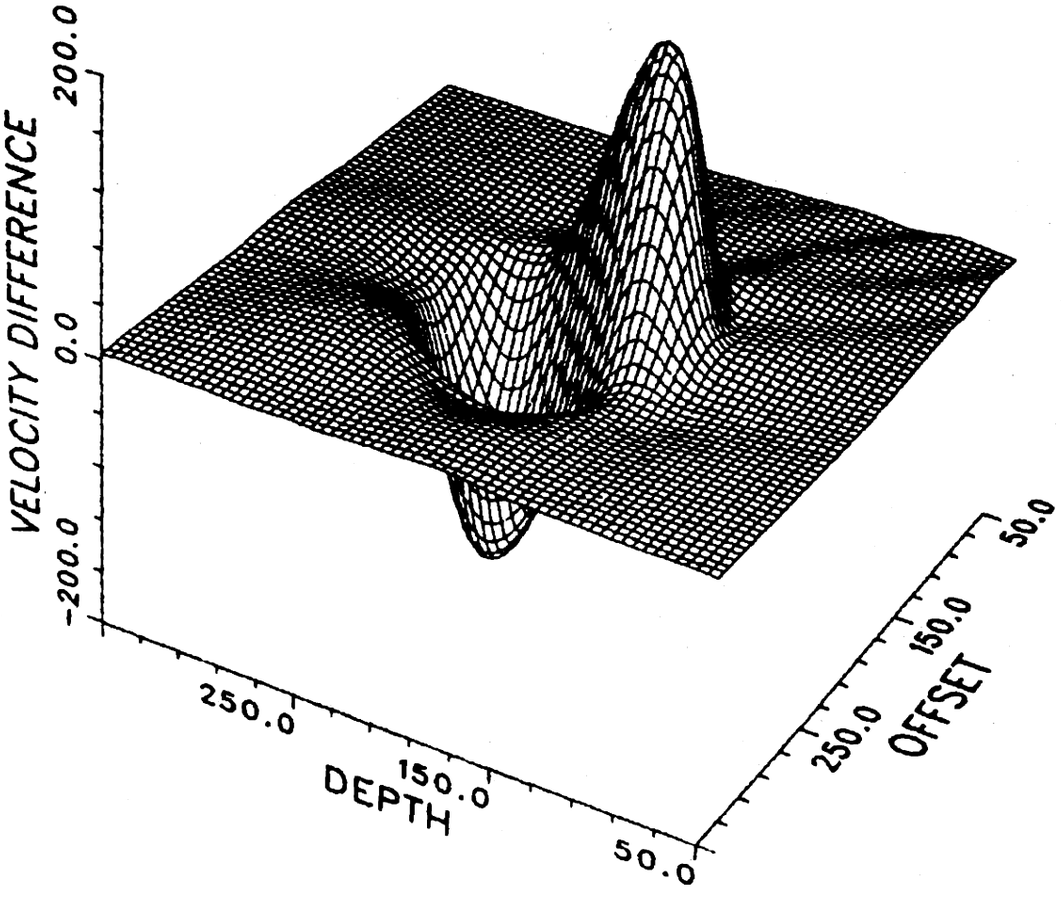

Figure 6.11 c) Velocities reconstructed by using all the receivers.

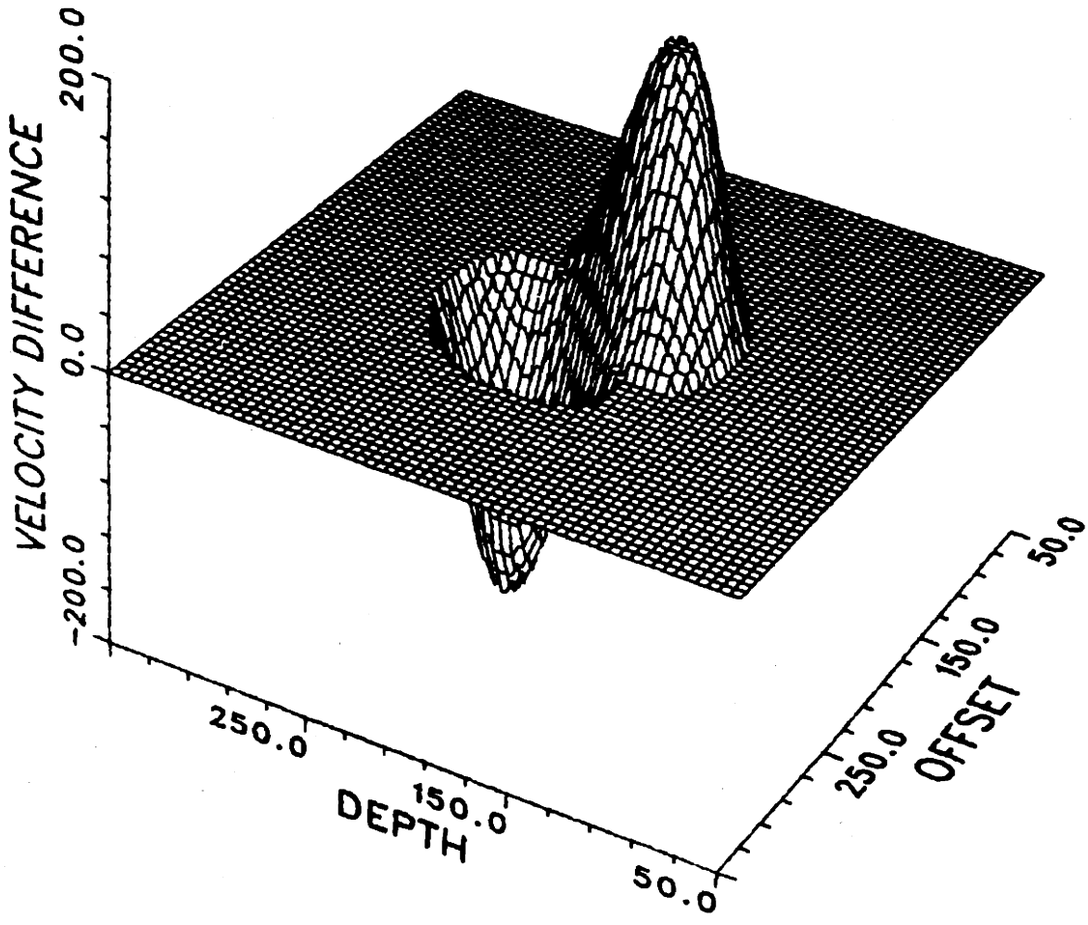

Figure 6.11 d) The true velocity model.

CHAPTER VII

Inversion for the 2½ Dimensional Zero-Offset Problem

One of the most common experimental geometries in exploration seismology consists of point sources and receivers located along a line on the surface of the earth. The source-receiver line is chosen so that it is perpendicular to the direction in which the medium velocities are approximately constant. The reflection experiment is repeated for each source and the field is recorded at a group of receivers. Clearly, for a given source and a group of receivers, this geometry resembles a 2½ dimensional problem of the type discussed in Section 6.3. The large volume of data obtained by repeating this experiment for many source locations is usually reduced by a stacking process known as Common Depth Point (CDP) stacking. The stacking is done in such a way that the after-stack data approximates a theoretical experiment model in which a point source-receiver pair is located everywhere along the observation line and an experiment is performed at every location. In this section a zero-time imaging method of inversion is presented for a 2½ dimensional zero-offset experiment. In the following discussion, we will not restrict the locations of the source-receiver pairs to be along a straight line. Instead, we consider the general receiver array model shown in Figure 4.5 by replacing receivers with source-receiver pairs. The zero-offset experiment differs from the single source experiments discussed previously in two aspects. First, in the zero-offset case the data represent many single source experiments and

thus do not represent a single physical wavefield. Second, since the sources and receivers are collocated in each experiment, only the backscattered field is observed. As will be shown shortly, the inversion problem for the zero-offset data turns out to be easier to solve than the corresponding inversion problem for the single source data. Moreover, the zero-offset experiment provides a complete reconstruction of the medium velocities with a source-receiver array with an angular aperture of 180°, whereas the single-source experiment requires a receiver array with an angular aperture of 360°. excitation.

It was shown in Chapter 4 that the extrapolated field $P_e^*(\underline{r},\omega)$ in the 2½ dimensional zero-offset problem is obtained by backpropagating the filtered scattered data $\bar{P}_s$, given by equation (4.4.2). As was pointed out in Section 4.4, the backpropagation medium in this case has a constant velocity $v = c/2$ where $c = \omega/k$ is the background velocity of the medium in which the scatterers are located. From equation (4.4.5) the extrapolated field can be expressed as

$$P_e^*(\underline{r},\omega) = \int_V d\underline{r}' \, \gamma(\underline{r}') \, E_0(\underline{r},\underline{r}',\omega) \, , \tag{7.1}$$

where, from equation (4.4.8), the zero-offset kernel E_0 is given by

$$E_0(\underline{r},\underline{r}',\omega) = \frac{i\,\mathrm{sgn}(\omega)}{4\pi} \int_{\alpha_2}^{\alpha_1} d\theta \; e^{i2\underline{k}\cdot(\underline{r}-\underline{r}')} \, . \tag{7.2}$$

Here, θ is the angle corresponding to the unit vector $\hat{\underline{k}}$, and $\underline{k} = k\hat{\underline{k}}$. Observe that there is no incident field term in equation (7.1) in contrast to equations (6.1.5),

(6.2.1) and (6.3.1). This is the major difference between the zero-offset and single source problems, aside from the fact that the extrapolated field kernels are different. Let $\hat{\gamma}(\underline{r})$ be the function obtained from the extrapolated field by imaging at time zero

$$\hat{\gamma}(\underline{r}) = \frac{4}{\pi c^2} \int_{-\infty}^{\infty} d\omega \; (-i\omega) \; P_e^*(\underline{r},\omega) \; . \tag{7.3}$$

The filter $(-i\omega)$ above corresponds to a differentiation operation in the time domain and can be combined with the prefilter in equation (4.4.2) that is used to obtain $\bar{P}_s$ from P_s. From equations (7.1),(7.2) and (7.3) the zero-time image $\hat{\gamma}$ can be written as

$$\hat{\gamma}(\underline{r}) = \int_V d\underline{r}' \; \gamma(\underline{r}') \; h(\underline{r}-\underline{r}') \; , \tag{7.4}$$

where the space invariant point spread function h is given by

$$h(\underline{r}-\underline{r}') = \frac{1}{\pi^2} \int_{\alpha_2}^{\alpha_1} d\theta \int_{-\infty}^{\infty} dk \; |k| \; e^{i2\underline{k}\cdot(\underline{r}-\underline{r}')} \; . \tag{7.5}$$

Let us briefly compare the point spread function given above with the point spread functions of the plane-wave source and point source problems, given by equations (5.3.7) and (6.2.16) respectively. First we see that the point spread function in the zero-offset case is spatially invariant as in the plane-wave source problem. The major difference, however, is that the angular variable θ in equation (7.5) is the angle corresponding to the unit vector $\hat{\underline{k}}$. This is the same angular variable involved in the

integral expression (7.2) of the extrapolated field kernel E_0. Obviously, this is due to the fact that there is no incident field term in equation (7.2). As a result, the integration limits in equation (7.5) are solely determined by the angular aperture $[\alpha_2 ; \alpha_1]$ of the source-receiver array. In contrast, the angular variable ϕ in equations (5.3.7) and (6.2.16) for the plane-wave source corresponds to the vector $\hat{\underline{k}}-\hat{\underline{k}}_s$. For fixed $\hat{\underline{k}}_s$, if we let θ vary in the range of angles $R_\alpha : [\alpha_2 ; \alpha_1]$ then the corresponding range of angles $R_\phi : [\phi_1 ; \phi_2]$ attained by ϕ can be computed from equation (5.1.18) or (6.2.17). It can be easily verified that the range R_ϕ of angles covered by ϕ is always smaller than R_α. This is the reason why a source-receiver array with an angular aperture of 180° is sufficient to obtain a complete reconstruction of the potential in the zero-offset case while a receiver array with an angular aperture of 360° is necessary for the single source case.

Let us now return to equation (7.5). Define an extended range of angles Θ such that, if $\theta \in [\alpha_2 ; \alpha_1]$ then both θ and $\theta + \pi \in \Theta$. Then, equation (7.5) can also be written as

$$h(\underline{r}-\underline{r}') = \frac{1}{\pi^2} \int_{\Theta} d\theta \int_0^\infty dk\ k\ e^{i2\underline{k}\cdot(\underline{r}-\underline{r}')} . \tag{7.6}$$

Finally, changing the radial variable from k to $u = 2k$ gives the point spread function

$$h(\underline{r}-\underline{r}') = \frac{1}{4\pi^2} \int_{\Theta} d\theta \int_0^\infty du\ u\ e^{i\underline{u}\cdot(\underline{r}-\underline{r}')}$$

$$= \frac{1}{4\pi^2} \int_{U_\Theta} d\underline{u} \; e^{i\underline{u} \cdot (\underline{r}-\underline{r}')} , \tag{7.7}$$

where $\underline{u} = u\hat{\underline{k}}$ and U_Θ denotes the cone in cartesian coordinates corresponding to the range of angles Θ shown in Figure 7.1. For example, if the source-receiver pairs are located along an infinite line on the x axis, then the angular aperture of the source-receiver array is given by [π ; 2π]. From Figure 7.1 it is seen that U_Θ in this case covers the whole $u_x - u_z$ plane and from equation (7.7) we obtain $h(\underline{r}-\underline{r}') = \delta(\underline{r}-\underline{r}')$. Thus the velocities can be reconstructed completely.

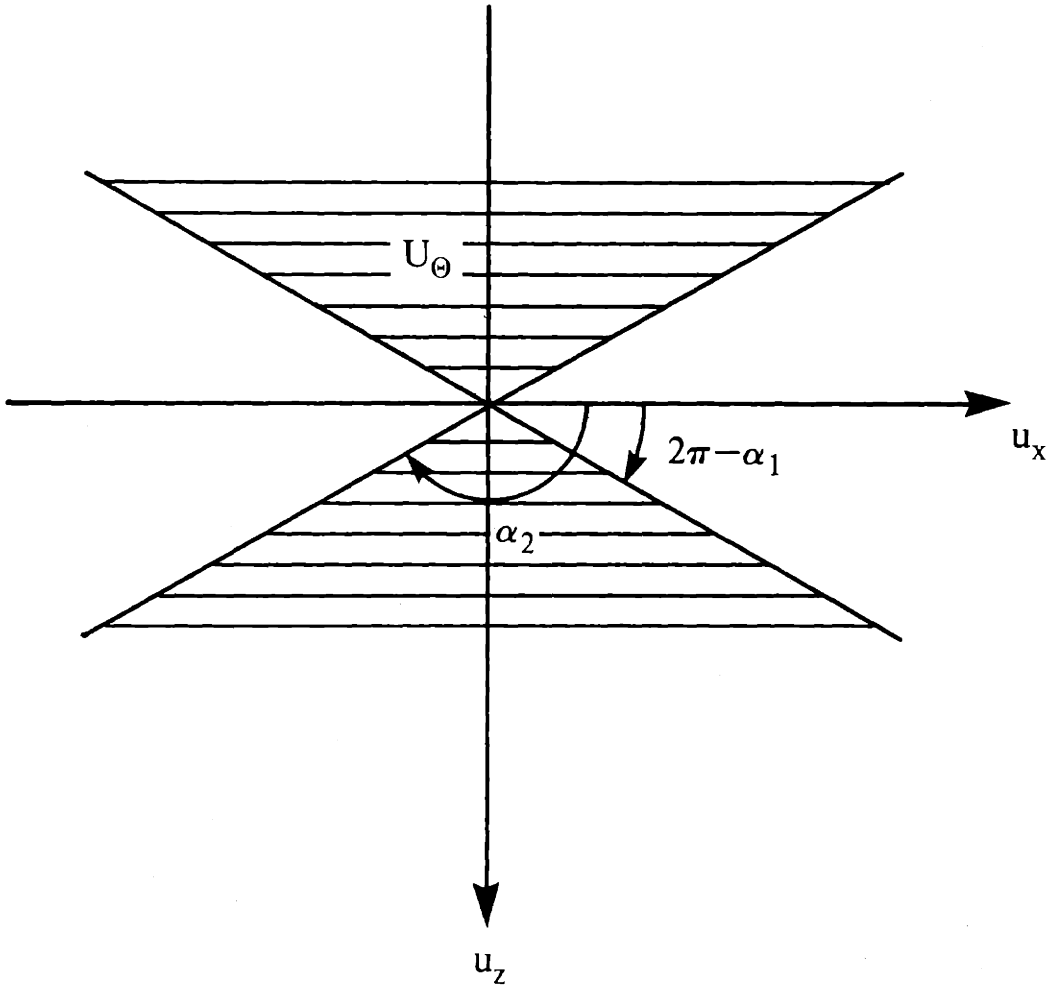

Figure 7.1. Fourier domain coverage in the zero-offset problem corresponding to a source-receiver pair array with angular aperture [α_2 ; α_1].

CHAPTER VIII

Conclusion and Suggestions for Further Research

8.1 Conclusion

In this thesis the multidimensional inverse scattering problem for a constant density acoustic medium was considered within the first Born approximation. The use of back-propagation in the inverse scattering problem was described in detail. The volume integral representation of the extrapolated field was derived in Chapter 4 for various experiment geometries, including complete and limited receiver arrays , 2 and 2½ dimensional problems and dimensional zero-offset problems. The velocity scattering potential γ of the medium and the extrapolated field P_e were related via this integral equation. We also presented several inversion methods for various types of excitations using the backpropagated field approach. In Chapter 5 the inversion problem for a wide-band plane-wave source was considered and two inversion methods, namely inversion by slant-stack and inversion by imaging the backpropagated field, were presented. The slant-stack method of inversion was developed by using the fact that the projections of the potential γ can be obtained directly from the slant-stacks of the observed traces (Section 5.1). It was shown that each slant-stack angle provides one projection of γ, where the projection angle and the slant-stack angle are analytically related. The imaging method of inversion is based on the relation between the potential γ and the source-travel time image of the backpropagated field. It was shown that the two were related by a spatially invariant multidimensional filter. An inverse filter,

which depends solely on the angle of incidence of the probing wave, was designed to obtain γ from the image. In Chapter 6 the inversion problem for a wide-band point source was considered and two methods, namely inversion by zero-time imaging and inversion by source-travel time imaging, were presented. It was shown that when the physical (outgoing) scattered field P_s^+ was backpropagated into the medium the incoming scattered field P_s^- was generated inside the medium in addition to P_s^+. Inversion by zero-time imaging was derived by showing that there is a one to one mapping between the projections of γ at various projection angles and the image obtained by taking a snapshot of the field P_s^- at time zero. In the case of complete receiver coverage a complete set of projections of γ is obtained, from which the potential can be fully reconstructed. Inversion by source-travel time imaging for a point source excitation was shown to be similar to the method obtained for the plane-wave source case. However, the source-travel time image and γ are related via a more complicated spatial filter in the point source case. It was shown that, as in the plane wave case, γ can be reconstructed from the source-travel time image partially or completely depending on the angular aperture of the receiver array. Also in Chapter 6 the zero-time and source-travel time imaging methods of inversion for the point source case were extended to the 2½ dimensional problem which was described in Chapter 2. Finally, in Chapter 7 we presented an inversion method for the 2½ dimensonal zero-offset problem described in Chapter 2, where we used the backpropagated field approach. It was shown in this chapter that the potential γ can be obtained directly by taking a snapshot of the extrapolated field at time zero. It was also pointed out that in the zero-offset case a coincident source-receiver pair array located on one side of the medium was sufficient for complete recovery of the potential.

8.2 Suggestions for Further Research

8.2.1 Inhomogeneous background model

In many applications some of the properties of the medium are known a priori or are obtained by previous experiments. For example, some major velocity changes in seismic problems can be determined from the general geological structure of the area, from simple reflection experiments and from borehole logs. As pointed out in Chapter 2, Born inversion methods, in general, are accurate only for small velocity variations with respect to the background velocity. Therefore, better inversion results can be obtained by incorporating known large velocity changes in the background model.

Compared to the previous Fourier transform methods of Born velocity inversion, the backpropagated field method described in this thesis offers more possibilities in handling inhomogeneous backgrounds. Suppose that the extrapolated field P_e is obtained by a finite difference algorithm. The time-reversed observed scattered field P_s^* is used as the boundary values at the receiver locations as described in Section 4.1. Now, if we use an inhomogeneous background medium (instead of a homogeneous medium) in the finite difference algorithm we obtain the extrapolated field given in equations (4.1.1) and (4.2.1) that corresponds to the given background model. In other words the extrapolated field in the inhomogeneous background case can be obtained the same way as in the homogeneous background case. During backpropagation, the scattered field propagates back towards the scattering medium along the original raypaths and arrives at the scattering points at the corresponding source-travel times. Therefore, by imaging the extrapolated field at the source-travel times com-

puted for an inhomogeneous background the scatterers are imaged close to their true locations. Reverse-time migration handles the varying background case precisely in this way. The difficulty in inhomogeneous background inversion is that we want to obtain the quantitative values of the scattering potential of the medium as well as the locations of the scatterers. In general, the scattering potential is obtained by solving an integral equation that relates the extrapolated field to the medium velocities. With an inhomongeneous background the volume integral representation of the backpropagated field becomes so complicated that an explicit inversion formula cannot be easily obtained. In the following we discuss the possibilities of extending some of the inversion methods presented in this thesis to tinhomogeneous background models.

Inversion by zero-time imaging

In Section 4.1 the integral representation of the extrapolated field P_e was derived for the case of complete receiver coverage. The integral representation given by equations (4.1.6) and (4.1.7) is valid for any inhomogeneous background model since it was obtained without using an explicit form of the background Green's function $G_0(\underline{r},\underline{r}',\omega)$. However, the inversion method presented in Section 6.1 is restricted to the homogeneous background case since the orthogonality property of the free space Green's function was exploited to obtain this method. Specifically, for a homogeneous background the travel time between two points in the medium is simply the distance divided by the constant velocity. The locus of points that have equal travel times to two points is the bisector of the line joining these two points. Therefore, as was shown in Section 6.1, the extrapolated field imaged at time zero gives the integrals of the velocity function along straight lines. For a background with varying

velocities, however, the distances and travel times are not proportional and the zero time imaged field corresponds to integrals of the velocity function along curved trajectories. Let $n_0(\underline{r})$ be the background model containing known large velocity changes. Then, the background wave operator and the velocity function are defined by

$$\mathbf{D}_0 = \nabla^2 + k^2 n_0^2(\underline{r}) \tag{8.2.1a}$$

$$\gamma(\underline{r},\omega) = k^2 [\, n^2(\underline{r}) - n_0^2(\underline{r}) \,] = k^2 \gamma(\underline{r}) \,. \tag{8.2.1b}$$

From equations (4.1.6) and (4.1.7) the representation of the extrapolated field for an impulse point source is given by

$$P_e^*(\underline{r},\omega) = k^2 \int_V d\underline{r}' \, \gamma(\underline{r}') \, G_0(\underline{r}',\underline{r}_s,\omega) \, 2i \, \mathrm{Im}[\, G_0(\underline{r},\underline{r}',\omega) \,] \,, \tag{8.2.2}$$

where the Green's function

$$\mathbf{D}_0 G_0(\underline{r},\underline{r}',\omega) = -\delta(\underline{r} - \underline{r}') \,, \tag{8.2.3}$$

is assumed to be known for the given background. From equation (8.2.2) by taking the real parts of both sides we have

$$P_e^R(\underline{r},\omega) = -2k^2 \int_V d\underline{r}' \, \gamma(\underline{r}') \, \mathrm{Im}[\, G_0(\underline{r}',\underline{r}_s,\omega) \,] \, \mathrm{Im}[\, G_0(\underline{r},\underline{r}',\omega) \,] \,. \tag{8.2.4}$$

Now, consider the geometrical optics approximation of the Green's function for a two dimensional medium given by equation (2.2.7). With this approximation the extrapolated field becomes (for $k > 0$)

$$P_e^R(\underline{r},\omega) = -2k \int_V d\underline{r}' \, \gamma(\underline{r}') \, a(\underline{r}',\underline{r}_s) \, a(\underline{r},\underline{r}')$$

$$\sin[\, k \, s(\underline{r}',\underline{r}_s) + \frac{\pi}{4} \,] \sin[\, k \, s(\underline{r},\underline{r}') + \frac{\pi}{4} \,] \, , \tag{8.2.5}$$

where a and s are the amplitude and phase terms of the background Green's function, and they can be obtained numerically for a given background model. As in equation (6.1.7), consider the following function obtained from the extrapolated field imaged at time zero

$$\hat{\gamma}(\underline{r}) = \frac{-1}{2\pi} \int_{-\infty}^{\infty} d\omega \, \frac{P_e(\underline{r},\omega)}{|\omega|} \, . \tag{8.2.6}$$

Using the orthogonality property of the $\sin(\cdot)$ function

$$\int_0^{\infty} dk \, \sin(kp) \, \sin(kq) = \frac{\pi}{2} \, \delta(p-q) \quad ; \quad p > 0 \, , \; q \geqslant 0 \, , \tag{8.2.7}$$

the zero-time image $\hat{\gamma}$ can be related to the scattering potential as follows

$$\hat{\gamma}(\underline{r}) = \frac{-1}{\pi} \int_0^{\infty} dk \, \frac{P_e^R(\underline{r},\omega)}{k}$$

$$= \int_V d\underline{r}' \, \gamma(\underline{r}') \, a(\underline{r}',\underline{r}_s) \, a(\underline{r},\underline{r}') \, \delta[s(\underline{r}',\underline{r}_s) - s(\underline{r},\underline{r}')] \, . \tag{8.2.8}$$

From this equation it is seen that $\hat{\gamma}(\underline{r})$ is essentially a weighted integral of $\gamma(\underline{r})$ along the points that have equal travel times to $\underline{r}_s$ and $\underline{r}$. For a homogeneous background

the locus of such points is a line. However, for an inhomogeneous background these points lie on a curve and $\hat{\gamma}(\underline{r})$ is not a simple straight line projection of $\gamma(\underline{r})$.

In the homogeneous background case the field scattered from a point $\underline{r}$ maps into circles when the field is imaged at time zero. According to equation (6.1.7), $\gamma(\underline{r})$ is reconstructed from $\hat{\gamma}(\underline{r})$ by integrating along the corresponding circle after a spatial filtering operation. For an inhomogeneous background the field scattered from $\underline{r}$ maps into a closed curve passing through the source point as shown in Figure 4.3. The reconstruction of $\gamma(\underline{r})$ in this case can be obtained by integrating along this curve. Nevertheless, the proper spatial filtering operation before integration is not known. The zero time curve associated to point $\underline{r}$ can be obtained by tracing rays from this point in all directions. Since this must be done for all points in the medium this method may be computationally impractical even if the proper spatial filtering operation is found.

Backpropagated field for limited receiver coverage

In the case of complete receiver coverage the integral representation of the backpropagated field kernel $E_c(\underline{r},\underline{r}',\omega)$ was derived without using an explicit form of the Green's function. This was made possible by the fact that, in this case, the receivers are located on a closed surface surrounding the medium. Then, we were able to replace the integral over the receivers in equation (4.1.1) with a volume integral over the medium by invoking the second theorem of Green. In the case of limited receiver coverage, however, the explicit form of the free space Green's function given in equation (4.2.6a) was used to obtain the backpropagated field kernel $E(\underline{r},\underline{r}',\omega)$. Thus, the kernel E given in equation (4.2.10) is valid only for the homogeneous background

case. An approximate representation of this kernel in the inhomogeneous background case can be obtained as follows. In Section 4.2 the discussion of the backpropagated field is valid for any background medium up to and including equation (4.2.5). Here, we continue the discussion starting from this equation. From equation (2.2.7), the background Green's function in a two dimensional inhomogeneous medium can be approximately written as

$$G_0(\underline{\xi},\underline{r}',\omega) \approx \lim_{\rho\to\infty} \frac{e^{i\frac{\pi}{4}sgn(\omega)}}{(8\pi)^{1/2}} \frac{e^{iks(\underline{\xi},\underline{r}')}}{|k|^{1/2}\,\rho^{1/2}} , \tag{8.2.9a}$$

$$G_0^*(\underline{r},\underline{\xi},\omega) \approx \lim_{\rho\to\infty} \frac{e^{-i\frac{\pi}{4}sgn(\omega)}}{(8\pi)^{1/2}} \frac{e^{-iks(\underline{r},\underline{\xi})}}{|k|^{1/2}\,\rho^{1/2}} , \tag{8.2.9b}$$

where $\underline{\xi}$ is located on the arc S of the circle of infinite radius centered at $\underline{r}'$ and ρ is the radial distance as shown in Figure 4.6. The function $s(\cdot)$ in the above equations represents the integral of the background refraction index $n_0(\underline{r})$ along the raypaths and is given by

$$s(\underline{\xi},\underline{r}') = \int_{R:\underline{r}'}^{\underline{\xi}} dl\; n_0(l) . \tag{8.2.10}$$

Also, note that in equations (8.2.9a,b) for $\rho \to \infty$ we have approximated the amplitude decay of the Green's function by $\rho^{-1/2}$. Then, from equations (4.2.5) and (8.2.9a,b) the backpropagated field kernel is obtained as

$$E(\underline{r},\underline{r}',\omega) = \frac{i\,sgn(\omega)}{4\pi} \int_{\alpha_2}^{\alpha_1} d\phi \; e^{ik[s(\underline{\xi},\underline{r}')-s(\underline{r},\underline{\xi})]} , \tag{8.2.11}$$

where ϕ is the polar angle as shown in Figure 4.6. Note that in general the limits of the above integral can be obtained by tracing rays starting from $\underline{r}'$ such that they become tangent to the receiver array R at the infinity. Nevertheless, here we will keep α_1 and α_2 as the approximate limits of this integral. The phase term in equation (8.2.11) is proportional to the difference of the travel times from points $\underline{r}'$ and $\underline{r}$ to the point $\underline{\xi}$ located at infinity. Therefore, for $\underline{r}$ close to $\underline{r}'$ we can make the following approximation

$$s(\underline{\xi},\underline{r}') - s(\underline{r},\underline{\xi}) \approx n_0(\underline{r})\, \hat{\underline{k}} \cdot (\underline{r}-\underline{r}') , \tag{8.2.12}$$

where $\hat{\underline{k}}$ is the unit vector corresponding to the angle ϕ and $n_0(\underline{r})$ is the refraction index of the background model at point $\underline{r}$. Finally, from equations (8.2.11) and (8.2.12) the kernel E is obtained as

$$E(\underline{r},\underline{r}',\omega) \approx \frac{i\,sgn(\omega)}{4\pi} \int_{\alpha_2}^{\alpha_1} d\phi \; e^{in_0(\underline{r})\hat{\underline{k}} \cdot (\underline{r}-\underline{r}')} . \tag{8.2.13}$$

Observe that for $n_0(\underline{r}) = 1$ the above expression reduces to the homogeneous background case. Using the kernel given above we can write an approximate volume integral representation of the extrapolated field. For example, for the plane-wave source problem the extraplated field is given by

$$P_e^*(\underline{r},\omega) = k^2\, S(\omega) \int_V d\underline{r}'\, \gamma(\underline{r}')\, e^{iks_p(\underline{r}')}\, E(\underline{r},\underline{r}',\omega)\ , \tag{8.2.14}$$

where $s_p(\underline{r}')$ is the integral of $n_0(\underline{r})$ of the form (8.2.10) along the raypath connecting the plane-wave source to the point $\underline{r}'$.

Inversion by source-travel time imaging

As in the homogeneous background case we define the source-travel time image as

$$\beta(\underline{r}) = -\frac{1}{2\pi} \int_{-\infty}^{\infty} d\omega\, \frac{P_e^*(\underline{r},\omega)}{i\omega\, S(\omega)}\, e^{-iks_p(\underline{r})}\ , \tag{8.2.15}$$

where $s_p(\underline{r})$ is proportional to the source-travel time to point $\underline{r}$ and for a given background medium it is obtained as described previously. From equations (8.2.13), (8.2.14) and (8.2.15) the image β can be expressed as

$$\beta(\underline{r}) = \int_V d\underline{r}'\, \gamma(\underline{r}')\, h(\underline{r},\underline{r}')\ , \tag{8.2.16}$$

where the point spread function h is given by

$$h(\underline{r},\underline{r}') = -\frac{1}{8\pi^2} \int_{\alpha_2}^{\alpha_1} d\theta \int_{-\infty}^{\infty} dk\, |k|\, e^{in_0(\underline{r})\underline{k}\cdot(\underline{r}-\underline{r}')}\, e^{-ik[s_p(\underline{r})-s_p(\underline{r}')]}\ . \tag{8.2.17}$$

Here θ is the angle corresponding to the vector $\underline{k}$. For $\underline{r}$ close to $\underline{r}'$, the phase term that represents the difference of the source-travel time to points $\underline{r}$ and $\underline{r}'$ can be approximated by

$$s_p(\underline{r}) - s_p(\underline{r}') \approx n_0(\underline{r})\, \hat{\underline{k}}_s(\underline{r}) \cdot (\underline{r}-\underline{r}') \,, \tag{8.2.18}$$

where $\hat{\underline{k}}_s(\underline{r})$ is the unit vector corresponding to the *local angle of incidence.* Since the background medium is inhomogeneous the incident plane wavefront of the source is distorted as it propagates into the medium. At a given point $\underline{r}$, $\hat{\underline{k}}_s(\underline{r})$ represents the incidence direction of the incident wave as observed at this point. Finally, from equations (8.2.17) and (8.2.18) the point spread function is obtained as

$$h(\underline{r},\underline{r}') = -\frac{1}{8\pi^2} \int_{\alpha_2}^{\alpha_1} d\theta \int_{-\infty}^{\infty} dk\, |k|\, e^{in_0(\underline{r})k[\hat{\underline{k}}-\hat{\underline{k}}_s(\underline{r})] \cdot (\underline{r}-\underline{r}')} \,. \tag{8.2.19}$$

Compared with the homogeneous background point spread function given in equation (5.3.6) the above expression has a similar form but is not space-invariant. The functions $n_0(\underline{r})$ and $\hat{\underline{k}}_s(\underline{r})$ are known a priori for a given background model, so that the point spread function can be computed at any point $\underline{r}$ in the medium. However, inverting equation (8.2.16) to obtain γ from the image β is not an easy task because inversion involves designing a space-variant inverse filter of the function $h(\underline{r},\underline{r}')$ given equation (8.2.19).

8.2.2 Simultaneous reconstruction of the velocity and density functions

Starting with equation (2.1), throughout this thesis we have assumed a constant density acoustic medium. In some practical problems the density variations of the medium are much smaller than the velocity variations and this assumption is justified. A more general problem is to reconstruct the velocities and densities simultaneously. When the variations of the density $\rho(\underline{r})$ are included, the acoustic wave equation

operator is given by

$$\mathbf{D} = \nabla^2 + k^2\, n^2(\underline{r}) - \frac{\nabla \rho(\underline{r})}{\rho(\underline{r})} \cdot \nabla \; . \tag{8.2.20}$$

It is seen that the velocities and densities enter the problem quite differently. Let us define the velocity scattering potential γ and the density scattering vector-potential $\underline{\beta}$ as follows

$$\gamma(\underline{r}) = n^2(\underline{r}) - 1 \tag{8.2.21a}$$

$$\underline{\beta}(\underline{r}) = \frac{\nabla \rho(\underline{r})}{\rho(\underline{r})} \; . \tag{8.2.21b}$$

Then, from equation (2.1.3) the differential equation satisfied by the scattered field can be written as

$$\mathbf{D}_0 P_s(\underline{r},\omega) = -k^2\, \gamma(\underline{r})\; P(\underline{r},\omega) + \underline{\beta}(\underline{r}) \cdot \nabla P(\underline{r},\omega) \; . \tag{8.2.22}$$

An integral solution of this equation is given in terms of the background Green's function G_0 by

$$P_s(\underline{r},\omega) = k^2 \int_V d\underline{r}'\; \gamma(\underline{r}')\; P(\underline{r}',\omega)\; G_0(\underline{r},\underline{r}',\omega) -$$

$$\int_V d\underline{r}'\; \underline{\beta}(\underline{r}') \cdot \nabla P(\underline{r}',\omega)\; G_0(\underline{r},\underline{r}',\omega) \; . \tag{8.2.23}$$

Using the Born approximation the incident field $P(\underline{r}',\omega)$ can be replaced by the back-

ground incident field $P_0(\underline{r}',\omega)$ and a more explicit expression for the scattered field can be obtained.

It is seen that in the varying density case the scattered field can be represented by the sum of two volume integrals; one for scattering from the velocity inhomogeneities, and one from the density inhomogeneities. Since there are now two unknown functions of the medium we need at least two different experiments for inversion. For example, with point sources two separate experiments with sources at different locations are required. Hooshyar and Weglein (1985) have recently extended the zero-time imaging method for the case of complete receiver coverage to the multiparameter case. They showed that velocity and density functions of the acoustic medium can be recovered simultaneously by using two point source experiments where the the distance between the source locations is small compared to the distance from the sources to the scatterers. In the plane-wave excitation case we must use two plane waves with different angles of incidence. In equation (8.2.23) there are two important differences between the velocity and the density scattering terms. First, the frequency weighting of the velocity term is k^2 whereas the density term is effectively weighted by k due to the gradient operation performed on the incident field. Second, the density scattering is proportional to the gradient of the density variations along the incident wave direction. By comparison, the velocity scattering is independent of the direction of the incident field. These differences in the behaviour of the velocity and density scattering terms with respect to the frequency and local direction of incidence of the probing wave may be useful in multiparameter inversion.

8.2.3 Obtaining an unknown part of the scattered field from an observed part

In addition to its practical importance, the incomplete observations problem has also some interesting theoretical aspects. For example, how much of the scattered field is needed in order to completely recover the medium velocities? Also, can we recover one part of the scattered field, which is not observed, from another observed part? These are questions for current and future research; their answers are not known for multidimensional media. For the one dimensional case, however, it can be shown that the transmitted waves can be recovered from the reflected waves. The argument is as follows. Consider the scattering problem shown in Figure 8.1. A one dimensional inhomogeneous medium of finite extent is probed by an impulsive plane wave with unit intensity and the reflected field $S(\omega)$ is observed above the medium. From the conservation of energy we have

$$|S(\omega)|^2 + |T(\omega)|^2 = 1 , \tag{8.2.24}$$

where $T(\omega)$ is the transmitted field. Hence, the Fourier magnitude of the transmitted waves can be recovered from the observed data by setting

$$|T(\omega)| = [\, 1 - |S(\omega)|^2 \,]^{1/2} . \tag{8.2.25}$$

A very interesting property of the transmitted waves in one dimension is that they are minimum phase (Faddeev, 1967). Therefore, the phase of the Fourier transform $T(\omega)$ can be obtained from its magnitude by a Hilbert transform in the complex cepstrum domain (Oppenheim and Schafer, 1975). This gives the complete recovery of the transmitted waves.

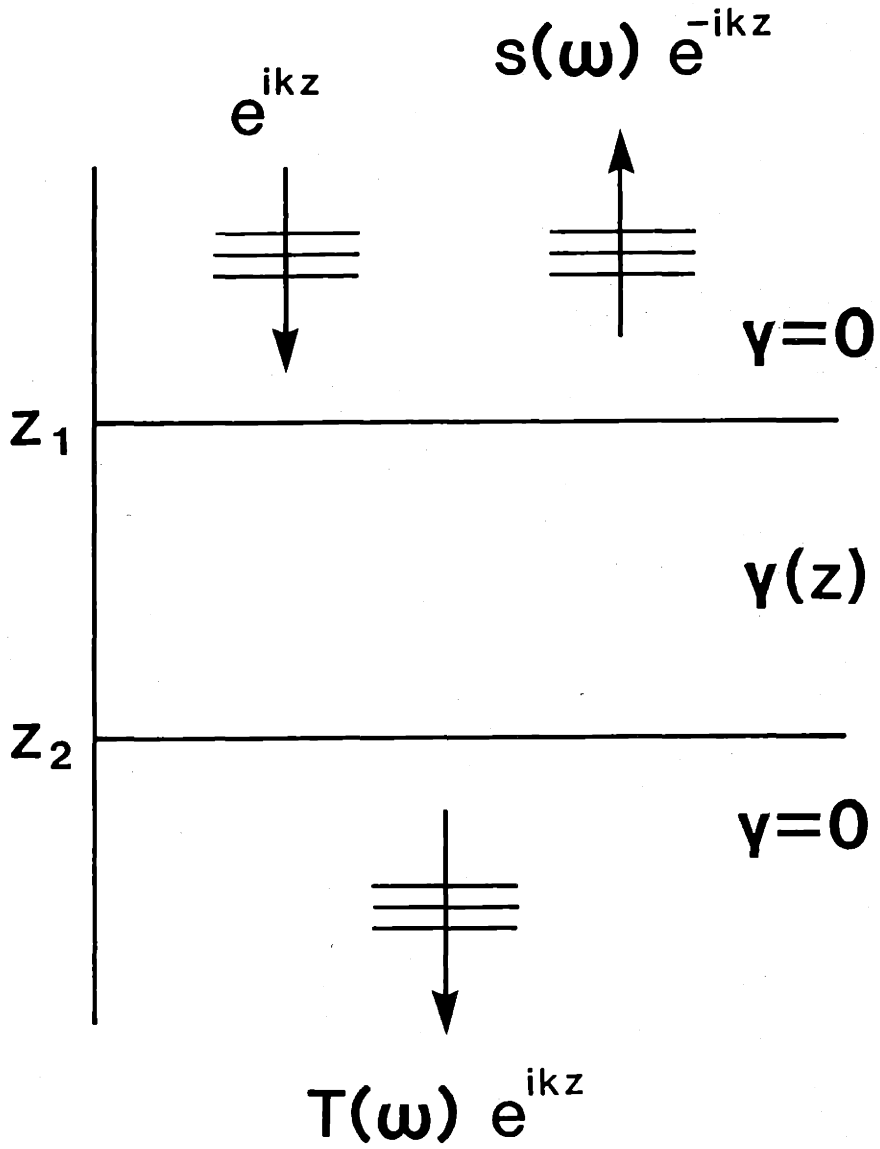

Figure 8.1. One dimensional scattering experiment.

The backpropagated field formulation may provide a convenient framework to investigate the questions stated above for multidimensional media. The backpropagated field obtained from incomplete observations of the scattered field was discussed in Section 4.2. Now, consider the field obtained by backpropagating the scattered field observed along the receiver array R_1 as shown in Figure 8.2. As was pointed out in Chapter 4, in the negative time direction the backpropagated field converges towards the scatterers, focuses at the scattering points and then diverges away from the scattering medium. The diverging portion of the scattered field P_s^- is called the incoming scattered field since it propagates towards the scatterers in the positive time direction. From equation (4.2.2) the volume integral representation of the scattered field is given by

$$P_s^{\bullet}(\underline{r},\omega) = \int_V d\underline{r}' \, \gamma(\underline{r}') \, P(\underline{r}',\omega) \, E^1(\underline{r},\underline{r}') \, , \tag{8.2.26}$$

where E^1 denotes the backpropagated field kernel associated to the receiver array R_1 and is given by equation (4.2.10). Next, consider the following decomposition of the extrapolated field

$$P_e^{\bullet}(\underline{r},\omega) = P_s^+(\underline{r},\omega) - P_s^-(\underline{r},\omega) \, . \tag{8.2.27}$$

Here P_s^+ and P_s^- are the outgoing and incoming parts of the extrapolated field. The outgoing part of the scattered field P_s^+ must correspond to the causal part of the extrapolated field kernel E^1. This is because the outgoing waves are the physical

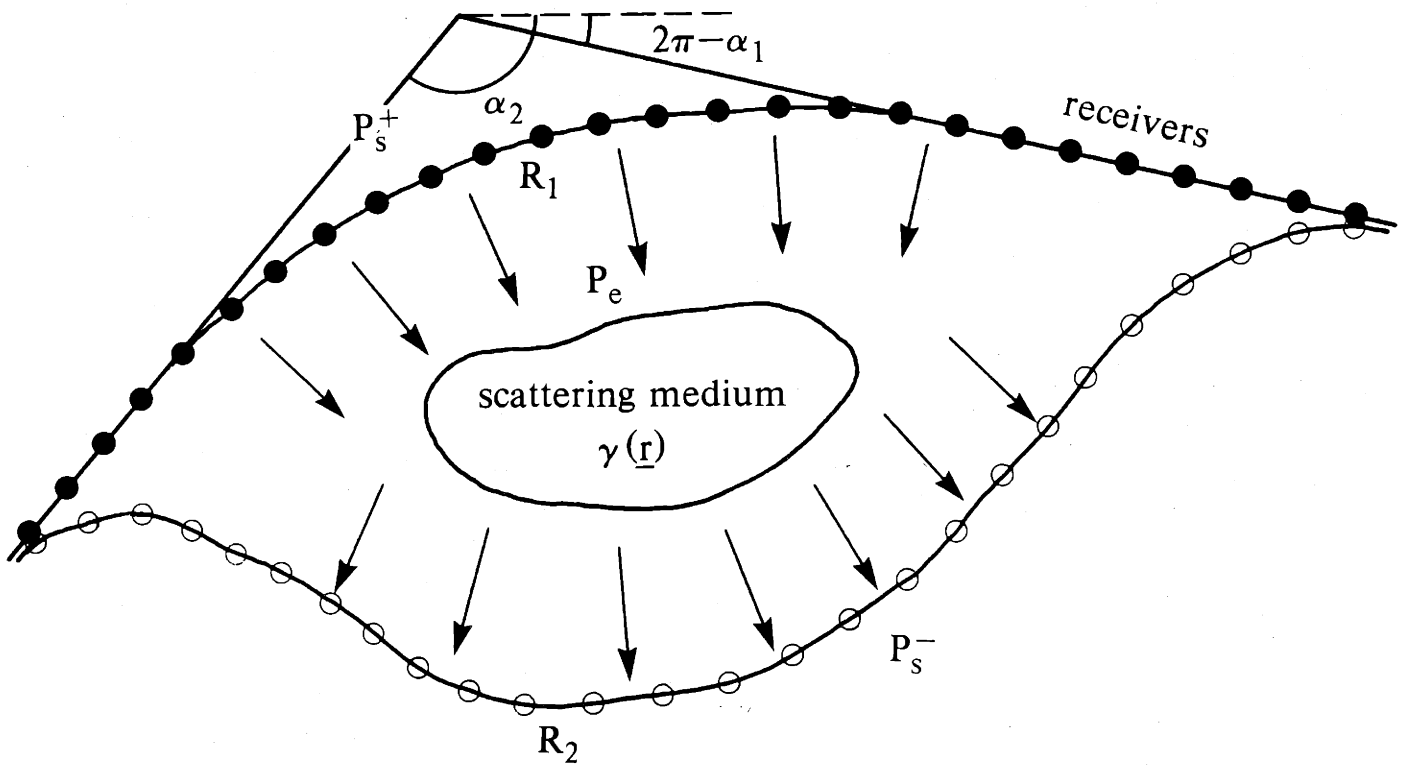

Figure 8.2. Obtaining P_s^- on R_2 from observations of P_s^+ on R_1.

scattered waves, therefore they are always causal. Then the outgoing waves are given by

$$P_s^+(\underline{r},\omega) = \int_V d\underline{r}'\ \gamma(\underline{r}')\ P(\underline{r}',\omega)\ E_{CA}^1(\underline{r},\underline{r}')\ , \tag{8.2.28}$$

where E_{CA}^1 denotes the causal part of E^1. The remaining part of the scattered field P_s^- corresponds to the anti-causal part of the extrapolated field kernel. Recall that the incoming waves P_s^- are generated by the backpropagated field after the converging waves passes the focus at the scattering points. Note again that "after" in reverse time means "before" in the positive time direction. Therefore, the incoming waves are always anti-causal because they are generated before the incident field reaches the scatterer. Then, the incoming waves are given by

$$P_s^-(\underline{r},\omega) = \int_V d\underline{r}'\ \gamma(\underline{r}')\ P(\underline{r}',\omega)\ E_{AC}^1(\underline{r},\underline{r}')\ , \tag{8.2.29}$$

where E_{AC}^1 denotes the anti-causal part of E^1. According to Figure 8.2 the outgoing field P_s^+ is known only along the receiver array $R_1 : [\ \alpha_1\ ;\ \alpha_2\ ]$, where α_2 and α_1 represents the angular range of the receiver array. The portion of the outgoing scattered field which is not known lies in the complementary angular aperture given by $R_2 : [2\pi-\alpha_1\ ;\ \alpha_2\ ]$. The interesting thing is that the known and unknown portions of the incoming field P_s^- are just the opposite of known and unknown portions of the outgoing field P_s^+. In other words, P_s^- is known in the aperture R_2 and unknown in the aperture R_1. Then the question stated at the beginning of this section can be restated as follows. Can we obtain P_s^+ from P_s^- in a given region in space, or vice versa?

More specifically, the unkown portion of the outgoing scattered field is given by

$$P_s^+(\underline{r},\omega) = \int_V d\underline{r}'\ \gamma(\underline{r}')\ P(\underline{r}',\omega)\ E_{CA}^2(\underline{r},\underline{r}')\ , \tag{8.2.30}$$

where E^2 is the extrapolated field kernel associated to the aperture R_2 and E_{CA}^2 denotes the causal part of E^2. Then the problem is to recover $P_s^+(\underline{r},\omega)$ given in equation (8.2.30) from $P_s^-(\underline{r},\omega)$ given in equation (8.2.29), where in both equations $\underline{r}$ is located along or below the curve R_2 shown in Figure 8.2. There are also other questions related to this problem. For example, P_s^+ given in equation (8.2.28) evaluated on the receiver array R_1 is the observed scattered field. Therefore, it is given by equation (2.1.4) in Chapter 2. Then, what is the relation between the causal part of the extrapolated field kernel E_{CA} and the background Green's function G_0? Under what conditions are they the same?

8.2.4 Finite bandwidth Sources

In Chapters 5, 6 and 7 we have assumed that the source wavelet $S(\omega)$ is such that $S(\omega) \neq 0$ at all frequencies. In the real world, however, we can only use bandlimited sources. In the examples presented in this thesis the synthetic scattered field data were generated by using bandlimited sources. As a result, sharp velocity changes in the medium were smoothed in the reconstructed image. A detailed analysis of the effects of the finite bandwidth in various inversion methods remains to be done. In the following we examine the problem for the zero-time imaging method with complete observations. We will consider a three dimensional medium with a point source excitation.

From equations (4.1.6) and (4.1.7) the extrapolated field for a bandlimited source can be written as

$$P_e^*(\underline{r},\omega) = k^2 \int_V d\underline{r}'\, \gamma(\underline{r}')\, S(\omega)\, G_0(\underline{r}',\underline{r}_s,\omega)\, 2i\, Im[\, G_0(\underline{r},\underline{r}',\omega)\,] \,. \tag{8.2.31}$$

Suppose that $S(\omega)$ is bandlimited so that

$$S(\omega) = 0 \quad ; \quad |\omega| > \omega_b \,. \tag{8.2.32}$$

For the frequencies within the source bandwidth we can divide both sides of equation (8.2.31) by $S(\omega)$

$$\frac{P_e^*(\underline{r},\omega)}{S(\omega)} = k^2 \int_V d\underline{r}'\, \gamma(\underline{r}')\, G_0(\underline{r}',\underline{r}_s,\omega)\, 2i\, Im[\, G_0(\underline{r},\underline{r}',\omega)\,] \,, \tag{8.2.33}$$

for $|\omega| < \omega_b$. Hence, in this frequency range we have an equation similar to equation (6.1.1). The bandlimited deconvolution operation in equation (8.2.33) can be performed on the observed data before extrapolation. The bandlimited version $\hat{\gamma}_b(\underline{r})$ of the zero time image field is given by

$$\hat{\gamma}_b(\underline{r}) = \frac{8\pi^2 c^2}{-\omega_b} |\underline{r}-\underline{r}_s|^2 \int_{-\omega_b}^{\omega_b} \frac{d\omega}{\omega^2}\, \mathrm{Re}\left\{ \frac{P_e^*(\underline{r},\omega)}{S(\omega)} \right\} . \tag{8.2.34}$$

Note that, in the three dimensional case the proper filtering operation is $1/\omega^2$, instead of $1/|\omega|$ which was used for the two dimensional problem in equation (6.1.7). The image function $\hat{\gamma}_b(\underline{r})$ can be expressed as

$$\hat{\gamma}_b(\underline{r}) = \frac{16\pi^2}{-k_b} |\underline{r}-\underline{r}_s|^2 \int_0^{k_b=\frac{\omega_b}{c}} \frac{dk}{k^2} \mathrm{Re}\left\{ \frac{P_e^*(\underline{r},\omega)}{S(\omega)} \right\} \tag{8.2.35a}$$

$$= |\underline{r}-\underline{r}_s|^2 \int_V d\underline{r}' \frac{\gamma(\underline{r}')}{|\underline{r}'-\underline{r}_s|\,|\underline{r}-\underline{r}'|} h_b(\underline{r}',\underline{r}) , \tag{8.2.35b}$$

where the bandlimited point spread function $h_b(\underline{r},\underline{r}')$ is given by

$$h_b(\underline{r},\underline{r}') = \frac{2}{k_b} \int_0^{k_b} dk \sin(k|\underline{r}'-\underline{r}_s|) \sin(k|\underline{r}-\underline{r}'|) . \tag{8.2.36}$$

Using the convolution property of the Fourier transform it can be shown that

$$h_b(\underline{r}',\underline{r}) = sinc[k_b(|\underline{r}'-\underline{r}_s|-|\underline{r}-\underline{r}'|)] - sinc[k_b(|\underline{r}'-\underline{r}_s|+|\underline{r}-\underline{r}'|)] , \tag{8.2.37}$$

where the $sinc(\cdot)$ function is defined by

$$sinc(k_b\ r) = \frac{\sin(k_b\ r)}{k_b\ r} . \tag{8.2.38}$$

If the source is a few wavelengths away from the medium then $|\underline{r}'-\underline{r}_s|+|\underline{r}-\underline{r}'| >> \lambda_b/2$ and we can neglect the second term in equation (8.2.37), so that

$$h_b(\underline{r}',\underline{r}) \approx sinc[\ k_b\ (\ |\underline{r}'-\underline{r}_s| - |\underline{r}-\underline{r}'|\ )\ ] . \tag{8.2.39}$$

Therefore, as a result of the finite source bandwith the projections obtained from the zero time image are smoothed by the $sinc(\cdot)$ function. The velocity function $\gamma_b(\underline{r})$

reconstructed from the smoothed projections $\hat{\gamma}_b(\underline{r})$ has a finite resolution which is roughly half of the minimum wavelength provided by the source. For a source bandwidth ω_b, the minimum wavelength is given by $\lambda_b = \frac{2\pi c}{\omega_b}$. Better resolution is obtained for a larger source bandwidth. Finally, for infinite bandwidth, as $k_b \rightarrow \infty$, $h_b(\underline{r}',\underline{r}) \rightarrow \delta(|\underline{r}'-\underline{r}_s|-|\underline{r}-\underline{r}'|)$ and an exact reconstruction of $\gamma(\underline{r})$ is obtained.

In the line source case the finite source bandwidth causes similar smoothing effects on the reconstructed velocities. However, since the Hankel transform does not have the convolution property the smoothing function $h_b(\underline{r}',\underline{r})$ becomes more complicated. For large bandwidth, the smoothing due to windowing the Hankel transform can be expressed as an approximate convolution operation (Mook, 1983), and an argument similar to the one above can be made for the line source case.

References

Aki, K. and Richards, P. G., *Quantitative Seismology, Theory and Methods, Volume 1,* W. H. Freeman and Company, San Francisco, 1980.

Alford, R. M., Kelly, K. R. and Boore, D. M.,"Accuracy of finite difference modeling of the acoustic wave equation," *Geophysics* , Vol. 39, No. 6, pp. 834-842, December 1974.

Bender, C. M. and Orszag, S. A., *Advanced Mathematical Methods for Scientists and Engineers,* McGraw-Hill Book Company, 1978.

Berkhout, A. J.,"Wavefield extrapolation techniques in seismic migration, a tutorial," *Geophysics* , Vol. 46, No. 12, pp. 1638-1656, December 1981.

Berkhout, A. J., *Seismic Migration, Imaging of Acoustic Energy by Wave Field Extrapolation, A. Theoretical Aspects,* Developments in Solid Earth Geophysics, 14A, Elsevier Scientific Publishing Company, 1982.

Beylkin, G.,"Imaging of Discontinuities in the Inverse Scattering Problem by Inversion of a Causal Generalized Radon Transform," *Journal of Mathematical Physics,* 26 (1), pp. 99-108, January 1985.

Bleistein, N. and Hanselman, R. A., *Asymptotic expansions of integrals,* Holt, Rinehart and Winston, New York, 1975.

Bojarski, N. N.,"A Survey of the Near-Field Far-Field Inverse Scattering Inverse Source Integral Equation," *IEEE Trans. Antennas and Propagation* , Vol. AP-30, No. 5, pp. 975-979, September 1982.

Cheng, G. and Coen, S.,"The relationship between Born inversion and migration for common-midpoint stacked data," *Geophysics* , Vol. 49, No. 12, pp. 2117-2131, December 1984.

Claerbout, J. F.,"Toward a Unified Theory of Reflector Mapping," *Geophysics* , Vol. 36, No. 3, pp. 467-481, 1971.

Claerbout, J. F. and Doherty S.,"Downward Continuation of Moveout Corrected Seismograms," *Geophysics* , Vol. 37, No. 5, 1972.

Clayton, R. W. and Stolt, R. H.,"A Born-WKBJ inversion method for acoustic reflection data," *Geophysics* , Vol. 46, No. 11, pp. 1559-1567, November 1981.

Cohen, J. K. and Bleistein, N.,"An inverse method for determining small variations in propagation speed," *SIAM J. Appl. Math.*, Vol. 32, No. 4, June 1977.

Cohen, J. K. and Bleistein, N.,"Velocity inversion procedure for acoustic waves," *Geophysics* , Vol. 44, No. 6, pp. 1077-1087, June 1979.

Devaney, A. J.,"A Filtered Backpropagation Algorithm for Diffraction Tomography," *Ultrasonic Imaging 4*, pp. 336-350, 1982.

Devaney, A. J.,"Geophysical diffraction tomography," *IEEE Trans. Geosience and Remote Sensing* , Vol. GE-22, No. 1, pp. 3-13, January 1984.

Devaney, A. J. and Beylkin, G."Diffraction tomography using arbitrary source-receiver surfaces," *Ultrasonic Imaging* , Vol. 6, pp. 181-193, 1984.

Devaney, A. J. and Oristaglio M. L.,"Inversion procedure for inverse scattering within the distorted-wave Born approximation," *Physical Review Letters,* Vol. 51, No. 4, pp. 237-240, July 1983.

Dudgeon, D. E. and Mersereau, R. M., *Multidimensional digital signal processing* , Prentice-Hall, Inc., New Jersey, 1984.

Faddeev, L. D.,"Properties of the S-Matrix of the One-Dimensional Schrödinger Equation," *American Mathematical Society, Translations,* Series 2, 65, 1967.

Gradshteyn, I. S. and Ryzhik. I. M., *Table of Integrals, Series, and Products,* Academic Press, 1980.

Gray S. H., Cohen J. K. and Bleistein, N.,"Velocity inversion in a stratified medium with separated source and receiver," *J. Acoust. Soc. Am.,* 68(1), July 1980.

Gray, S. H.,"A second order procedure for one dimensional velocity inversion," *SIAM J. Appl. Math.,* Vol. 39, No. 3, December 1980.

Gray S. H.,"Velocity inversion in a stratified medium with separated source and receiver. II," *J. Acoust. Soc. Am.,* 69(3), March 1981.

Greenleaf, J. K.,"Computerized tomography with ultrasound," *Proc. IEEE* , Vol. 71, No. 3, pp. 330-337, March 1983.

Hagin, F. G. and Gray, S. H.,"Travel time(like) variables and the solution of velocity inverse problems," *Geophysics* , Vol. 49, No. 6, June 1984.

Hooshyar, M. A. and Weglein, A. B.,"Inversion of the two dimensional SH elastic wave equation for the density and shear modulus," submitted to *J. Acoust. Soc. Am.*, 1985.

Jain, S. and Wren, E. A.,"Migration before stack-Procedure and significance," *Geophysics* , Vol. 45, No. 2, February 1980.

Lahlou, M., Cohen, J. and Bleistein, N.,"Highly accurate inversion methods for three-dimensional stratified media," *SIAM J. Appl. Math.*, Vol. 43, No. 4, August 1983.

Ludwig, D."The Radon Transform on Euclidean Space," *Comm. Pure and Applied Mathematics,* Vol. XIX, 1966.

Miller, D., Oristaglio M. and Beylkin G.,"A New Formalism and an Old Heuristic for Seismic Migration," *SEG 1984, Extended Abstracts.*

Morse, P. M. and Feshbach H., *Methods of Theoretical Physics, Part I* , McGraw-Hill, 1953.

Mueller, R. K., Kaveh, M. and Wade G.,"Reconstructive tomography and applications to ultrasonics," *Proc. IEEE* , Vol. 67, No. 4, pp. 567-587, April 1979.

Norton, S. J. and Linzer, M.,"Ultrasonic reflectivity imaging in three dimensions: Exact inverse scattering solutions for plane, cylindrical, and spherical

apertures," *IEEE Trans. Biomedical Eng.* , BME-28, pp. 202-220, 1981.

Oppenheim, A. V. and Schafer, R. W., *Digital Signal Processing,* Prentice-Hall, Inc., Englewood Cliffs, New Jersey, 1975.

Oristaglio, M. L., private communication, 1984.

Porter, R. P.,"Diffraction Limited, Scalar Image Formation with Holograms of Arbitrary Shape," *Journal of the Optical Society of America* , Vol. 60, No. 8, pp. 1051-1059, August 1970.

Porter, R. P., *The Theory of Holographic Image Formation with Scalar and Electromagnetic Waves,* Ph. D. Thesis, Northeastern University, 1969.

Raz, S.,"Direct reconstruction of velocity and density profiles from scattered field data," *Geophysics* , Vol. 46, No. 6, June 1981a.

Raz, S.,"Three-dimensional velocity profile inversion from finite-offset scattering data," *Geophysics* , Vol. 46, No. 6, pp. 837-842, June 1981b.

Raz, S.,"A direct profile inversion: Beyond the Born model," *Radio Science* , Vol. 16, No. 3, May-June 1981c.

Raz, S.,"A procedure for multidimensional inversion of seismic data," *Geophysics* , Vol. 47, No. 10, October 1982.

Santosa, F. and Schwetlick, H.,"The inversion of acoustical impedance profile by methods of characteristcs," *Wave Motion* , 4, pp. 99-110, 1982.

Schneider, W. A.,"Integral formulation for migration in two and three dimensions," *Geophysics* , Vol. 43, No. 1, February 1978.

Stolt, R. H.,"Migration by Fourier Transform," *Geophysics* , Vol. 43, No. 1, February 1978.

Taylor, J. R., *Scattering Theory* ,John-Wiley & Sons, Inc., 1972.

Temme, P.,"A comparison of common-midpoint, single-shot and plane wave depth migration," *Geophysics* , Vol. 49, No. 11, pp. 1896-1907, November 1984.

Weglein, A. B.,"Multidimensional seismic analysis: migration and inversion," *Geoexploration* , 20, pp. 47-60, 1982.

Weglein, A. B. and Gray, S. H.,"The sensitivity of Born inversion to the choice of reference velocity: A simple example," *Geophysics* , Vol. 48, No. 1, January 1983.

Wolf, E.,"Three-dimensional structure determination of semi-transparent objects from holographic data," *Optics Communications* , Vol. 1, pp. 153-156, 1969.

Yagle, A. E. and Levy, B. C.,"Application of the Schur algorithm to the inverse problem for a layered acoustic medium," *J. Acoust. Soc. Am.* 76(1), July 1984.

Appendix A

First and Second Theorems of Green

In this thesis we have repeatedly utilized the second theorem of Green. Particularly in Chapter 4 we have used this powerful theorem to relate a surface integral over the receiver locations to a volume integral containing the scattering potential of the medium. In the following we present a brief derivation of the first and the second theorems of Green starting from Gauss' theorem. All scalar and vectoral quantities introduced below are functions of two or three space coordinates and frequency or time. For notational simplicity the arguments of these functions will be dropped. Let $\underline{a}$ be a vector field given in a volume V which is surrounded by the closed surface S. Then, the theorem of Gauss states that

$$\int_V dv \, (\nabla \cdot \underline{a}) = \int_S ds \, (\underline{a} \cdot \hat{\underline{n}}) , \tag{a1}$$

where $\hat{\underline{n}}$ is the outward-normal unit vector on the surface S. The first theorem of Green is obtained from Gauss' theorem by simply representing the vector $\underline{a}$ in terms of two scalar functions f and g as

$$\underline{a} = f \nabla g , \tag{a2}$$

$$\nabla \cdot \underline{a} = f\nabla^2 g + \nabla f \cdot \nabla g \,, \tag{a3}$$

where ∇^2 denotes the Laplacian with respect to the spatial coordinates. Equations (a1) and (a3) give the first theorem of Green as follows

$$\int_V dv \, (f\nabla^2 g + \nabla f \cdot \nabla g) = \int_S ds \, f \, (\nabla g \cdot \underline{\hat{n}}) \,. \tag{a4}$$

The second theorem of Green is obtained from the above equation in two steps. First we rewrite equation (a4) by interchanging the functions f and g, and then we subtract the resulting equation from equation (a4). The end result is given by

$$\int_V dv \, (f\nabla^2 g - g\nabla^2 f) = \int_S ds \, (f\nabla g - g\nabla f) \cdot \underline{\hat{n}} \,. \tag{a5}$$

Note that since the two terms on the left hand side of the above equation are subtracted we can generalize this relation to any operator of the form $\mathbf{D} = \nabla^2 + \gamma$. Then

$$\int_V dv \, (f\mathbf{D}g - g\mathbf{D}f) = \int_S ds \, (f\nabla g - g\nabla f) \cdot \underline{\hat{n}} \,, \tag{a6}$$

where γ is also a function of the space coordinates and frequency.

Appendix B

Impulse Invariant Design of a Square-Root Integrator

In Chapters 4 and 6 it was shown that, in the preprocessing stage of the two and 2½ dimensional point source problems, the observed traces must be filtered by a filter with frequency repsonse

$$H(\omega) = \left(\frac{1}{-i\omega} \right)^{1/2} = \frac{e^{i\frac{\pi}{4} sgn(\omega)}}{|\omega|^{1/2}} . \tag{b1}$$

Note that if this filter is applied to a trace twice the resulting operation is simply the integration of the trace in time. Consequently, this filter is called here as a square-root integrator. In this appendix we will obtain an impulse invariant design of the digital square-root integrator. First the continuous time impulse response $h_a(t)$ of the filter $H(\omega)$ will be derived. Then, the impulse response $h(n)$ of the corresponding digital filter is obtained by setting $h(n) = h_a(nT)$, where T is the sampling period. The inverse Fourier transform of the frequency response $H(\omega)$ in equation (b1) is given by

$$h_a(t) = \frac{1}{2\pi} \int_{-\infty}^{\infty} d\omega \, \frac{e^{i\frac{\pi}{4} sgn(\omega)}}{|\omega|^{1/2}} \, e^{-i\omega t} .$$

$$= \frac{1}{2\pi} \int_{-\infty}^{\infty} d\omega \, \frac{e^{-i sgn(\omega)(|\omega| t - \frac{\pi}{4})}}{|\omega|^{1/2}} \, . \tag{b2}$$

In the above integral the imaginary part of the integrand cancels out since it is odd symmetric in frequency ω. Then we have

$$h_a(t) = \frac{1}{\pi} \int_{0}^{\infty} d\omega \, \frac{\cos(\omega t - \frac{\pi}{4})}{|\omega|^{1/2}} \, . \tag{b3}$$

Using the trigonometric expansion of the $\cos(\cdot)$ term above and noting that $\cos(\pi/4) = \sin(\pi/4) = 1/\sqrt{2}$ we obtain

$$h_a(t) = \frac{1}{\pi\sqrt{2}} \int_{0}^{\infty} d\omega \left[\frac{\cos(\omega t)}{|\omega|^{1/2}} + \frac{\sin(\omega t)}{|\omega|^{1/2}} \right] . \tag{b4}$$

This expression can be evaluated by using the Fourier cosine and sine transforms (Gradshteyn and Ryzhik, 1980) given by

$$\int_{0}^{\infty} d\omega \, \frac{\cos(\omega t)}{|\omega|^{1/2}} = \sqrt{\pi/2} \, \frac{1}{|t|^{1/2}} \, , \tag{b5}$$

$$\int_{0}^{\infty} d\omega \, \frac{\sin(\omega t)}{|\omega|^{1/2}} = \sqrt{\pi/2} \, \frac{sgn(t)}{|t|^{1/2}} \, . \tag{b6}$$

Using equations (b5) and (b6) in equation (b4) the continuous time impulse response is obtained as

$$h_a(t) = (\pi t)^{-1/2} \quad ; \quad t > 0$$

$$= 0 \quad ; \quad \text{otherwise} . \tag{b7}$$

The impulse invariant design of the corresponding digital filter is obtained by sampling $h_a(t)$ at sampling points $t = nT$. This gives

$$h(n) = (\pi Tn)^{-1/2} \quad ; \quad n = 1,2,3, \cdots ,$$

$$= 0 \quad ; \quad n < 0 . \tag{b7}$$

Note that since $h_a(0) = \infty$ we cannot obtain the zero sample $h(0)$ by sampling the impulse response. A reasonable value for $h(0)$ can be obtained by selecting

$$h(0) = \frac{1}{T} \int_0^T dt \; h_a(t) = 2h(1) . \tag{b9}$$

Appendix C

Generating Synthetic Scattered Field Data by a Finite Difference Algorithm

The synthetic data used in the examples in this thesis were generated by a finite difference algorithm. Also, the extrapolated field P_e was obtained with the finite difference method where the time-reversed synthetic scattered field was used to specify the boundary values at the receiver locations. The finite difference method simulates wave propagation on a computer. The medium of interest is discretized in space yielding a finite number of grid points. The differential equation governing the wave equation is converted into an approximate difference equation in terms of the coordinates of the grid points and discrete time samples. There are many ways to implement the wave equation in discretized space and time. The finite difference program used in this thesis is based on an algorithm developed by Oristaglio (1984), which uses 4th order accurate difference formula for the Laplacian. For a constant density acoustic medium the 4th order formula is

$$P^{t+1}_{x,z} = (2-5r_{x,z})\, P^{t}_{x,z} - P^{t-1}_{x,z} + (4r_{x,z}/3)\,(\, P^{t}_{x-1,z} + P^{t}_{x+1,z} + P^{t}_{x,z-1} + P^{t}_{x,z+1}\,)$$

$$- (r_{x,z}/12)\,(\, P^{t}_{x-2,z} + P^{t}_{x+2,z} + P^{t}_{x,z-2} + P^{t}_{x,z+2}\,)\,. \tag{c1}$$

Here, $P^{t}_{x,z}$ denotes the pressure at grid point x,z and at time t, and $r_{x,z} = \dfrac{T^2\, v^2_{x,z}}{D^2}$

where T and D are the time step and grid spacing, and $v_{x,z}$ is the velocity at grid point x,z. The fourth order scheme is known to produce accurate seismograms with a grid spacing twice as coarse as the one required by the more commonly used second order scheme (Alford et. al., 1974). The fact that fewer grid points are used implies that we obtain substantial savings in computer memory requirements and computation time.

Recall that in Chapter 2 the scattered field $P_s(\underline{r},\omega)$ is defined as the difference between the total field $P(\underline{r},\omega)$ and the background field $P_0(\underline{r},\omega)$. One way to obtain the synthetic scattered field is as follows. First, the forward problem is solved for a given velocity structure and source specifications. This gives the total field $P(\underline{r},\omega)$ recorded at the receiver locations. Then, the forward problem is solved again this time for the background velocity model and the background field $P_0(\underline{r},\omega)$ is recorded at the receivers. The scattered field is obtained by subtracting the receiver traces of P_0 from the total field traces P.

In this thesis P_s is obtained directly by an alternative method (Oristaglio) where we need to run the finite difference program only once. The method consists of implementing an inhomogeneous wave equation satisfied by the scattered field. From equation (2.1.8) the scattered field P_s satisfies

$$\mathbf{D}\, P_s(\underline{r},\omega) = -k^2\, \gamma(\underline{r})\, P_0(\underline{r},\omega)\ , \tag{c2}$$

where $\mathbf{D} = \nabla^2 + k^2\, n^2(\underline{r})$ and $n(\underline{r}) = c/v(\underline{r})$ is the refraction index of the medium. In equation (c2) $\gamma(\underline{r}) = n^2(\underline{r}) - n_0^2(\underline{r})$ is the velocity scattering potential and $P_0(\underline{r},\omega)$ is the background incident field. Note that equation (c2) is exact and we are free to

choose any background model we want. A natural choice of the background model is a homogeneous medium ($n_0(\underline{r}) = 1$) for which the incident field P_0 is known analytically. The scattering potential $\gamma(\underline{r}) = n^2(\underline{r}) - 1$ is computed from the given velocity structure and the right hand side of equation (c2) (the source term) is completely determined. Then, the scattered field P_s is obtained by the finite difference algorithm as follows. Each grid point for which $v(\underline{r}) \neq c$ is considered as a source point. At each time step the source time samples associated to all source points are computed using the analytical solution of the background field P_0. The field created by these distributed sources is then propagated in the medium with refraction index $n(\underline{r})$. According to equation (c2) the wavefield generated in this manner gives the scattered field at every point in the medium. The observed scattered field is, then, obtained by recording this wavefield at the receiver locations.